NASA-CR-196403

P-222

INTERFACE BEHAVIOR OF A MULTI-LAYER FLUID CONFIGURATION SUBJECT TO ACCELERATION IN A MICROGRAVITY ENVIRONMENT

SUPPLEMENT I

NASA CONTRACT NAG 8-149
(PROJECT JOVE)

Dr. M.J. Lyell, P.I.
M. Roh, Graduate Student

Mechanical and Aerospace Engineering Dept.
Box 6106
West Virginia University
Morgantown, WV 26506-6106

INTERFACE BEHAVIOR OF A MULTI-LAYER FLUID CONFIGURATION SUBJECT TO ACCELERATION IN A MICROGRAVITY ENVIRONMENT

SUPPLEMENT I

NASA CONTRACT NAG 8-149
(PROJECT JOVE)

Dr. M.J. Lyell, P.I.
M. Roh, Graduate Student

Mechanical and Aerospace Engineering Dept.
Box 6106
West Virginia University
Morgantown, WV 26506-6106

INTERFACE BEHAVIOR OF A MULTI-LAYER FLUID CONFIGURATION SUBJECT TO ACCELERATION IN A MICROGRAVITY ENVIRONMENT

THESIS

Submitted to the College of Engineering

of

In Partial Fulfillment of the Requirements for

The Degree of Master of Science in Mechanical Engineering

by

Michael Roh, B.S.M.E.

Morgantown

West Virginia

1991

ACKNOWLEDGEMENTS

The author wishes to express his upmost gratitude to Dr. Margaret Lyell in appreciation for her invaluable guidance and support as advisor. Though risking triteness, may I say it truly could not have been done without you.

Particular thanks are extended to the other members of the examining committee, Dr. John Kuhlman and Dr. Gary Morris, for their assistance and encouragement. In addition, the helpful suggestions from Drs. F. Leslie and N. Ramachandran and Ms. C. Winter of NASA-Marshall are greatly appreciated.

Special gratitude is extended to Dr. Larry Padgett for his generous assistance with computational resources. Also the author wishes to thank his family and friends for their constant understanding and patience.

This research was performed as part of Project JOVE (NAG8-149), a joint venture project between West Virginia University and NASA.

This thesis is dedicated to Francis Otieno, Sarah Bellum, and the gang at Gene's. May the burdens they shoulder have weights pertinent to a microgravity environment.

ABSTRACT

With the increasing opportunities for research in a microgravity environment, there arises a need for understanding fluid mechanics under such conditions. In particular, a number of material processing configurations involve fluid-fluid interfaces which may experience instabilities in the presence of external forcing. In a microgravity environment, these accelerations may be periodic or impulse-type in nature. This research investigates the behavior of a multi-layer idealized fluid configuration which is infinite in extent. The analysis is linear, and each fluid region is considered inviscid, incompressible, and immiscible.

An initial parametric study of configuration stability in the presence of a constant acceleration field is performed. The zero mean gravity limit case serves as the base state for the subsequent time-dependent forcing cases. A stability analysis of the multi-layer fluid system in the presence of periodic forcing is investigated. Floquet theory is utilized. A parameter study is performed, and regions of stability are identified. For the impulse-type forcing case, asymptotic stability is established for the configuration. Using numerical integration, the time response of the interfaces is determined.

TABLE OF CONTENTS

LIST OF FIGURES

NOMENCLATURE

English

A	constant coefficent, dimensional (Chapter 2) (also B,C,D,E,F)
A(t)	time-dependent coefficient, nondimen. (Chp. 3,4) (also, B(t),C(t),D(t),E(t),F(t))
$\underset{\sim}{A}$, $\underset{\sim}{B}$	matrices representing final system (Chp. 3)
$Bo_{2,3}$	nondimen. Bond type parameter: $(\rho_D H^2 G_o/\gamma_{II,III})$ of upper,lower interface respectively
c	propagation speed, $c = c_R + ic_I$ (Chp. 2)
Fe	equilibrium interface, nondimensionalized
Fr	nondimen. Froude type parameter: $(G_o/(H\omega_f^2))$
G_o	peak value of forcing, dimensional
g	constant gravitational term, dimensional (Chp. 2)
g(t)	forcing term, nondimensional (Chp. 3,4)
h	height of middle layer (Chp.2)
H	height of middle layer (Chp.3,4)
k	wave number of perturbation, nondimensional
$\underline{\hat{n}}$	outward pointing unit normal to interface
p	pressure field, nondimensional
$\underset{\sim}{P}(t)$	time-dependent matrix (Chp. 4)
$\underset{\sim}{R}$	constant matrix (Chp. 4)
$\underline{u}$	velocity field, nondimensional
t	time
$\underline{x},\underline{y},\underline{z}$	spatial variables

Greek

ϕ	velocity potential, nondimensional
γ	surface tension
η	interface shape (Chp. 2)
ε	small parameter
λ	Floquet exponent, eigenvalue (Chp. 3)
ρ	density
ρ_D	density difference parameter $(\lvert\rho_2-\rho_1\rvert+\lvert\rho_3-\rho_1\rvert)/2$
$\rho_{21,31,D1}$	density ratios of $\rho_2:\rho_1$, $\rho_3:\rho_1$, and $\rho_D:\rho_1$
ω_f	frequency of periodic acceleration (forcing)
ξ	perturbation amplitude (Chp. 2)

Subscripts

1	middle layer fluid region of height H (finite)
2	upper layer fluid region (unbounded)
3	lower layer fluid region (unbounded)
II,III	upper,lower interface respectively

CHAPTER 1

INTRODUCTION

1.1 Literature review

The microgravity environment aboard the space shuttle has given rise to an number of research opportunities which will increase when space station becomes operational. In particular, materials processing , which generally involves fluid configurations, will involve processes which exhibit significantly different behavior in a microgravity environment. The gravity-induced fluid-thermal flows; ie. buoyancy-driven convection in liquids, will no longer contribute. This physical phenomenon masked the presence of thermo-capillary flows, which will now assume a greater role in a microgravity environment[1].

The effect of gravity has been greatly reduced in low-gravity aircraft flights and drop tubes which provide short periods of microgravity, sufficient for some research, but certainly too brief for most materials processing experiments. The advent of extended spaceflight has dramatically increased the opportunities for long-duration research and development in space. There are numerous technological applications which are envisioned in a microgravity environment.

The growth of crystals for electronic materials has not reached theoretical performance limits due to defects caused in

part by the presence of gravity. During the spacelab missions, scientists were able to monitor growth of a crystal through each stage of its formation. In earth-grown crystals, it can be observed where the seed crystal stops and the new growth begins. The introduction of such a defect was not detected in space due to the lack of gravity-induced convection[20].

The great reduction in convection is also relevant to metallurgical manufacturing. A microgravity environment provides greater understanding of how liquefied metals diffuse through each other prior to solidification. Such knowledge is important for the production of improved and novel alloys.

Containerless processing makes possible the production of much improved glasses and ceramics. In such a process, the sample is suspended and manipulated by acoustical and electromagnetic forces without the contamination of a container. Large samples can be dealt with in a microgravity environment[20].

Biological processing also benefits from space. Large, pure crystals allow analysis of many unknown protein structures which are essential to the design of new and improved drugs. There is also effort towards the separation and purification of biological substances for pharmaceutical purposes[17,21].

In the absence of gravity, fluid behavior which might normally be hidden by gravity-driven flows in a terrestrial environment can be observed and analyzed. Drop and fluid column dynamics in microgravity permit experimentation of basic

fluid physics theories. Experiments have been performed concerning the stability of liquid bridges in a short term microgravity on a rocket[18]. Also, experimental work has been done on board Spacelab to investigate the shapes of rotating free drops in a microgravity environment[28]. In fact, the fluid configurations of drop dynamics and liquid columns will occur not only in fundamental studies, but also in materials processing applications. For example, the proposed solidification of novel alloys could take place in an acoustic levitation chamber, with the liquid sample having a drop configuration.

A float zone configuration can be utilized in the growth of crystals. The float zone itself is modeled by a liquid column. In materials processing applications, heat and mass transfer effects are present in addition to the fluid dynamics. In fact, Marangoni convection would occur in the liquid column in a realistic processing scenario. It is currently thought that this convection could be reduced via the addition of a surrounding layer of fluid around the float zone. This would result in a multi-layer, compound fluid column configuration[2].

The environment on board a spacecraft is not strictly a microgravity environment. Rather, residual accelerations exist which could affect any ongoing materials science or space processing experiments. A recent summary[22] indicates that on board the space shuttle, accelerations include those in the frequency range up to ten hertz, with acceleration levels

ranging from $10^{-5}*g_{earth}$ to $10^{-3}*g_{earth}$. In addition to periodic accelerations (g-jitter), residual accelerations may be of impulse type, due to such causes as station-keeping maneuvers and astronaut motion[27].

Most processes involve fluid dynamics, and in particular, fluid interfaces. This study does not investigate a specific process per se, but instead considers the stability of initially planar fluid interfaces.

Previous work on fluid interfaces in microgravity has focused predominantly on the application of fuel slosh in tanks. Most recently, this has included work done by Hung et al[9], which considered g-jitter in a slosh tank. A brief review of earlier work, as well as an extension of the previous efforts, was given by Gu et al[7]. These investigations all involved liquid in a container of specified shape with a free surface.

The stability of a single planar free surface subjected to periodic forcing in the direction perpendicular to the interface has been investigated[3,6]. Both studies were done in a 1-g ambient environment and required the use of a container. In the work of Benjamin and Ursell[3], the container was cylindrical in shape. The analysis led to a Mathieu equation which governed the time-dependent amplitude of the disturbance. They were able to make statements concerning the interface stability based upon known mathematical properties of Mathieu equations. The case of a rectangular container has been

addressed recently by Gu[6], and the results extended into the nonlinear regime. Both of these investigations utilized an inviscid analysis.

Viscous effects on the stability properties have been investigated recently in idealized infinite or semi-infinite configurations which have one fluid-fluid interface[8,12]. The forcing was periodic and directed perpendicular to the interface. The work of Jacqmin and Duval[12] assumed a zero mean g-level and pertained to a microgravity environment. A Floquét analysis was applied to the fluid system for the case of sinusoidal forcing. Stability boundaries were obtained from the results.

Recently, Jacqmin has studied the stability of an oscillated fluid with a uniform density gradient[11]. The case of forcing perpendicular to the density gradient was investigated. Such a problem involves the Kelvin-Helmholtz instability.

1.2 Objectives

This research will consider a multi-layer fluid configuration unbounded in space. Multi-layer fluid configurations are finding applications in materials processing scenarios in microgravity. Although the infinite, multiple layer fluid system is not physically realistic, it is the logical extension of work done previously in the one interface,

infinite system. As such, it will provide insight into the behavior of configurations with multiple interfaces in the presence of forcing.

A layer of finite height will be situated between two semi-infinite layers of fluid. The analysis is linear, and each fluid region is considered inviscid, irrotational, incompressible, and immiscible. A normal mode approach in the spatial variables will be assumed. Surface tension is the only property of each interface and is taken to be constant. Jacqmin and Duval showed that the presence of even weak surface tension can overwhelm the effects of viscosity, making the viscous analysis of secondary importance[12].

The objective is to investigate the configuration behavior in the presence of microgravity environment acceleration fields. As stated previously, these may manifest as periodic or non-periodic impulse-type accelerations. It is recognized that in practice, the true acceleration field will be random in magnitude and orientation. Two subcases will be investigated: 1) periodic forcing directed normal to the interface (a cosine forcing function will be assumed), 2) non-periodic but time-dependent normal impulse forcing.

As a preliminary step to this investigation, the stability of the configuration in the presence of a constant acceleration field will be investigated (Chapter 2). Regions of stability and various parametric trends will be established. The zero mean gravity limit case will ultimately serve as the base state

for the investigation of the time-dependent acceleration cases.

The periodic forcing case results in a system of four ordinary differential equations (in time) with periodic time-dependence. Such a problem is well-posed for application of Floquet theory[5,25] in which the time-dependent coefficients are expressed in terms of a Floquet exponent. Previous work in fluid mechanics has utilized Floquet theory[5,12]. It is, however, more generally applied to dynamical systems[25]. One recent application involved the analysis of a spin-stabilized satellite in orbit[26]. In the periodic forcing case, the system of fluid equations can be converted to an infinite algebraic eigensystem. The nature of the real component of the eigenvalue will determine configuration stability. The effect of six non-dimensional parameters will be investigated.

For the non-periodic case, asymptotic stability will be established according to mathematical theory. The system results in four linear differential equations which will be integrated numerically. The time response of each interface will be determined, and parametric trends will be discerned.

CHAPTER 2

MULTI-LAYER FLUID CONFIGURATION STABILITY IN THE PRESENCE OF CONSTANT ACCELERATION FIELDS

2.1 Problem description

Prior to an analysis of stability of a multi-layered configuration in the presence of time-dependent forcing, cases will be considered in which the body force is due entirely to a constant gravitational acceleration. The limit cases of $1*g_{earth}$ and $0*g_{earth}$ are studied, as well as various intermediate values. The $0*g_{earth}$ mean state will ultimately serve as a basis for investigating the effects of residual accelerations in Chapters 3 and 4.

The configuration to be considered is comprised of three horizontal fluid layers. No rigid boundaries are present. The layers extend to infinity in the horizontal directions. The top and bottom layers are considered to be semi-infinite in nature, while the middle layer has a finite height. The geometry of the figure is given by Figure 2.1.

The base state is one of zero mean motion in each of the three fluid regions. The fluids are immiscible and will be taken as inviscid, irrotational and incompressible. Surface tension is a property of the interfaces. A normal mode approach is assumed. That is, the small amplitude perturbations are wavelike in nature.

The fluids considered in this study are water, air, and

Configuration Geometry

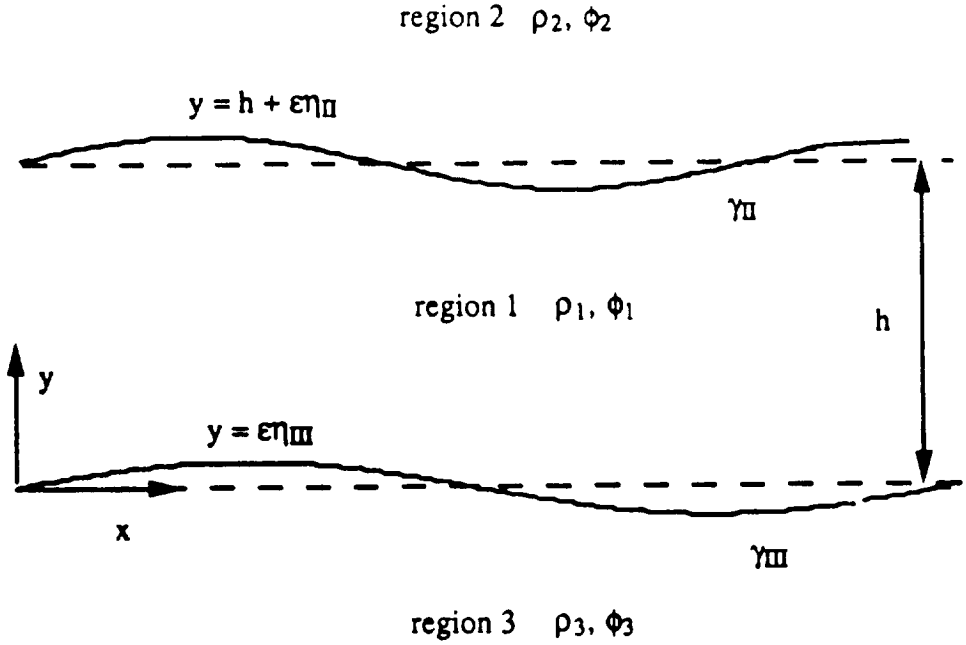

ρ = density of subscripted region

ϕ = potential function of subscripted region

γ = surface tension of subscripted interface

η = perturbation of subscripted interface

Figure 2.1

silicone oil. Four different cases are examined in the following configurations:

CASE 1: air/silicone oil/water (region 2/region 1/region 3)
CASE 2: air/water/air "
CASE 3: air/silicone oil/air "
CASE 4: water/silicone oil/water "

The parameters to be varied include height of the middle slab, wave number of the interfacial perturbation, and the value of the constant gravitational acceleration. By varying these quantities, the propagation speed of the perturbations can be calculated for different parameter conditions. A positive value of the imaginary component of the propagation speed will indicate an instability on the fluid system.

Several of the cases to be investigated have a configuration such that the density of the upper fluid is greater than that of the lower fluid, giving rise to a motion driven by gravity. This type of instability is known as the Rayleigh-Taylor instability. It will be shown that the growth rate of these instabilities is determined by the nature of the solution to the dispersion relation. More specifically, if a certain configuration generates non-zero imaginary components of the propagation speed, then depending on the sign of the quantity, the Rayleigh-Taylor instability will occur.

2.2 Equation development

2.2a Governing equations

As stated previously, a normal mode perturbation has been utilized. The waveform of the disturbance is given by the following:

$$\eta(x,t) = \xi e^{ik(x-ct)} \tag{2.1}$$

where ξ = amplitude (small)
k = wave number (real number)
c = propagation speed (complex number)
η = interface shape

The governing equations of incompressible fluid mechanics are the continuity equation and the momentum equation. The analysis is inviscid, irrotational, and linear. Linearization is done about a base state of zero mean motion. The following equations govern fluid behavior.

$$\nabla \cdot \underline{u}' = 0 \tag{2.2}$$

$$\rho \frac{\partial \underline{u}'}{\partial t} = -\nabla p' \tag{2.3a}$$

$$0 = -\nabla p_{mean} + \rho g \hat{e}_y \tag{2.3b}$$

Note the momentum equation has been split into the perturbation (2.3a) and mean (2.3b) equations Henceforth, primes will be omitted for perturbation values.

A potential function, ϕ, with $\underline{u} = \nabla\phi$, is defined. Substitution into equation (2.2) yields Laplace's equation.

$$\nabla^2\phi = 0 \tag{2.4}$$

Laplace's equation must be solved in all three regions. Separation of variables yields the following solutions for the potential functions.

$$\phi_1 = \left[Ae^{ky} + Be^{-ky} \right] e^{ik(x-ct)} \tag{2.5}$$

$$\phi_2 = Ce^{-ky}e^{ik(x-ct)} \tag{2.6}$$

$$\phi_3 = De^{ky}e^{ik(x-ct)} \tag{2.7}$$

where A, B, C, and D are constant coefficients.

Furthermore, at each interface the perturbation is defined as

$$\eta_{II} = Ee^{ik(x-ct)} \tag{2.8}$$

$$\eta_{III} = Fe^{ik(x-ct)} \tag{2.9}$$

2.2b Boundary conditions

The dispersion relation is obtained by applying three boundary conditions at each interface. These three conditions are: (1) the kinematic boundary condition, (2) the matching of the normal component of the velocity, and (3) the normal force balance.

The kinematic condition states that a particle of fluid which is at some point on the surface will always remain on that surface. This can be written as:

$$\frac{D(y-\varepsilon\eta)}{Dt} = 0 \tag{2.10}$$

By converting into Eulerian form, and noting that x, y, and t are independent and that the waveform depends solely on x and t, the equation (after linearization) becomes:

$$\frac{\partial \eta}{\partial t}(x,t) = \frac{\partial \phi}{\partial y}(x, y_o + \varepsilon\eta, t) \qquad (y_o = 0 \text{ or } h) \tag{2.11}$$

By applying a Taylor expansion and again neglecting quadratically small terms, the kinematic boundary condition at each interface simplifies to:

$$\frac{\partial \phi}{\partial y}(x,h,t) = \frac{\partial \eta_{II}}{\partial t}(x,t) \tag{2.12}$$

$$\frac{\partial \phi}{\partial y}(x,0,t) = \frac{\partial \eta_{III}}{\partial t}(x,t) \tag{2.13}$$

Imposition of the condition that the normal component of velocity be continuous across the interface yields:

$$\frac{\partial \phi_1}{\partial y} = \frac{\partial \phi_2}{\partial y} \qquad \text{at} \quad y = h \tag{2.14}$$

$$\frac{\partial \phi_1}{\partial y} = \frac{\partial \phi_3}{\partial y} \qquad \text{at} \quad y = 0 \tag{2.15}$$

Finally, the third boundary condition is imposed. Taking

into account the surface tension, the normal force balance takes the following form:

$$P_{lower} - P_{upper} = \gamma \nabla \cdot \hat{n} \tag{2.16}$$

where γ = surface tension
$\hat{n}$ = the outward pointing normal to the interface

By noting that the perturbation is a function of x and t only, the final boundary conditions can be derived at each interface.

$$\rho_2 \frac{\partial \phi_2}{\partial t} - \rho_1 \frac{\partial \phi_1}{\partial t} + g(\rho_2 - \rho_1)\eta_{II} = -\gamma_{II} \frac{\partial^2 \eta_{II}}{\partial x^2} \tag{2.17}$$

$$\rho_1 \frac{\partial \phi_1}{\partial t} - \rho_3 \frac{\partial \phi_3}{\partial t} + g(\rho_1 - \rho_3)\eta_{III} = -\gamma_{III} \frac{\partial^2 \eta_{III}}{\partial x^2} \tag{2.18}$$

2.2c Dispersion relation

These six algebraic equations (2.12-2.15,2.17,2.18) form a homogeneous system in unknowns A,B,C,D,E, and F. In order to have a solution, the determinant corresponding to this system must equal zero. This results in the following dispersion relation.

$$\left[(\rho_1+\rho_3)(\rho_1+\rho_2)e^{2kh} + (\rho_2-\rho_1)(\rho_1-\rho_3)\right] c^4$$

$$+ \left[\left\{(\rho_1+\rho_3)\left(\frac{q}{k}(\rho_2-\rho_1)-\gamma_{II}\,k\right) + (\rho_1+\rho_2)\left(\frac{q}{k}(\rho_1-\rho_3)-\gamma_{III}k\right)\right\} e^{2kh}\right.$$

$$\left. + (\rho_2-\rho_1)\left(\frac{q}{k}(\rho_3-\rho_1)+\gamma_{III}k\right) + (\rho_1-\rho_3)\left(\frac{q}{k}(\rho_2-\rho_1)-\gamma_{II}k\right)\right] c^2$$

$$+ \left[\left\{\left(\frac{q}{k}(\rho_1-\rho_3)-\gamma_{III}k\right)\left(\frac{q}{k}(\rho_2-\rho_1)-\gamma_{II}k\right)\right\} e^{2kh}\right.$$

$$\left. + \left(\frac{q}{k}(\rho_2-\rho_1)-\gamma_{II}k\right)\left(\frac{q}{k}(\rho_3-\rho_1)-\gamma_{III}k\right)\right] = 0 \qquad (2.19)$$

Thus, this propagation speed, c, is given by the solution of a fourth order polynomial. It is also the eigenvalue. From the theory of roots of a polynomial, it is readily seen that there exists the possibility of complex roots to the dispersion relation. The propagation speed can be written as a complex number.

$$c = c_R + ic_I \qquad (2.20)$$

Hence, the perturbation equations can actually be written as:

$$\eta_{II} = Ee^{ikx}\, e^{(-ikc_R t)}\, e^{(kc_I t)} \qquad (2.21)$$

$$\eta_{III} = Fe^{ikx}\, e^{(-ikc_R t)}\, e^{(kc_I t)} \qquad (2.22)$$

The first two exponential terms of each equation are oscillatory in nature. The third exponential factor is a real number. An imaginary component equal to zero implies a neutral disturbance, while if the value is less than zero, the exponential term decays in time, and the system remains stable. However, if this imaginary component, c_I, is positive, the exponential term grows in time, resulting in an instability. This case is known as the Rayleigh-Taylor instability. An analytical limit case can be obtained from the full dispersion relation for the special case in which the ratios of the top and bottom densities to the middle density are negligibly small.

$$\left[e^{2kh}-1\right]c^4 + \left[(e^{2kh}+1)\left(\frac{-\gamma_{II}^{\,k}}{\rho_1} - \frac{\gamma_{III}^{\,k}}{\rho_1}\right)\right]c^2$$

$$+ \left[(e^{2kh}-1)\left(\frac{g}{k} - \frac{\gamma_{III}^{\,k}}{\rho_1}\right)\left(\frac{-g}{k} - \frac{\gamma_{II}^{\,k}}{\rho_1}\right)\right] = 0 \qquad (2.23)$$

For such cases, the configuration will remain stable if the following inequality holds true.

$$\frac{\gamma_{III}}{\rho_1} k^2 \geq g \qquad \text{for } \frac{\rho_2}{\rho_1}, \frac{\rho_3}{\rho_1} \ll 1 \qquad (2.24)$$

The scope of this study is to analyze the four previously stated cases under various parameter conditions. That is, by allowing the parameters to vary over a specified range, the roots of the dispersion relation can be calculated ;and hence, interface stability can be determined. The parameters that are considered are the height of the middle layer, the wave number, and the value of the gravitational constant. For our ultimate purposes, we are most interested in the case in which the time-independent gravitational body force is zero.

2.3 Results

The dispersion relation was solved numerically using the DZPORC routine of the IMSL library. The DZPORC routine makes use of the Jenkins-Traub three-stage algorithm[13], in which the roots are computed one at a time for real roots and two at a time for complex conjugate pairs. As the roots are found, the real root or quadratic factor is removed by polynomial deflation.

The fourth order polynomial (in c) has four roots. Because of the nature of the dispersion relation, the roots were generated in pairs. That is, for any given solution, there exist two pairs of roots, where each pair consists of the positive and negative values of a number. Physically, for real roots, this means the perturbation may propagate in either the positive or negative direction. For imaginary roots, it implies an instability will occur since these roots occur in complex conjugate pairs. If all the roots are real, the system will be stable.

Figure 2.2 shows the four roots of the dispersion relation for Case 1 (air/silicone oil/water). The roots are plotted over a range of gravity ratios (g/g_{earth}) from 0 to 1.0. As is expected, since heavier fluids underlie lighter ones this case is stable for all parametric conditions. (Note that the non-zero roots are exclusively real.) A less dense fluid above a more dense fluid is stable to small perturbations in the presence of constant gravitational forcing.

Figures 2.3, 2.4, and 2.5 show the dispersion solution for Cases 2,3, and 4, respectively. Each of these cases reveals the presence of a positive imaginary root, which in turn, implies an unstable configuration. This behavior is expected as each case involves a more dense fluid above a less dense fluid in its configuration.

Since an instability depends solely on the presence of

positive imaginary roots, the subsequent figures will display these particular roots exclusively.

The effect of wave number,(k), on configuration stability is elucidated in Figures 2.6-2.8. As k values increase, the configuration becomes more stable. Since k is inversely proportional to wavelength, the configuration is unstable to long wavelength perturbations. The restoring force required to maintain stability is greater in the long wavelength regime.

Note that all cases are stable at $0*g_{earth}$. The results of Case 1 do not appear since the configuration is stable for all parameter space.

The effect of surface tension can be readily seen by comparing Figure 2.6 with 2.7, where the middle layers are water and silicone oil, respectively. Thus, while their densities are effectively the same, the water-air interfaces have surface tension values nearly three times that of the oil-air interfaces. With the increased restoring force, it is expected and confirmed that Figure 2.6 will be more stable than Figure 2.7. In the water case (Fig. 2.6), for a k value of 3, the system is stable up to $g=0.65*g_{earth}$. For the oil case (Fig. 2.7), for k=3, the configuration becomes unstable at $g=0.23*g_{earth}$.

From Figure 2.9, it is tempting to conclude that the middle slab height,(h), has no effect on the stability of the configuration. This conclusion is valid for values of h which are large in comparison to the wavelength (recall $\lambda = 2\pi/k$).

When the nondimensional quantity, h/λ, is greater than or on the order of one, middle layer height has little effect on the stability. In Figure 2.9, this corresponds roughly to values of $h \geq 5cm$ (for $k=1cm^{-1}$). For h=1cm, the quantity, h/λ, equals 0.16 which is less than O(1). From Figure 2.9 it is seen that this height is associated with the fastest growing instabilities.

The effect of middle layer height is even more dramatic in Figures 2.10 and 2.11. The fastest growing instabilities for a given wavelength perturbation are associated with configurations with the smallest values of h/λ. In Figure 2.10, the smallest value of h/λ equals 0.04 (corresponding to $h=0.25cm$, $k=1.0cm^{-1}$). Note that this value relates to the fastest growing instability.

The limit case (eq. 2.24) simulates a liquid layer situated between two layers of a gas, and its accuracy can be verified by comparing it to either Figure 2.6 or 2.7. According to (2.24), for Case 2 (air/water/air), and h=1cm, the instability should originate at $g/g_{earth}=0.073$ for k=1, and at $g/g_{earth}=0.661$ for k=3.

For Case 2 (air/silicone oil/air), and h=1cm, the instability should start at $g/g_{earth}=0.027$ for k=1, $g/g_{earth}=0.230$ for k=3, and $g/g_{earth}=0.657$ for k=5. The results from Figures 2.6 and 2.7 confirm these values.

It is seen that in the case of zero gravity, each configuration remains stable. Although we might expect

Rayleigh-Taylor type instabilities for Cases 2,3, and 4, there is no body force which would drive the density difference; hence, the system will remain stable.

This zero mean gravity state will be taken as the base state for the remainder of the investigations of this thesis.

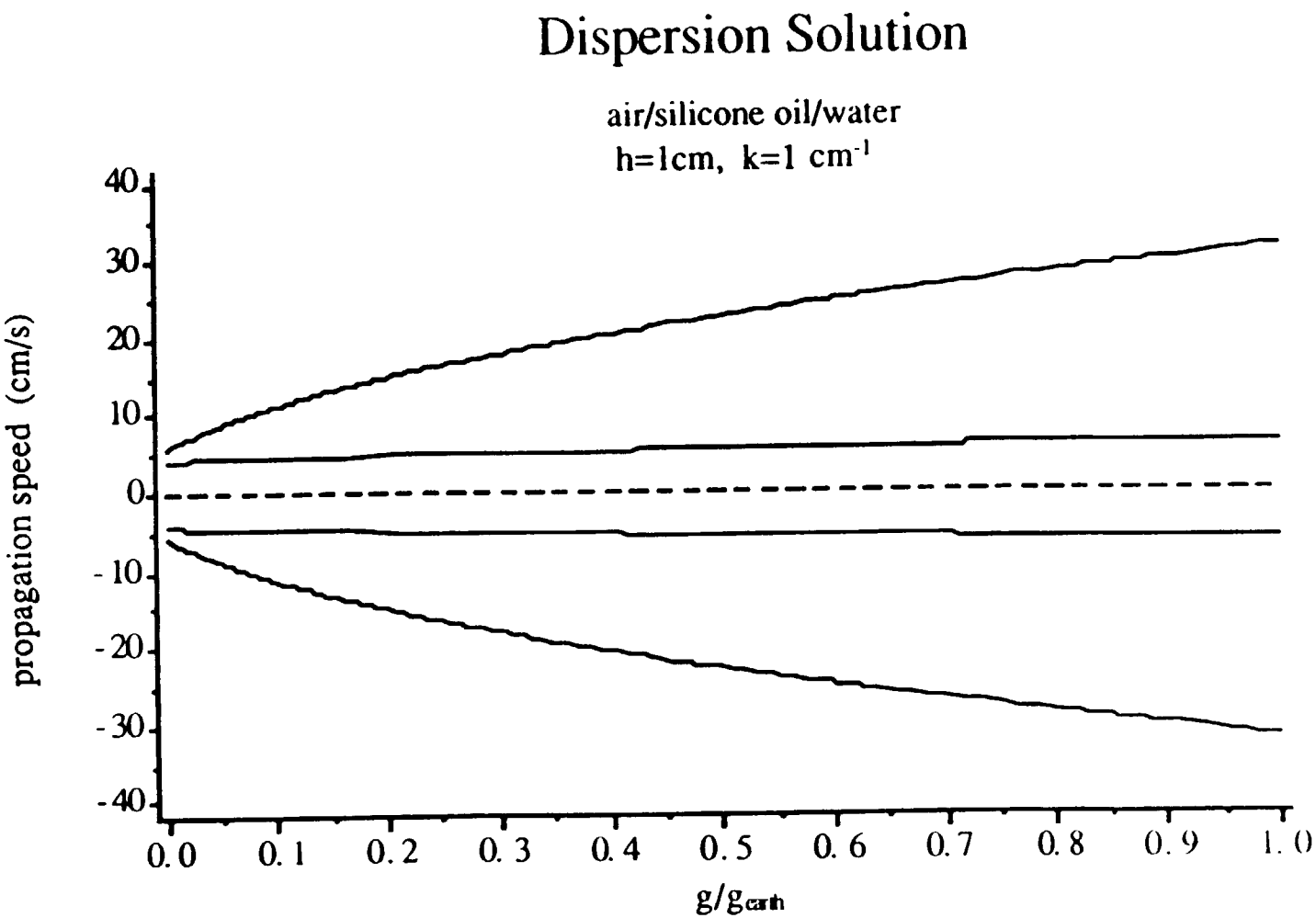

solid line: real root (stable solution)
dashed line: imaginary root (positive values yield unstable solutions)

Figure 2.2

Dispersion Solution

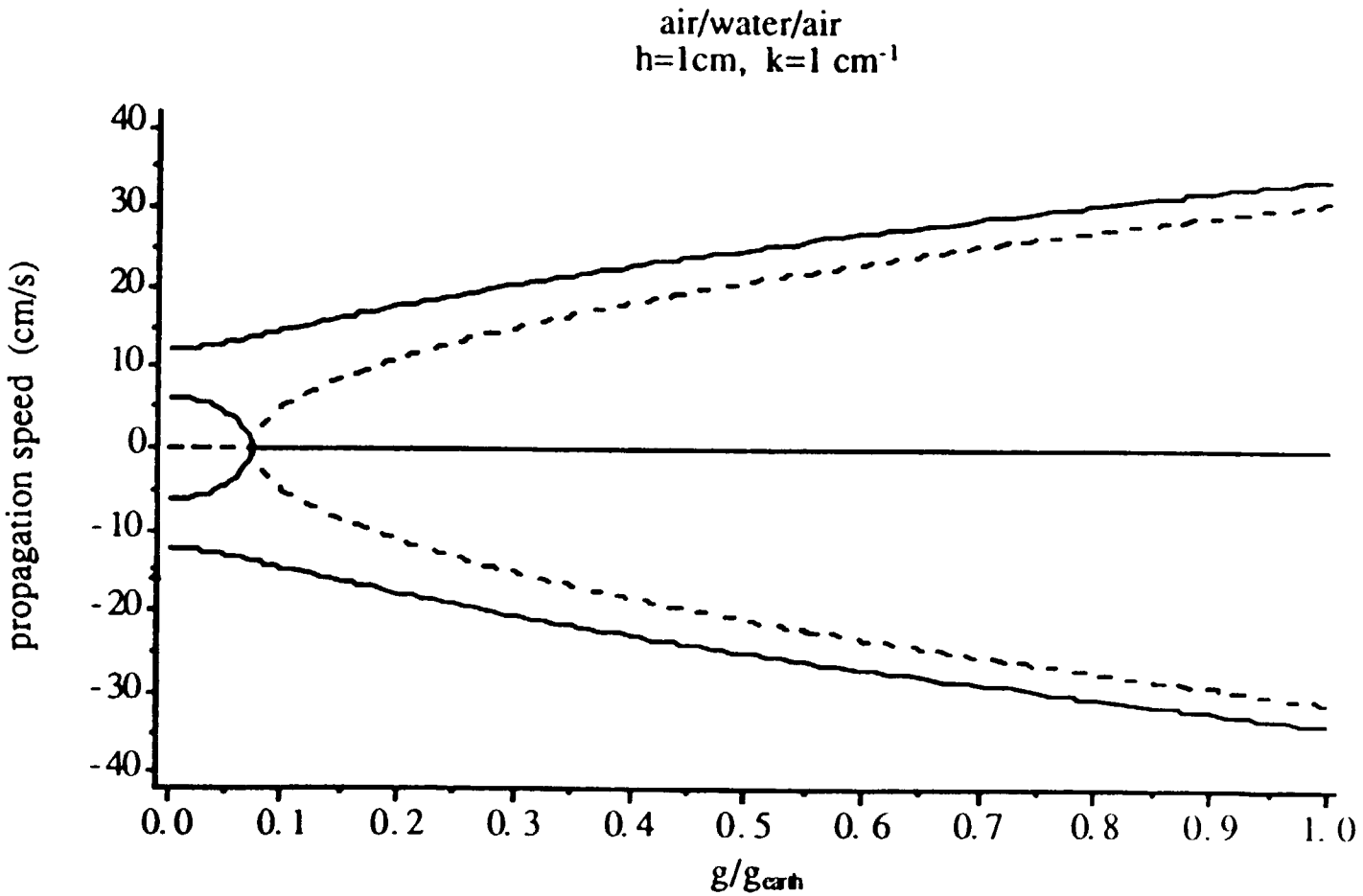

solid line: real root (stable solution)
dashed line: imaginary root (positive values yield unstable solutions)

Figure 2.3

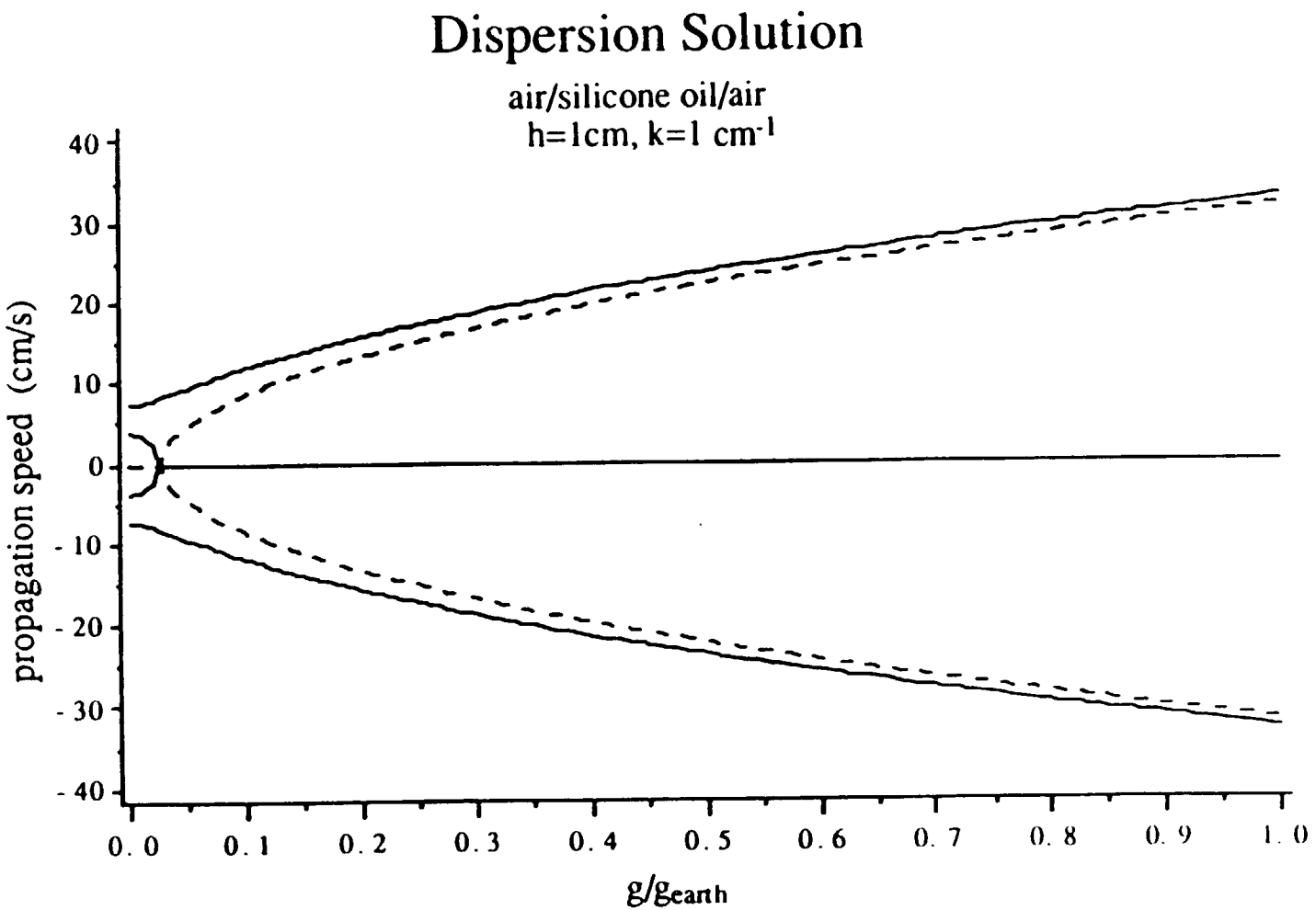

solid line: real root (stable solution)
dashed line: imaginary root (positive values yield unstable solutions)

Figure 2.4

Dispersion Solution

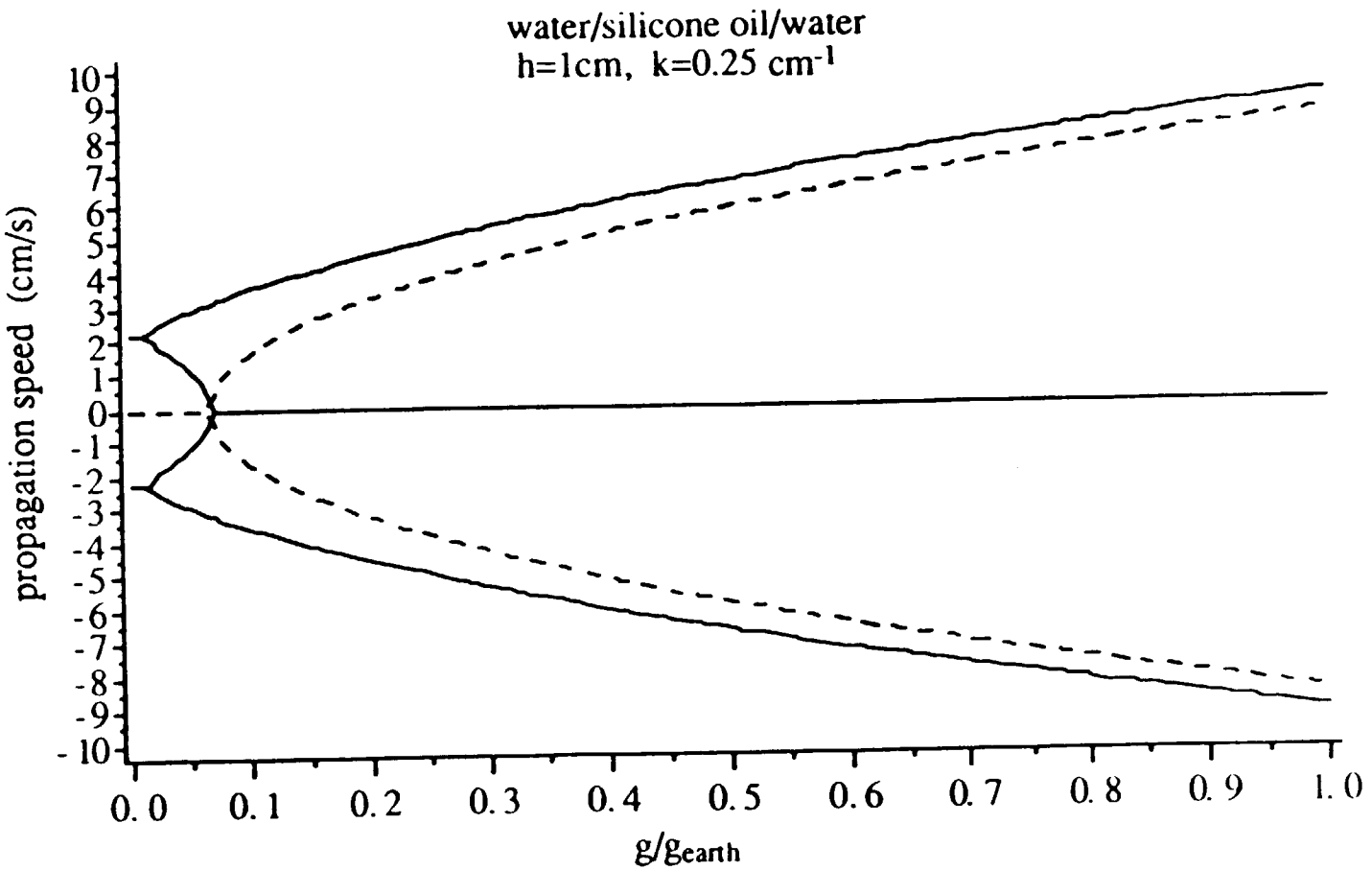

solid line: real root (unstable solution)
dashed line: imaginary root (positive values yield unstable solutions)

Figure 2.5

Effect of Wave Number on Stability

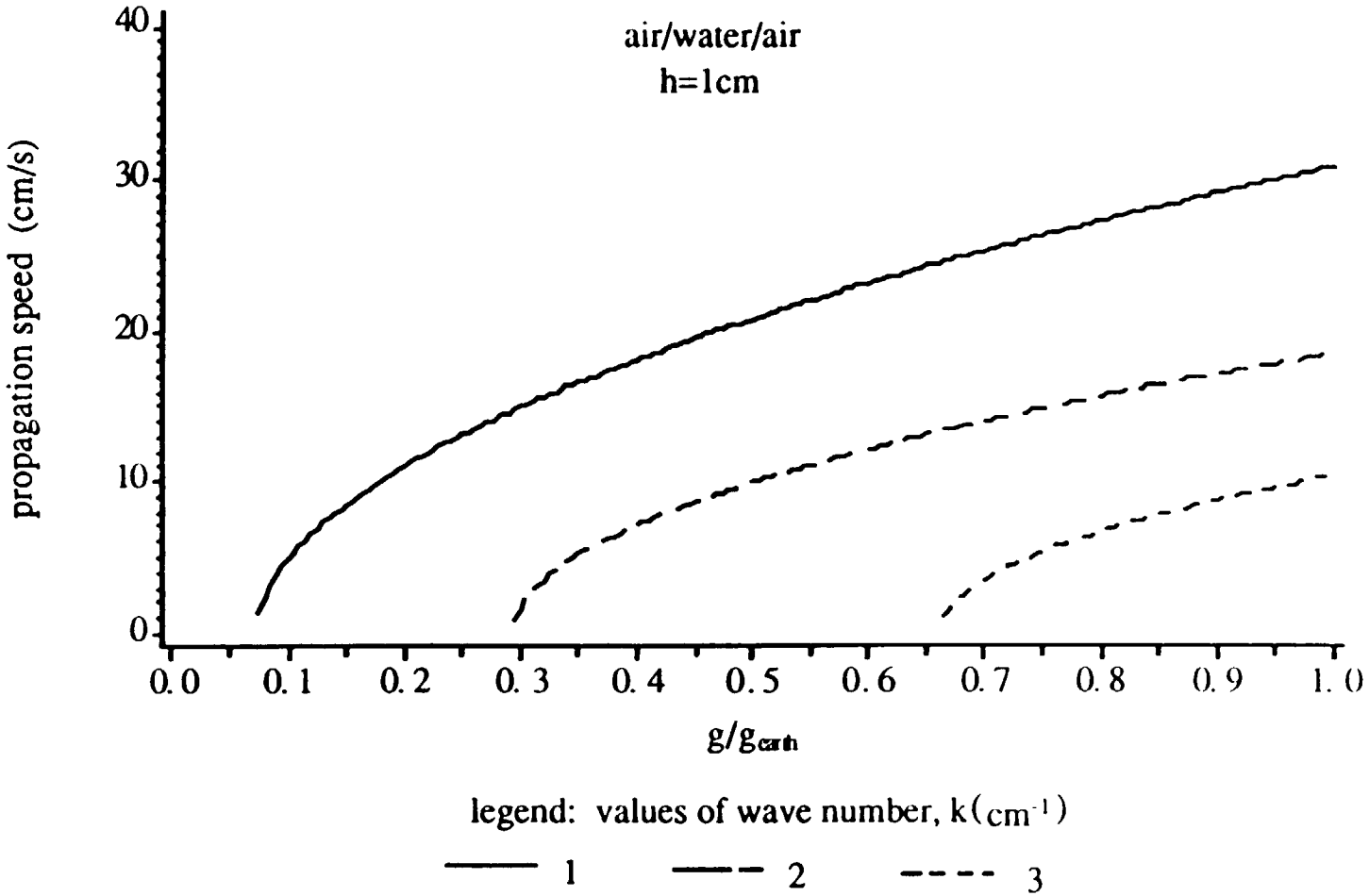

Figure 2.6

Effect of Wave Number on Stability

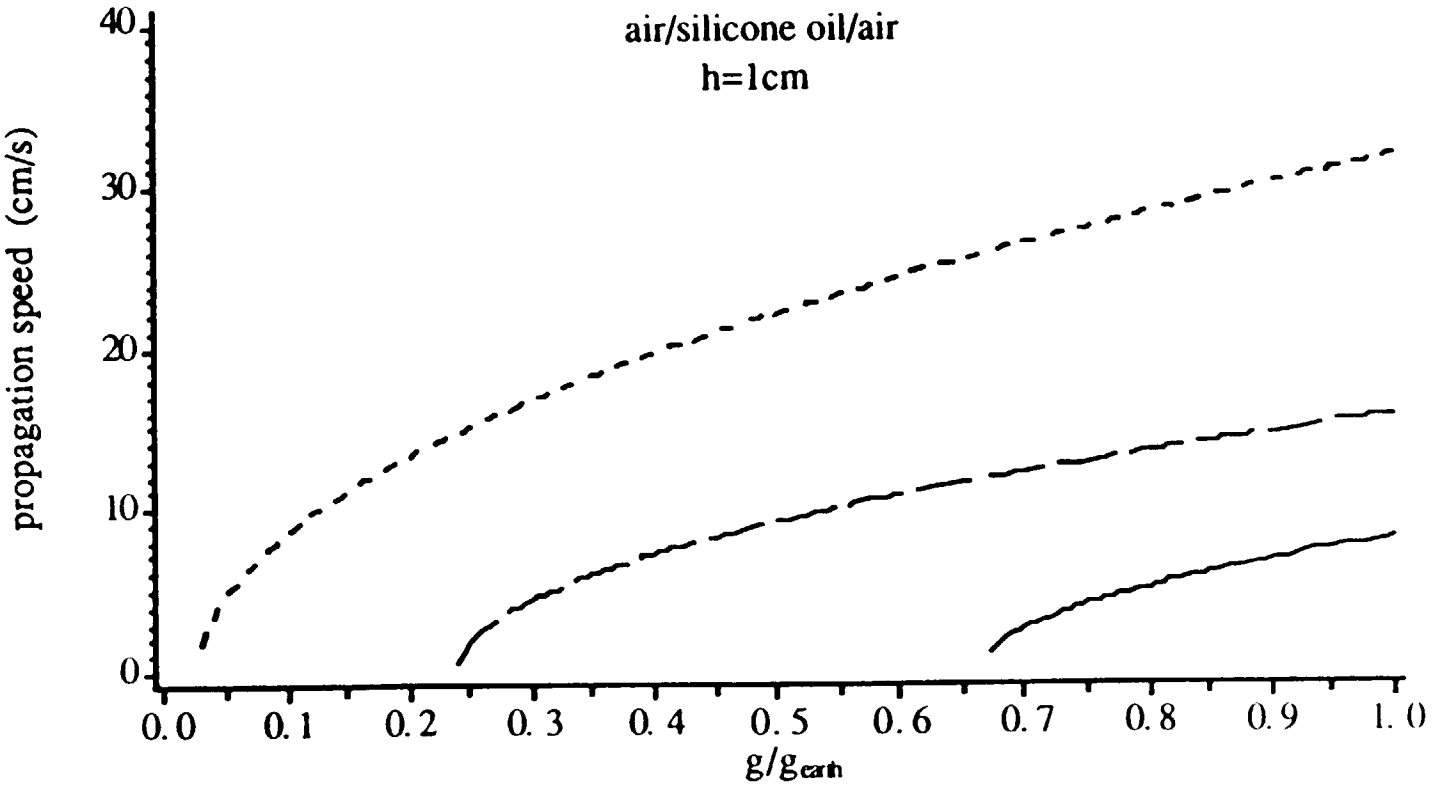

Figure 2.7

Effect of Wave Number on Stability

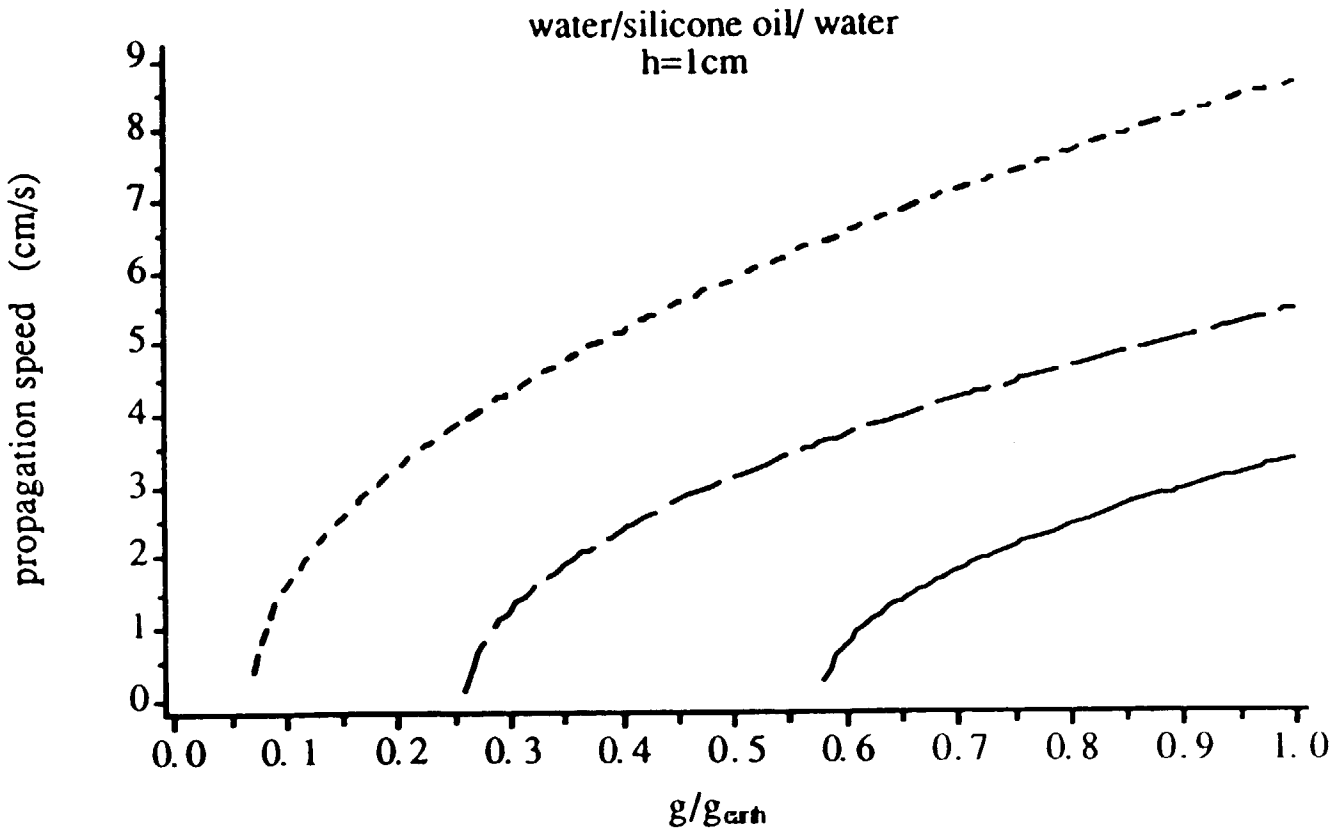

Figure 2.8

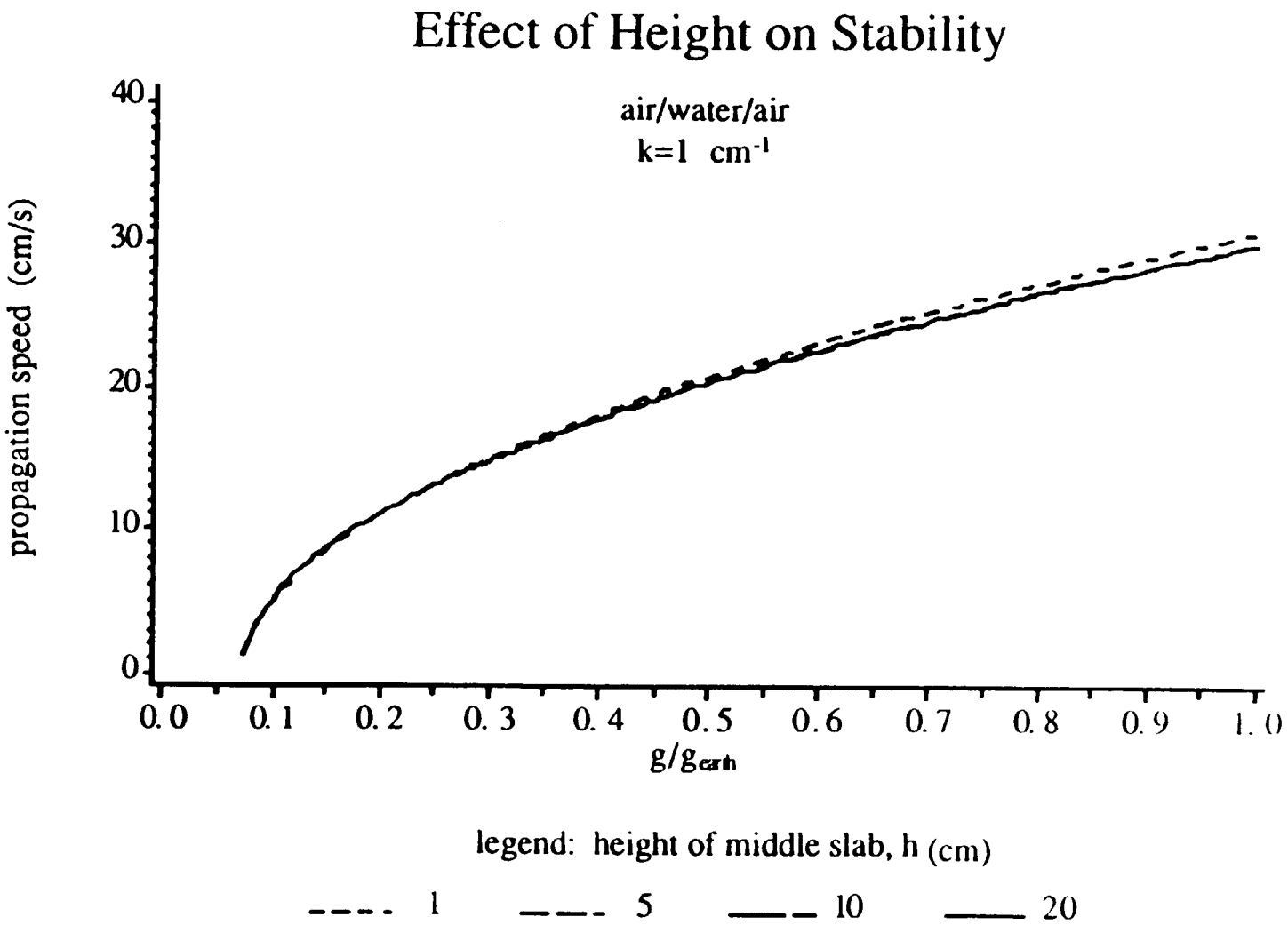
Effect of Height on Stability
air/water/air
k=1 cm-1
propagation speed (cm/s)
40
30
20
10
0
0.0
0.1
0.2
0.3
0.4
0.5
0.6
0.7
0.8
0.9
1.0
g/gearth
legend: height of middle slab, h (cm)
1
5
10
20

Figure 2.9

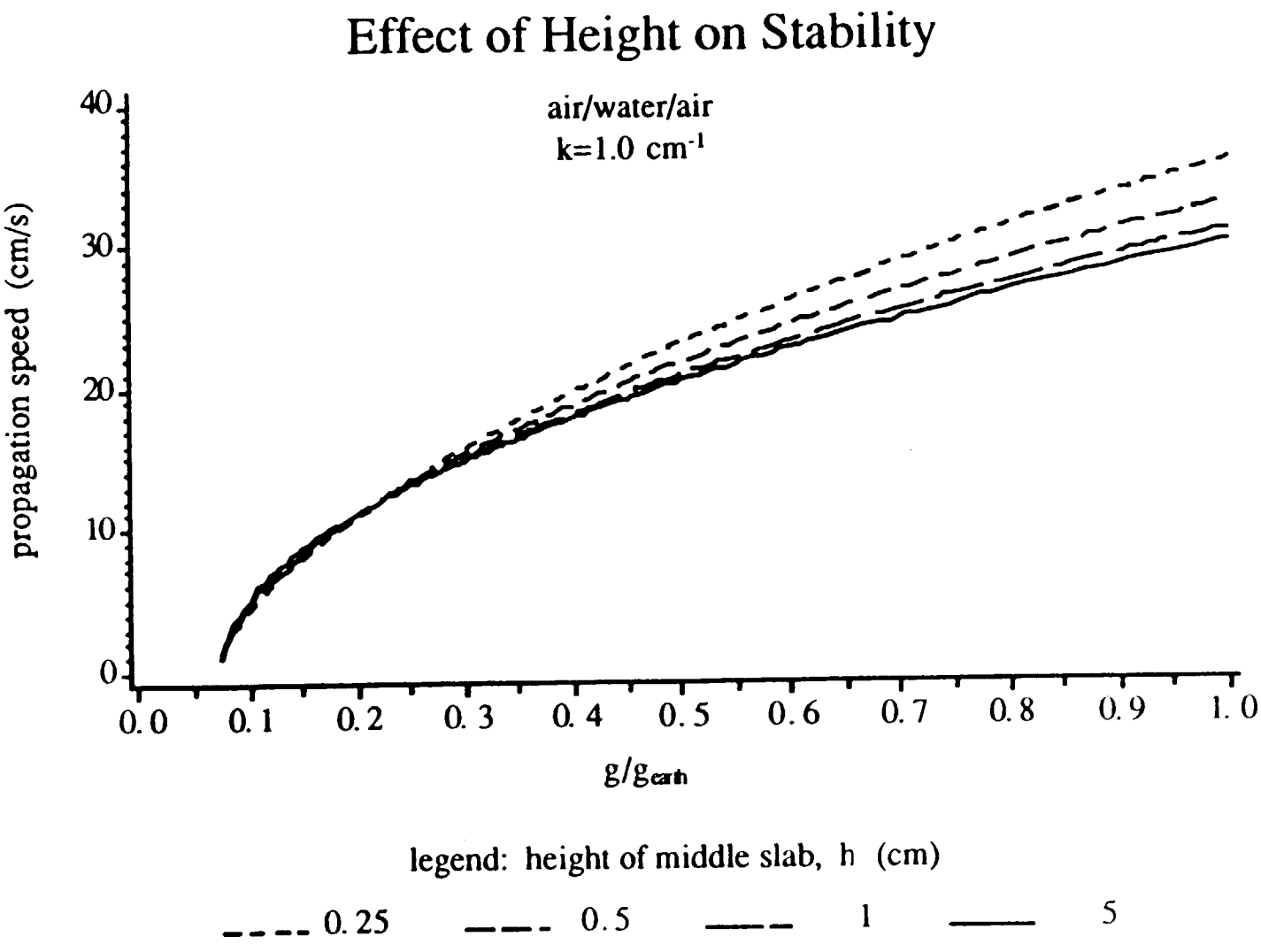
Effect of Height on Stability
air/water/air
k=1.0 cm-1
propagation speed (cm/s)
40
30
20
10
0
0.0
0.1
0.2
0.3
0.4
0.5
0.6
0.7
0.8
0.9
1.0
g/gearth
legend: height of middle slab, h (cm)
0.25
0.5
1
5

Figure 2.10

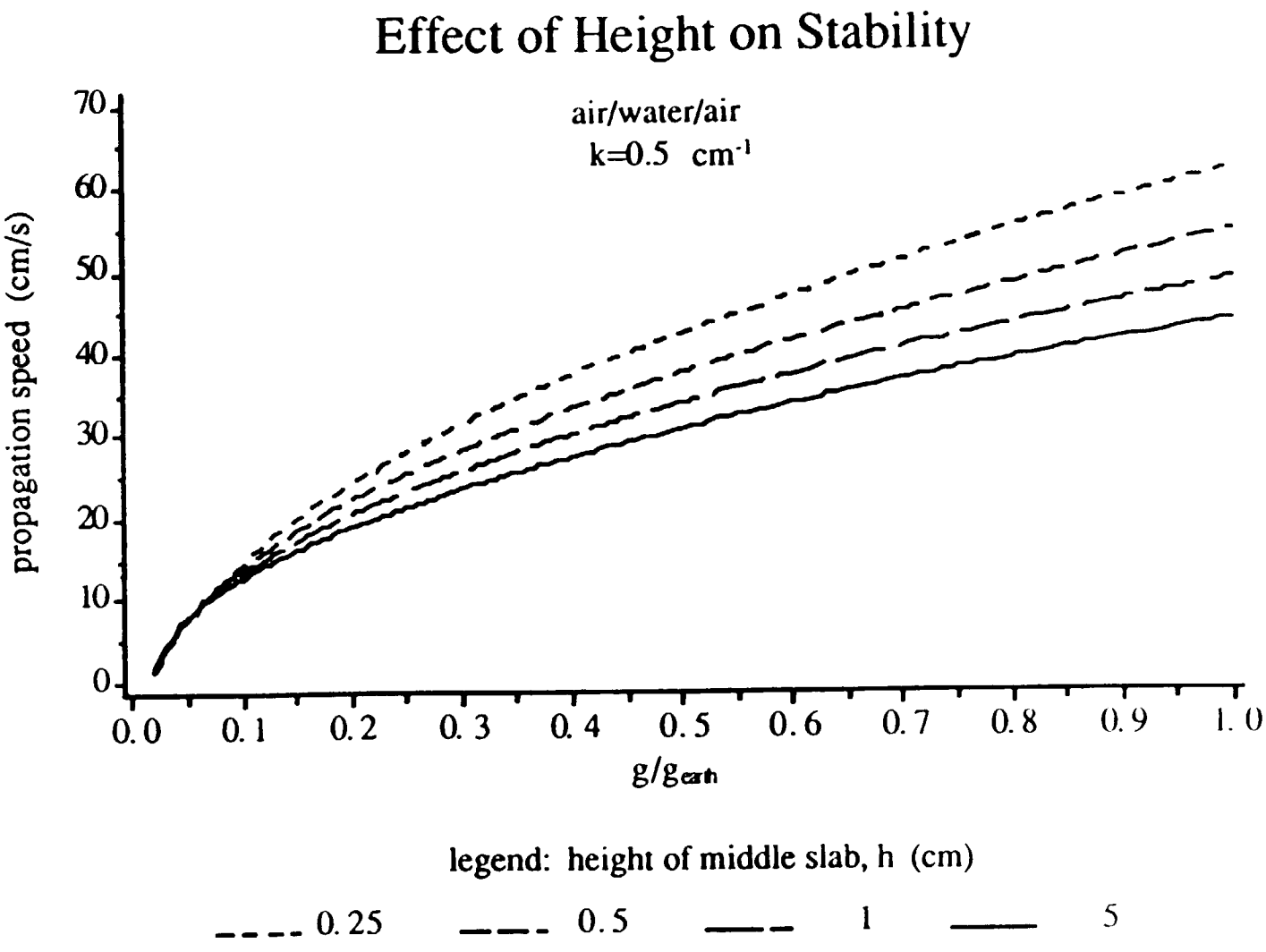
Effect of Height on Stability
air/water/air
k=0.5 cm-1
propagation speed (cm/s)
70
60
50
40
30
20
10
0
0.0
0.1
0.2
0.3
0.4
0.5
0.6
0.7
0.8
0.9
1.0
g/gearth
legend: height of middle slab, h (cm)
0.25
0.5
1
5

Figure 2.11

CHAPTER 3

MULTI-LAYER FLUID CONFIGURATION STABILITY IN THE PRESENCE OF A TIME-DEPENDENT PERIODIC ACCELERATION FIELD

3.1 Problem description

The results from Chapter 2 illustrated that for constant zero gravity the fluid configuration is stable for all parameter values. This, however, is a highly idealized case. A recent summary[22] indicates that the environment of board space shuttle is subjected to residual accelerations ranging from 10^{-5} to $10^{-3} * g_{earth}$ at a frequency range up to 10 Hz.

This chapter investigates the effect of periodic accelerations on the interface stability of a multi-layer fluid configuration without rigid boundaries. The configuration consists of a layer with finite height situated between two semi-infinite layers. All three layers extend to infinity in the horizontal plane. (See Figure 3.1). The accelerations are periodic about a zero mean gravity level, and are oriented normal (in the $\hat{e}_z$ direction) to the interfaces.

The three fluids are inviscid, incompressible, irrotational, and immiscible. Surface tension is a property of the interfaces. The spatial dependence of the perturbation is considered to be wavelike.

The dynamics of the above system are again governed by the continuity and Euler equations. These are non-dimensionalized

Configuration Geometry

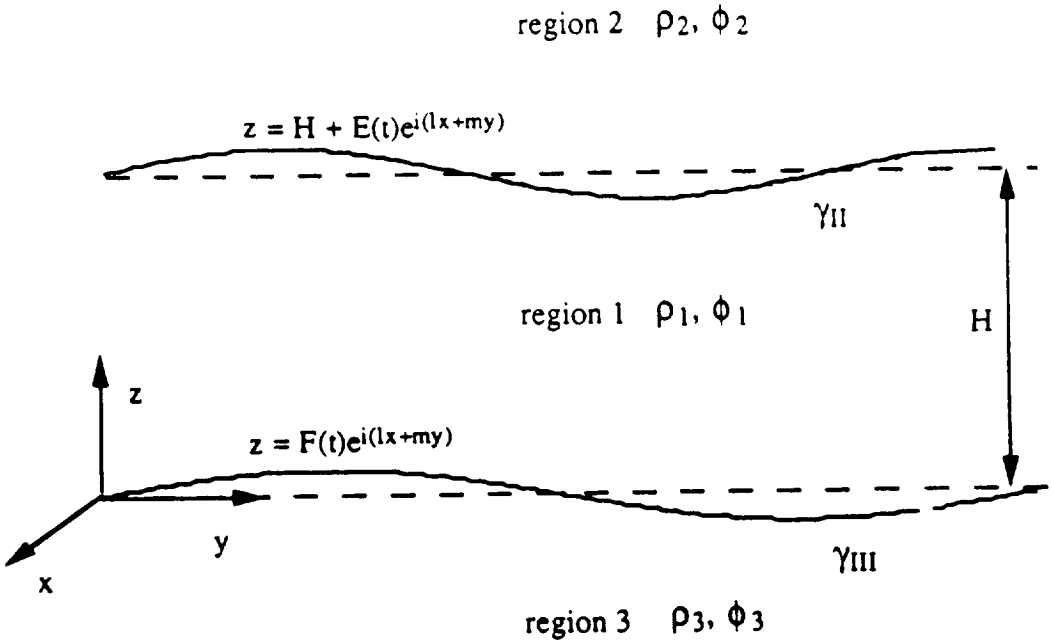

ρ = density of subscripted region

ϕ = potential function of subscripted region

γ = surface tension of subscripted interface

Figure 3.1

and linearized, resulting in a system of linear equations with time-dependent coefficients.

A Floquet analysis is applied. The resulting system can be viewed as an eigensystem in the Floquet exponent. It is the value of this exponent which will determine the stability of the configuration. The linear stability of a perturbation to the interface is thus dependent upon six non-dimensional parameters: the density ratios of the outer to middle slabs, the Froude type number, the Bond type number at each interface, and the wave number.

3.2 Equation development

3.2a Governing equations and non-dimensionalization

The governing equations are the continuity and the conservation of momentum equations for an incompressible and inviscid fluid.

$$\nabla \cdot \underline{u} = 0 \tag{3.1}$$

$$\rho \frac{\partial \underline{u}}{\partial t} + \rho \underline{u} \cdot \nabla \underline{u} = -\nabla p - \rho G_o \, g(\omega_f t) \hat{e}_z \tag{3.2}$$

where the time-dependence is apparent in the body force term. G_o represents the peak value of the acceleration due to the periodic g-jitter. Equation (3.2) is to be linearized about a state of zero mean motion. Quadratically small terms are neglected (after expansion in a small disturbance parameter, ε).

Expansions of pressure and velocity fields are as follows:

$$p = p_{mean} + \varepsilon p' ..+.. \text{ (h.o.t.)} \tag{3.3}$$

$$\underline{u} = 0 + \varepsilon \underline{u}' ..+.. \text{ (h.o.t.)} \tag{3.4}$$

(Note the analysis considers zero mean motion ($\underline{u}_{mean}=0$).)

The governing equations can be non-dimensionalized to yield:

$$\tilde{\nabla} \cdot \tilde{\underline{u}}' = 0 \tag{3.5}$$

$$\frac{\rho}{\rho_D} \frac{\partial \tilde{\underline{u}}'}{\partial t} = -\tilde{\nabla} \tilde{p}' \tag{3.6a}$$

$$0 = -\tilde{\nabla} \tilde{p}_{mean} - \frac{\rho}{\rho_D} \left(\frac{G_o}{H\omega_f^2} \right) g(\tilde{t}) \hat{e}_z \tag{3.6b}$$

where $\underline{u} = H\omega_f \tilde{\underline{u}}$ (3.7)

$\underline{x} = H \tilde{\underline{x}}$ (3.8)

$t = (1/\omega_f)\ \tilde{t}$ (3.9)

$p = \rho_D H^2 \omega_f^2 \tilde{p}$ (3.10)

(Note that ρ_D is the average of the density differences across each interface, and ω_f is the forcing frequency.)

Equation (3.6b) is the mean conservation of momentum equation, and (3.5,3.6a) represents the perturbed system.

Note that due to the periodic time-dependence, the mean pressure field will also be periodic in time. The parameter $(G_o/H\omega_f^2)$ in equation (3.6b) is taken to be roughly of order one; this ensures the mean pressure to be of the same order.

For convenience, the tildes will be omitted from this point forth in Chapter 3. All quantities are henceforth non-dimensional. Also, the primes will be dropped from perturbation quantities.

The analysis is incompressible, inviscid, irrotational, and linear. A potential function can be utilized, giving rise to Laplace's equation. Perturbations are taken to be wave-like in the (xy) plane. The resulting differential equations (in z) are solved by separation of variables to yield:

$$\phi_1 = \left[A(t)e^{kz} + B(t)e^{-kz}\right] e^{i(lx+my)} \tag{3.11}$$

$$\phi_2 = \left[C(t)e^{-kz}\right] e^{i(lx+my)} \tag{3.12}$$

$$\phi_3 = \left[D(t)e^{kz}\right] e^{i(lx+my)} \tag{3.13}$$

A, B, C, and D are time-dependent coefficients, and k represents the wave number ($k^2 = l^2 + m^2$). ϕ is the potential function. Subscripts indicate the region of interest. The pressure (both mean and perturbation) can be obtained from equations (3.6a) and (3.6b).

A normal mode perturbation approach in the spatially independent variables is utilized; thus, the equations of each equilibrium interface can be written as:

$$Fe_{II} = z - 1 - \varepsilon E(t)e^{i(lx+my)} \tag{3.14}$$

$$Fe_{III} = z - 0 - \varepsilon F(t)e^{i(lx+my)} \tag{3.15}$$

where Fe defines the equation of each equilibrium interface, and E and F are time-dependent coefficients.

3.2b Boundary conditions:

Three boundary conditions are imposed on each of the interfaces: (1) the kinematic boundary condition, (2) continuity of the normal component of velocity, and (3) the normal force balance across the interface.

The kinematic boundary condition states that at each interface

$$\frac{D(Fe)}{Dt} = 0 \tag{3.16}$$

which can be expressed as:

$$\frac{\partial Fe}{\partial t} + \underline{u}\cdot\nabla\,(Fe) = 0 \tag{3.17}$$

Note that after linearization, the gradient of the interface equation has a contribution in the $\hat{e}_z$-direction only. Imposition of this kinematic condition on each of the two interfaces yields the following:

$$\text{on } Fe_{II}, \qquad \dot{E}(t) + k\,C(t)e^{-k} = 0 \tag{3.18}$$

$$\text{on } Fe_{III}, \qquad -\dot{F}(t) + k\,D(t) = 0 \tag{3.19}$$

A second boundary condition can be imposed in which the normal component of the velocity is continuous across the interface.

$$\text{on } Fe_{II}, \qquad \frac{\partial \phi_1}{\partial z} = \frac{\partial \phi_2}{\partial z} \tag{3.20}$$

$$\text{on } Fe_{III}, \qquad \frac{\partial \phi_1}{\partial z} = \frac{\partial \phi_3}{\partial z} \tag{3.21}$$

After a Taylor series expansion at each interface, the following relationships are obtained:

$$A(t)e^{2k} - B(t) = -C(t) \tag{3.22}$$

$$A(t) - B(t) = D(t) \tag{3.23}$$

And finally, a (linearized) normal force balance across the interface is implemented.

$$p_{lower} - p_{upper} = \gamma \nabla \cdot \hat{n} \tag{3.24}$$

or, in non-dimensional form:

$$\frac{\rho_D H^3 \omega_f^2}{\gamma} \left(p_{lower} - p_{upper} \right) = \nabla \cdot \hat{n} \qquad (3.25)$$

where γ = surface tension

$\hat{n}$ = linearized outward pointing normal to the interface

Recall that the upper and lower pressures each have both a mean and a perturbation component. Contributions to the pressure at $O(\varepsilon)$ (needed in equation (3.25)) involve both the perturbation pressure given in equation (3.26a) and a second term due to the wave itself. This second term is listed in equation (3.26b).

$$\varepsilon p = \varepsilon \left(\frac{-\rho}{\rho_D} \frac{\partial \phi}{\partial t} \right) \qquad (3.26a)$$

$$\text{second term} = \frac{\rho^{u,l}}{\rho_D} \left[\frac{G_o}{H \omega_f^2} \right] g(t) \; \varepsilon E(t) e^{i(lx+my)} \qquad (3.26b)$$

Note that the second term also contributes at the lower interface, with E(t) replaced by F(t).
(Recall that primes have been dropped from the perturbation pressure.)

Substitution of equations (3.26a,b) into equation (3.25) for each respective interface results in the following relationships at $O(\varepsilon)$:

on Fe_{II},

$$\frac{Bo_2}{Fr}\left[\frac{(\rho_2-\rho_1)}{\rho_D}\,Fr\cdot g(t)E(t) - \frac{\rho_1}{\rho_D}\left(\dot{A}(t)e^{k}+\dot{B}(t)e^{-k}\right)\right.$$

$$\left. + \frac{\rho_2}{\rho_D}\left(\dot{C}(t)e^{-k}\right)\right] = k^2E(t) \qquad (3.27)$$

on Fe_{III},

$$\frac{Bo_3}{Fr}\left[\frac{(\rho_1-\rho_3)}{\rho_D}\,Fr\cdot g(t)F(t) + \frac{\rho_1}{\rho_D}\left(\dot{A}(t)+\dot{B}(t)\right)\right.$$

$$\left. - \frac{\rho_3}{\rho_D}\left(\dot{D}(t)\right)\right] = k^2F(t) \qquad (3.28)$$

where $$Bo_{2,3} = \frac{\rho_D H^2 G_o}{\gamma_{II,III}} \quad ; \quad Fr = \frac{G_o}{H\omega_f^2}$$

$Bo_{2,3}$ and Fr are Bond and Froude number type parameters.

By utilizing equations (3.22,3.23), the C and D time-dependent coefficients can be eliminated from (3.18,3.19) and (3.27,3.28) to yield the following system.

$$\dot{A}(t)\left[\frac{-(1+\rho_{21})e^{k}}{\rho_{D1}}\right] + \dot{B}(t)\left[\frac{(\rho_{21}-1)e^{-k}}{\rho_{D1}}\right] + E(t)\left[\frac{(\rho_{21}-1)}{\rho_{D1}}\ (Fr)g(t)\right] = \frac{Fr}{Bo_2}\,k^2\,E(t) \tag{3.29}$$

$$\dot{A}(t)\left[\frac{(1-\rho_{31})}{\rho_{D1}}\right] + \dot{B}(t)\left[\frac{(1+\rho_{31})}{\rho_{D1}}\right] + F(t)\left[\frac{(1-\rho_{31})}{\rho_{D1}}\ (Fr)g(t)\right] = \frac{Fr}{Bo_3}\,k^2\,F(t) \tag{3.30}$$

$$\dot{E}(t) = k\left[A(t)e^{k} - B(t)e^{-k}\right] \tag{3.31}$$

$$\dot{F}(t) = k\left[A(t) - B(t)\right] \tag{3.32}$$

where $\rho_{21} = \frac{\rho_2}{\rho_1}$, $\rho_{31} = \frac{\rho_3}{\rho_1}$, $\rho_{D1} = \frac{\rho_D}{\rho_1}$

Thus, the system has been reduced to four ordinary differential equations (in time) with four time-dependent unknowns: A,B,E,F. The time-varying forcing function is chosen to be periodic, with

$$g(t) = \cos(t) = \frac{1}{2} (e^{it} + e^{-it}) \qquad (3.33)$$

3.3 Application of Floquet theory

Floquet theory can then be applied to system (3.29-3.32). This is done by expressing the four time-dependent coefficients as

$$[A(t),B(t),E(t),F(t)] = \sum_{n=-\infty}^{+\infty} [A_n,B_n,E_n,F_n]\ e^{int}\ e^{\lambda t} \qquad (3.34)$$

where λ is the Floquet exponent.

By substitution of equation (3.34) into the system (3.29-3.32), the four ordinary differential equations in time can be expressed as an infinite algebraic system with the Floquet exponent appearing as a parameter.

$$(\lambda+in)\left[\frac{-(1+\rho_{21})e^{k}}{\rho_{D1}}\right]A_n + (\lambda+in)\left[\frac{(\rho_{21}-1)e^{-k}}{\rho_{D1}}\right]B_n$$

$$+\left[\frac{(\rho_{21}-1)}{\rho_{D1}}\frac{Fr}{2}\right](E_{n-1}+E_{n+1}) - \left[\frac{Fr}{Bo_2}k^2\right]E_n = 0 \qquad (3.35)$$

$$(\lambda+in)\left[\frac{(1-\rho_{31})}{\rho_{D1}}\right]A_n + (\lambda+in)\left[\frac{(1+\rho_{31})}{\rho_{D1}}\right]B_n$$

$$+\left[\frac{(1-\rho_{31})}{\rho_{D1}}\frac{Fr}{2}\right](F_{n-1}+F_{n+1}) - \left[\frac{Fr}{Bo_3}k^2\right]F_n = 0 \qquad (3.36)$$

$$(\lambda+in)E_n + kB_n e^{-k} - kA_n e^{k} = 0 \qquad (3.37)$$

$$(\lambda+in)F_n + kB_n - kA_n = 0 \qquad (3.38)$$

where n varies from $-\infty$ to $+\infty$. This results in an infinite system of equations. The set of homogeneous equations (3.35-3.38) can be written in the form

$$(\underset{\sim}{A} - \lambda \underset{\sim}{B})\ \underline{X} = 0 \tag{3.39}$$

or

$$\underset{\sim}{A}\ \underline{X} = \lambda\ \underset{\sim}{B}\ \underline{X} \tag{3.40}$$

which is the generalized eigenvalue problem. The Floquet exponent, λ , acts as the eigenvalue. $\underline{X}$ is an infinite column vector containing the following terms:

$$\underline{X} = \begin{pmatrix} \vdots \\ E_{n-1} \\ F_{n-1} \\ A_{n-1} \\ B_{n-1} \\ E_n \\ F_n \\ A_n \\ B_n \\ E_{n+1} \\ F_{n+1} \\ A_{n+1} \\ B_{n+1} \\ \vdots \end{pmatrix}$$

$(\underset{\sim}{A} - \lambda \underset{\sim}{B})$ is the coefficient matrix of $\underline{X}$. It is generated in groups of four rows corresponding to a particular value of n. Matrices $\underset{\sim}{A}$ and $\underset{\sim}{B}$ are shown in Figures 3.2 and 3.3.

$$
\begin{vmatrix}
\vdots & \vdots & \vdots & \vdots & \vdots & \vdots & \vdots & \vdots & \vdots & \vdots & \\
\cdots\ 0 & 0 & 0 & 0 & in & 0 & -ke^{k} & ke^{k} & 0 & 0 & \cdots \\
\cdots\ 0 & 0 & 0 & 0 & 0 & in & -k & k & 0 & 0 & \cdots \\
\cdots \left[\left(\frac{1-\rho 21}{1+\rho 21}\right)\left(\frac{Fr}{2e^{k}}\right)\right] & 0 & 0 & 0 & \left[\frac{Fr\,k^{2}\,\rho_{D1}}{Bo_{2}(1+\rho 21)e^{k}}\right] & 0 & in\left[\left(\frac{in}{e^{2k}}\right)\left(\frac{1-\rho 21}{1+\rho 21}\right)\right] & \left[\left(\frac{1-\rho 21}{1+\rho 21}\right)\left(\frac{Fr}{2e^{k}}\right)\right] & 0 & \cdots \\
\cdots\ 0 & \left[\left(\frac{1-\rho 31}{1+\rho 31}\right)\left(\frac{Fr}{2}\right)\right] & 0 & 0 & 0 & \left[\frac{Fr\,k^{2}\,\rho_{D1}}{-Bo_{3}(1+\rho 31)}\right] & \left[in\left(\frac{1-\rho 31}{1+\rho 31}\right)\right] & in & 0 & \left[\left(\frac{1-\rho 31}{1+\rho 31}\right)\left(\frac{Fr}{2}\right)\right] & \cdots \\
\vdots & \vdots & \vdots & \vdots & \vdots & \vdots & \vdots & \vdots & \vdots & \vdots &
\end{vmatrix}
$$

matrix A

$-\infty < n < +\infty$

Figure 3.2

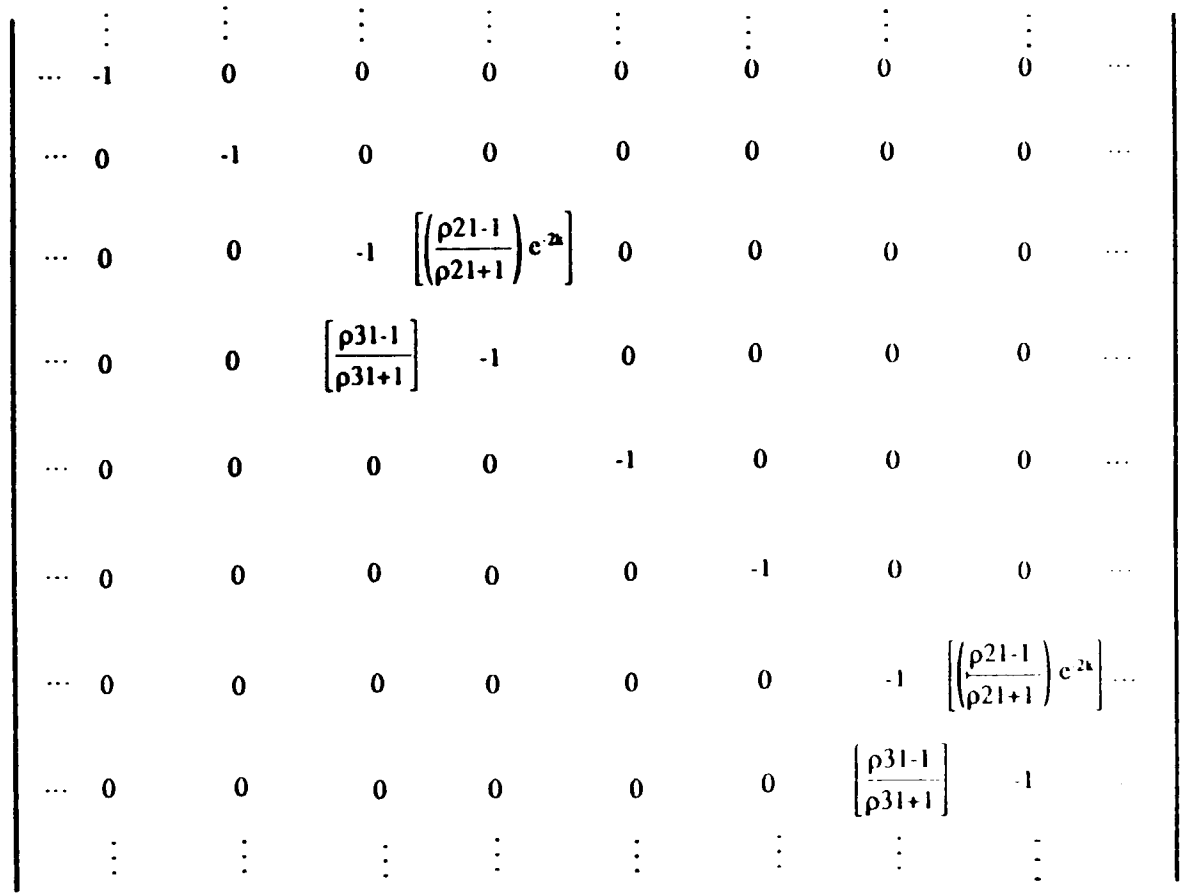

matrix B

Figure 3.3

The solution to the single interface problem (Jacqmin and Duval)[12], utilized Floquet theory and truncated at n = |24|. It was decided that the multi-layer system should be truncated at least at this level. In our analysis, n is truncated at |25| . This generates a system of 204 equations in which the Floquet exponent is determined by eigenvalue methods. (A generalized eigenvalue routine is used). Details of the algorithms are found in Kaufman (1974)[14,15] and Moler and Stewart (1973)[19].

3.4 Solution methodology

To solve the large, sparse generalized eigensystem, a routine DGVLCG from the IMSL library package is utilized. (See Appendix 5.) This routine is based on the LZ algorithm described by Kaufman (1974), which in turn is similar to the QZ algorithm (Moler and Stewart,1973) except that it uses elementary transformations whereas the latter uses orthogonal transformations.

3.4a Preliminary checks

Four checks were performed to verify the accuracy of the solutions.

1) The system was converted to a standard eigensystem of form, $(\underset{\sim}{C} - \lambda \underset{\sim}{I})\ \underline{X} = 0$,which was analyzed using DEVLCG from IMSL. This particular routine converts the matrix into a complex upper Hessenberg matrix, in which the eigenvalues are generated via the QR algorithm (Smith, 1976)[24]. There is agreement of the solution values. (See Appendix 6.)

2) The original matrix was truncated at $n = |50|$, producing a much larger matrix. The same eigenvalues were obtained, with greater multiplicity of each root.

3) The generated Floquet exponents were resubstituted into the linear system to compute the determinant by Gauss' method. The checks show our eigenvalues to be accurate. (See Appendix 7.)

4) A limit case of the two interface system was investigated. In this case, $\rho_{21} = 1.0$ and $Bo_2 = \infty$. The physical interpretation of such a system is that the top and middle slabs have the same density, and their interface has zero surface tension. Hence, the system can be considered as a one interface configuration at Fe_{III}.

To compare the results of the limit case, an analysis was performed for a one interface system following the methodology of sections 3.2-3.3. This new system reduces to two linear differential equations which are solved via Floquet analysis in the same manner as was done for the two interface system. (See Appendices 2 and 8.) A parameter, Q, appears with

$$Q = 1.0 * Bo_3$$

(The constant of unity exists due to fact that the Froude number identically equals one according to a comparison of the non-dimensionalizations.)

A comparison of the two interface limit case with the one interface system for the same physical configuration is shown in Figures 3.4 and 3.5. The correlation between the two systems is evident.

The results of these four separate checks provide great confidence in the numerical results.

3.4b Solution interpretation

The stability of the system can be determined by the numerical value of the complex eigenvalues. It is readily seen from equation (3.34) that the time-dependent coefficients will grow exponentially for positive real components of the Floquet exponents. Such a case will imply an instability of the fluid system. Thus, as the eigenvalues are generated, the presence of a single positive real part of λ will dominate the system, causing it to be unstable. As this is a linear analysis, no information can be obtained concerning the finite amplitude (nonlinear) form of the configuration.

The system of algebraic equations is non-dimensional. Thus, the linear stability of the fluid layers depends on six non- dimensional parameters: the two density ratios, the Froude

number, the Bond type number at each interface, and the wave number.

A parametric study is performed to investigate the effects of parameter variation on the stability of the fluid system. The parameter space is defined by appropriate values of the six non-dimensional parameters pertinent to a microgravity environment.

As stated previously, the complex Floquet exponent (λ) is the eigenvalue of the system. The presence of a single positive real component implies exponential growth of the interface and hence, a subsequent instability. Thus, we are concerned solely with the largest real component of the Floquet exponent. The values of this quantity are charted throughout the parameter space. A positive value of the largest real component of the Floquet exponent indicates an instability; a zero or negative value indicates stability.

3.5 Results

To display most effectively the regions of instability, the largest (fastest growing) real component of the Floquet exponent is plotted as a function of the wave number for fixed values of Bond and Froude numbers and density ratios.

The range for the parameters is as follows:

$$0.1 < k < 5.0$$

$$Bo_2 = 1.0,\ 0.1,\ 0.01, 0.001$$

$$Bo_3 = 1.0(Bo_2),\ 2.0(Bo_2)$$

$$Fr = 5.0,\ 1.0,\ 0.5,\ 0.1$$

(Note that the quantities are nondimensional.)

These values correspond to physically realistic configurations which might be expected in a microgravity environment as well as satisfying conditions for linear analysis.

For each case, if the forcing function, g(t), were set to zero instead of cos(t), the configuration would be stable for all parameter space. The interfaces would simply oscillate with no growth of the amplitude. It is only with the forcing, and in the indicated parameter regions, that instabilities may occur.

In Figures 3.6-3.25, the effect of $Bo_2(Bo_3)$ on stability for different values of Fr and density ratios is illustrated. For Fig.3.6, ρ_{21} =1.0, ρ_{31} =0.001225, Fr=5.0, and Bo_2 is set equal to Bo_3. The unstable wave number region is broadest for

the largest $Bo_2(Bo_3)$ values. As $Bo_2(Bo_3)$ is decreased, the unstable wave number region shrinks to encompass a smaller k range and tends towards lower k values. For low $Bo_2(Bo_3)$ values, the configuration is unstable to longer wavelength perturbations in the presence of periodic forcing.

In Figure 3.7, Fr is reduced to 1.0 while other parameter values remain the same. Though the general qualitative trends follow, it is seen that the range of unstable wave numbers is broader than in Figure 3.6.

Figure 3.8 shows an order of magnitude drop in Fr. Again as $Bo_2(Bo_3)$ is increased, the range of unstable wave numbers broadens. Likewise, as Fr decreases the unstable region encompasses a broader range of wave numbers.

Similar results are elucidated in Figures 3.9-3.20, keeping parameter ranges the same for various density ratios. As $Bo_2(Bo_3)$ values are increased, the range of unstable wave numbers widens (corresponding to smaller wavelength disturbances).

The density ratios in Figures 3.21-3.23 pertain to a gas/liquid/gas configuration. The qualitative trends of varying Fr and $Bo_2(Bo_3)$ continue. However, the behavior is observed to be more peaky, with occasional regions of stability punctuating unstable wave number bands. For the lowest Fr (Figure 3.23), the unstable band shifts away from the low k region. Note that in Figure 3.21, the configuration is

stable when $Bo_2(Bo_3)$ is 0.001. Positive values of the real component of λ occur only for larger $Bo_2(Bo_3)$ values.

Figures 3.24 and 3.25 show the effect of Bo_2 not equal to Bo_3. In Figure 3.24 the Bo values are equal, whereas in Figure 3.25, Bo_3 is twice Bo_2, keeping all other parameters the same. Physically, the increase of Bo_3 while keeping Fr fixed can be interpreted as decrease in the surface tension value at the lower interface. The dominant effect is to broaden the range of unstable wave numbers for each set of Bo values. Note that Figure 3.25 shows a narrow band of wave number stability near k=1.95. In general, the numerical value of the real part of the Floquet exponent (λ) is increased for Bo_3 twice the value of Bo_2, indicating a faster growing "fastest growing" disturbance.

The effect of varying Fr while holding $Bo_2(Bo_3)$ values fixed is illustrated in Figures 3.26-3.29. As Fr is decreased, the range of unstable wave numbers increases. Physically, this can be interpreted as a decrease in configuration stability for larger frequencies of the g-jitter. The behavior is typical for the various density ratios and Bo values which were considered.

The effect of density ratio difference on stability is presented in Figures 3.30-3.34. Values of ρ_{21} and ρ_{31} represent the density ratios of the upper and lower regions to that of the middle layer, respectively. Among cases indicated, the largest value of ρ_{D1} [$=(|\rho_{21}-1|+|\rho_{31}-1|)/2$] corresponds

to the case having the largest range of unstable wave numbers. Furthermore, it also corresponds to the largest values of the real component of the Floquet exponent. In general, as ρ_{D1} is decreased, the band of unstable wave numbers becomes more narrow. Results are typical and illustrative for the parameter space of concern. Note that Figure 3.34 compares three configurations of gas/liquid/gas with different gas densities. The three cases have similar results, indicating that the density of the gas layers is not too significant.

In addition, the case in which both density ratios were set to unity, indicating equal densities in all three regions, was addressed. In such a case, ρ_{D1} equals zero; hence, $Bo_2(Bo_3)$ values are identically zero. Under the action of g-jitter, lack of density differences between the layers results in a stable configuration. One would expect the interfaces to merely oscillate in time. As a further check, the system was derived using a different definition of ρ_D [$\rho_D=(\rho_1+\rho_2+\rho_3)/3$]. Hence, Bo values are non-zero for equal densities in each region. Numerical results showed stability for all parameter values.

The height of the finite middle slab is a physical quantity which appears in both the Bo and Fr nondimensional parameters. In particular, Fr is inversely proportional to the height, while Bo depends on the square of the height. An increase in height, H, implies a decrease in Fr and an increase in Bo. As was seen in Figures 3.6-3.25, an increase in Bo

corresponds to a larger region of unstable wave number space. From Figures 3.26-3.29, it is seen that the broadest region of unstable wave numbers occurs at smaller values of Fr. Thus, it is expected that an increase in H will result in a more unstable fluid configuration. This is confirmed in Figure 3.35. Results are presented graphically for the case G_o = $(10^{-4}*g_{earth})$, ω_f=0.1 Hz, and $\gamma_{II}=\gamma_{III}$=50 dynes/cm. In addition, ρ_{21} =0.8, and ρ_{31} =1.2. Larger values of H correspond to a larger range of unstable wave numbers.

The wave number at which the subharmonic (λ=1/2) occurs is plotted in Figures 3.36 and 3.37 for a range of Fr with given values of $Bo_2(Bo_3)$. It is seen that there is a gradual shift of the subharmonic to lower wave numbers (or longer wavelengths) as Fr is increased (ie., as the forcing frequency decreases). Figure 3.37 represents the case of unequal Bo values ($Bo_3=2*Bo_2$). Physically, this implies the surface tension of the lower interface is halved. It is seen that this case has subharmonics occurring at larger values of the wave number than the case of $Bo_3=Bo_2$ (as shown in Figure 3.36).

Stability boundaries of Fr versus k are plotted in Figures 3.38 and 3.39. This is done for configurations of different density ratios (as indicated by the different area fill patterns). Moreover, on each graph, multiple values of $Bo_{2,3}$ are represented. The unstable regions are indicated by the rectangular "filled" regions. No meaning is ascribed to the width of the rectangles. In general, it is seen that an

increase in Fr while holding other parameter values fixed (corresponding to low frequency forcing) results in a smaller range of unstable wave numbers. Likewise, an increase in Bo values (corresponding to a decrease in the surface tension) relates to a broader region of instability, in terms of k.

In general, fluid systems involving larger values of ρ_{D1} have wider bands of unstable wave numbers. This is evident in both Figures 3.38 and 3.39. Note also the "gaps" in the band of unstable wave numbers. These represent regions of stability of the fluid configuration. It is generally at higher k values ($k > 1$) that these bands of stability occur.

The limit case (ρ_{21} =1.0, $Bo_2=\infty$) was used to compare the stability of the one interface configuration with that of the multi-layer fluid system. To compare the two, the parameters in each case are set equal at interface Fe_3. In this way, the parameters are consistent in both problems. From Figures 3.40-3.41, it is readily seen that the multi-layered configuration is more unstable than the one interface fluid system. The range of unstable wave numbers is broader for the multi-layered case. In particular, note the contrast in the low k region (corresponding to large wavelengths). That is, in the two interface system the very low k region is generally an unstable region as compared to the one interface case. In the one interface model, bands of instability are more frequently punctuated by narrow regions of wave number stability. These results are typical and illustrative for various density ratios.

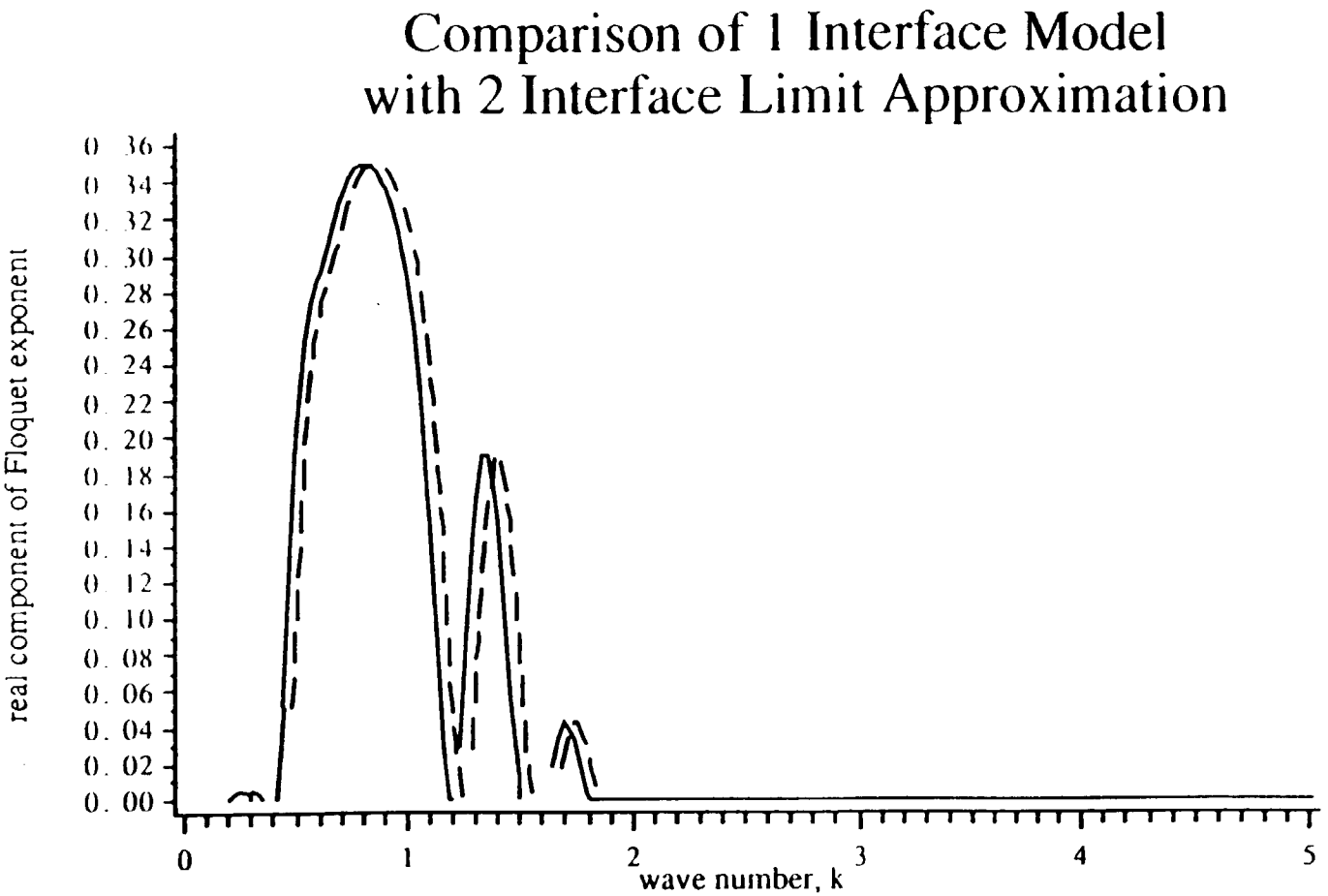
Comparison of 1 Interface Model
with 2 Interface Limit Approximation
real component of Floquet exponent
0.36
0.34
0.32
0.30
0.28
0.26
0.24
0.22
0.20
0.18
0.16
0.14
0.12
0.10
0.08
0.06
0.04
0.02
0.00
0
1
2
3
4
5
wave number, k
1 interface model
ρ21=0.001225
Q=1.0
2 interface limit approximation
ρ21=1.0, ρ31=0.001225
Bo2=∞, Bo3=1.0, Fr=1.0

Figure 3.4

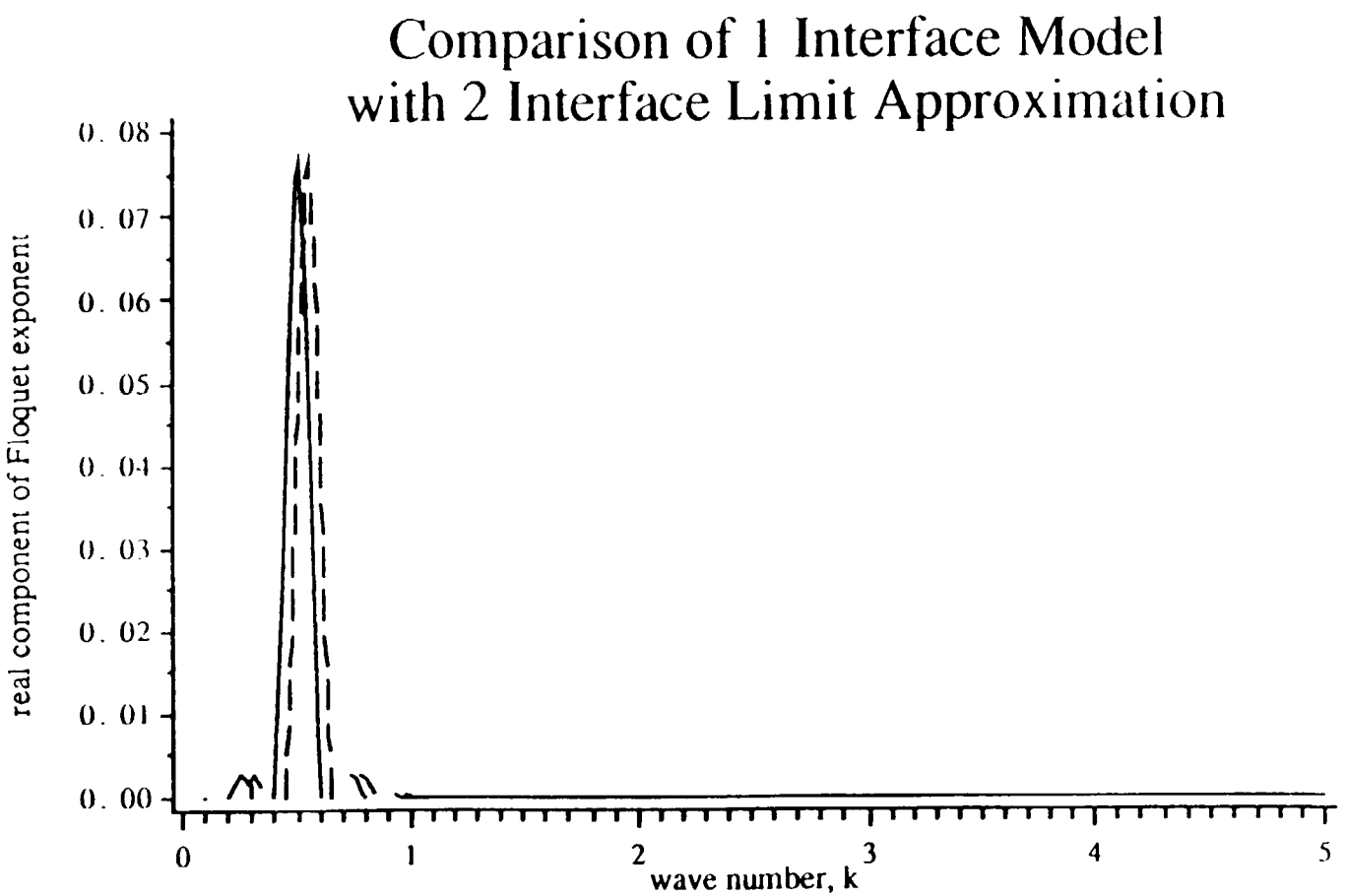
Comparison of 1 Interface Model
with 2 Interface Limit Approximation
real component of Floquet exponent
0.08
0.07
0.06
0.05
0.04
0.03
0.02
0.01
0.00
0
1
2
3
4
5
wave number, k
1 interface model
ρ21=0.5
Q=0.1
2 interface limit approximation
ρ21=1.0, ρ31=0.5
Bo2=∞, Bo3=0.1, Fr=1.0

Figure 3.5

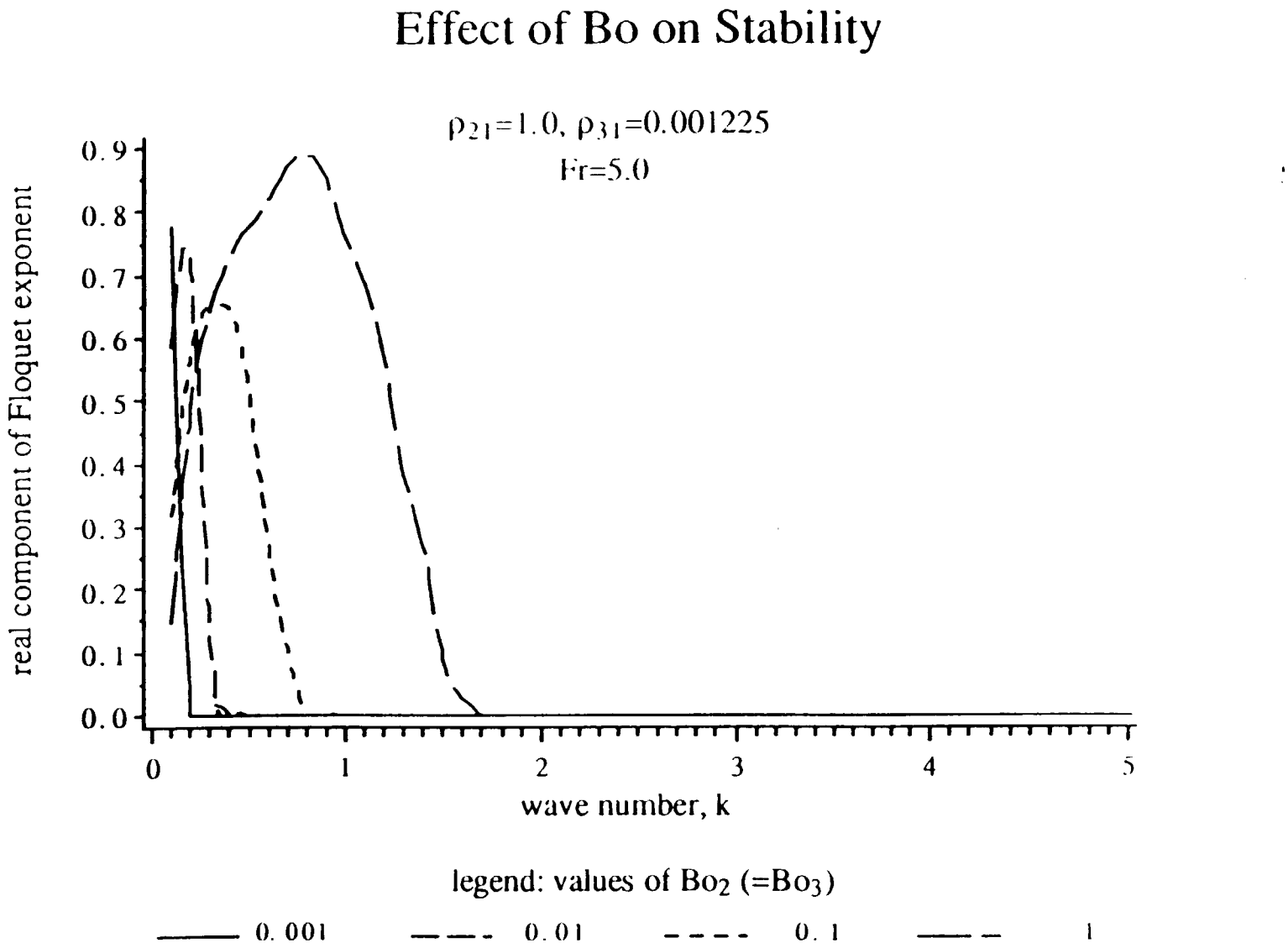
Effect of Bo on Stability
ρ_{21}=1.0, ρ_{31}=0.001225
Fr=5.0
real component of Floquet exponent
0.9
0.8
0.7
0.6
0.5
0.4
0.3
0.2
0.1
0.0
0
1
2
3
4
5
wave number, k
legend: values of Bo_2 (=Bo_3)
0.001
0.01
0.1
1

Figure 3.6

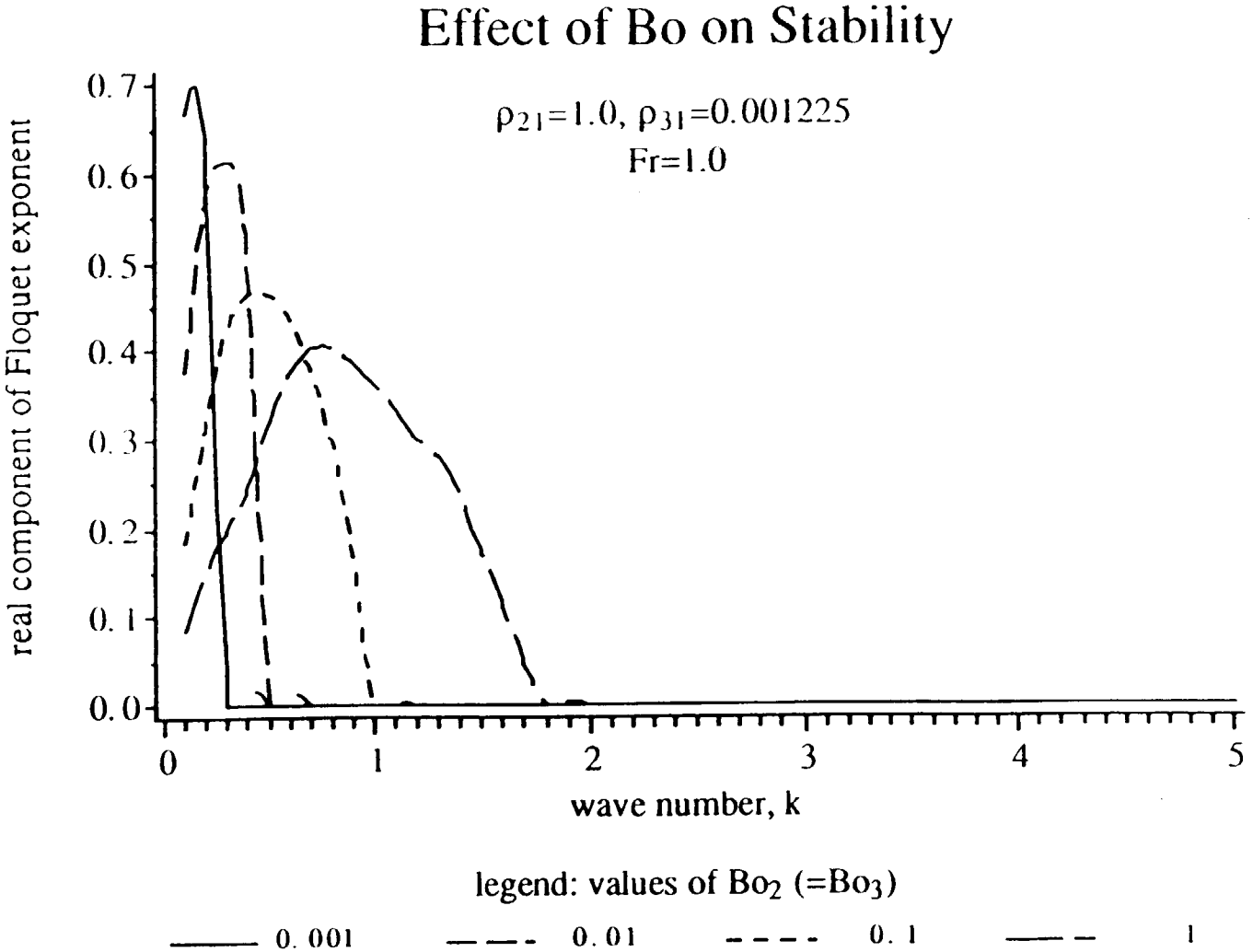
Effect of Bo on Stability
ρ_{21}=1.0, ρ_{31}=0.001225
Fr=1.0
real component of Floquet exponent
0.7
0.6
0.5
0.4
0.3
0.2
0.1
0.0
0
1
2
3
4
5
wave number, k
legend: values of Bo_2 (=Bo_3)
0.001
0.01
0.1
1

Figure 3.7

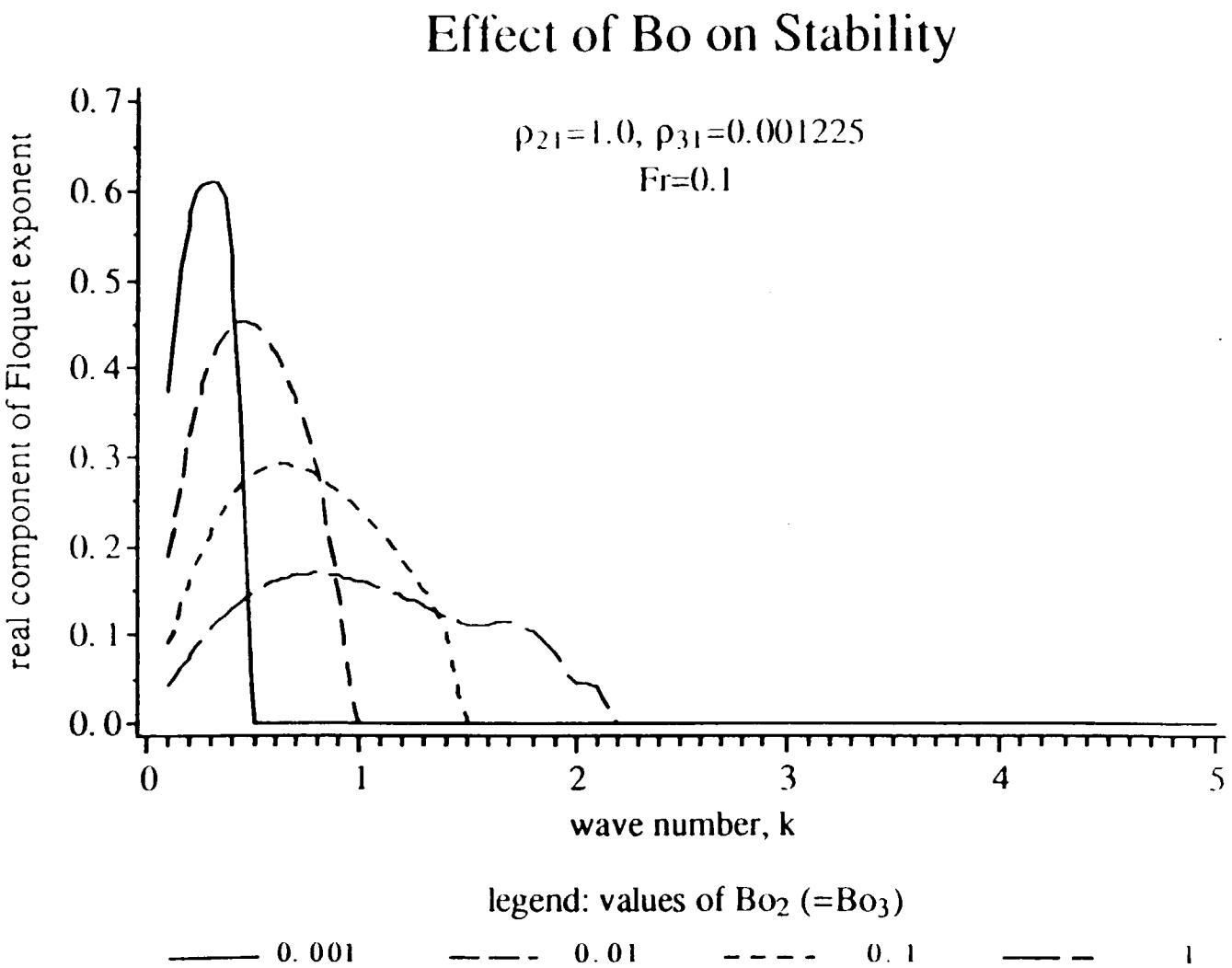
Effect of Bo on Stability
ρ_{21}=1.0, ρ_{31}=0.001225
Fr=0.1
real component of Floquet exponent
0.7
0.6
0.5
0.4
0.3
0.2
0.1
0.0
0
1
2
3
4
5
wave number, k
legend: values of Bo_2 (=Bo_3)
0.001
0.01
0.1
1

Figure 3.8

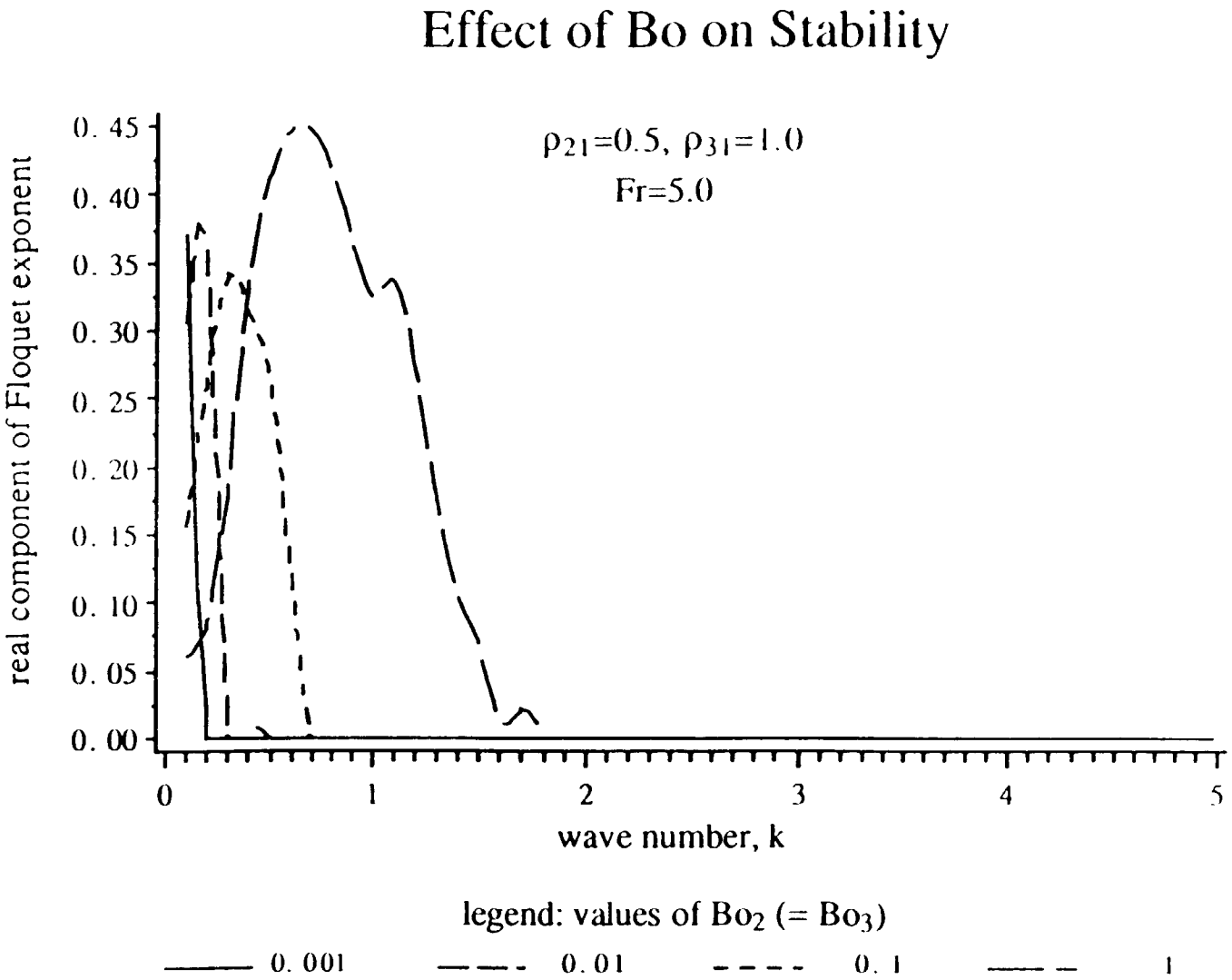
Effect of Bo on Stability
ρ_{21}=0.5, ρ_{31}=1.0
Fr=5.0
real component of Floquet exponent
0. 45
0. 40
0. 35
0. 30
0. 25
0. 20
0. 15
0. 10
0. 05
0. 00
0
1
2
3
4
5
wave number, k
legend: values of Bo_2 (= Bo_3)
0. 001
0. 01
0. 1
1

Figure 3.9

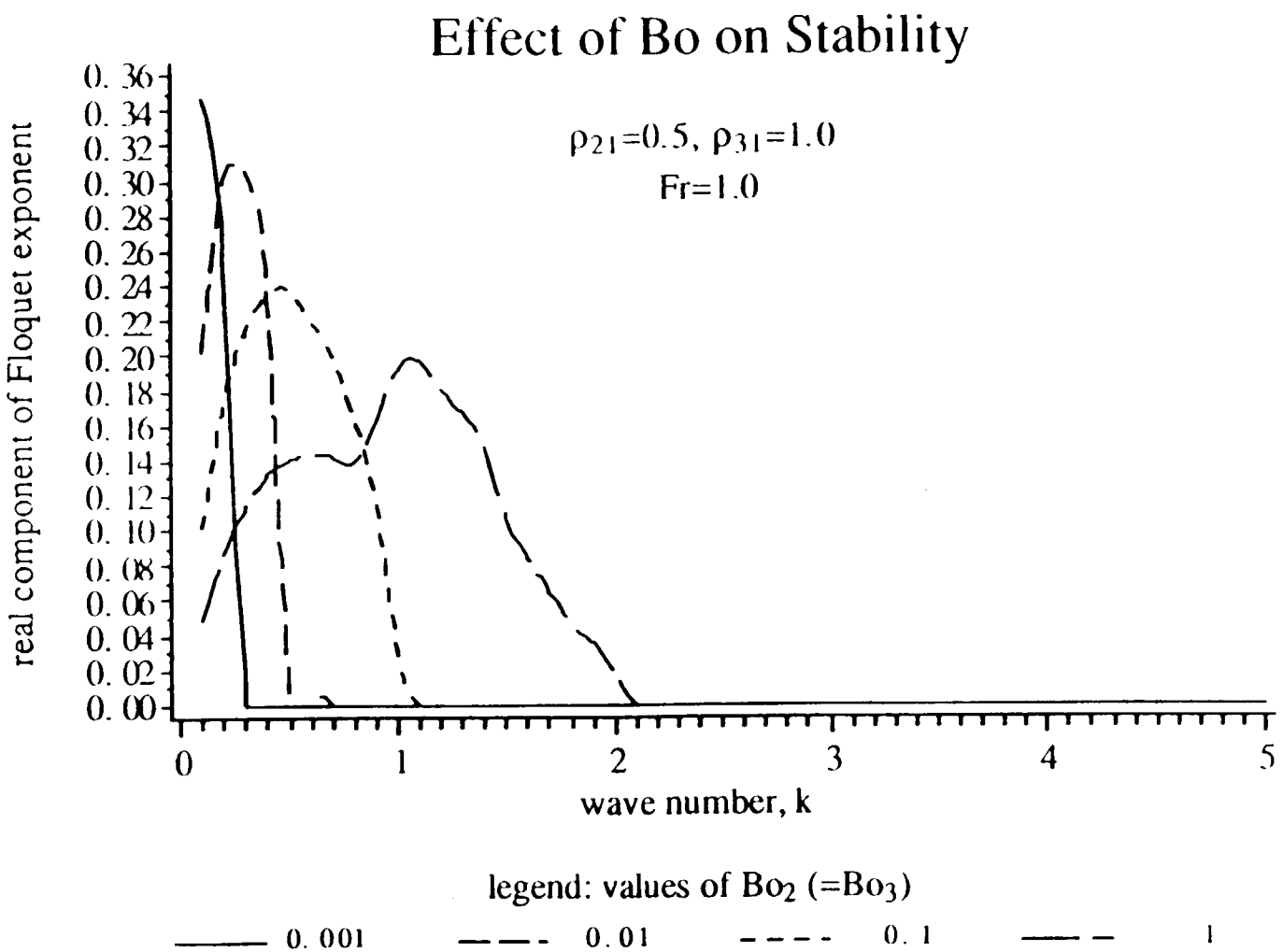
Effect of Bo on Stability
ρ_{21}=0.5, ρ_{31}=1.0
Fr=1.0
real component of Floquet exponent
0.36
0.34
0.32
0.30
0.28
0.26
0.24
0.22
0.20
0.18
0.16
0.14
0.12
0.10
0.08
0.06
0.04
0.02
0.00
0
1
2
3
4
5
wave number, k
legend: values of Bo_2 (=Bo_3)
0.001
0.01
0.1
1

Figure 3.10

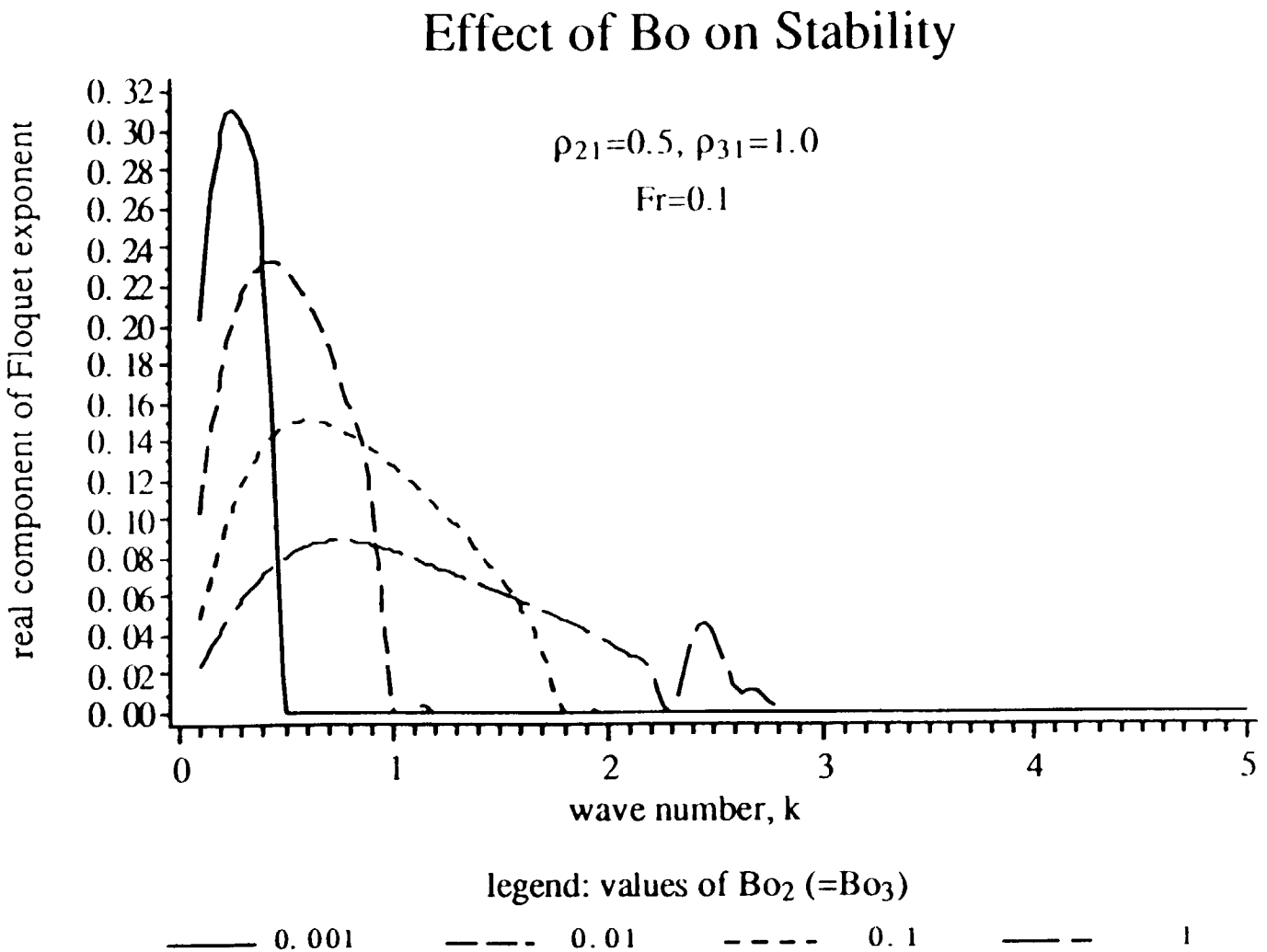
Effect of Bo on Stability
ρ_{21}=0.5, ρ_{31}=1.0
Fr=0.1
real component of Floquet exponent
0.32
0.30
0.28
0.26
0.24
0.22
0.20
0.18
0.16
0.14
0.12
0.10
0.08
0.06
0.04
0.02
0.00
0
1
2
3
4
5
wave number, k
legend: values of Bo_2 (=Bo_3)
0.001
0.01
0.1
1

Figure 3.11

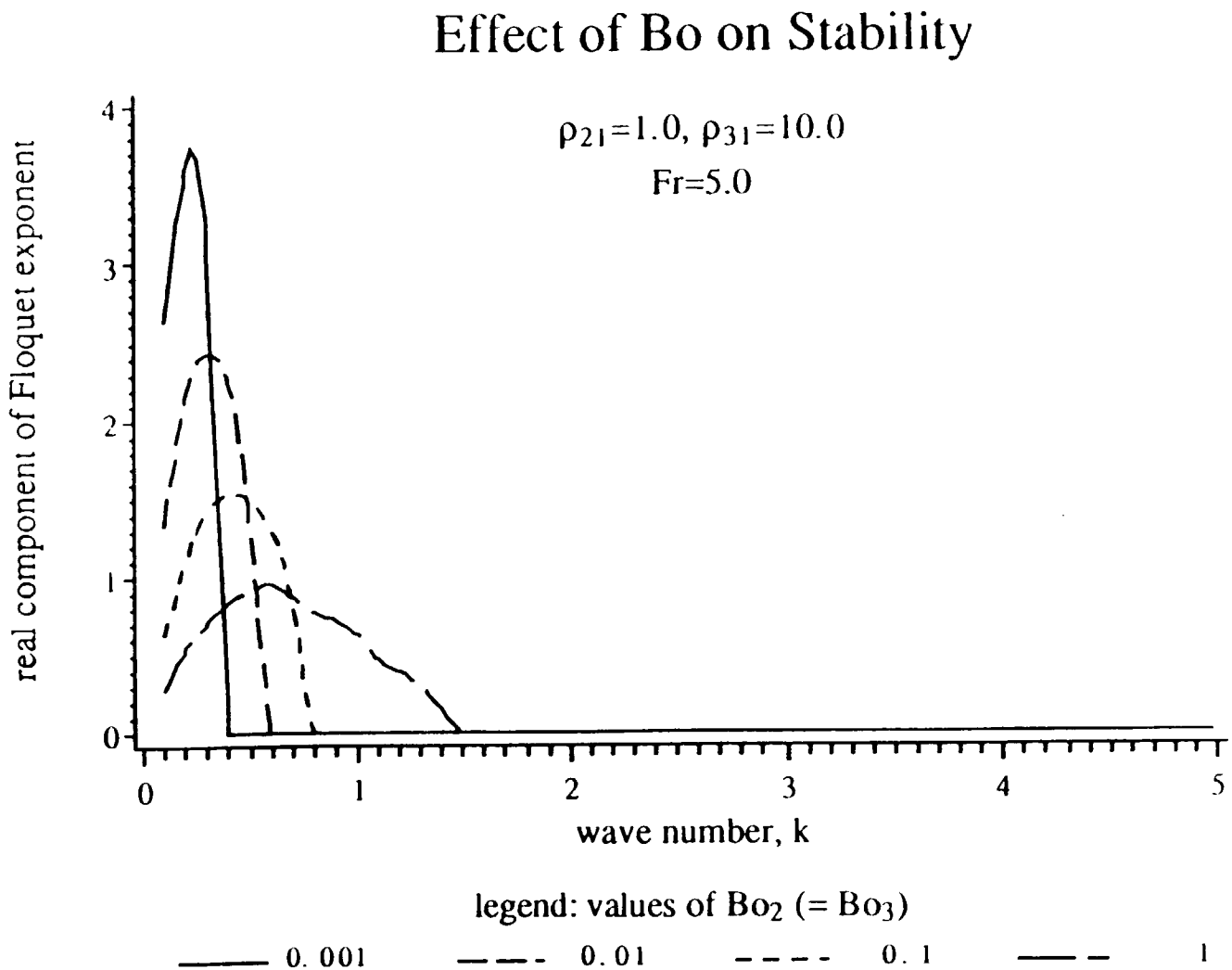
Effect of Bo on Stability
ρ_{21}=1.0, ρ_{31}=10.0
Fr=5.0
real component of Floquet exponent
0
1
2
3
4
0
1
2
3
4
5
wave number, k
legend: values of Bo_2 (= Bo_3)
0. 001
0. 01
0. 1
1

Figure 3.12

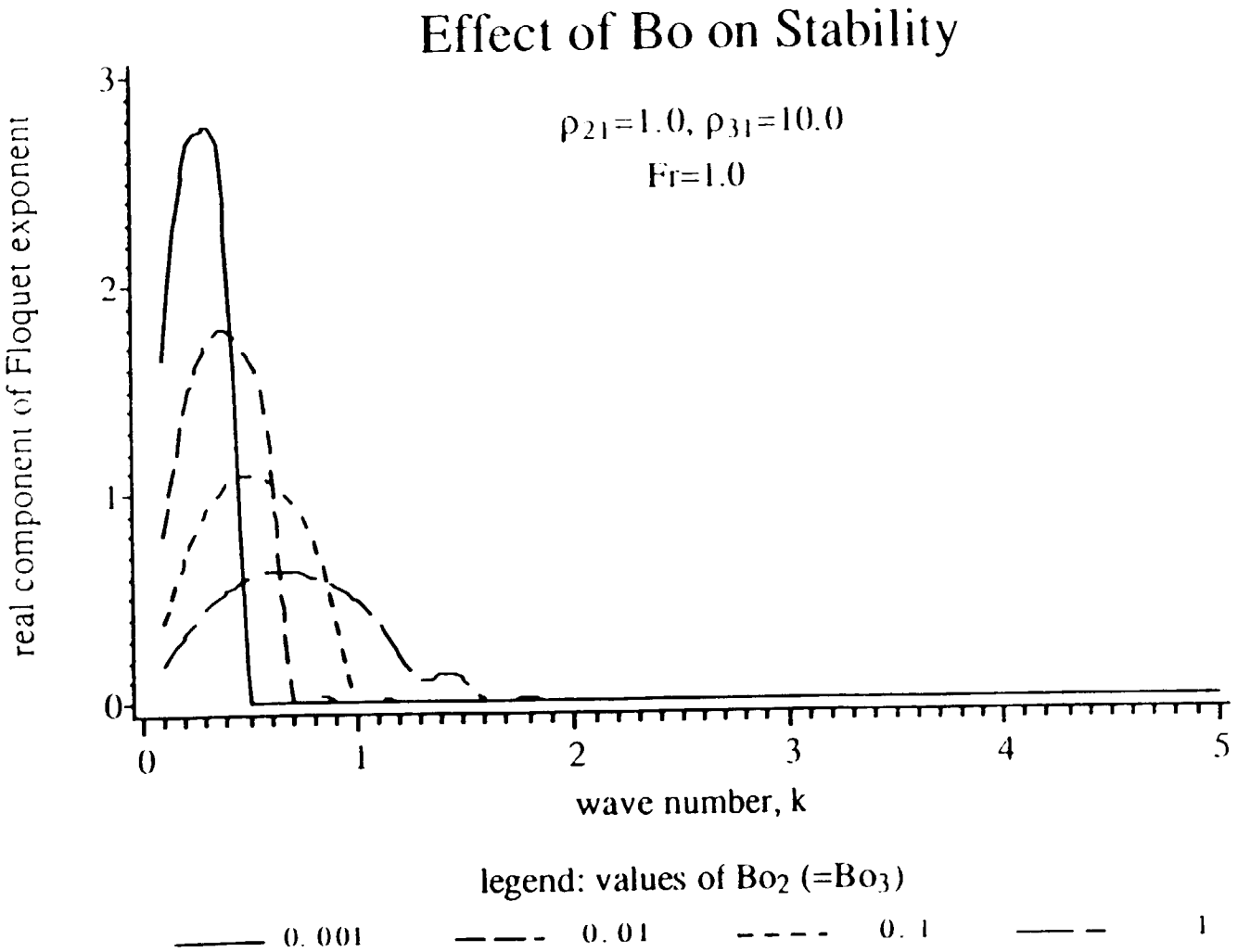
Effect of Bo on Stability
ρ_{21}=1.0, ρ_{31}=10.0
Fr=1.0
real component of Floquet exponent
0
1
2
3
0
1
2
3
4
5
wave number, k
legend: values of Bo_2 (=Bo_3)
0.001
0.01
0.1
1

Figure 3.13

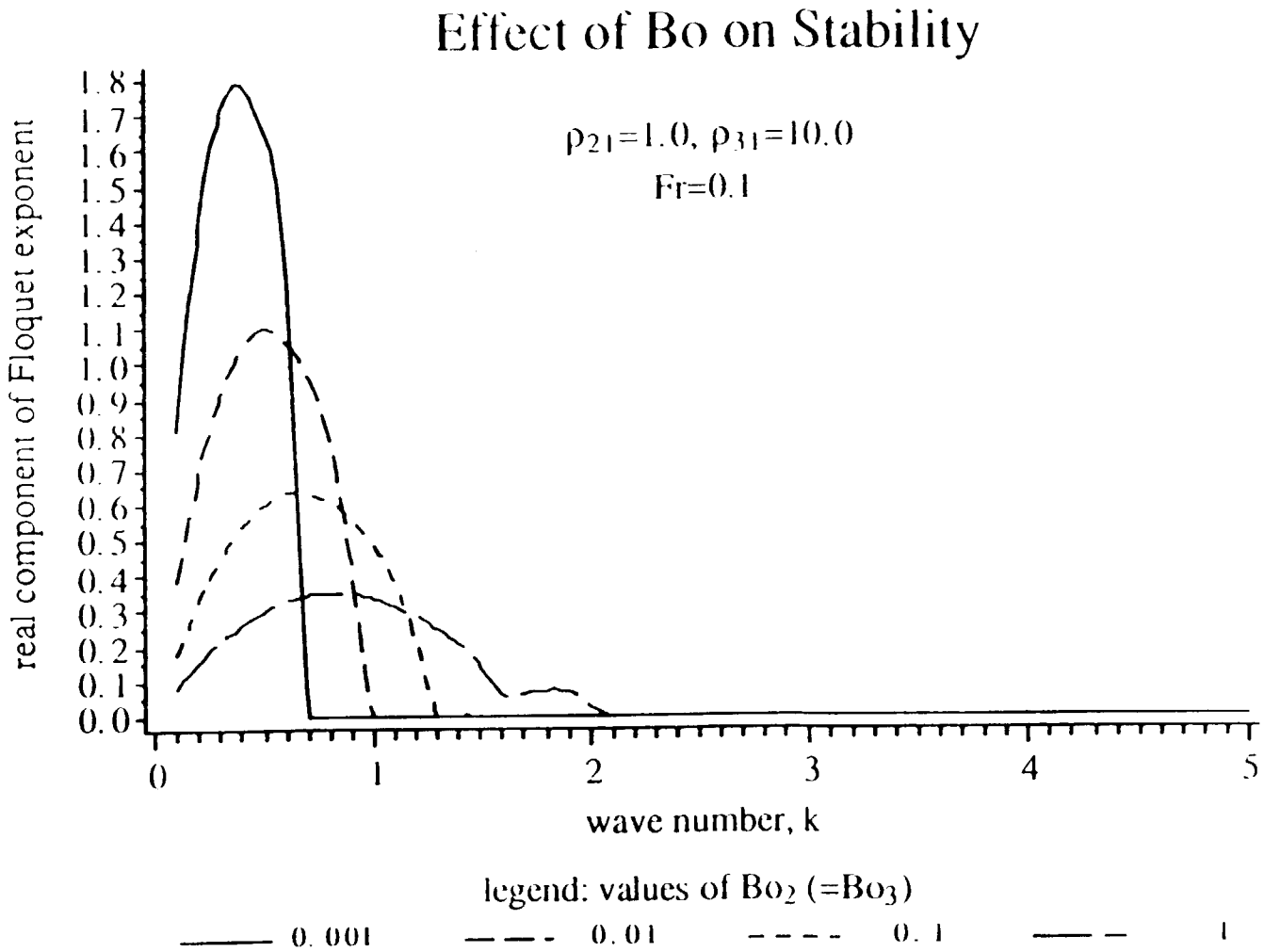
Effect of Bo on Stability
ρ_{21}=1.0, ρ_{31}=10.0
Fr=0.1
real component of Floquet exponent
1.8
1.7
1.6
1.5
1.4
1.3
1.2
1.1
1.0
0.9
0.8
0.7
0.6
0.5
0.4
0.3
0.2
0.1
0.0
0
1
2
3
4
5
wave number, k
legend: values of Bo_2 (=Bo_3)
0.001
0.01
0.1
1

Figure 3.14

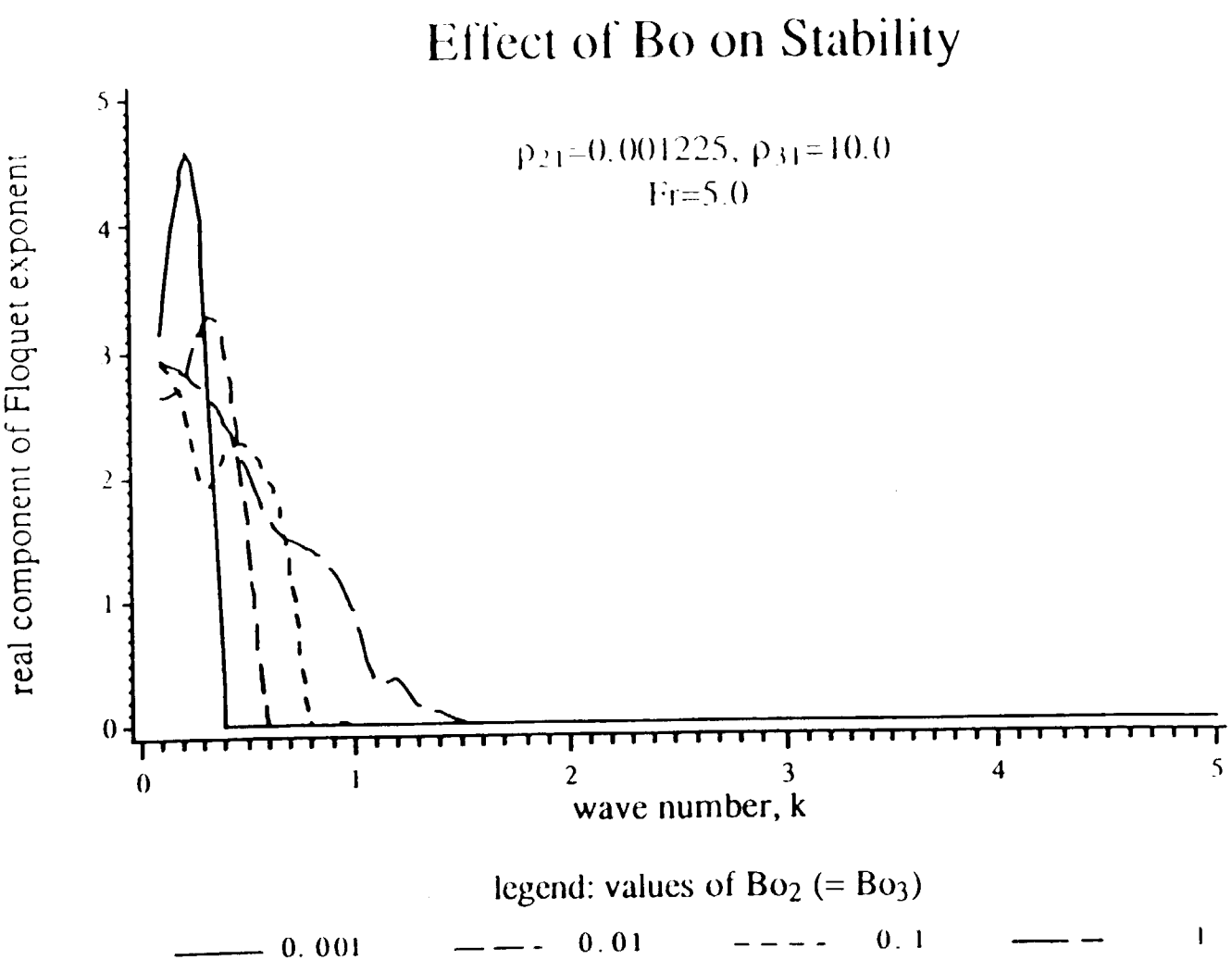
Effect of Bo on Stability
ρ_{21}=0.001225, ρ_{31}=10.0
Fr=5.0
real component of Floquet exponent
wave number, k
0
1
2
3
4
5
legend: values of Bo_2 (= Bo_3)
0.001
0.01
0.1
1

Figure 3.15

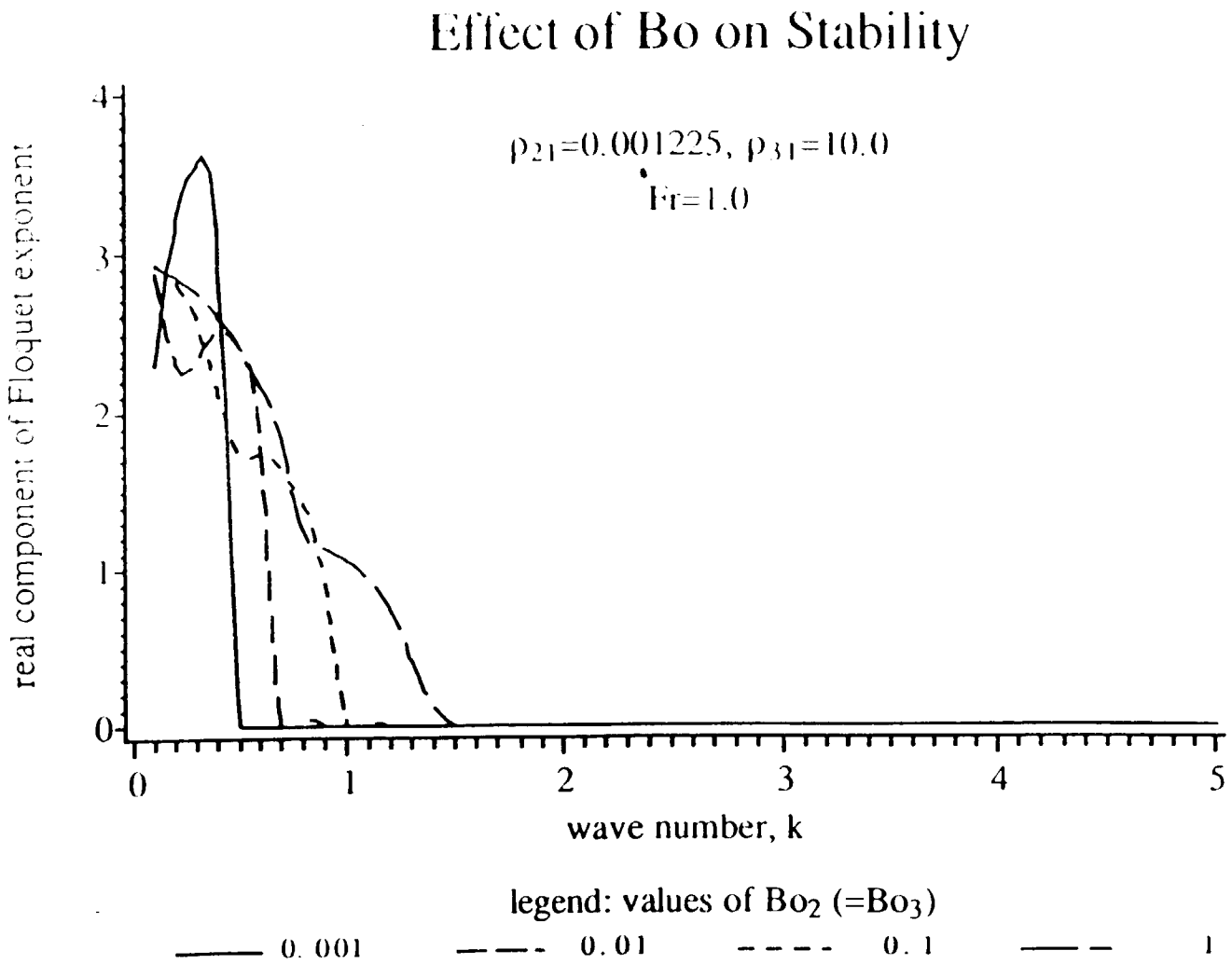
Effect of Bo on Stability
ρ21=0.001225, ρ31=10.0
Fr=1.0
real component of Floquet exponent
0
1
2
3
4
0
1
2
3
4
5
wave number, k
legend: values of Bo2 (=Bo3)
0.001
0.01
0.1
1

Figure 3.16

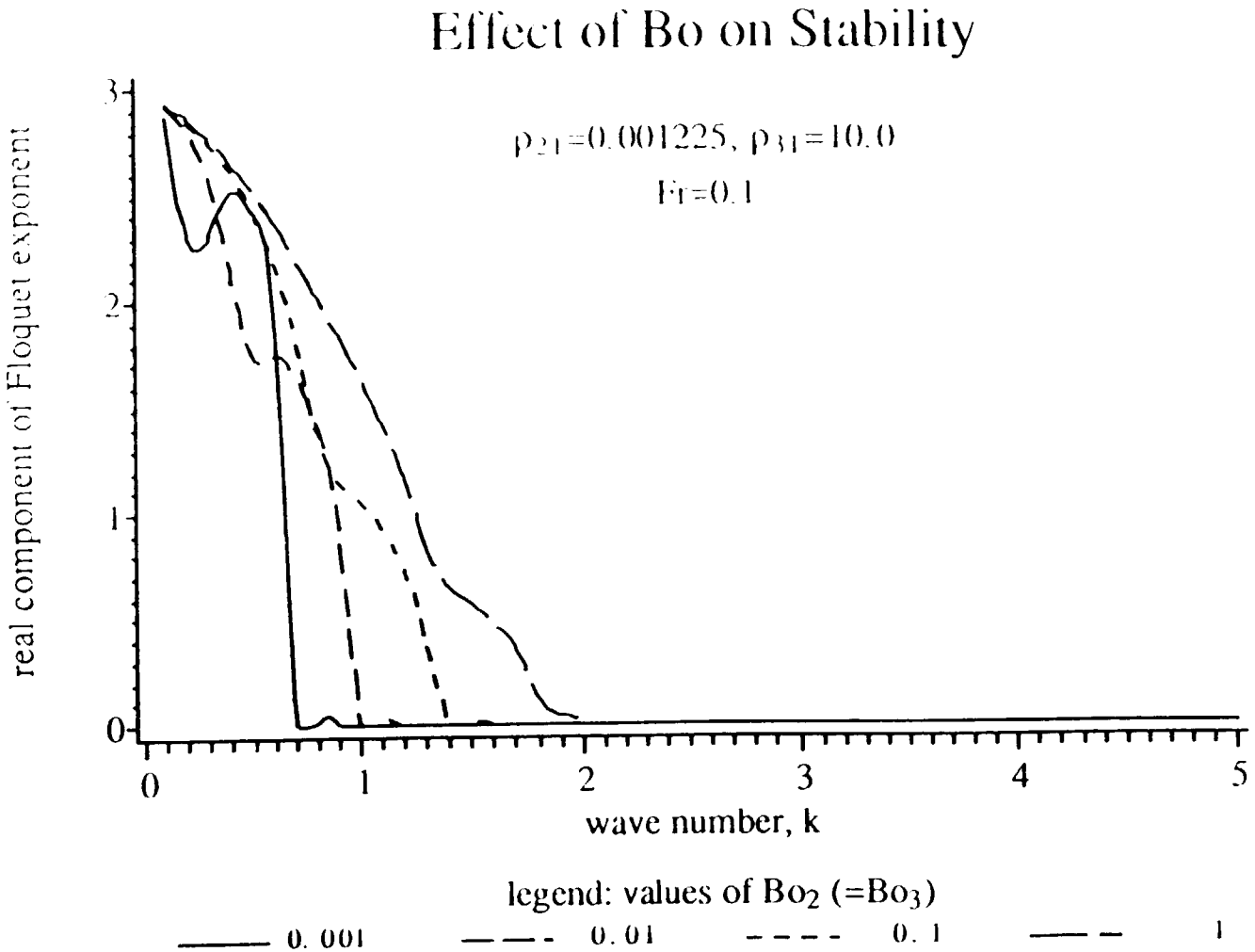
Effect of Bo on Stability
ρ_{21}=0.001225, ρ_{31}=10.0
Fr=0.1
real component of Floquet exponent
0
1
2
3
0
1
2
3
4
5
wave number, k
legend: values of Bo_2 (=Bo_3)
0. 001
0. 01
0. 1
1

Figure 3.17

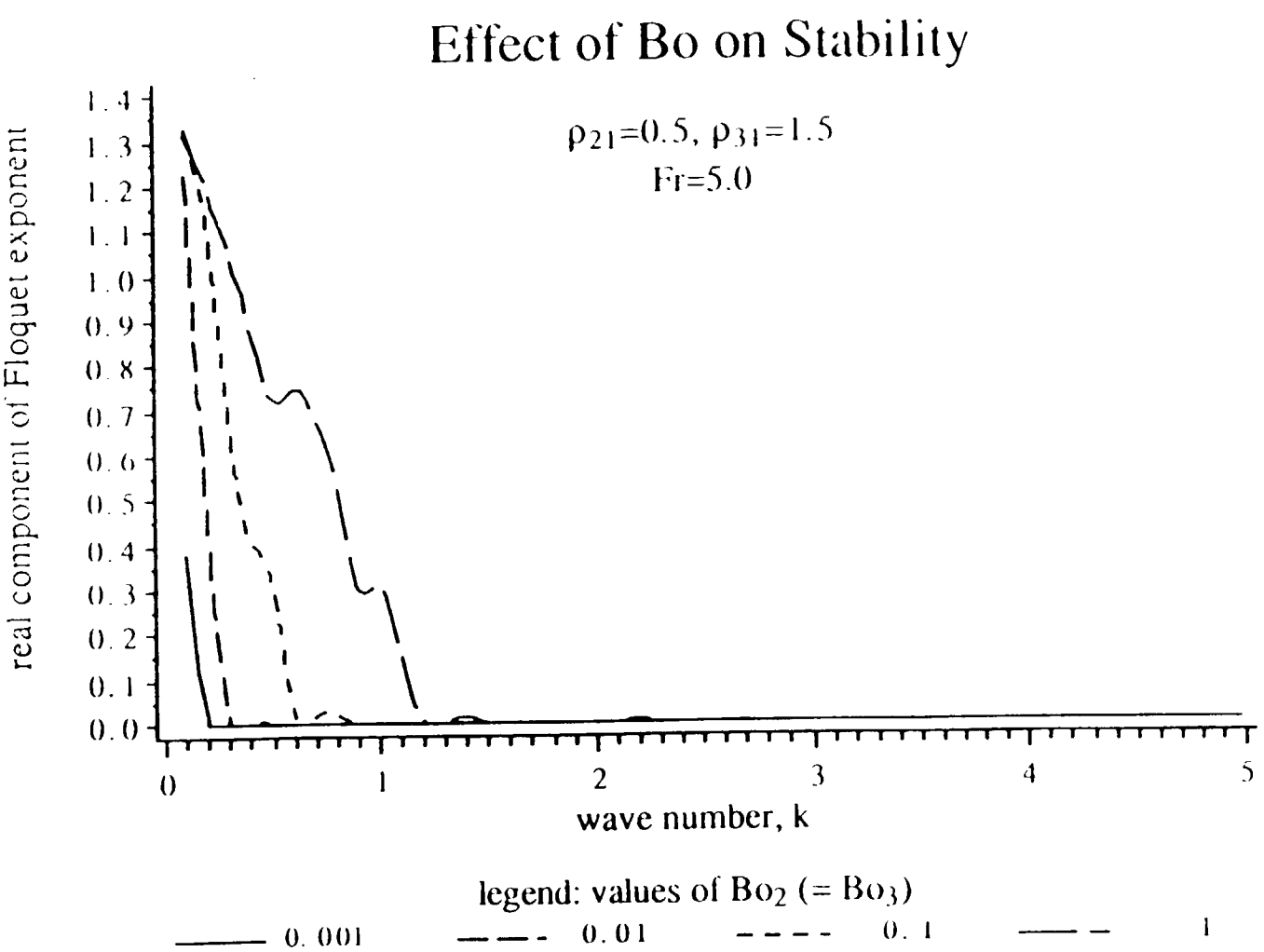
Effect of Bo on Stability
ρ_{21}=0.5, ρ_{31}=1.5
Fr=5.0
real component of Floquet exponent
1.4
1.3
1.2
1.1
1.0
0.9
0.8
0.7
0.6
0.5
0.4
0.3
0.2
0.1
0.0
0
1
2
3
4
5
wave number, k
legend: values of Bo_2 (= Bo_3)
0.001
0.01
0.1
1

Figure 3.18

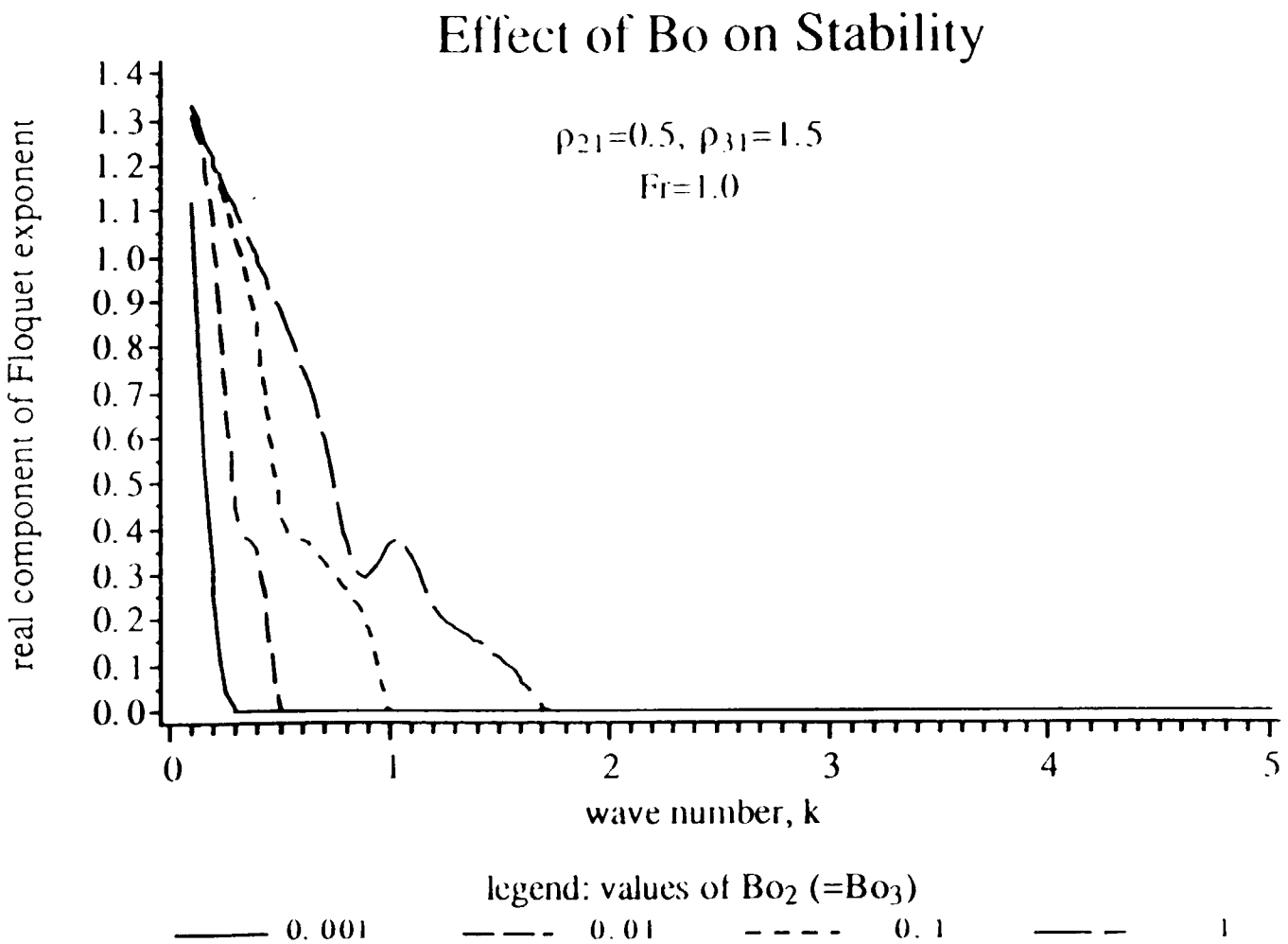
Effect of Bo on Stability
ρ_{21}=0.5, ρ_{31}=1.5
Fr=1.0
real component of Floquet exponent
1.4
1.3
1.2
1.1
1.0
0.9
0.8
0.7
0.6
0.5
0.4
0.3
0.2
0.1
0.0
0
1
2
3
4
5
wave number, k
legend: values of Bo_2 (=Bo_3)
0.001
0.01
0.1
1

Figure 3.19

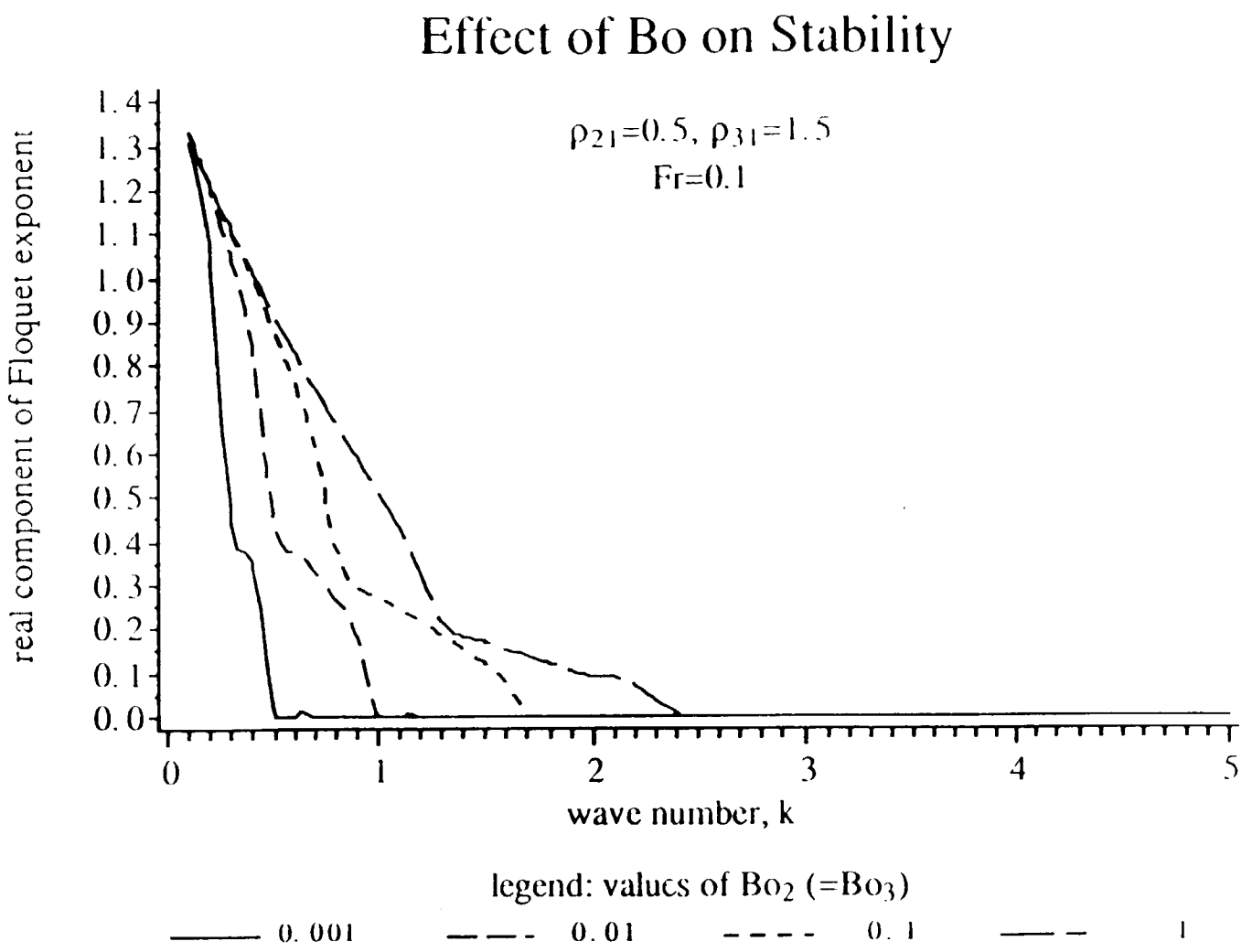
Effect of Bo on Stability
ρ21=0.5, ρ31=1.5
Fr=0.1
real component of Floquet exponent
1.4
1.3
1.2
1.1
1.0
0.9
0.8
0.7
0.6
0.5
0.4
0.3
0.2
0.1
0.0
0
1
2
3
4
5
wave number, k
legend: values of Bo2 (=Bo3)
0.001
0.01
0.1
1

Figure 3.20

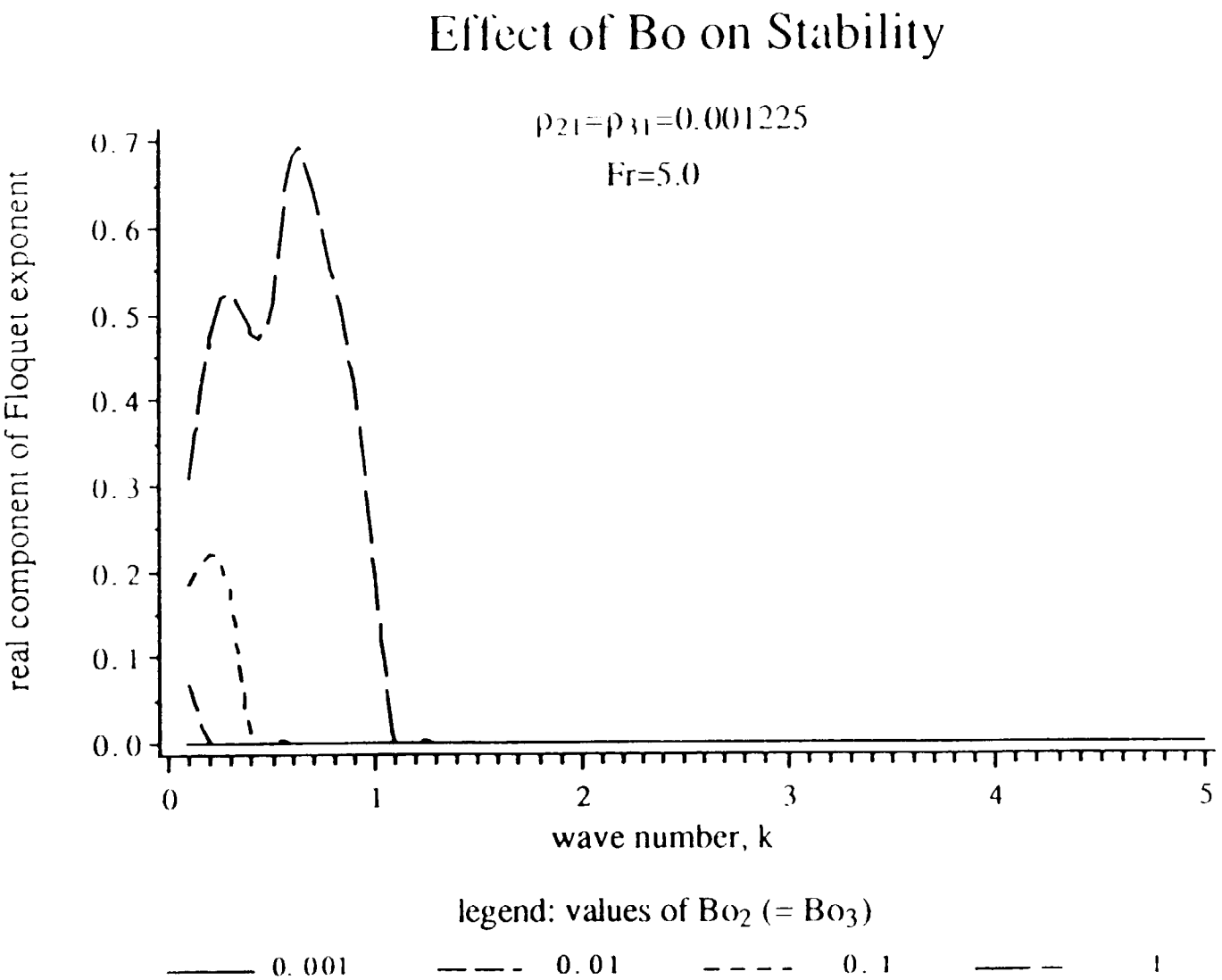
Effect of Bo on Stability
ρ21=ρ31=0.001225
Fr=5.0
real component of Floquet exponent
0.7
0.6
0.5
0.4
0.3
0.2
0.1
0.0
0
1
2
3
4
5
wave number, k
legend: values of Bo2 (= Bo3)
0.001
0.01
0.1
1

Figure 3.21

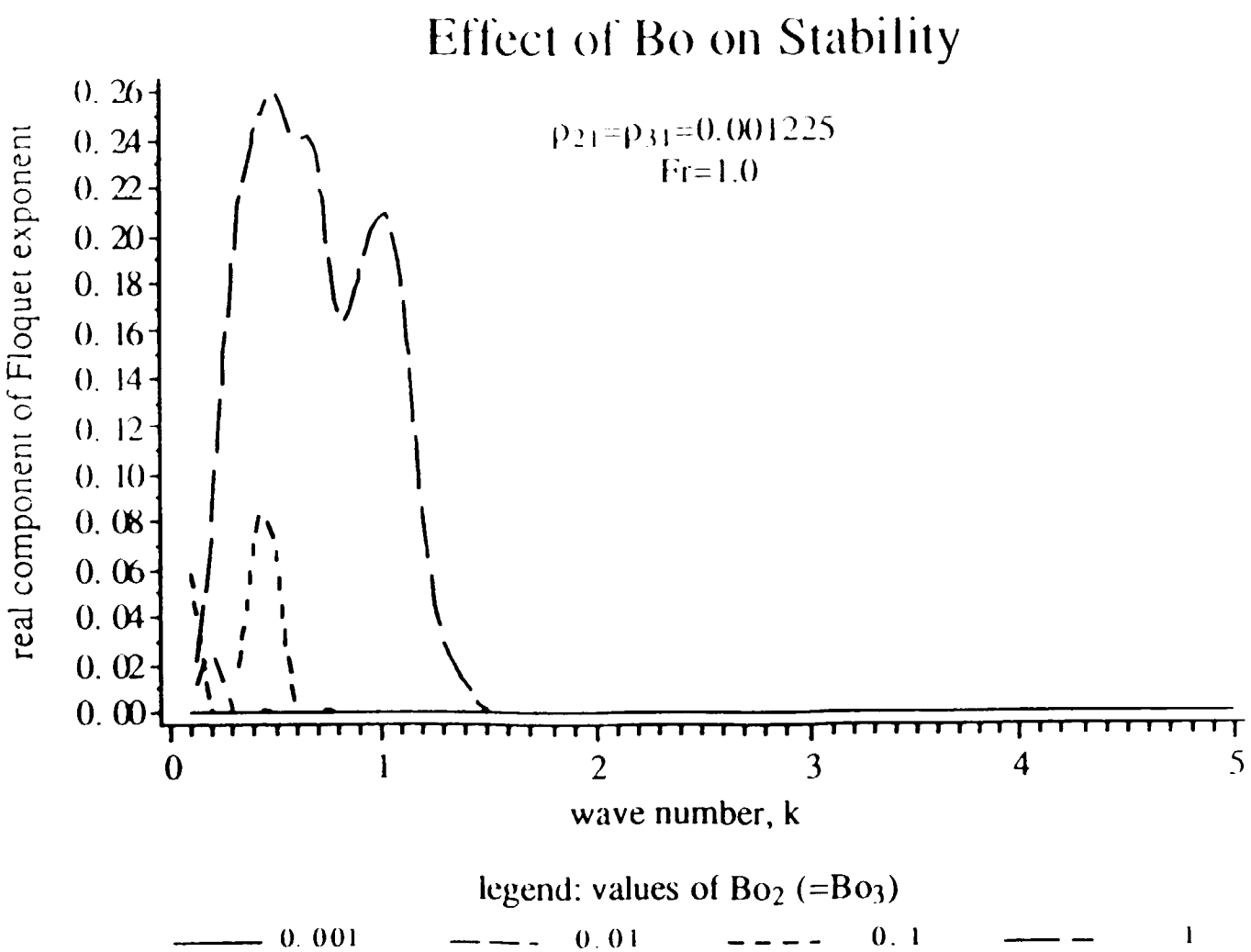
Effect of Bo on Stability
ρ21=ρ31=0.001225
Fr=1.0
real component of Floquet exponent
0. 26
0. 24
0. 22
0. 20
0. 18
0. 16
0. 14
0. 12
0. 10
0. 08
0. 06
0. 04
0. 02
0. 00
0
1
2
3
4
5
wave number, k
legend: values of Bo2 (=Bo3)
0. 001
0. 01
0. 1
1

Figure 3.22

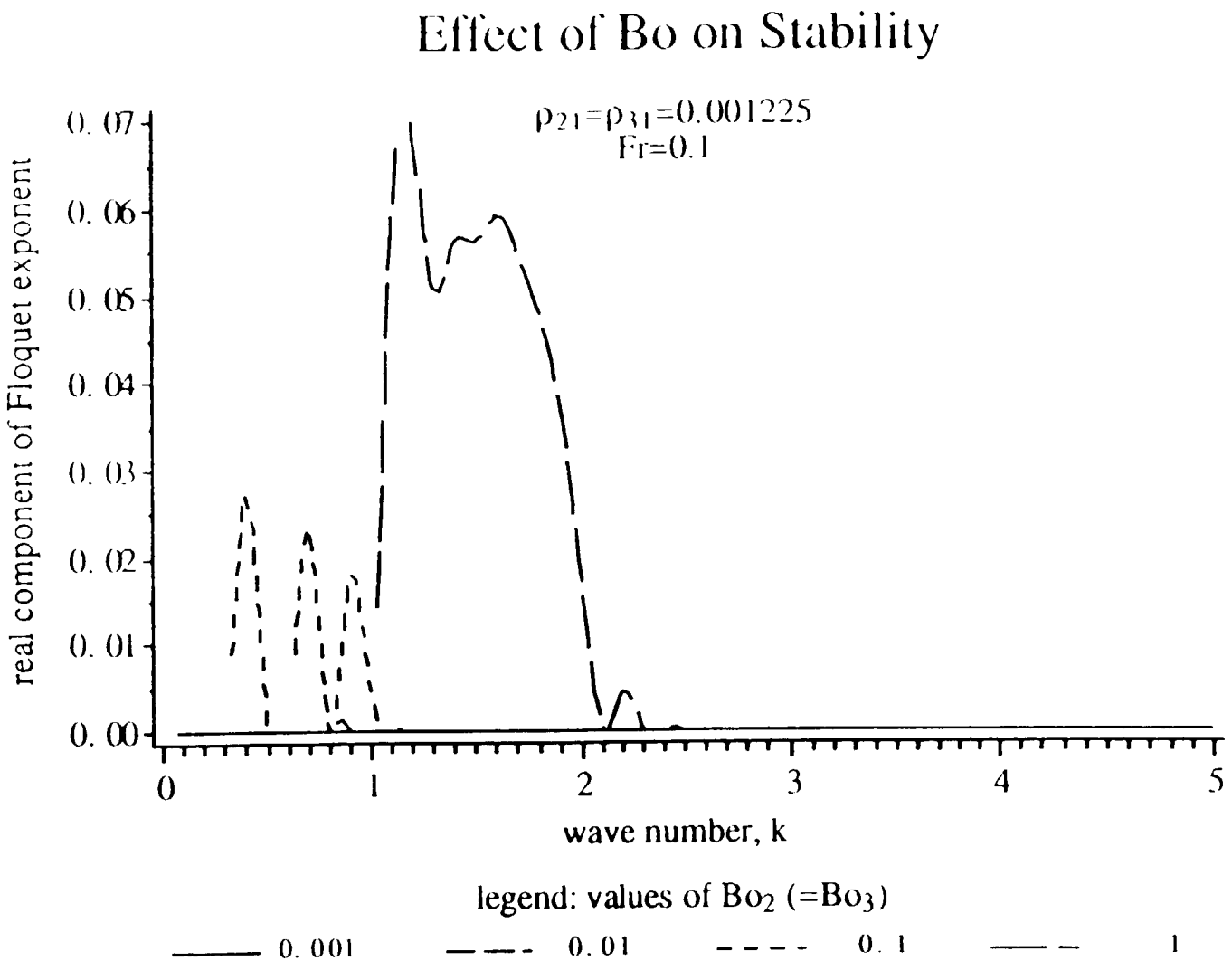
Effect of Bo on Stability
$\rho_{21}=\rho_{31}=0.001225$
Fr=0.1
real component of Floquet exponent
0. 07
0. 06
0. 05
0. 04
0. 03
0. 02
0. 01
0. 00
0
1
2
3
4
5
wave number, k
legend: values of Bo_2 (=Bo_3)
0. 001
0. 01
0. 1
1

Figure 3.23

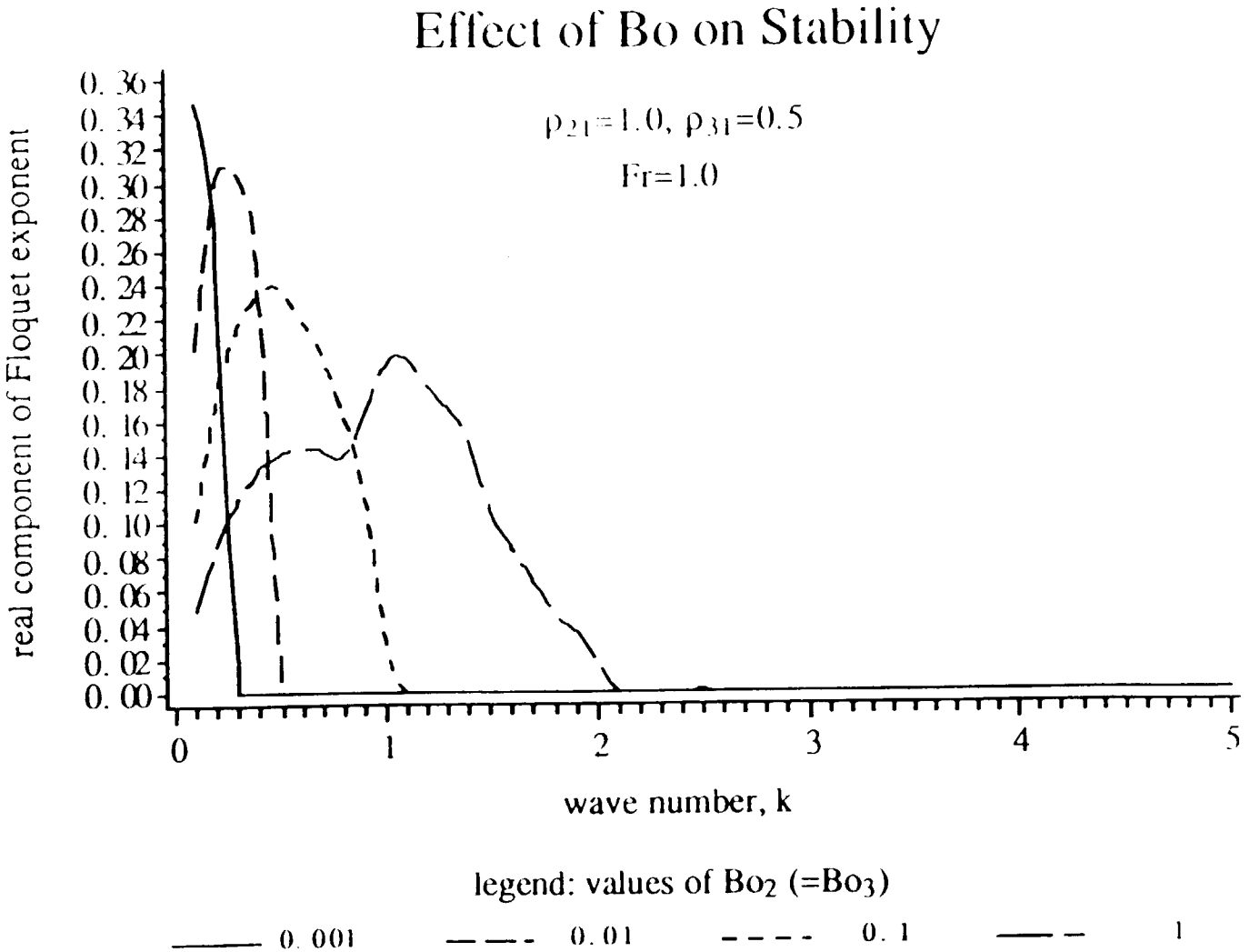
Effect of Bo on Stability
ρ_{21}=1.0, ρ_{31}=0.5
Fr=1.0
real component of Floquet exponent
0.36
0.34
0.32
0.30
0.28
0.26
0.24
0.22
0.20
0.18
0.16
0.14
0.12
0.10
0.08
0.06
0.04
0.02
0.00
0
1
2
3
4
5
wave number, k
legend: values of Bo_2 (=Bo_3)
0.001
0.01
0.1
1

Figure 3.24

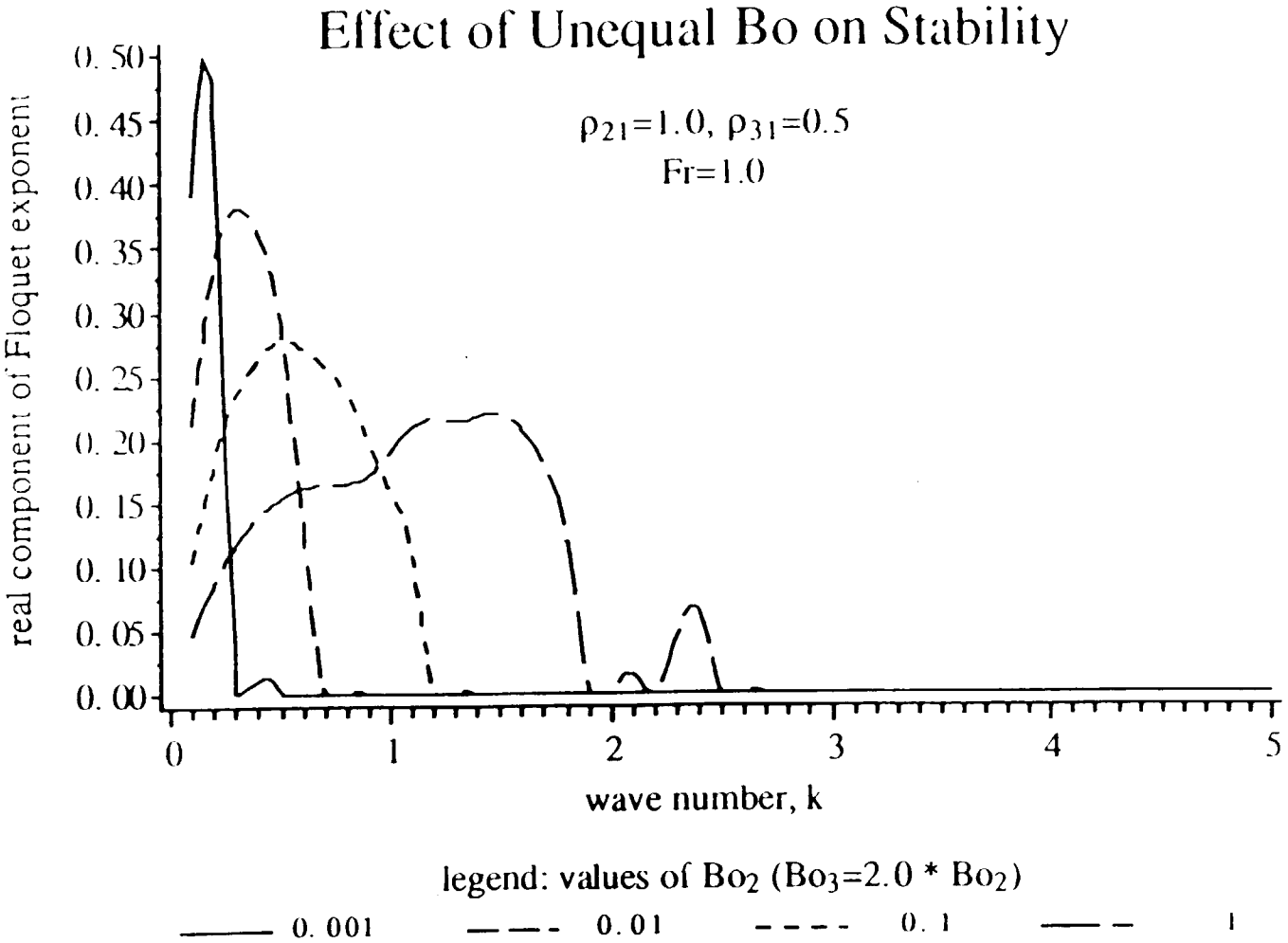
Effect of Unequal Bo on Stability
ρ_{21}=1.0, ρ_{31}=0.5
Fr=1.0
real component of Floquet exponent
0.50
0.45
0.40
0.35
0.30
0.25
0.20
0.15
0.10
0.05
0.00
0
1
2
3
4
5
wave number, k
legend: values of Bo_2 (Bo_3=2.0 * Bo_2)
0.001
0.01
0.1
1

Figure 3.25

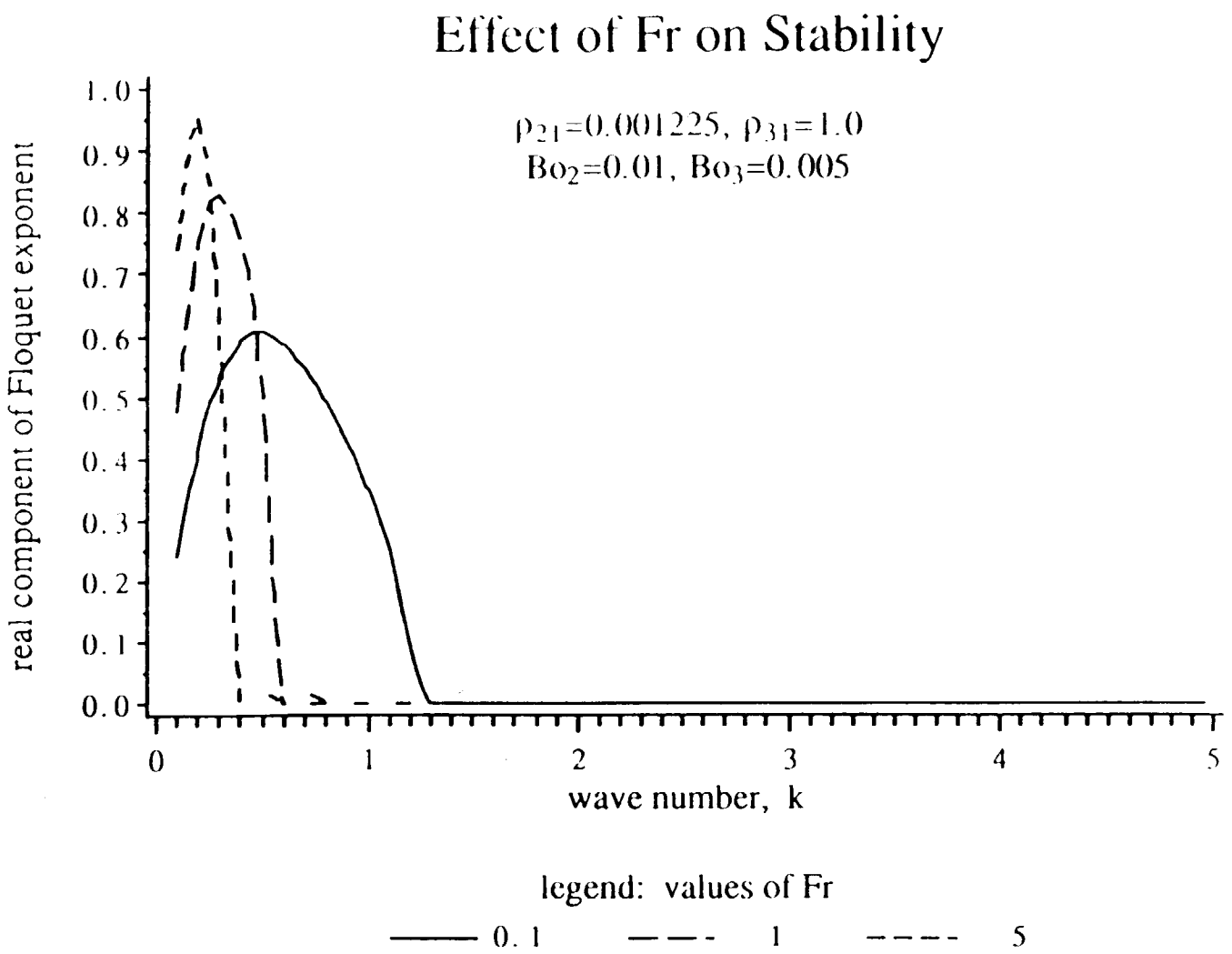
Effect of Fr on Stability
ρ_{21}=0.001225, ρ_{31}=1.0
Bo_2=0.01, Bo_3=0.005
real component of Floquet exponent
1.0
0.9
0.8
0.7
0.6
0.5
0.4
0.3
0.2
0.1
0.0
0
1
2
3
4
5
wave number, k
legend: values of Fr
0.1
1
5

Figure 3.26

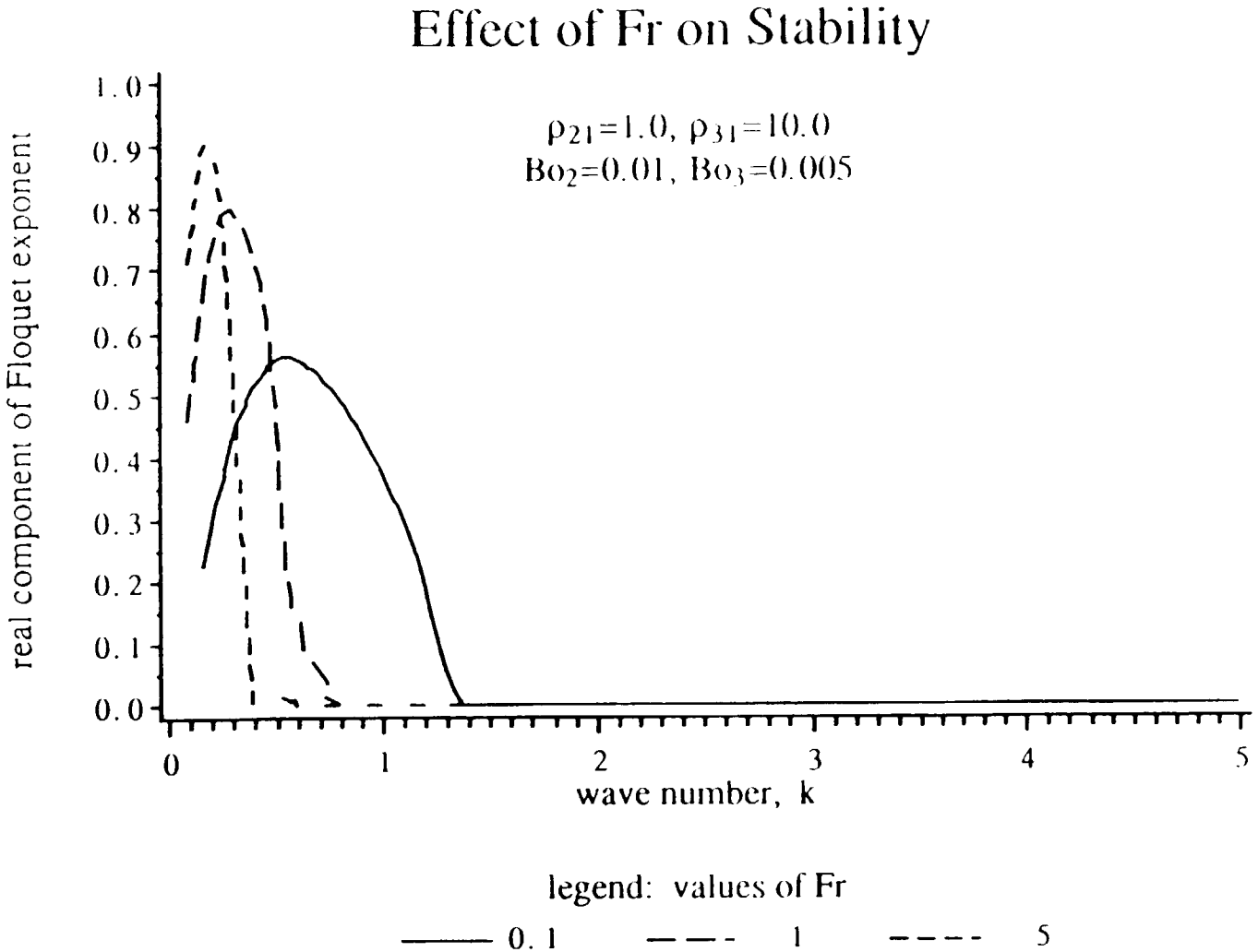
Effect of Fr on Stability
ρ_{21}=1.0, ρ_{31}=10.0
Bo_2=0.01, Bo_3=0.005
real component of Floquet exponent
1.0
0.9
0.8
0.7
0.6
0.5
0.4
0.3
0.2
0.1
0.0
0
1
2
3
4
5
wave number, k
legend: values of Fr
0.1
1
5

Figure 3.27

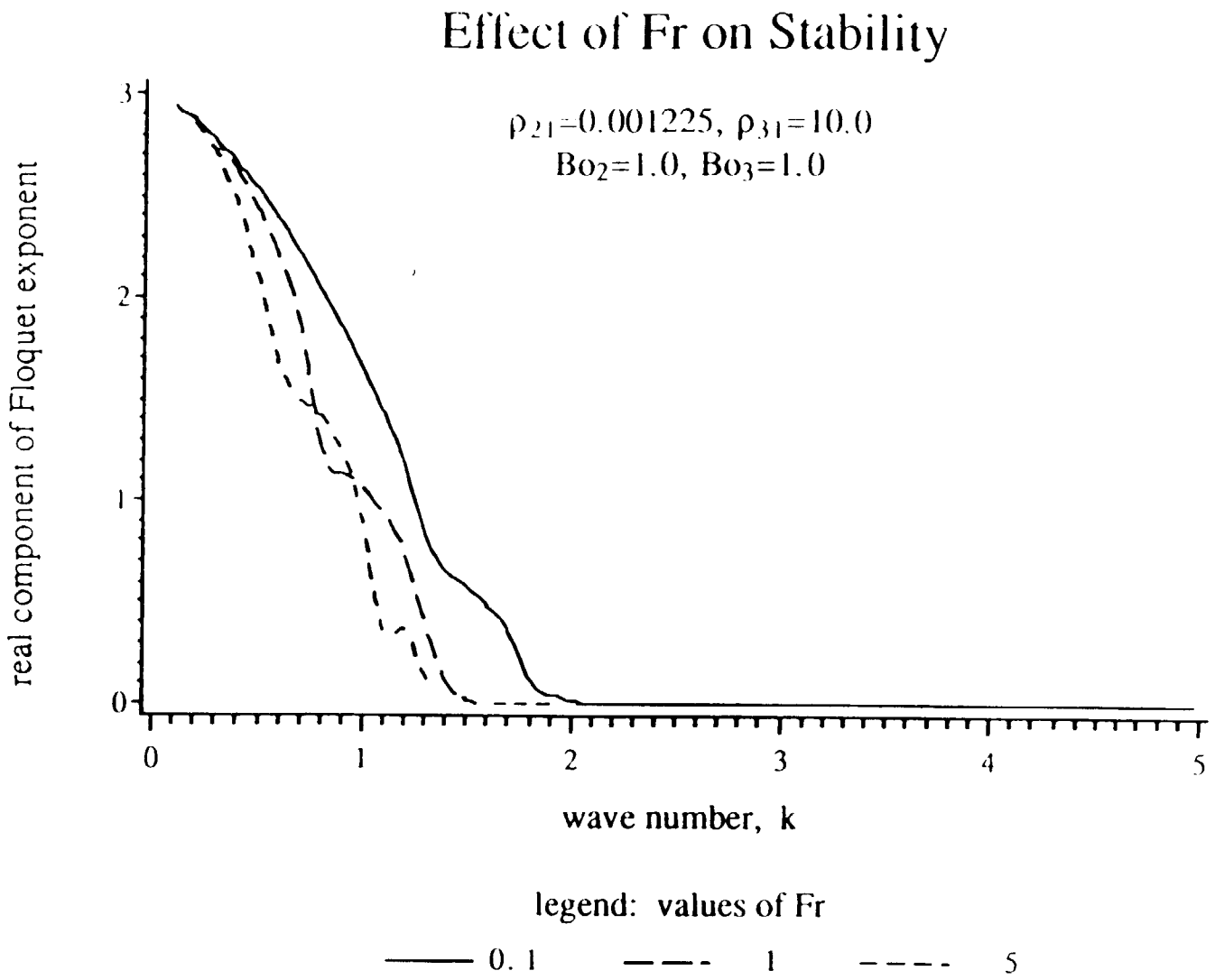
Effect of Fr on Stability
ρ_{21}=0.001225, ρ_{31}=10.0
Bo_2=1.0, Bo_3=1.0
real component of Floquet exponent
0
1
2
3
0
1
2
3
4
5
wave number, k
legend: values of Fr
0.1
1
5

Figure 3.28

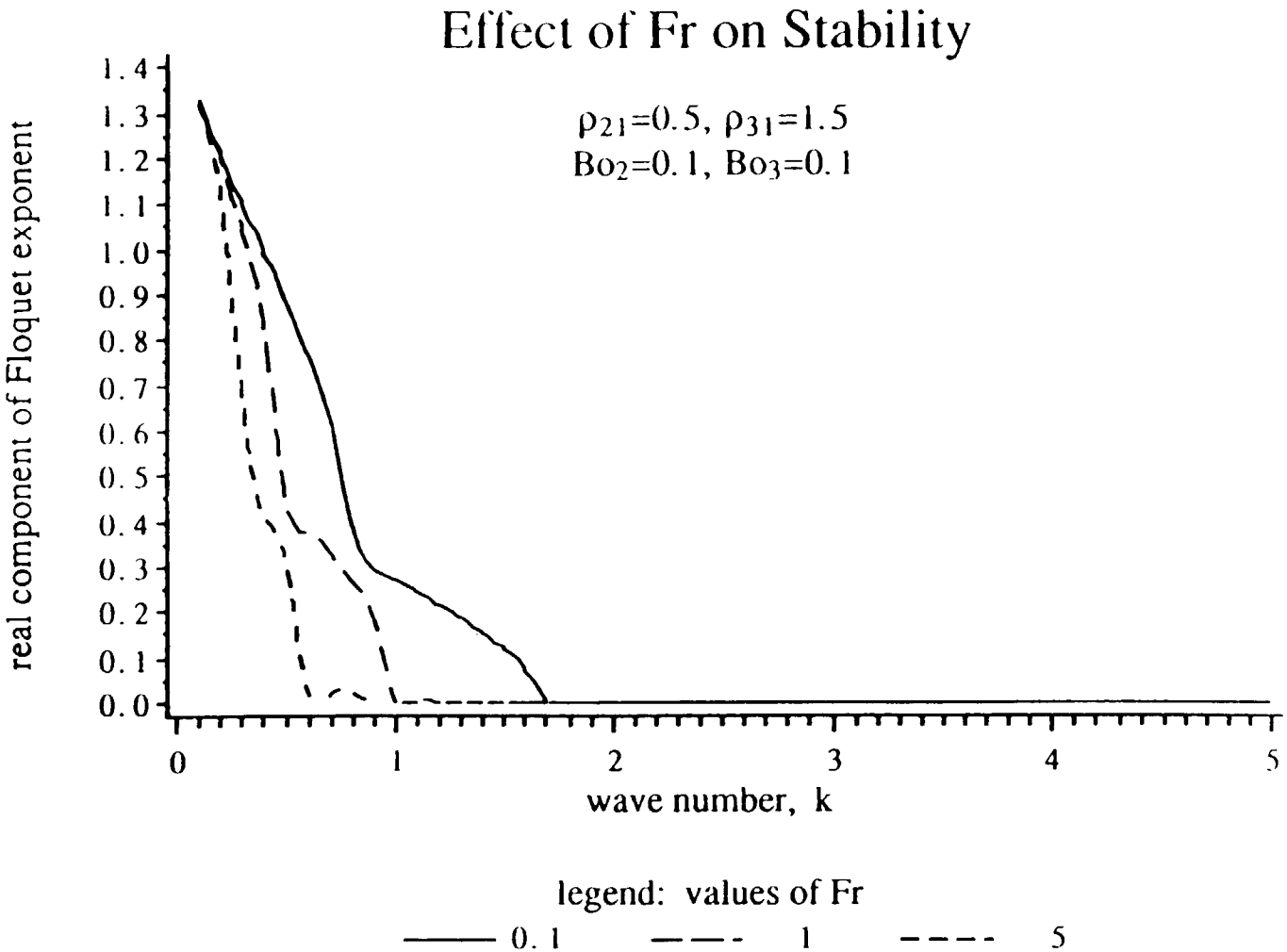
Effect of Fr on Stability
ρ_{21}=0.5, ρ_{31}=1.5
Bo_2=0.1, Bo_3=0.1
real component of Floquet exponent
1.4
1.3
1.2
1.1
1.0
0.9
0.8
0.7
0.6
0.5
0.4
0.3
0.2
0.1
0.0
0
1
2
3
4
5
wave number, k
legend: values of Fr
0.1
1
5

Figure 3.29

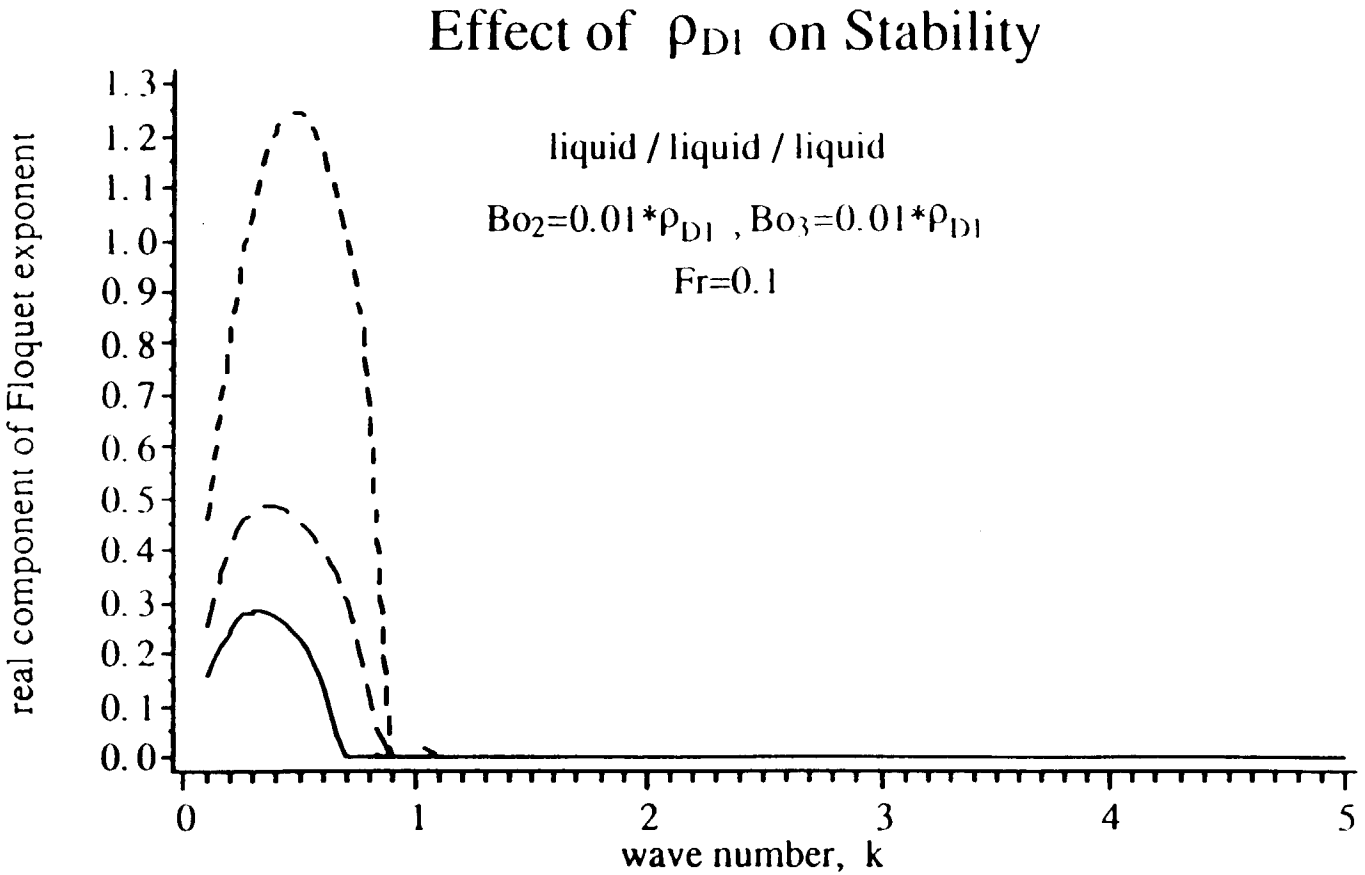
Effect of ρ_{D1} on Stability
liquid / liquid / liquid
$Bo_2=0.01*\rho_{D1}$, $Bo_3=0.01*\rho_{D1}$
Fr=0.1
real component of Floquet exponent
1.3
1.2
1.1
1.0
0.9
0.8
0.7
0.6
0.5
0.4
0.3
0.2
0.1
0.0
0
1
2
3
4
5
wave number, k
ρ_{21}= 1.0
ρ_{31}= 0.5
ρ_{D1}= 0.25
ρ_{21}= 1.0
ρ_{31}= 2.0
ρ_{D1}= 0.5
ρ_{21}= 1.0
ρ_{31}= 10.0
ρ_{D1}= 4.5

Figure 3.30

Effect of ρ_{D1} on Stability

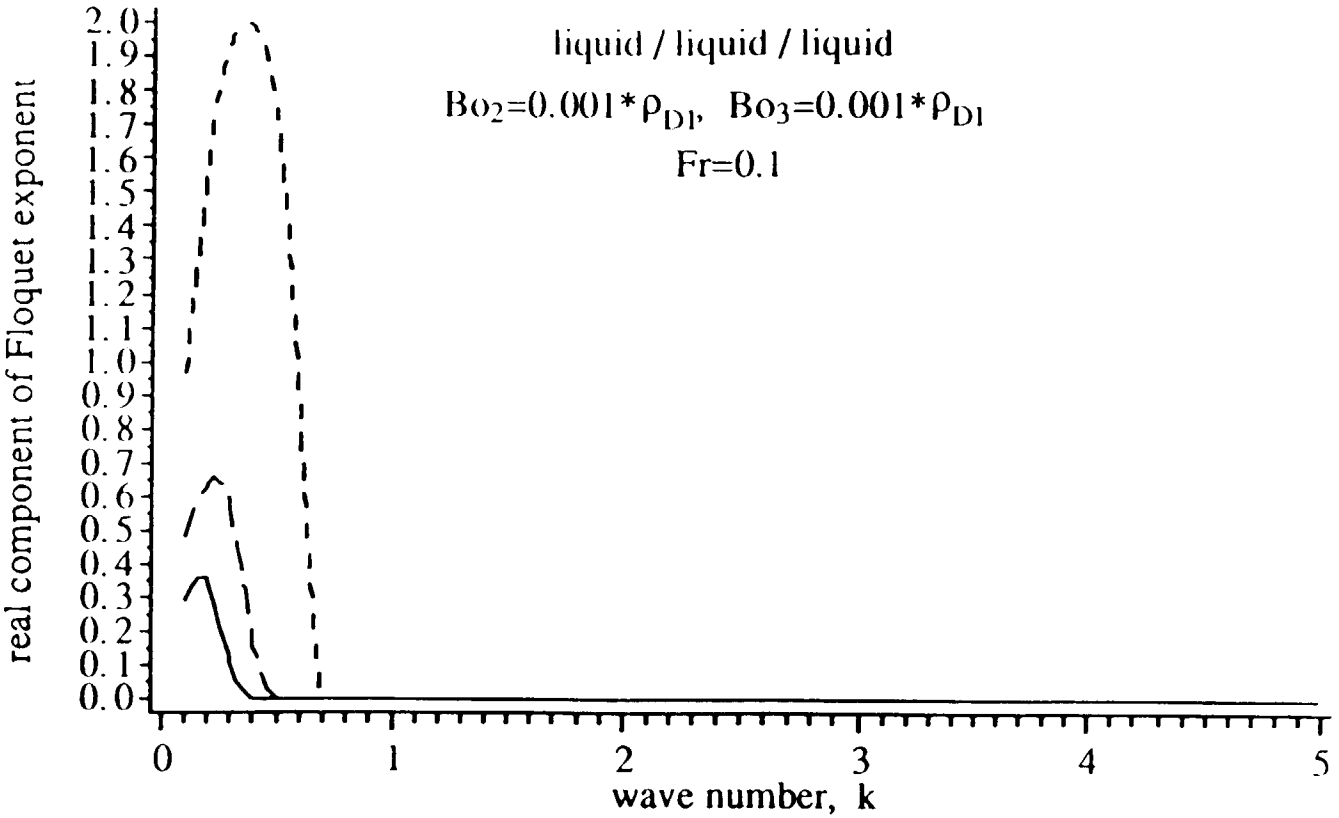

Figure 3.31

Effect of ρ_{D1} on Stability

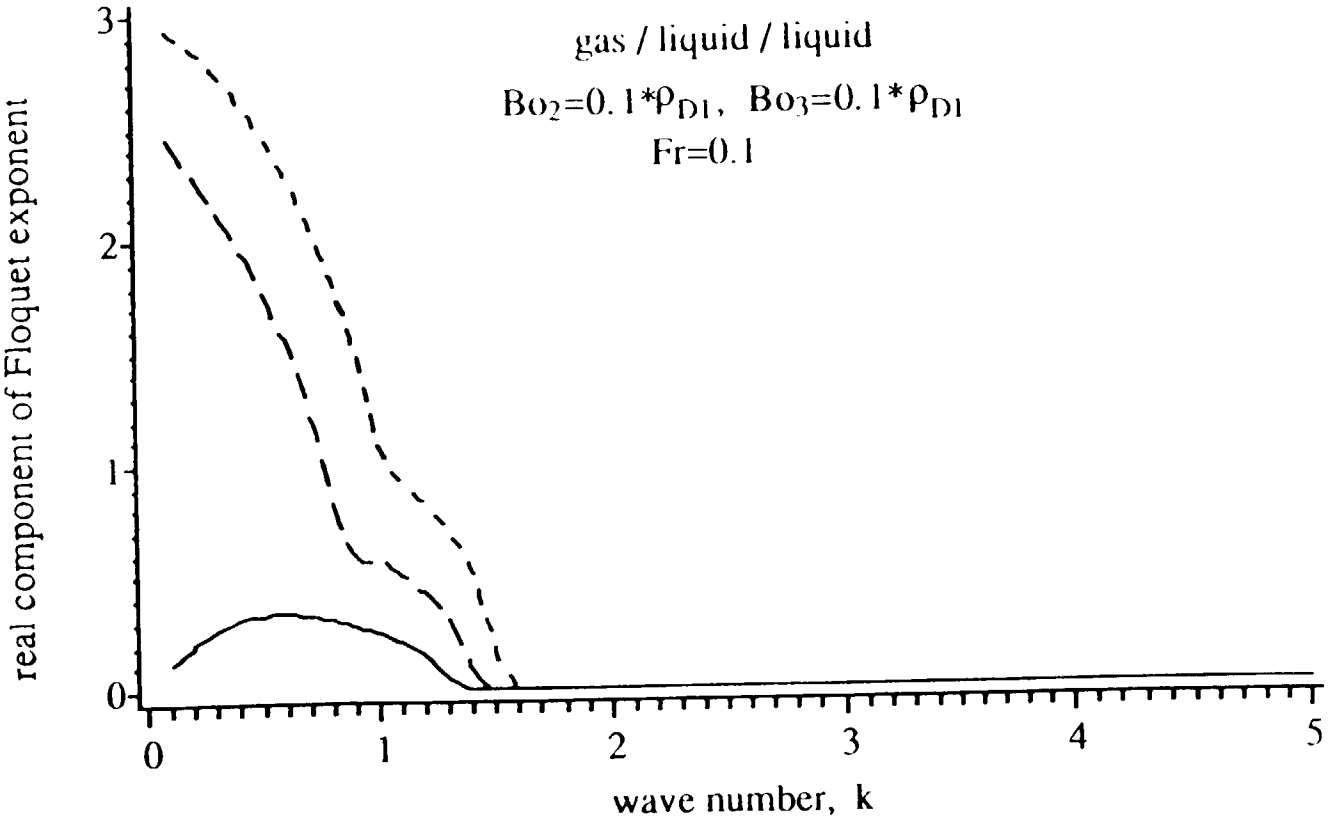

ρ_{21}= 0.001225	ρ_{21}= 0.001225	ρ_{21}= 0.001225
ρ_{31}= 1.0	ρ_{31}= 2.0	ρ_{31}= 10.0
ρ_{D1}= 0.5	ρ_{D1}= 1.0	ρ_{D1}= 5.0
———	— — -	- - - -

Figure 3.32

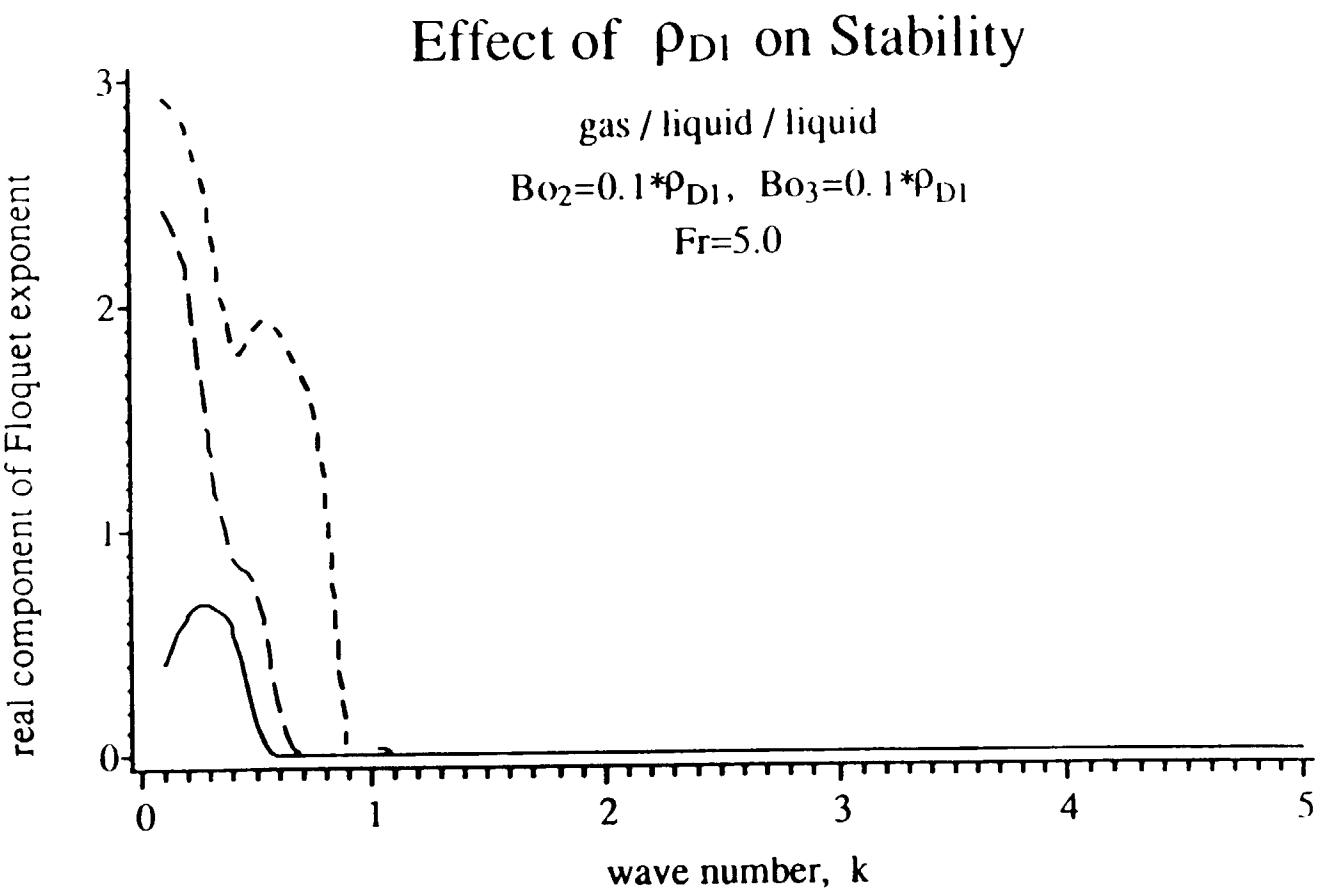
Effect of ρ_{D1} on Stability
gas / liquid / liquid
$Bo_2=0.1*\rho_{D1}$, $Bo_3=0.1*\rho_{D1}$
Fr=5.0
real component of Floquet exponent
0
1
2
3
0
1
2
3
4
5
wave number, k
ρ_{21}= 0.001225
ρ_{31}= 1.0
ρ_{D1}= 0.5
ρ_{21}= 0.001225
ρ_{31}= 2.0
ρ_{D1}= 1.0
ρ_{21}= 0.001225
ρ_{31}= 10.0
ρ_{D1}= 5.0

Figure 3.33

Effect of ρ_{D1} on Stability

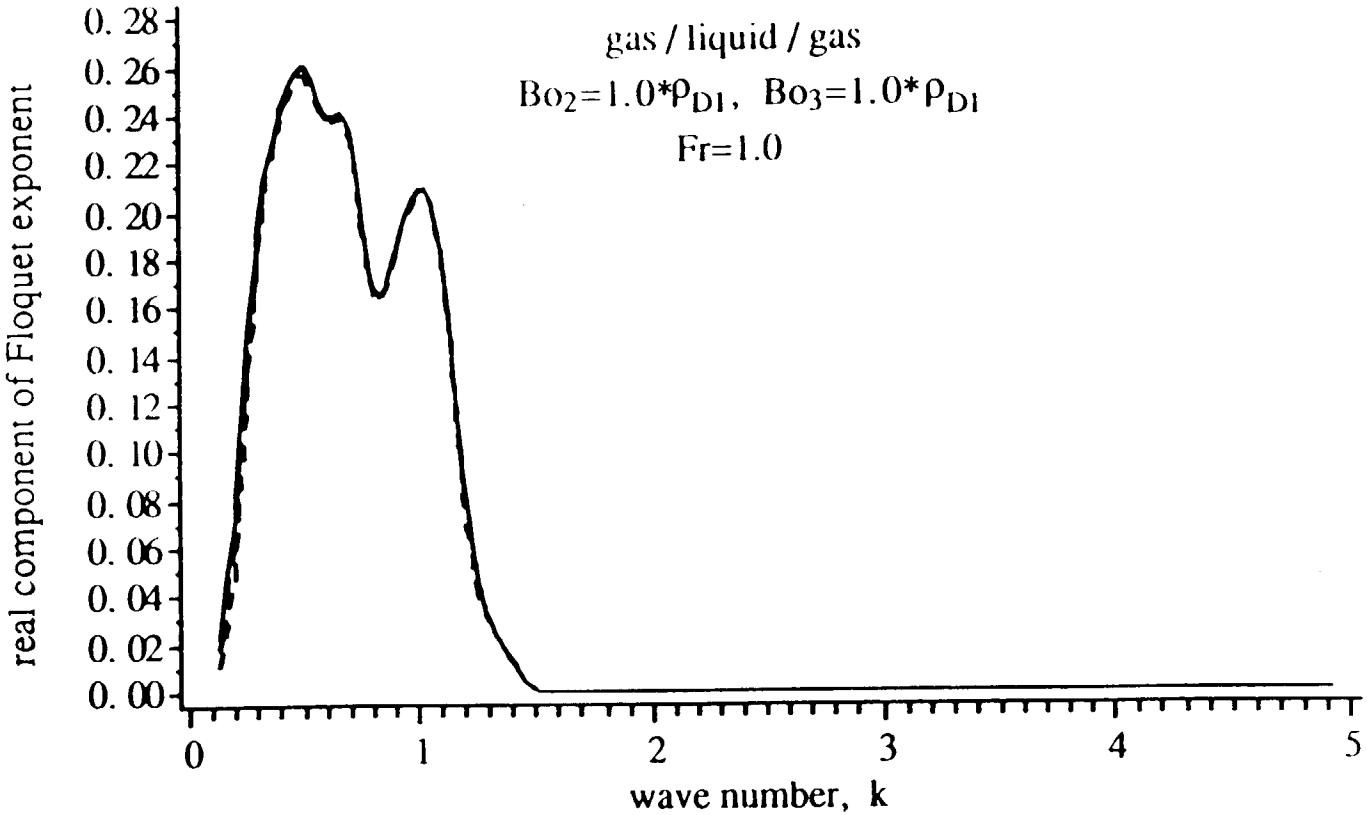

ρ_{21}= 0.001225	ρ_{21}= 0.00500	ρ_{21}= 0.01000
ρ_{31}= 0.001225	ρ_{31}= 0.00500	ρ_{31}= 0.01000
ρ_{D1}= 0.9988	ρ_{D1}= 0.995	ρ_{D1}= 0.990
———	— — -	- - - -

Figure 3.34

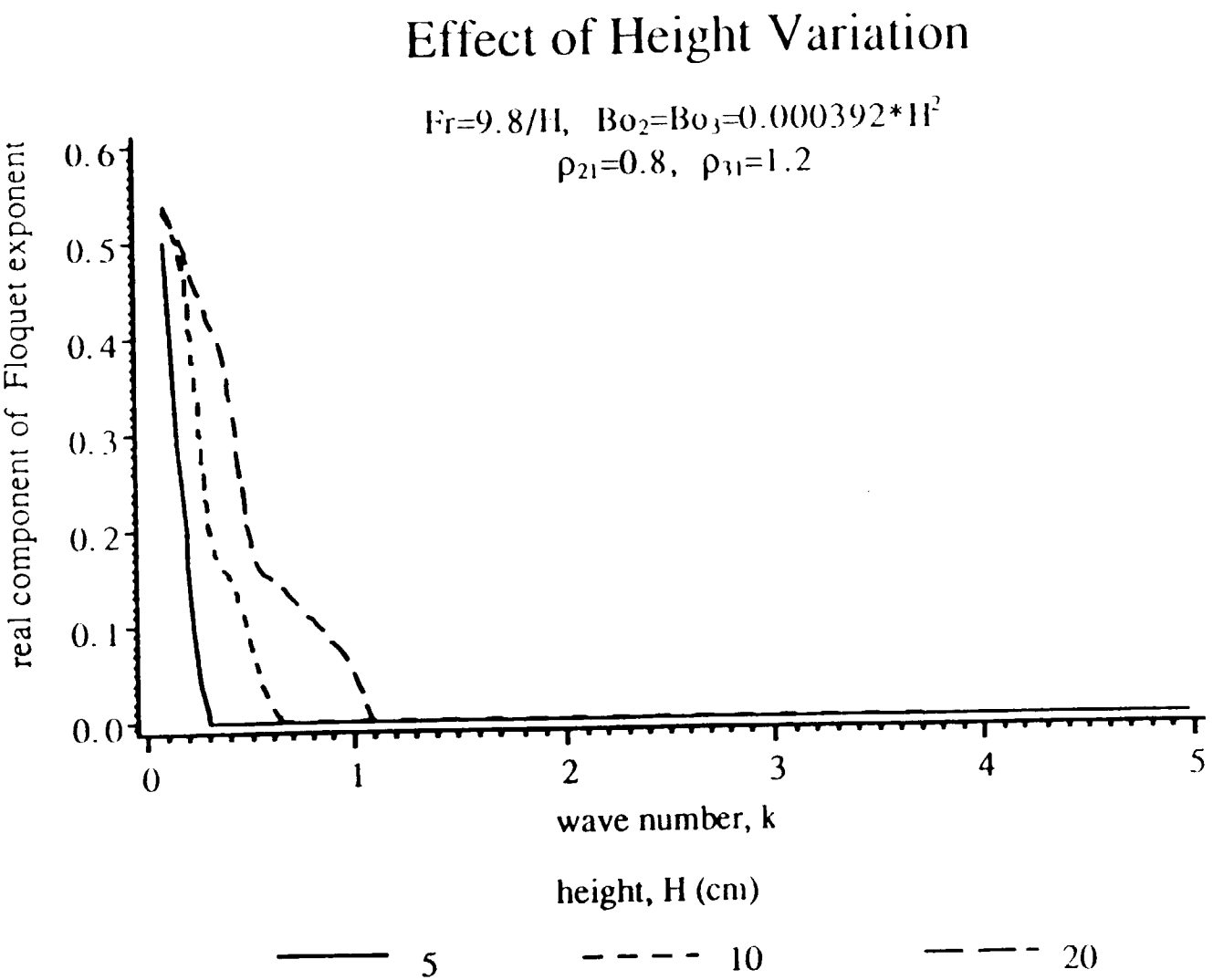
Effect of Height Variation
Fr=9.8/H, Bo2=Bo3=0.000392*H^2
ρ21=0.8, ρ31=1.2
real component of Floquet exponent
0.6
0.5
0.4
0.3
0.2
0.1
0.0
0
1
2
3
4
5
wave number, k
height, H (cm)
5
10
20

Figure 3.35

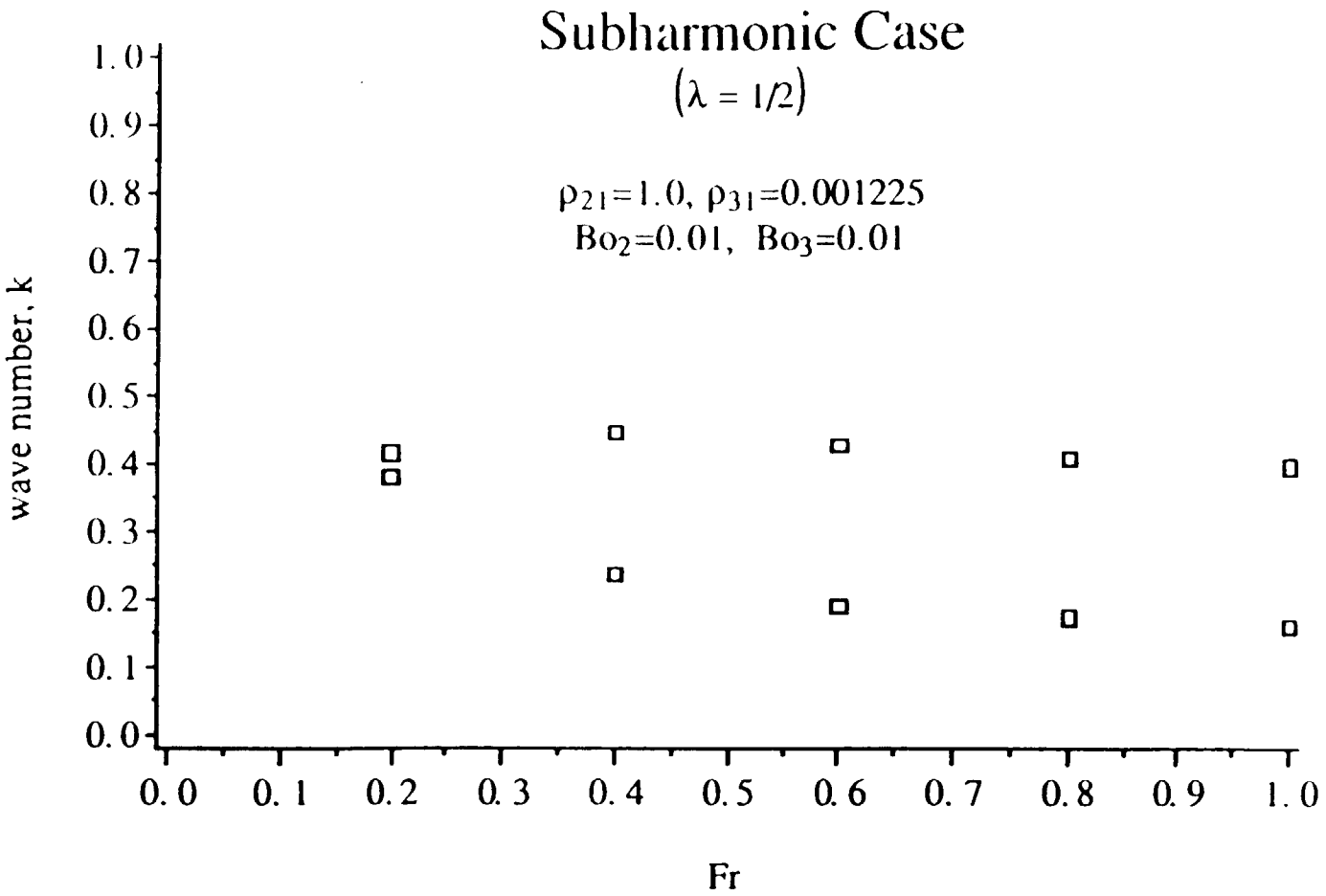
Subharmonic Case
(λ = 1/2)
ρ21=1.0, ρ31=0.001225
Bo2=0.01, Bo3=0.01
wave number, k
1.0
0.9
0.8
0.7
0.6
0.5
0.4
0.3
0.2
0.1
0.0
0.0 0.1 0.2 0.3 0.4 0.5 0.6 0.7 0.8 0.9 1.0
Fr

Figure 3.36

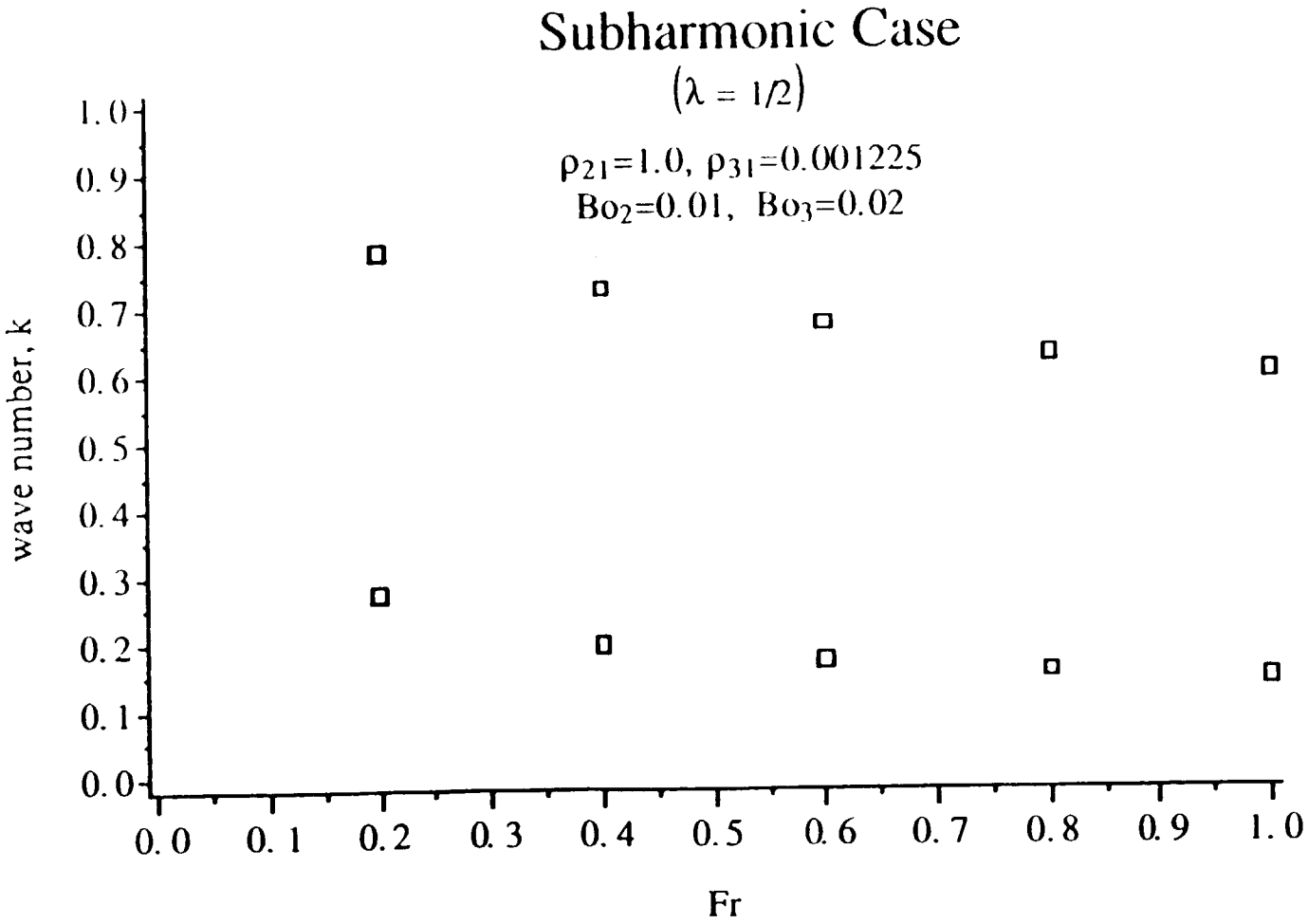
Subharmonic Case
(λ = 1/2)
ρ21=1.0, ρ31=0.001225
Bo2=0.01, Bo3=0.02
wave number, k
1.0
0.9
0.8
0.7
0.6
0.5
0.4
0.3
0.2
0.1
0.0
0.0 0.1 0.2 0.3 0.4 0.5 0.6 0.7 0.8 0.9 1.0
Fr

Figure 3.37

Stability Boundaries

for given density ratios

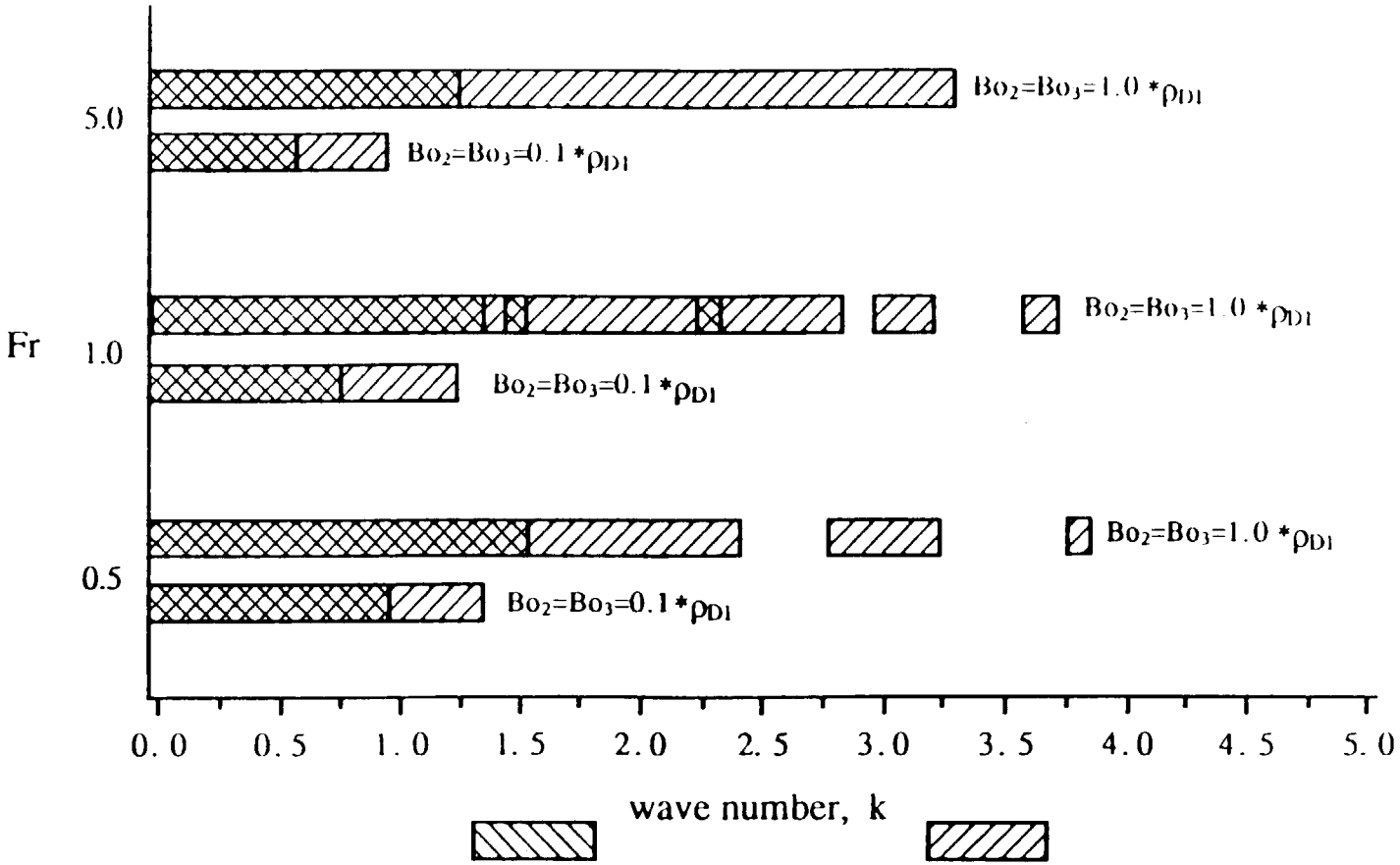

ρ_{21}=0.001225
ρ_{31}= 1.0
ρ_{D1}=0.499

ρ_{21}= 0.001225
ρ_{31}= 10.0
ρ_{D1}=4.999

Figure 3.38

Stability Boundaries

for given density ratios

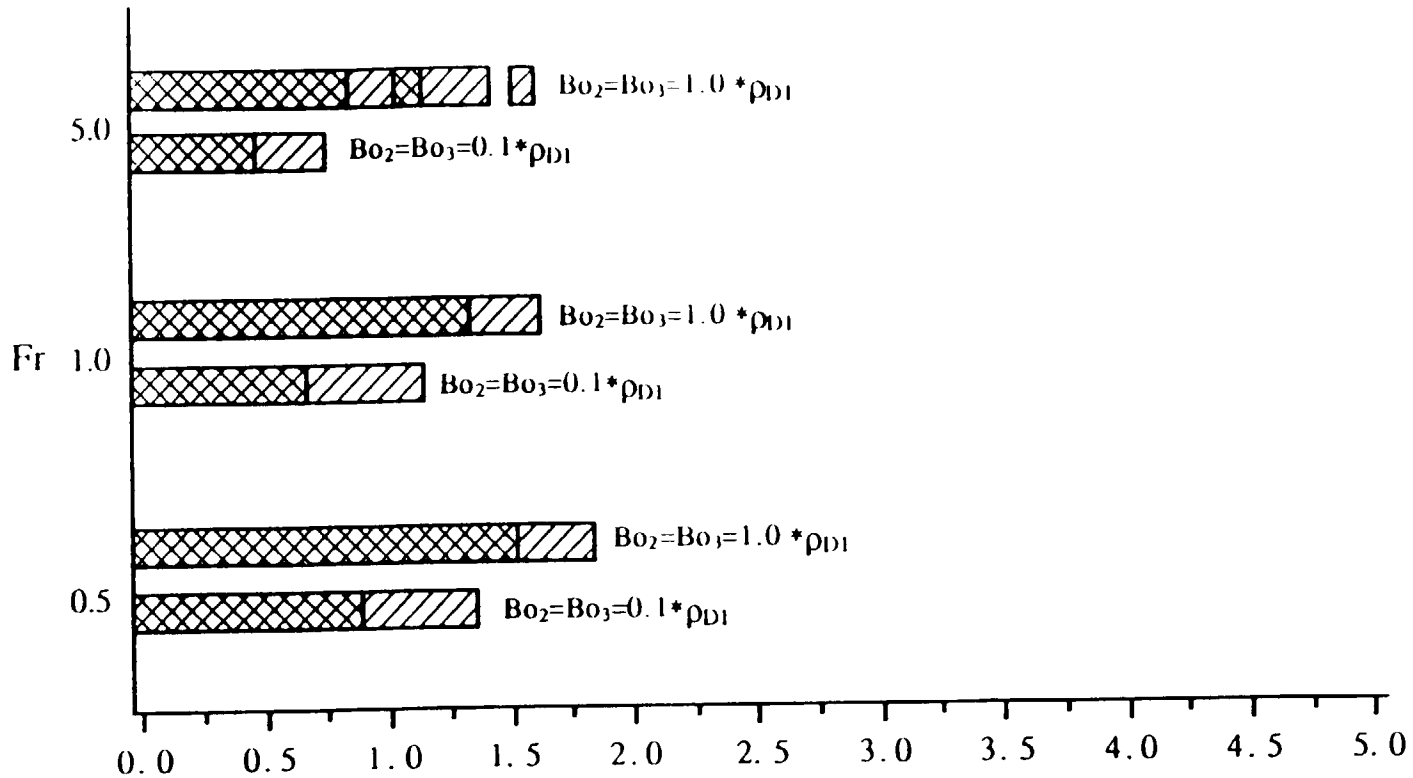

ρ21=1.0
ρ31= 0.5
ρD1=0.25

ρ21 =1.0
ρ31= 2.0
ρD1=0.50

Figure 3.39

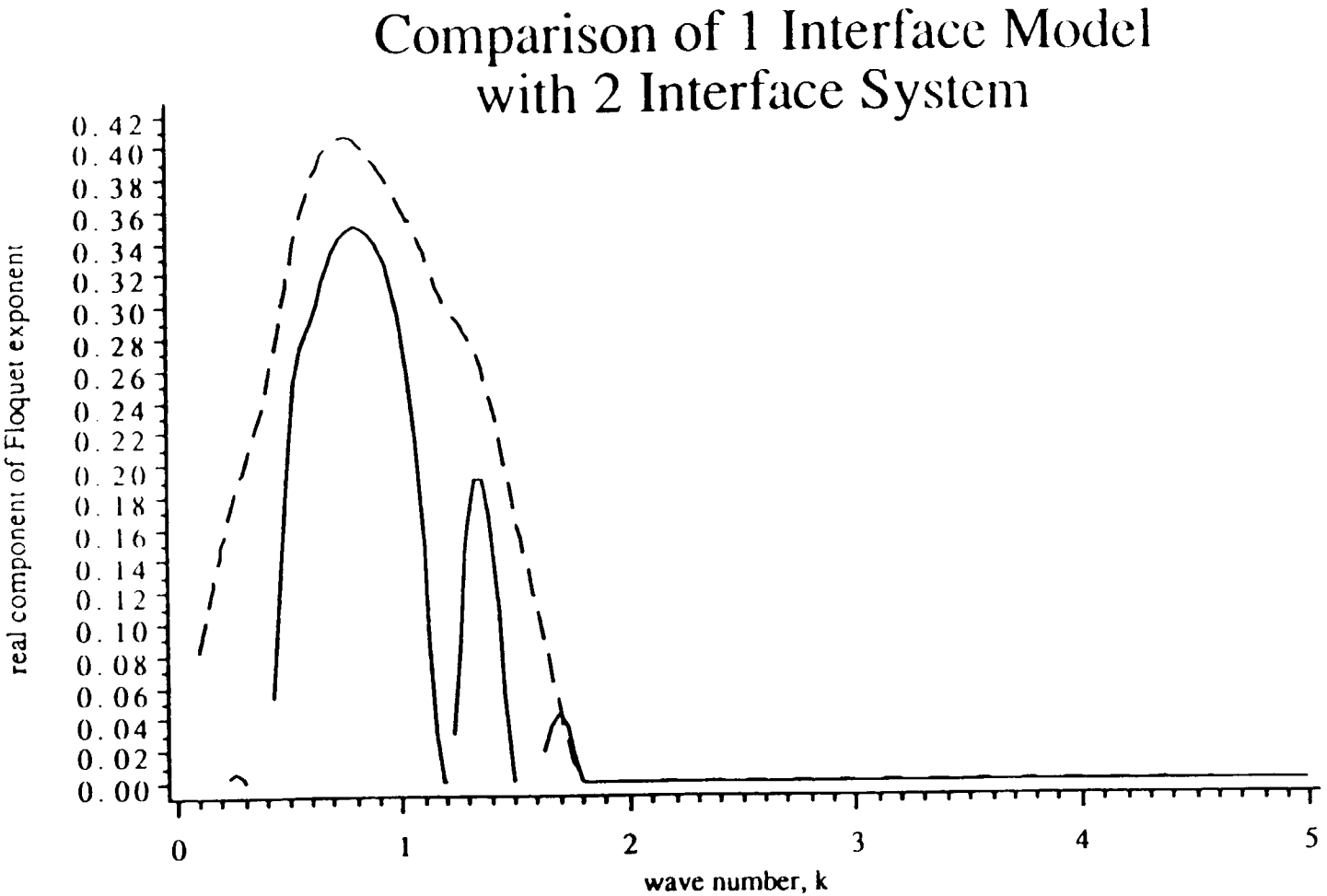
Comparison of 1 Interface Model
with 2 Interface System
real component of Floquet exponent
0.42
0.40
0.38
0.36
0.34
0.32
0.30
0.28
0.26
0.24
0.22
0.20
0.18
0.16
0.14
0.12
0.10
0.08
0.06
0.04
0.02
0.00
0
1
2
3
4
5
wave number, k
1 interface model
ρ21=0.001225
Q=1.0
2 interface system
ρ21=1.0, ρ31=0.001225
Bo2=Bo3=1.0, Fr=1.0

Figure 3.40

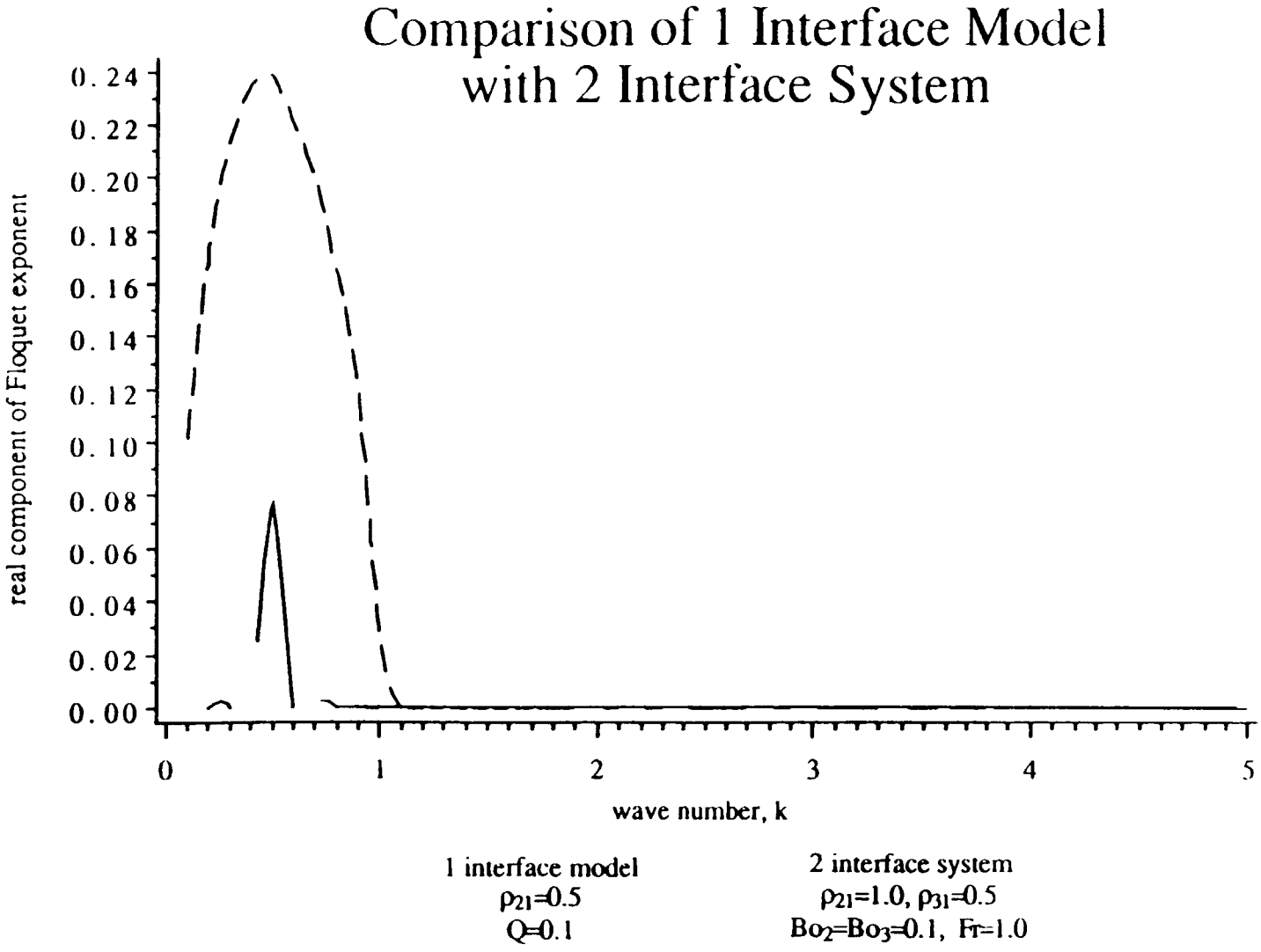
Comparison of 1 Interface Model
with 2 Interface System
real component of Floquet exponent
0.24
0.22
0.20
0.18
0.16
0.14
0.12
0.10
0.08
0.06
0.04
0.02
0.00
0
1
2
3
4
5
wave number, k
1 interface model
ρ21=0.5
Q=0.1
2 interface system
ρ21=1.0, ρ31=0.5
Bo2=Bo3=0.1, Fr=1.0

Figure 3.41

CHAPTER 4

RESPONSE OF MULTI-LAYER FLUID CONFIGURATION TO SHORT-DURATION NON-PERIODIC TIME-DEPENDENT FORCING

4.1 Problem description and stability considerations

The residual accelerations which occur in a microgravity environment are generally time-dependent in nature. The special case of periodic g-jitter was addressed in Chapter 3. In addition to periodic forcing, residual accelerations may be of impulse type, due to such causes as station-keeping maneuvers and astronaut motion. This forcing, though non-periodic, would certainly still be time-dependent.

This chapter investigates the effect of time-dependent, non-periodic accelerations on the interface stability of an idealized fluid configuration. The geometry of the system is the same as in Chapter 3 (see Figure 3.1). The accelerations are again oriented normal (in the $\hat{e}_z$ direction) to the interfaces and have a zero initial value condition. Moderate-duration responses will primarily be investigated.

The three fluids are assumed inviscid, incompressible, irrotational, and immiscible. Surface tension is a property of the interfaces and is taken to be constant. The spatial dependence of the perturbation is considered to be wavelike. The fluid system is governed by the continuity and Euler equations. These equations are non-dimensionalized and linearized, resulting in a system of linear equations with time-dependent coefficients.

Two forcing functions will be considered: 1) An exponential ramp followed by exponential decay, and 2) a ramped step function with both positive and negative values. These idealized functions were chosen to represent general impulses.

An analytical approach is used to ascertain the asymptotic (mathematical) stability of the non-autonomous system. This analysis is presented in Section 4.3, with additional reference to Appendix 3. Note that the system is non-autonomous due to the explicit appearance of time in g(t).

The system of first-order differential equations is integrated numerically utilizing Gear's stiff method[4] in order to solve for the time-dependent coefficients, which describe the response of the interfaces. The interface responses are plotted as a function of time.

The presence of the "short duration" non-periodic body force functions do not modify the asymptotic stability of the multi-layer fluid configuration. Interest is in the level of system disturbance in the presence of the acceleration. Since the effects of viscosity are not incorporated into the analysis, the long time behavior of the system, predicted by the model, is not physically meaningful.

4.2 Equation development

4.2a Governing equations and non-dimensionalization

The governing equations remain those of conservation of mass and momentum for an incompressible fluid. Again, the analysis is inviscid. Linearization is performed about a state of zero mean motion. (Quadratically small terms are neglected after expansion in ε.) The forcing function is of the form

$$G_o g(t)$$

where $g(t)$ is non-periodic, and may be represented by a ramp function, for example. G_o is taken to be the peak magnitude of the forcing function. A positive forcing value is oriented in the negative $\hat{e}_z$ direction.

For this non-periodic forcing case, the non-dimensionalizations used are:

$$\underline{u} = \sqrt{HG_o}\ \tilde{\underline{u}} \tag{4.1}$$

$$\underline{x} = H\ \tilde{\underline{x}} \tag{4.2}$$

$$t = \sqrt{H/G_o}\ \tilde{t} \tag{4.3}$$

$$p = \rho_D\ HG_o\ \tilde{p} \tag{4.4}$$

The non-dimensionalized disturbance governing equations assume the following form:

$$\tilde{\nabla}\cdot\tilde{\underline{u}}' = 0 \tag{4.5}$$

$$\frac{\rho}{\rho_D}\frac{\partial\tilde{\underline{u}}'}{\partial\tilde{t}} = -\tilde{\nabla}\,\tilde{p}' \tag{4.6a}$$

$$0 = -\tilde{\nabla}\,\tilde{p}_{mean} - \frac{\rho}{\rho_D}\,g(\tilde{t})\,\hat{e}_z \tag{4.6b}$$

where tildes indicate non-dimensional quantities and primes denote perturbation values. Equation (4.6b) says the mean pressure instantaneously adopts a hydrostatic distribution with a magnitude governed by the instantaneous value of g(t). Henceforth, the tildes will be dropped, and all quantities are to be considered non-dimensional. Also, the primes are dropped.

As in Chapter 3, the pressure and velocity fields were expanded into a mean and perturbation component. The mean velocity, as stated previously, equals zero.

An inviscid, irrotational, and incompressible analysis gives rise to a potential function ($\underline{u} = \nabla\phi$), which can be substituted into equation (4.5) to yield Laplace's equation. This equation is solved in each region, yielding the same potential functions as in Chapter 3.

$$\phi_1 = \left[A(t)e^{kz} + B(t)e^{-kz}\right] e^{i(lx+my)} \tag{4.7}$$

$$\phi_2 = \left[C(t)e^{-kz}\right] e^{i(lx+my)} \tag{4.8}$$

$$\phi_3 = \left[D(t)e^{kz}\right] e^{i(lx+my)} \tag{4.9}$$

where A,B,C,D are time-dependent coefficients. k represents the wave number, where $k^2 = l^2 + m^2$.

The interface shapes are identical to Chapter 3. Repeating them here, they are

$$Fe_{II} = z - 1 - \varepsilon E(t)e^{i(lx+my)} \tag{4.10}$$

$$Fe_{III} = z - 0 - \varepsilon F(t)e^{i(lx+my)} \tag{4.11}$$

4.2b Boundary conditions

Three boundary conditions are imposed at each interface: (1) the kinematic condition, (2) continuity of the normal component of the velocity, and (3) a normal force balance across each interface.

Imposition of the kinematic condition yields the following relationships between the time-dependent coefficients:

$$\text{on } Fe_{II}, \qquad -\dot{E} - kCe^{-k} = 0 \tag{4.12}$$

$$\text{on } Fe_{III}, \qquad -\dot{F} + kD = 0 \tag{4.13}$$

The normal component of the velocity must match across each interface. Applying this condition gives the following relationships:

$$\text{on } Fe_{II}, \qquad Ae^{2k} - B = -C \tag{4.14}$$

$$\text{on } Fe_{III}, \qquad A - B = D \tag{4.15}$$

The linearized normal force balance across each interface states:

$$\frac{\rho_D (H^2 G_o)}{\gamma} \left[p_{lower} - p_{upper} \right] = \nabla \cdot \hat{n} \tag{4.16}$$

Note the upper and lower pressures each have a mean and perturbation component. Substitution into equation (4.16) follows the same methodology as that discussed in Chapter 3, resulting in the following system of equations:

$$\left[\frac{-(1+\rho_{21})e^{k}}{\rho_{D1}}\right]\dot{A}(t) + \left[\frac{(\rho_{21}-1)e^{-k}}{\rho_{D1}}\right]\dot{B}(t)$$

$$+\left[\frac{(\rho_{21}-1)g(t)}{\rho_{D1}} - \frac{k^2}{Bo_2}\right]E(t) = 0 \qquad (4.17)$$

$$\left[\frac{(1-\rho_{31})}{\rho_{D1}}\right]\dot{A}(t) + \left[\frac{(1+\rho_{31})}{\rho_{D1}}\right]\dot{B}(t)$$

$$+\left[\frac{(1-\rho_{31})g(t)}{\rho_{D1}} - \frac{k^2}{Bo_3}\right]F(t) = 0 \qquad (4.18)$$

$$\dot{E}(t) = k\left[A(t)e^{k} - B(t)e^{-k}\right] \qquad (4.19)$$

$$\dot{F}(t) = k\left[A(t) - B(t)\right] \qquad (4.20)$$

Note that E(t) and F(t) represent the displacement of the interface due to the perturbation.

This system has thus been reduced to four linear, non-autonomous differential equations of the form:

$$\dot{\underline{X}} = \left(\underset{\sim}{B} + \underset{\sim}{P}(t) \right) \underline{X} \qquad (4.21)$$

where $\underline{X}$ is the unknown vector function containing the time-dependent coefficients. $\underset{\sim}{B}$ is a constant matrix and $\underset{\sim}{P}(t)$ is the time-dependent matrix. (See Figure 4.1.)

4.3 Asymptotic stability

According to Sanchez[23], non-autonomous linear systems of equations (in the form of equation (4.21)) are asymptotically stable if three conditions are satisfied:

(1) the characteristic polynomial of $\underset{\sim}{B}$ is stable,

(2) the matrix $\underset{\sim}{P}(t)$ is continuous on $0 \leq t < \infty$,

(3) $\int_0^\infty || \underset{\sim}{P}(t)|| \, dt < \infty$.

The functions which are selected will be shown to satisfy conditions (2) and (3). Condition (1) is ascertained by checking the characteristic polynomial of matrix $\underset{\sim}{B}$. For a stable solution of equation (4.21), the four roots of the characteristic polynomial of $\underset{\sim}{B}$ must have non-positive real components (see Appendix 3). Hence, solutions of equation (4.21) are bounded and stable.

Having ascertained the asymptotic stability of the fluid configuration, the time response of the interfaces in the

$$\begin{vmatrix} \dot{A} \\ \dot{B} \\ \dot{E} \\ \dot{F} \end{vmatrix} = \left[\begin{vmatrix} 0 & 0 & \delta_{11}\left(\frac{k^2}{Bo_2}\right) & \delta_{12}\left(\frac{k^2}{Bo_3}\right) \\ 0 & 0 & \delta_{21}\left(\frac{k^2}{Bo_2}\right) & \delta_{22}\left(\frac{k^2}{Bo_3}\right) \\ ke^{k} & -ke^{-k} & 0 & 0 \\ k & -k & 0 & 0 \end{vmatrix} + \begin{vmatrix} 0 & 0 & \frac{\delta_{11}(1-\rho 21)g(t)}{\rho_{D1}} & \frac{\delta_{12}(\rho 31-1)g(t)}{\rho_{D1}} \\ 0 & 0 & \frac{\delta_{21}(1-\rho 21)g(t)}{\rho_{D1}} & \frac{\delta_{22}(\rho 31-1)g(t)}{\rho_{D1}} \\ 0 & 0 & 0 & 0 \\ 0 & 0 & 0 & 0 \end{vmatrix} \right] \begin{vmatrix} A \\ B \\ E \\ F \end{vmatrix}$$

$$\dot{X} = (R+P(t))\,X$$

where $\delta_{11} \equiv \dfrac{(1+\rho 31)\rho_{D1}}{-\left[(1+\rho 21)(1+\rho 31)e^{k} + (1-\rho 31)(1-\rho 21)e^{-k}\right]}$

$\delta_{12} \equiv \dfrac{(\rho 21-1)\rho_{D1}e^{-k}}{\left[(1+\rho 21)(1+\rho 31)e^{k} + (1-\rho 31)(1-\rho 21)e^{-k}\right]}$

$\delta_{21} \equiv \dfrac{(1-\rho 31)\rho_{D1}}{-\left[(1+\rho 21)(1+\rho 31)e^{k} + (1-\rho 31)(1-\rho 21)e^{-k}\right]}$

$\delta_{22} \equiv \dfrac{(1+\rho 21)\rho_{D1}e^{k}}{\left[(1+\rho 21)(1+\rho 31)e^{k} + (1-\rho 31)(1-\rho 21)e^{-k}\right]}$

Figure 4.1

presence of forcing is investigated. The "short duration" non-periodic body force functions which have been constructed do not modify the asymptotic stability of the multi-layer fluid configuration. Interest is in the level of system disturbance in the presence of the acceleration, (eg. E(t) and F(t)). Since the effects of viscosity are not incorporated into the analysis, the long time behavior of the system is not physically meaningful. However, long-duration responses will be examined to investigate asymptotic stability.

Note that for asymptotic stability, the forcing function must be bounded. That is, if g(t) was chosen to be periodic (say a cosine function), condition (3) of Sanchez would be violated, and the system of equations would not be asymptotically stable. This does not imply that the fluid configuration is unstable to periodic forcing. In Chapter 3, it was shown that there exist regions of parametric stability in the presence of periodic forcing.

4.4 Results

4.4a Solution methodology

The system of first-order differential equations, (4.17-4.20), is integrated via DIVPAG of the IMSL library. This routine utilizes Gear's method to solve for the time-dependent coefficients[4]. (See Appendix 9.)

It was found to be more convenient to represent the fourth order system in terms of $(E,F,\dot{E},\dot{F})$. This is accomplished by differentiating equations (4.19,20) and substituting into equations (4.17,18) to eliminate A(t) and B(t). This system is given as follows:

$$\ddot{E} = \left[k\beta_1(\beta_2+\beta_3) + k(\beta_4-\beta_5) \right] F - k\beta_1(\beta_6-\beta_7)\, E \qquad (4.22)$$

$$\ddot{F} = \left[k\beta_8(\beta_2+\beta_3) + k(\beta_9-\beta_{10}) \right] F - k\beta_8(\beta_6-\beta_7)\, E \qquad (4.23)$$

where

$$\beta_1 = \frac{(-(1+\rho_{31})e^{k} - e^{-k}(1-\rho_{31}))\,\rho_{D1}}{(1+\rho_{21})(1+\rho_{31})e^{k} + (\rho_{21}-1)(1-\rho_{31})e^{-k}}$$

$$\beta_2 = \frac{-(1+\rho_{21})g(t)e^{k}}{\rho_{D1}} \qquad \beta_3 = \frac{(1+\rho_{21})k^2e^{k}}{(1-\rho_{31})Bo_3}$$

$$\beta_4 = \frac{k^2\rho_{D1}e^{k}}{Bo_3(1-\rho_{31})} \qquad \beta_5 = g(t)e^{k}$$

$$\beta_6 = \frac{(\rho_{21}-1)g(t)}{\rho_{D1}} \qquad \beta_7 = \frac{k^2}{Bo_2}$$

$$\beta_8 = \frac{-2\rho_{D1}}{(1+\rho_{21})(1+\rho_{31})e^{k} + (\rho_{21}-1)(1-\rho_{31})e^{-k}}$$

$$\beta_9 = \frac{k^2\rho_{D1}}{Bo_3(1-\rho_{31})} \qquad \beta_{10} = g(t)$$

The system was integrated for specified non-zero $(\dot{E}_o, \dot{F}_o)$ values with E_o, F_o both taken to be zero. The E(t) and F(t) coefficients define the time-development of the interface. $\dot{E}_o$ and $\dot{F}_o$ are determined from equations (4.12,4.13) where C_o=-0.05 and D_o=0.05. These values were chosen arbitrarily but are required to be small to satisfy the restriction to linearity. The signs were chosen to ensure that both interfaces had the same direction for their respective velocity fields. This was decided solely to provide a more realistic physical system. Different values of C_o and D_o were investigated with qualitatively similar results.

Two time-dependent forcing cases (for $t \geq 0$) are investigated and are defined as follows:

$$1: \quad g(t) = te^{(-t+1)}$$

$$2: \quad g(t) \begin{cases} = 0 & \text{if } 0 \leq t < 1 \\ = t-1 & \text{if } 1 \leq t < 2 \\ = 1 & \text{if } 2 \leq t < 3 \\ = -t+4 & \text{if } 3 \leq t < 5 \\ = -1 & \text{if } 5 \leq t < 6 \\ = t-7 & \text{if } 6 \leq t < 7 \\ = 0 & \text{if } t \geq 7 \end{cases}$$

Case 1 represents exponential growth followed by exponential decay. Case 2 represents a ramped step function with forcing in the positive and negative $\hat{e}_z$ directions. Each forcing function is shown in Figures (4.11-4.34) as a solid line. Both cases have an initial value of zero forcing and are continuous on $0 \leq t < \infty$; hence, condition (2) for asymptotic stability is satisfied.

Condition 3) requires that the integral over infinity of the absolute value of the forcing function be finite. For forcing case 1 (exponential ramp), the integral is solved by integration by parts.

$$\int_0^{\infty} || te^{(-t+1)} || \, dt = e^1 < \infty$$

For the step forcing function, case 2, the integral is subdivided into appropriate time steps and is found to equal 4. (Note that due to the absolute value in the integral, negative values of the forcing do not cancel out positives.) Hence, for both forcing cases the integral is finite, and condition (3) of Sanchez is satisfied.

The time interval extends in the range, $0 \leq t < t_o$, where t_o is a value of time significantly greater than the outer bound of the forcing function.

The time response of each forcing case is investigated for parameter values pertinent to a microgravity environment.

$$k = 0.5,\ 1.0,\ 2.0$$
$$Bo_2 = 1.0,\ 0.1$$
$$Bo_3 = 1.0(Bo_2),\ 2.0(Bo_2)$$

These values correspond to physically realistic configurations where values of G_o range from 10^{-3} to 10^{-5} * g_{earth}.

Two fluid systems are considered:

1) gas/liquid/gas ($\rho_{21}=\rho_{31}=0.001225$)

2) liquid/liquid/liquid ($\rho_{21}=1.0,\ \rho_{31}=1.5$)

The reverse of system 2), ($\rho_{21}=1.5,\ \rho_{31}=1.0$), is investigated since the forcing cases are directional, and the behavior is fundamentally different.

4.4b Numerical results

The shape of the interface is defined by E(t) and F(t), which are the perturbation displacements. The time response of E(t) and F(t) are examined for the said parameter space as described in section (4.4a).

Discussion of zero forcing:

The case of zero forcing was studied to show the time behavior of E(t) and F(t) in the absence of transient accelerations. As expected, the numerical results were consistent with the fact that the configuration is asymptotically stable[23]. Results show an oscillatory pattern that neither grows nor decays exponentially in time (See Figures (4.2-4.10)). The perturbations are wavelike. Note that the variation of the interface perturbations in the zero forcing case is not uniform and sinusoidal. This is due to the coupling effect of the two interfaces, which have different velocities according to equations (4.12,4.13). With careful selection of constants C_o and D_o for a specific wave number, the initial velocities of each interface could be set equal ($\dot{E}(t)=\dot{F}(t)$). In the subcase of $\dot{E}(t)=\dot{F}(t)$ and $\rho_{21}=\rho_{31}$, the time variation of the perturbations is sinusoidal. Although equal interface velocities provides a more uniform wave on the interfaces, it is recognized as a special case. The general case, with fixed C_o and D_o and hence unequal $\dot{E}$ and $\dot{F}$, is investigated in the results.

Also note that as the wave number increases (Figures 4.2,4.3,4.4), the amplitude of the perturbation becomes larger in magnitude. This is due to the k dependence of the interface velocities (equations 4.12,4.13). Moreover, note that the selection of C_o and D_o must be such that all quantities do not violate linear theory.

For a fixed wave number for the zero forcing cases, the amplitudes of E and F are smaller for the gas/liquid/gas configuration than for the liquid/liquid/liquid systems (compare figure 4.9 with 4.3,4.6 where k=1.0). This is due to decreased dynamical effects from the gas regions. Different wave numbers provide similar results.

Discussion of impulse forcing (exponential ramp):

Figures 4.11-4.28 show moderate-duration responses of each interface to impulse forcing for the specified parameter space. Figures 4.11-4.19 correspond to the exponential ramp forcing case. Note that the forcing function is displayed on the graphs as a solid line. Physically, this function simulates short-duration impulse forcing which might be due to disturbances such as astronaut motion. By no way do the selected functions represent the entire class of possible impulses. It should be pointed out that positive values of the forcing correspond to accelerations in the negative $\hat{e}_z$ direction.

Figure 4.11 represents a liquid/liquid/liquid configuration with the most dense fluid being on the bottom (ρ_{21}=1.0, ρ_{31}=1.5). The interfaces oscillate in time with a fairly periodic motion. It is clear that the response is greater in magnitude for higher values of $Bo_2(Bo_3)$. Bo values are inversely proportional to surface tension; hence, an increase in Bo is associated with a decrease in the restoring force at the interfaces. A decreased restoring force will lead to enhancement of the interface displacement. This trend is typical throughout the results. Note also that there is an increase in the period of the perturbation for higher Bo values. Henceforth, discussion will pertain to responses for $Bo_2(Bo_3)$=1.0 unless otherwise noted.

Comparing Figure 4.11 with 4.2 (the same fluid system with no forcing, k=0.5), there is an enhancement of the interface displacements in the presence of forcing. The upper interface in the zero forcing case has ΔE_{max}= 0.13 which increased to 0.21 in the presence of the ramp forcing. This is a 62% amplification due to impulse forcing. Likewise, at the lower interface, ΔF_{max} increased from 0.14 to 0.24 for a 72% enhancement. (Note: $\Delta E_{max} = E_{max} - E_{min}$).

The wave number in Figure 4.12 is increased to 1.0 while holding other parameters fixed. Oscillatory motion still occurs. Comparing with Figure 4.3 (zero forcing for the same configuration), there is no enhancement at either interface. In Figure 4.13 (k=2.0), the ramp forcing results in a smaller

interface displacement as compared to that of the zero forcing case (Figure 4.4). Recall that positive values of g(t) correspond to accelerations in the negative $\hat{e}_z$ ("downward") direction. The greatest forcing for the ramp function occurs between t=0 and t=5. During this time period, the interfaces for Bo=1.0, particularly the lower interface (F), are accelerating in the positive $\hat{e}_z$ direction. The net acceleration is smaller than for the zero forcing case, hence the "negative enhancements" of -30% and -40% at the upper and lower interfaces, respectively.

Note that in both Figures 4.4 and 4.13, for Bo=0.1 and k=2.0, both interfaces are accelerating in the negative $\hat{e}_z$ direction during the time period in which the peak of the ramp forcing occurs. Note again that the ramp function is in the negative $\hat{e}_z$ direction. Thus the net acceleration is greater for the forced case with amplitude enhancements at upper and lower interfaces of 15% and 30%, respectively.

Note that the results are contrary for Bo=1.0 and Bo=0.1 at this k value of 2.0.

The configuration is inverted for Figures 4.14-4.16, that is, ρ_{21}=1.5, ρ_{31}=1.0. Such a configuration has an unfavorable density gradient with respect to the direction of the forcing (ie., a more dense fluid is oriented above a less dense one). The enhancement of the perturbation amplitude due to forcing (Figure 4.14) compared to the zero forcing case (Figure 4.5) for k=0.5 is 67% at the upper interface (E) and 90% at the

lower interface (F). For k=1.0, the upper and lower interface amplifications due to ramp forcing are 12% and 11%, respectively. As with Figure 4.13 (ρ_{21}=1.0, ρ_{31}=1.5), the situation is reversed for k=2.0, with the non-forced case exhibiting larger perturbation amplitudes. Inspection of the interfaces for zero forcing (Figure 4.7) at Bo=1.0 show perturbation accelerations in the opposite direction of the impulse forcing during the critical time period (t=0 to t=5).

In general, the enhancements for the unfavorable density gradient configuration (ρ_{21}=1.5, ρ_{31}=1.0) are greater than those of the favorable one.

Figures 4.17-4.19 correspond to a gas/liquid/gas configuration. Difference between forced and unforced cases are most dramatic at k=2.0. In Figure 4.19, there is "negative enhancement" for the ramp forcing as compared to the zero forcing (Figure 4.10). The upper interface exhibits little change, but the lower interface (F) has a 31% decrease in perturbation amplitude in the forced case. As in the liquid/liquid/liquid configurations, the cause is an interface acceleration in the opposite direction of the impulse forcing.

In general, in the presence of ramp forcing the enhancement is greater at the lower interface. Recall that the forcing is mono-directional (downward); hence there is a true "upper" and a "lower" interface in terms of the acceleration field.

Discussion of impulse forcing (bi-directional step):

The step forcing function is employed in Figures 4.20-4.28. This implies that the acceleration is bi-directional (that is, an interface may experience a favorable density gradient at one moment and an unfavorable one at another time in its history).

Figures 4.20-4.22 correspond to a liquid/liquid/liquid configuration (ρ_{21}=1.0, ρ_{31}=1.5). Again it is observed that high surface tension (low Bo values) relate to minimal distortion of the interfaces. As with the exponential ramp forcing function, there is enhancement of perturbation amplitude at low wave numbers as compared to the zero forcing cases. In Figure 4.20 (k=0.5) the upper and lower interfaces are enhanced by 160% and 200%, respectively. This amplification due to the step function is considerably larger than the enhancement of the same configuration in the presence of ramp forcing (Figure 4.11). For k=1.0 (Figure 4.21) there is slight enhancement of 3% and 10% for interfaces E and F. Figure 4.22 (k=2.0) shows "negative enhancement". Note on Figure 4.22, the lower interface response for Bo=1.0 is in "phase" with the step forcing function but opposite in direction. During the period of forcing (t=1 to t=7), the perturbation is in effect opposed, hence the reduction in amplitude. The long wavelength perturbations (low k values) are not "in phase" with the selected forcing functions; therefore, enhancement occurs even if the interface acceleration is opposite in direction to the forcing.

Figures 4.23-4.25 are for the case with the density ratios reversed and offer qualitatively similar results. Since the configuration is subjected to bi-directional forcing, there is no true "upper" or "lower" interface with respect to the orientation of the forcing. Figure 4.23 (k=0.5) shows enhancements of 215% and 170% for interfaces E and F, respectively. For k=1.0 (Figure 4.24), the amplification of E as compared to the zero forcing case is 17% and for F, 21%. For k=2.0 (Figure 4.25), there is "negative enhancement" at both interfaces. Again, note the "phasing" between the lower interface response and the period of the forcing.

It should be pointed out that the greatest enhancement in perturbation amplitude for the bi-directional forcing occurs at the interface with $\rho_{21}(\rho_{31})$=1.5 rather than 1.0. That is, the interface with a density difference across it experiences greater enhancement. In general, this trend is typical for Figures 4.20-4.25.

The gas/liquid/gas configuration in the presence of step function forcing is represented by Figures 4.26-4.28. In general, such configurations have more uniform oscillations. As occurred with exponential ramp forcing, it is the k=2.0 configuration in which differences between the forced and unforced case are most dramatic. For k=2.0 in the forced case (Figure 4.28), there is an increase in the amplitude of the interfaces: E (25%) and F (32%). Recall that for all other cases with k=2.0, there is "negative enhancement". The

"phasing" between the interface response and the forcing period is the critical factor. Note on Figure 4.28, when the forcing is clipped (t=7), both interfaces are perturbed at a large amplitude, hence a "positive enhancement". Comparing with Figure 4.25, both perturbations have small displacements at t=7; the oscillation is in "phase" with the forcing period. Therefore, this case has "negative enhancement". At low k values (long wavelengths), for the selected forcing functions, phasing does not occur; thus in general, the impulse forcing enhances the perturbation.

The effect of unequal Bo values is addressed in Figures 4.29-31, where in each case $Bo_3=2*Bo_2$. That is, the surface tension of the bottom interface is half that of the top. Note that the case of equal Bo values appears on the graphs for purposes of comparison. The cases involving the doubling of one of the Bo values show an enhancement of the interface displacement as compared to the equal Bo case. In Figure 4.29, the amplification for $Bo_3=2*Bo_2$ is 28% greater at E and 100% larger at F as compared to the equal Bo case. Figure 4.30 shows a different configuration but similar results. The effect of doubling Bo_3 actually has a slight "negative enhancement" (-1%) on interface E, but a 100% amplification on F. Figure 4.31 represents a gas/liquid/gas configuration subjected to ramp forcing. Doubling Bo_3 corresponds to amplifications of 26% on interface E and 58% on interface F. In all cases of $Bo_3=2*Bo_2$, the greatest enhancement occurs on interface F.

doubling the Bo value on this interface corresponds to halving its surface tension. It is of interest that in the liquid/liquid/liquid configurations (Figures 4.29,4.30), doubling the Bo value of an interface corresponds to a 100% amplification of that interface.

It has been discussed that consideration of "long-duration" responses is not physically realistic due to the absence of viscosity. Surely viscous effects would play an important damping role (ie., in time, we would expect that long after the forcing dies out, the perturbation amplitude should be damped). For an inviscid system the perturbations, even in the absence of any forcing, continue to oscillate ad infinitum. Therefore, there is no physical relevance to the long-duration response. However, the extension of calculations out to these larger times yielded numerical results which are consistent with the known (mathematical) asymptotic stability of the configuration.

Figures 4.32-4.34 display long-duration responses for various parameters. The two figures in each left column represent zero forcing. The oscillatory nature of the perturbation is apparent. The two figures in the right column represent the same configuration in the presence of the designated forcing. Although all three figures show an enhancement in the amplitude in the case of forcing, this is not to suggest that impulse forcing causes enhancement of the zero forcing case for all parameter space. (Recall the ramp forcing case for k=2.0 where negative enhancements occur.) The

period of the oscillation in the forced cases is approximately equal to the period of the zero forcing case. During this time period ($0<t<200$), the response of the interfaces is not growing exponentially in time. Nondimensional time periods up to $t=1000$ were examined with similar results.

In general, the presence of impulse forcing causes enhancement of interface displacement (in the case of low k, long wavelength disturbances). Depending on the phasing between the oscillation of the interface and the period of the forcing function, a reduction in interface amplitude may occur for some parameter space, particularly at higher wave numbers.

The interface behavior for a given configuration may be very different for various impulse accelerations. Recall that the displacements for the gas/liquid/gas configuration at $k=2.0$ were smaller in the presence of ramp forcing but were enhanced when subjected to step forcing. The possibility of enhancement could cause adverse effects on materials processing applications.

Time Response of the Interfaces

$g(t)=0$

$\rho_{21} = 1.0 \quad \rho_{31} = 1.5$

$k=0.5$

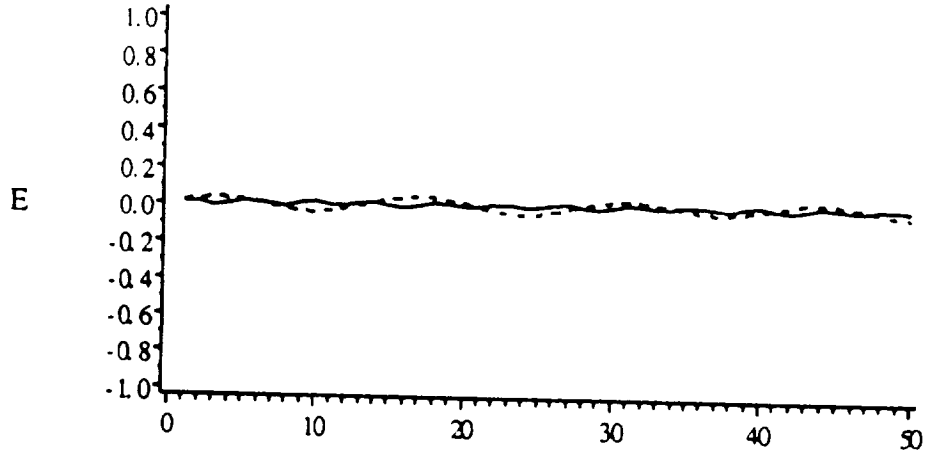

Bo values: $Bo_2 = Bo_3$

—— 0.1 ---- 1

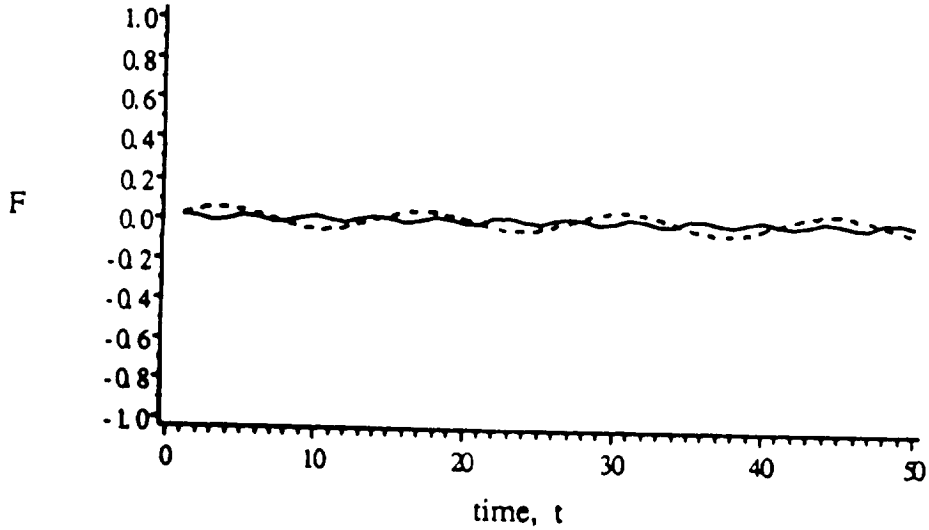

Bo values: $Bo_2 = Bo_3$

—— 0.1 ---- 1

Figure 4.2

Time Response of the Interfaces

$g(t)=0$

$\rho_{21} = 1.0 \quad \rho_{31} = 1.5$

$k=1.0$

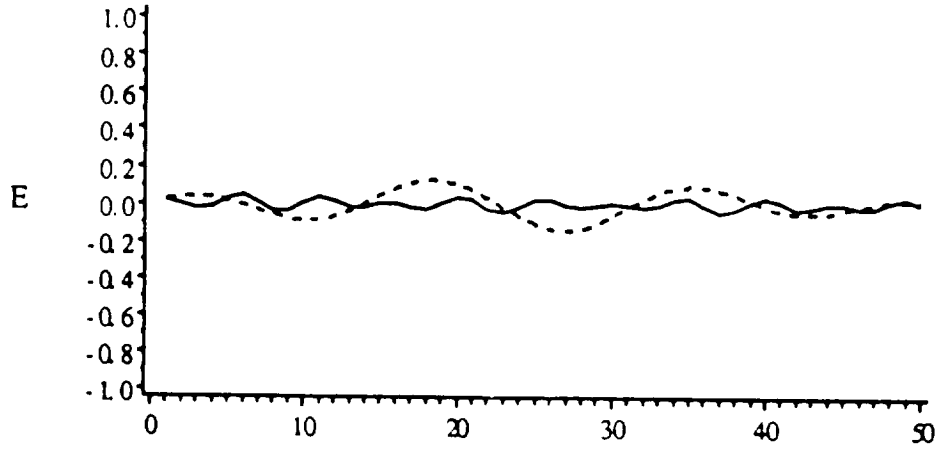

Bo values: $Bo_2 = Bo_3$

—— 0.1 ---- 1

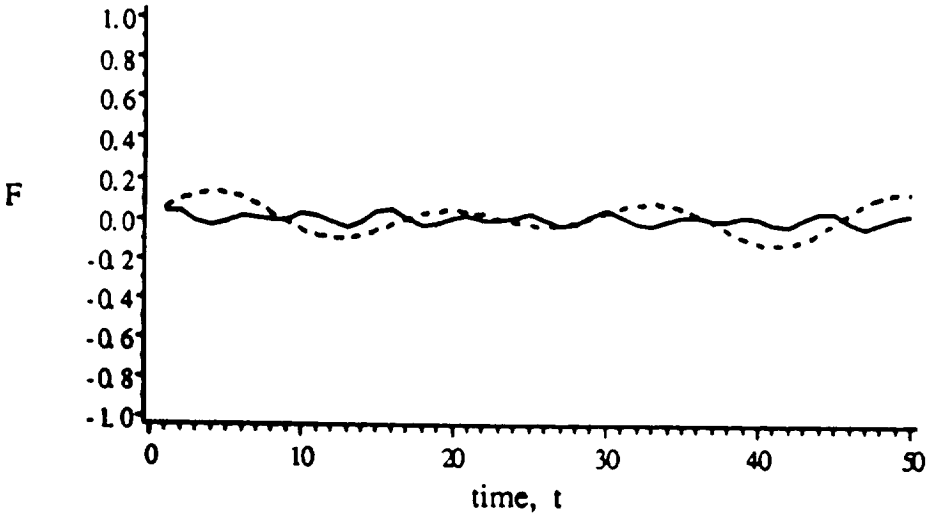

Bo values: $Bo_2 = Bo_3$

—— 0.1 ---- 1

Figure 4.3

Time Response of the Interfaces

$g(t)=0$

$\rho_{21} = 1.0 \quad \rho_{31} = 1.5$

$k=2.0$

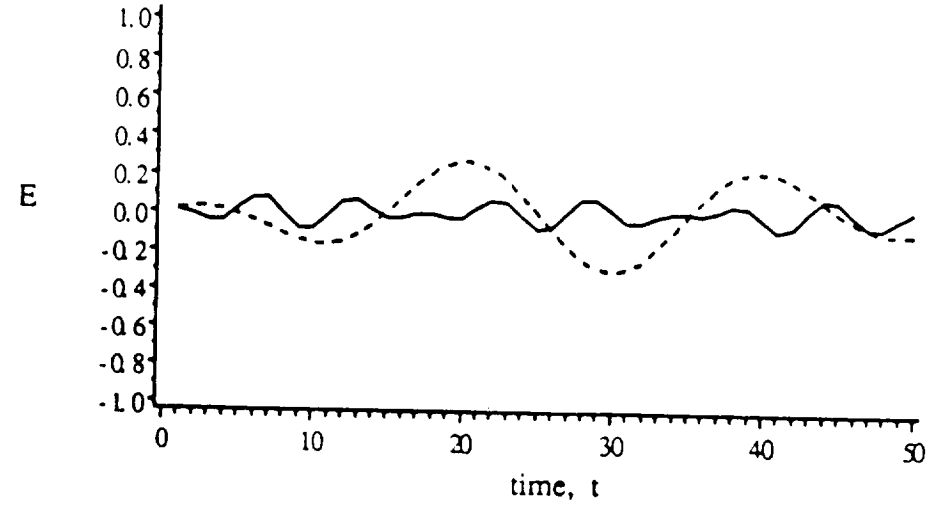

Bo values: $Bo_2 = Bo_3$

—— 0.1 ---- 1

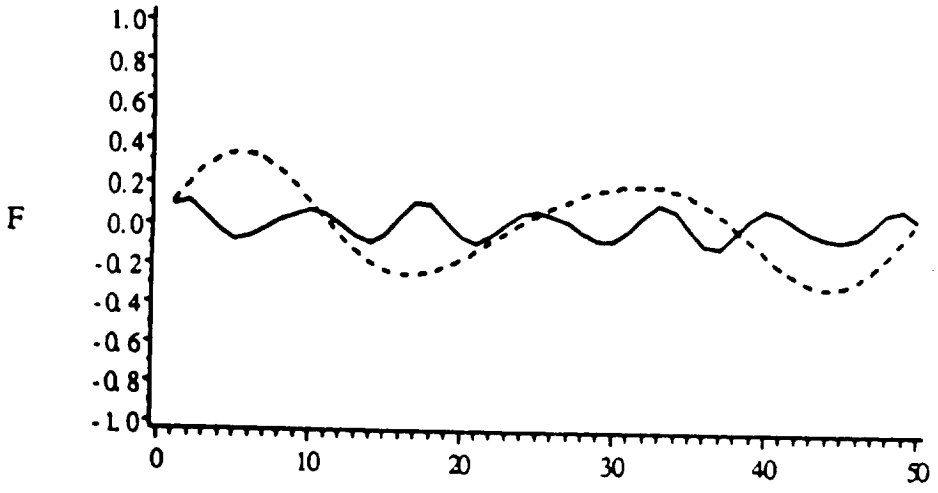

Bo values: $Bo_2 = Bo_3$

—— 0.1 ---- 1

Figure 4.4

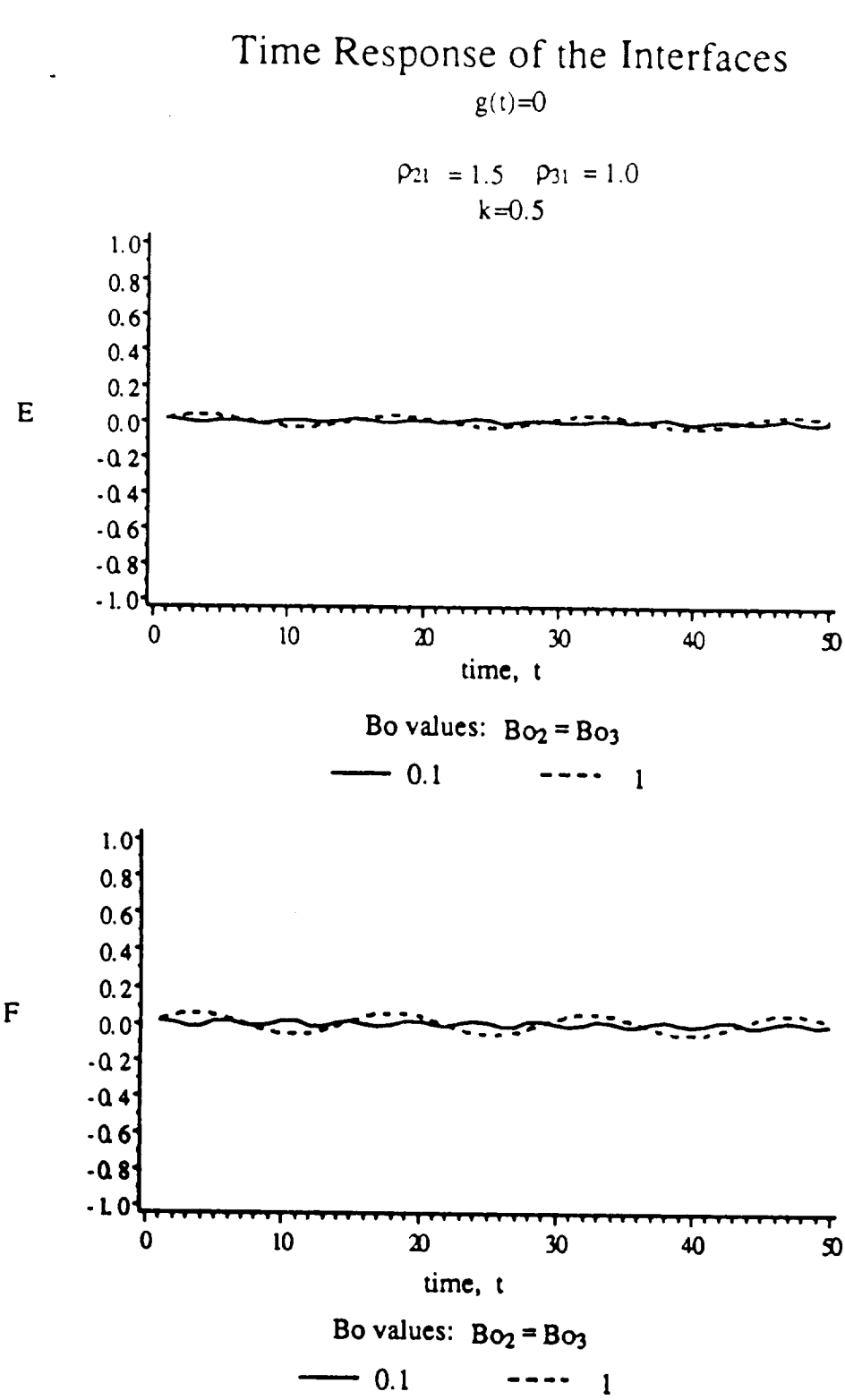
Time Response of the Interfaces
g(t)=0
ρ21 = 1.5 ρ31 = 1.0
k=0.5
E
1.0
0.8
0.6
0.4
0.2
0.0
-0.2
-0.4
-0.6
-0.8
-1.0
0
10
20
30
40
50
time, t
Bo values: Bo2 = Bo3
0.1
1
F
1.0
0.8
0.6
0.4
0.2
0.0
-0.2
-0.4
-0.6
-0.8
-1.0
0
10
20
30
40
50
time, t
Bo values: Bo2 = Bo3
0.1
1

Figure 4.5

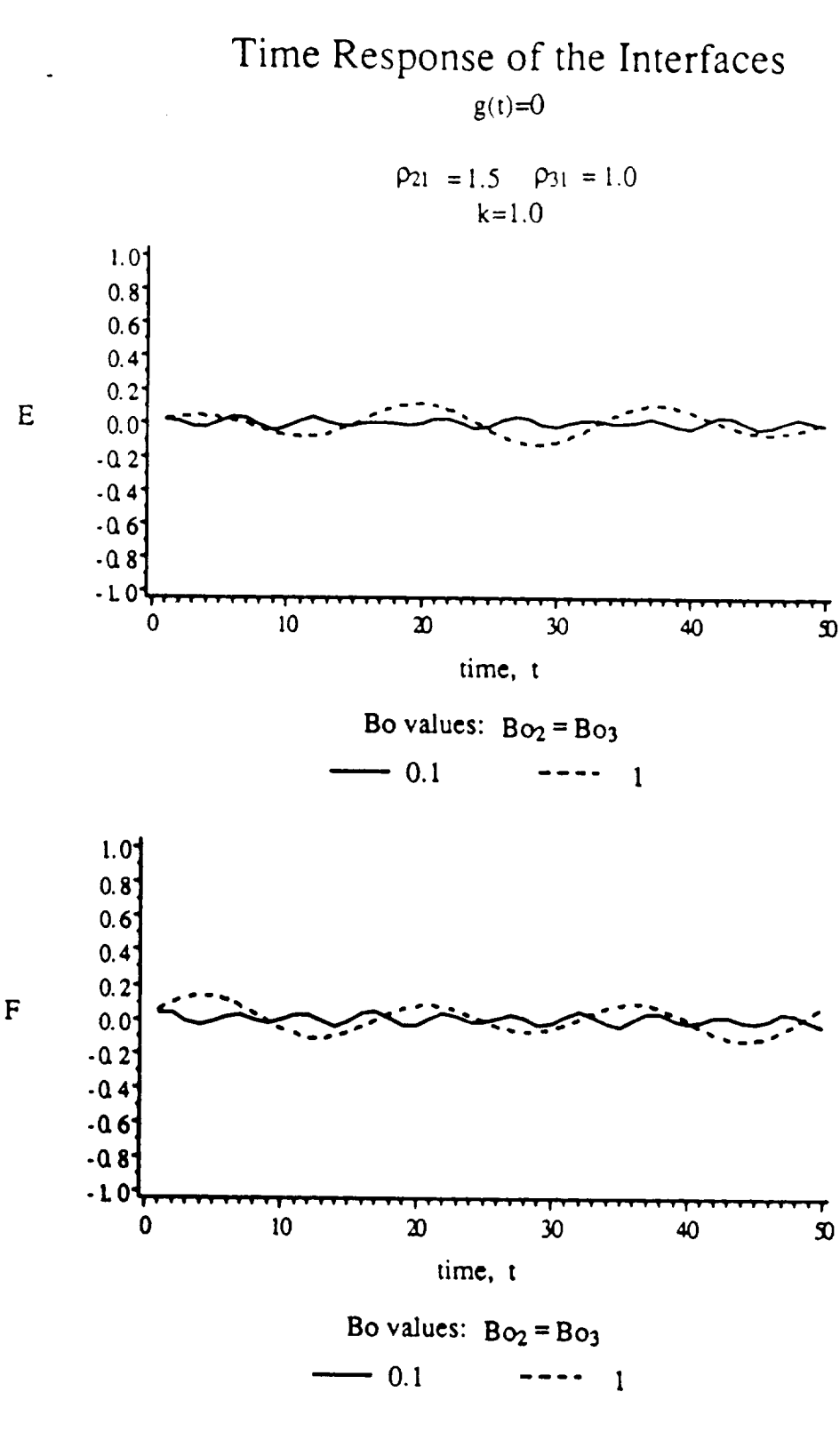
Time Response of the Interfaces
g(t)=0
ρ21 = 1.5 ρ31 = 1.0
k=1.0
E
1.0
0.8
0.6
0.4
0.2
0.0
-0.2
-0.4
-0.6
-0.8
-1.0
0
10
20
30
40
50
time, t
Bo values: Bo2 = Bo3
0.1
1
F
1.0
0.8
0.6
0.4
0.2
0.0
-0.2
-0.4
-0.6
-0.8
-1.0
0
10
20
30
40
50
time, t
Bo values: Bo2 = Bo3
0.1
1

Figure 4.6

Time Response of the Interfaces

$g(t)=0$

$\rho_{21} = 1.5 \quad \rho_{31} = 1.0$

$k=2.0$

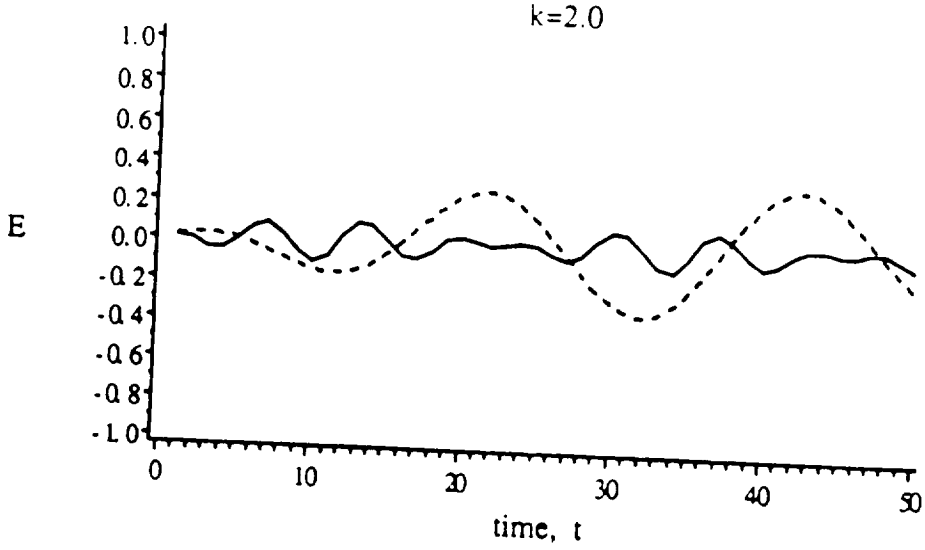

Bo values: $Bo_2 = Bo_3$

—— 0.1 ---- 1

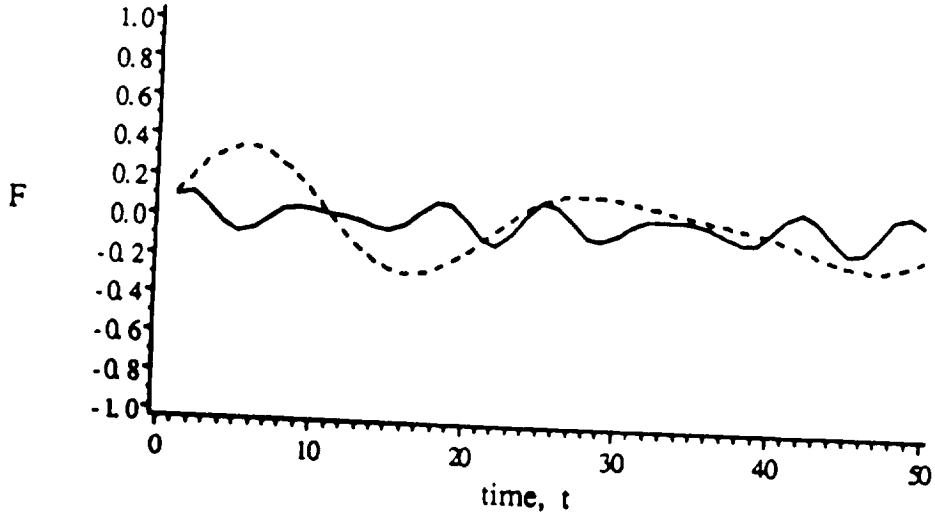

Bo values: $Bo_2 = Bo_3$

—— 0.1 ---- 1

Figure 4.7

Time Response of the Interfaces

$g(t)=0$

$\rho_{21} = \rho_{31} = 0.001225$

$k=0.5$

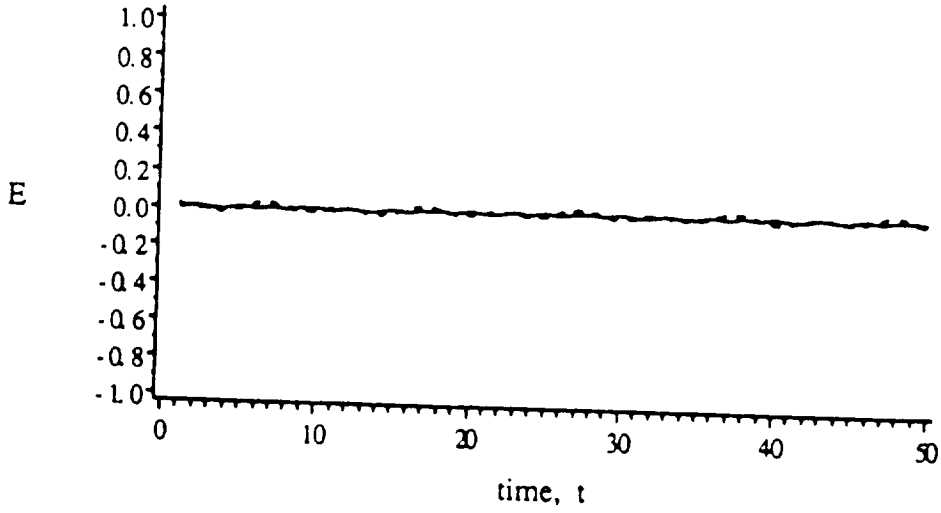

Bo values: $Bo_2 = Bo_3$

—— 0.1 ---- 1

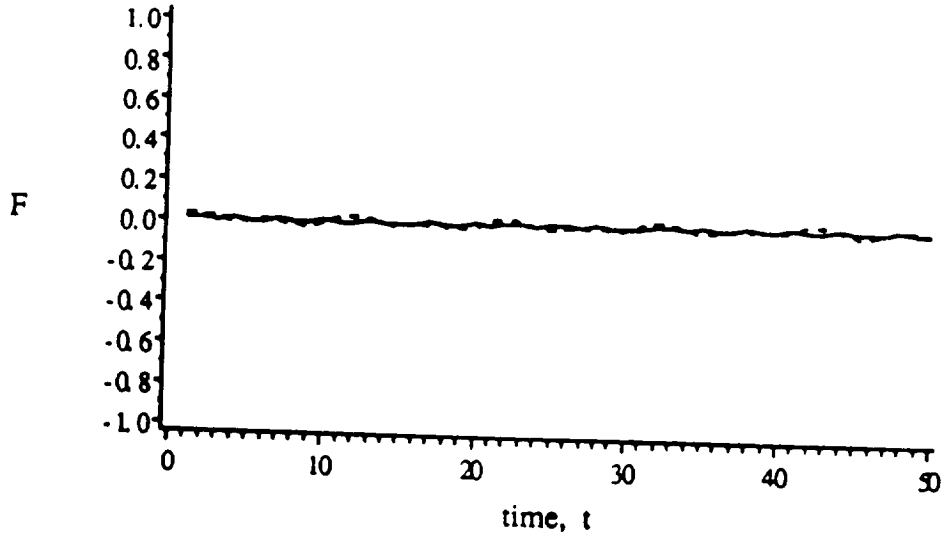

Bo values: $Bo_2 = Bo_3$

—— 0.1 ---- 1

Figure 4.8

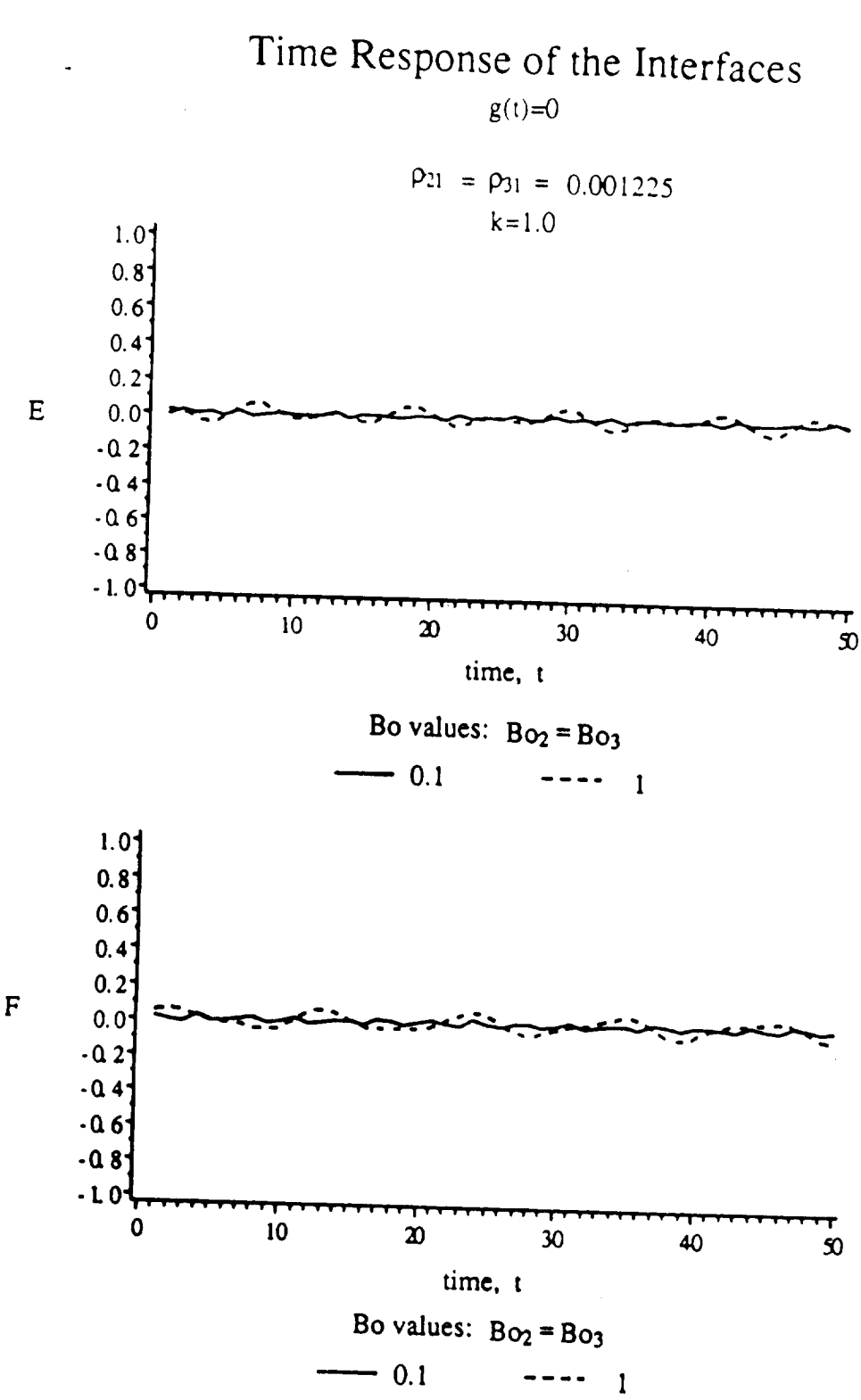
Time Response of the Interfaces
g(t)=0
ρ21 = ρ31 = 0.001225
k=1.0
E
1.0
0.8
0.6
0.4
0.2
0.0
-0.2
-0.4
-0.6
-0.8
-1.0
0
10
20
30
40
50
time, t
Bo values: Bo2 = Bo3
0.1
1
F
1.0
0.8
0.6
0.4
0.2
0.0
-0.2
-0.4
-0.6
-0.8
-1.0
0
10
20
30
40
50
time, t
Bo values: Bo2 = Bo3
0.1
1

Figure 4.9

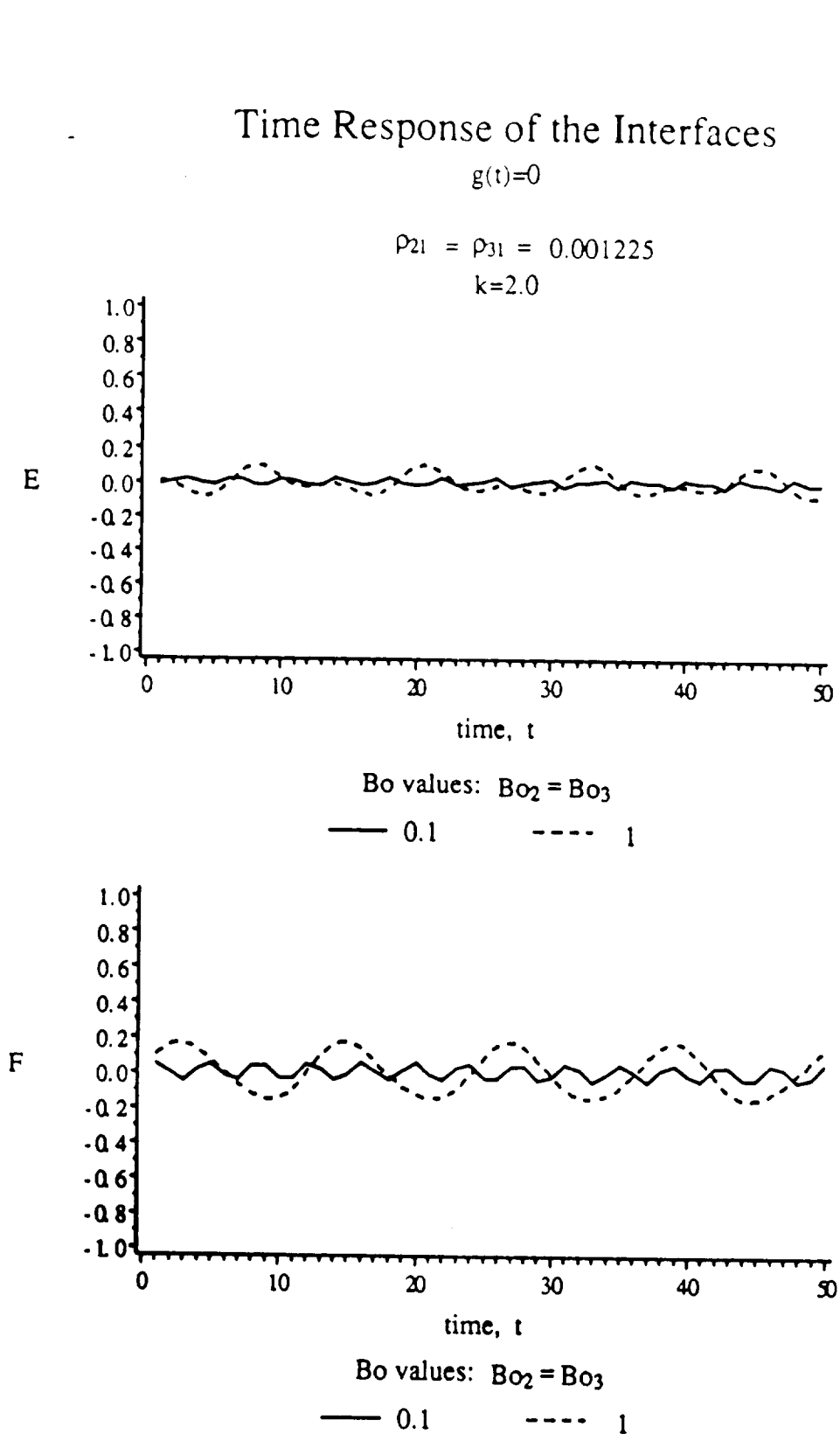
Time Response of the Interfaces
g(t)=0
ρ21 = ρ31 = 0.001225
k=2.0
E
1.0
0.8
0.6
0.4
0.2
0.0
-0.2
-0.4
-0.6
-0.8
-1.0
0
10
20
30
40
50
time, t
Bo values: Bo2 = Bo3
0.1
1
F
1.0
0.8
0.6
0.4
0.2
0.0
-0.2
-0.4
-0.6
-0.8
-1.0
0
10
20
30
40
50
time, t
Bo values: Bo2 = Bo3
0.1
1

Figure 4.10

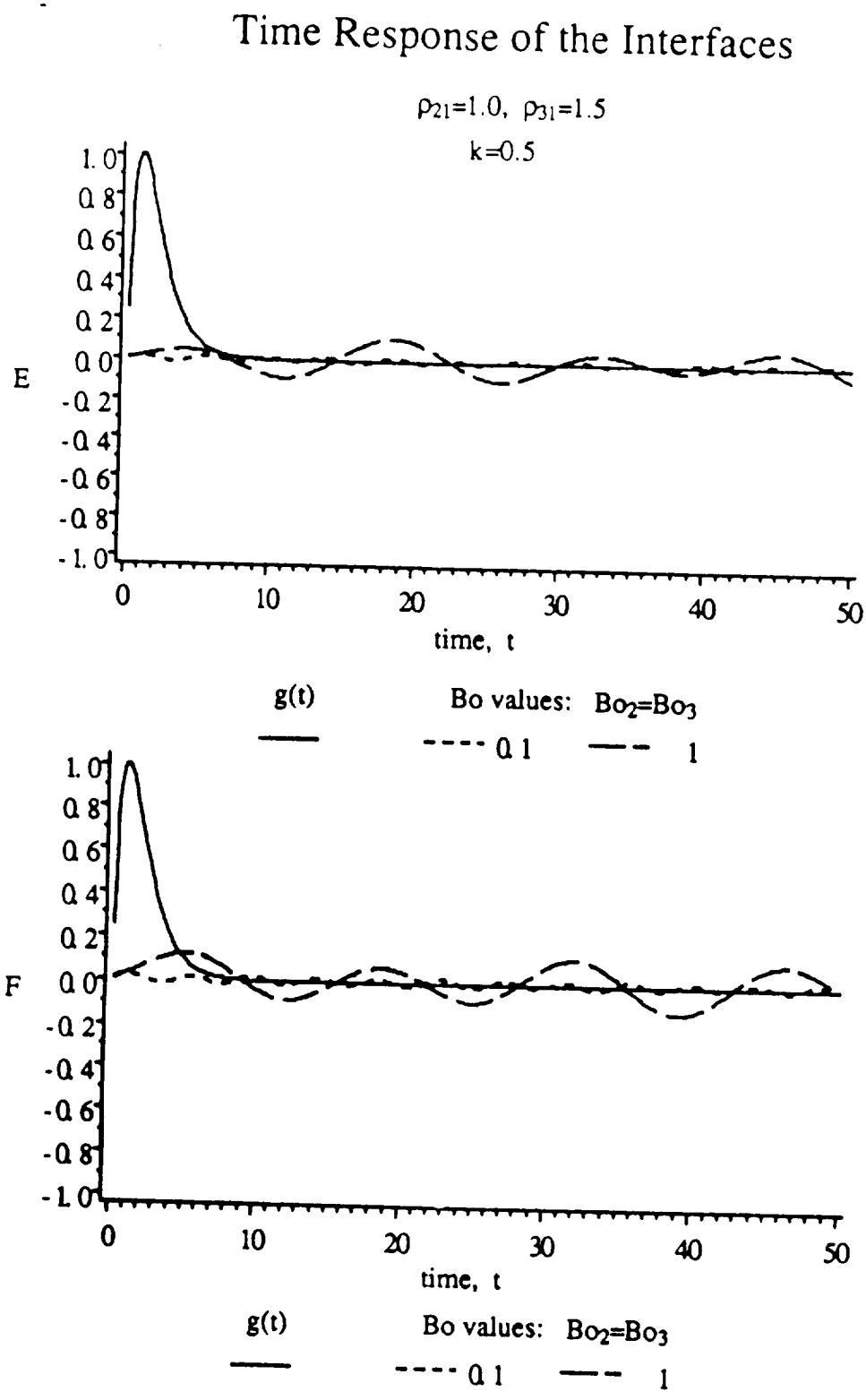
Time Response of the Interfaces
ρ_{21}=1.0, ρ_{31}=1.5
k=0.5
E
1.0
0.8
0.6
0.4
0.2
0.0
-0.2
-0.4
-0.6
-0.8
-1.0
0
10
20
30
40
50
time, t
g(t)
Bo values: Bo_2=Bo_3
0.1
1
F
time, t
g(t)
Bo values: Bo_2=Bo_3
0.1
1

Figure 4.11

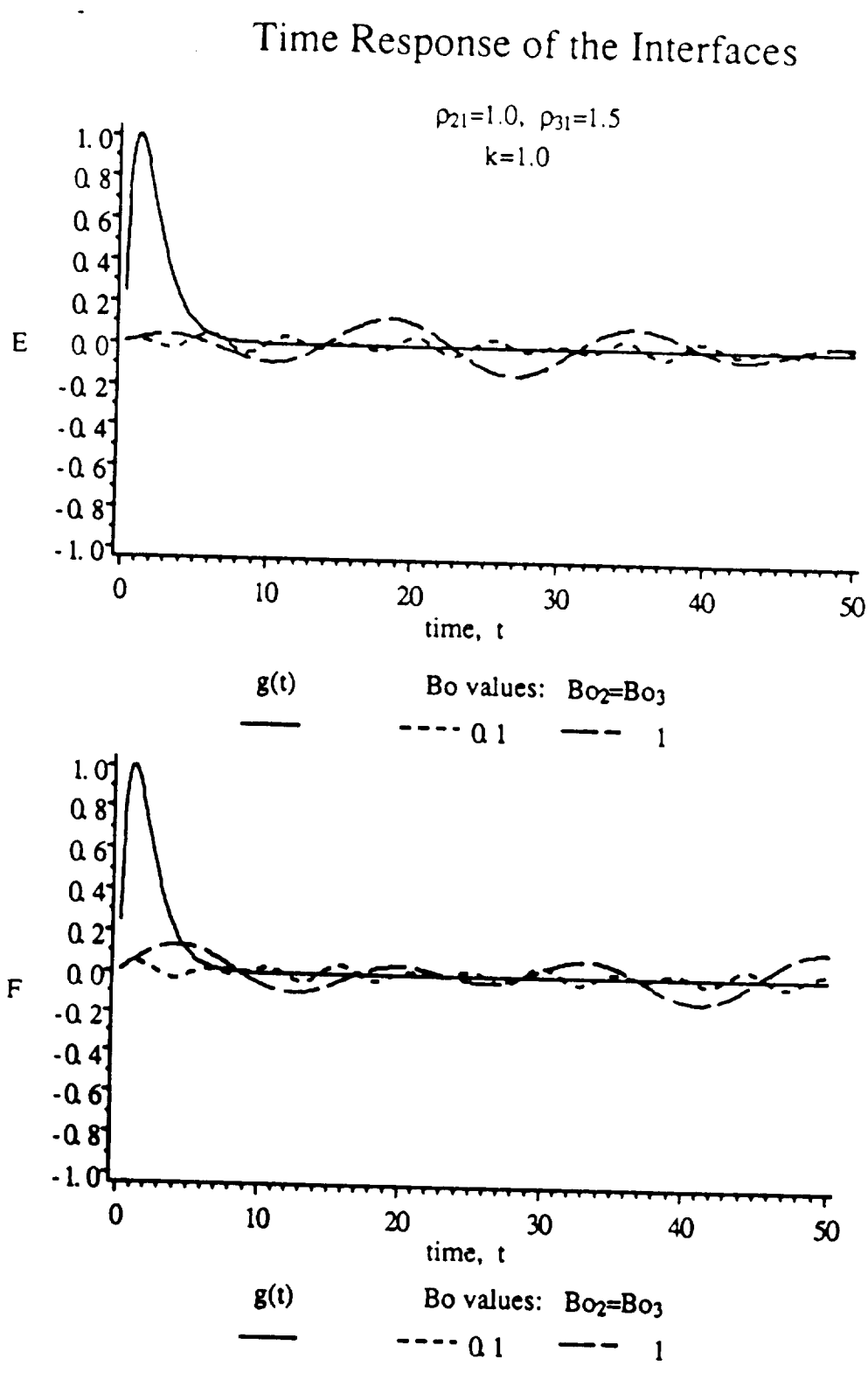
Time Response of the Interfaces
ρ21=1.0, ρ31=1.5
k=1.0
E
1.0
0.8
0.6
0.4
0.2
0.0
-0.2
-0.4
-0.6
-0.8
-1.0
0
10
20
30
40
50
time, t
g(t)
Bo values: Bo2=Bo3
0.1
1
F
1.0
0.8
0.6
0.4
0.2
0.0
-0.2
-0.4
-0.6
-0.8
-1.0
0
10
20
30
40
50
time, t
g(t)
Bo values: Bo2=Bo3
0.1
1

Figure 4.12

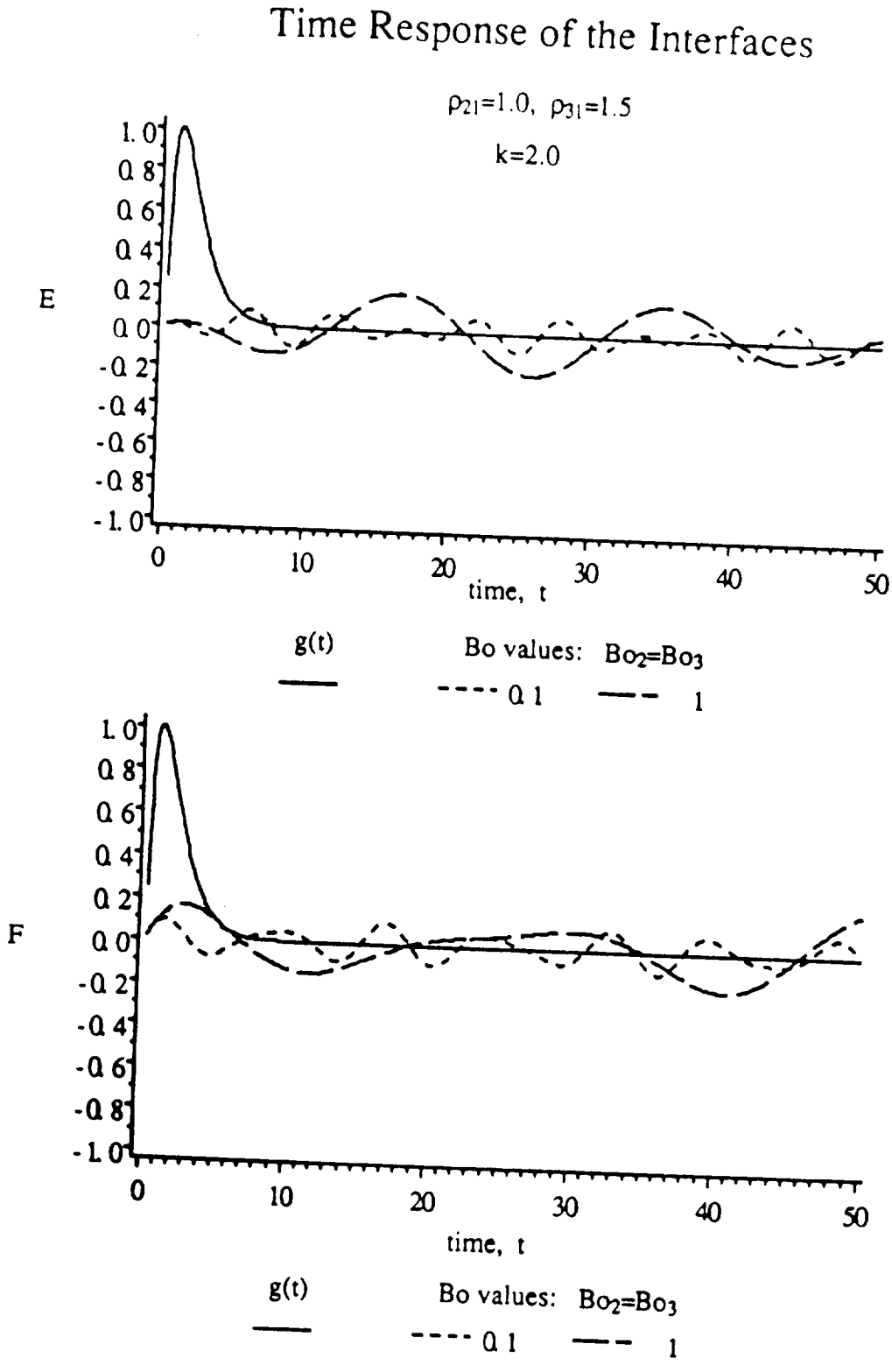
Time Response of the Interfaces
ρ_{21}=1.0, ρ_{31}=1.5
k=2.0
E
1.0
0.8
0.6
0.4
0.2
0.0
-0.2
-0.4
-0.6
-0.8
-1.0
0
10
20
30
40
50
time, t
g(t)
Bo values: Bo_2=Bo_3
0.1
1
F
1.0
0.8
0.6
0.4
0.2
0.0
-0.2
-0.4
-0.6
-0.8
-1.0
0
10
20
30
40
50
time, t
g(t)
Bo values: Bo_2=Bo_3
0.1
1

Figure 4.13

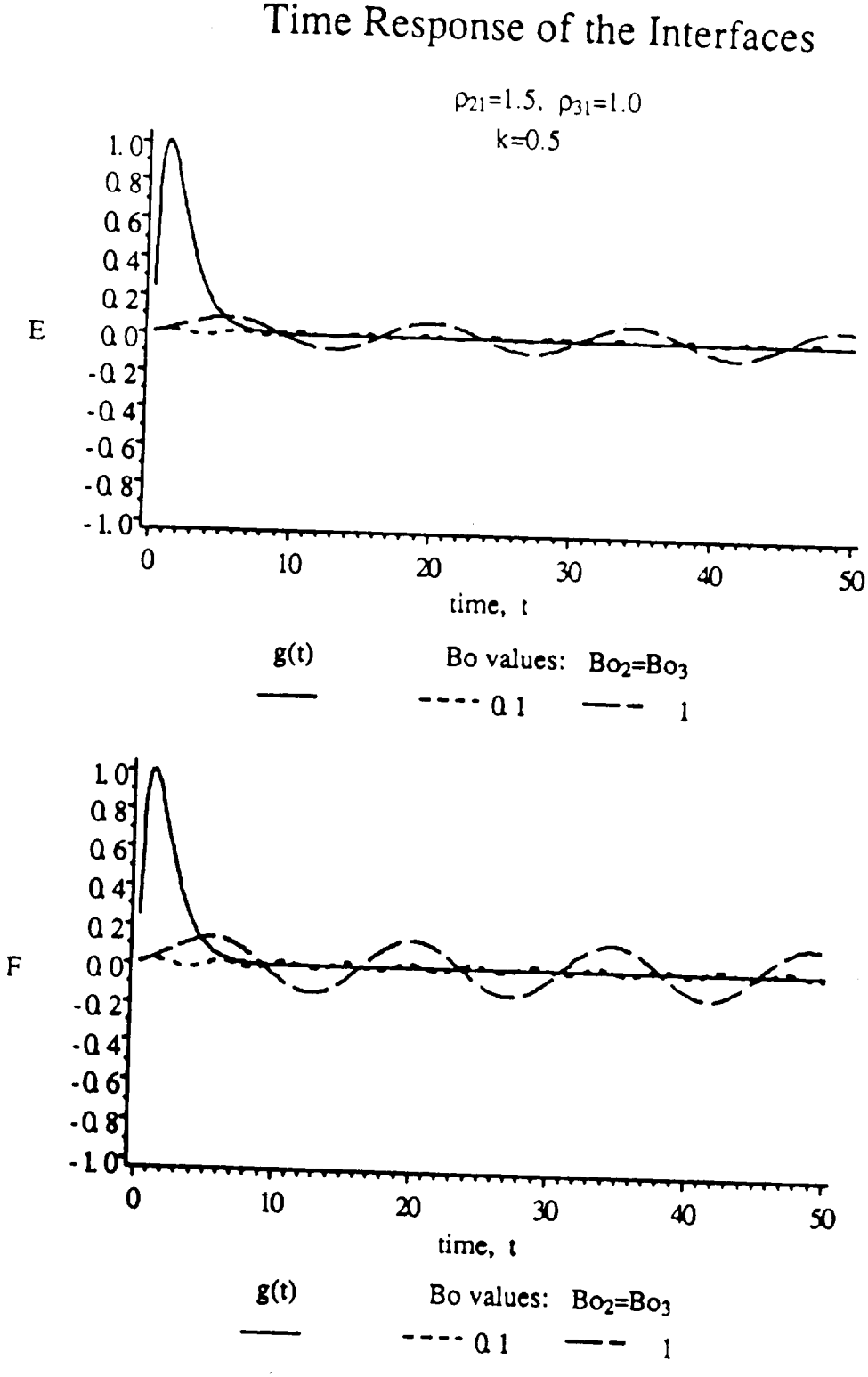
Time Response of the Interfaces
ρ_{21}=1.5, ρ_{31}=1.0
k=0.5
E
1.0
0.8
0.6
0.4
0.2
0.0
-0.2
-0.4
-0.6
-0.8
-1.0
0
10
20
30
40
50
time, t
g(t)
Bo values: Bo_2=Bo_3
0.1
1
F
1.0
0.8
0.6
0.4
0.2
0.0
-0.2
-0.4
-0.6
-0.8
-1.0
0
10
20
30
40
50
time, t
g(t)
Bo values: Bo_2=Bo_3
0.1
1

Figure 4.14

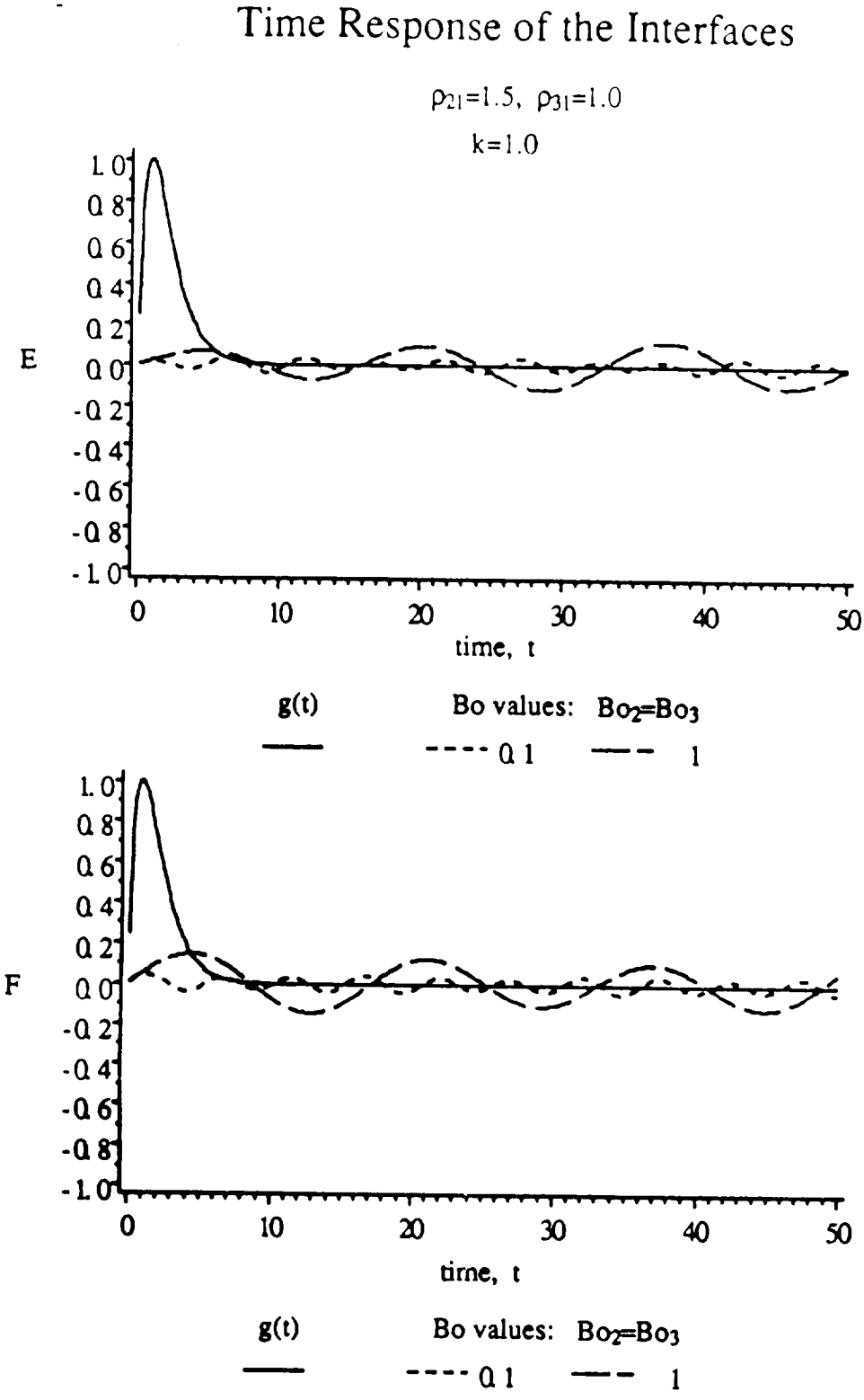
Time Response of the Interfaces
ρ_{21}=1.5, ρ_{31}=1.0
k=1.0
E
1.0
0.8
0.6
0.4
0.2
0.0
-0.2
-0.4
-0.6
-0.8
-1.0
0
10
20
30
40
50
time, t
g(t)
Bo values: Bo_2=Bo_3
0.1
1
F
time, t
g(t)
Bo values: Bo_2=Bo_3
0.1
1

Figure 4.15

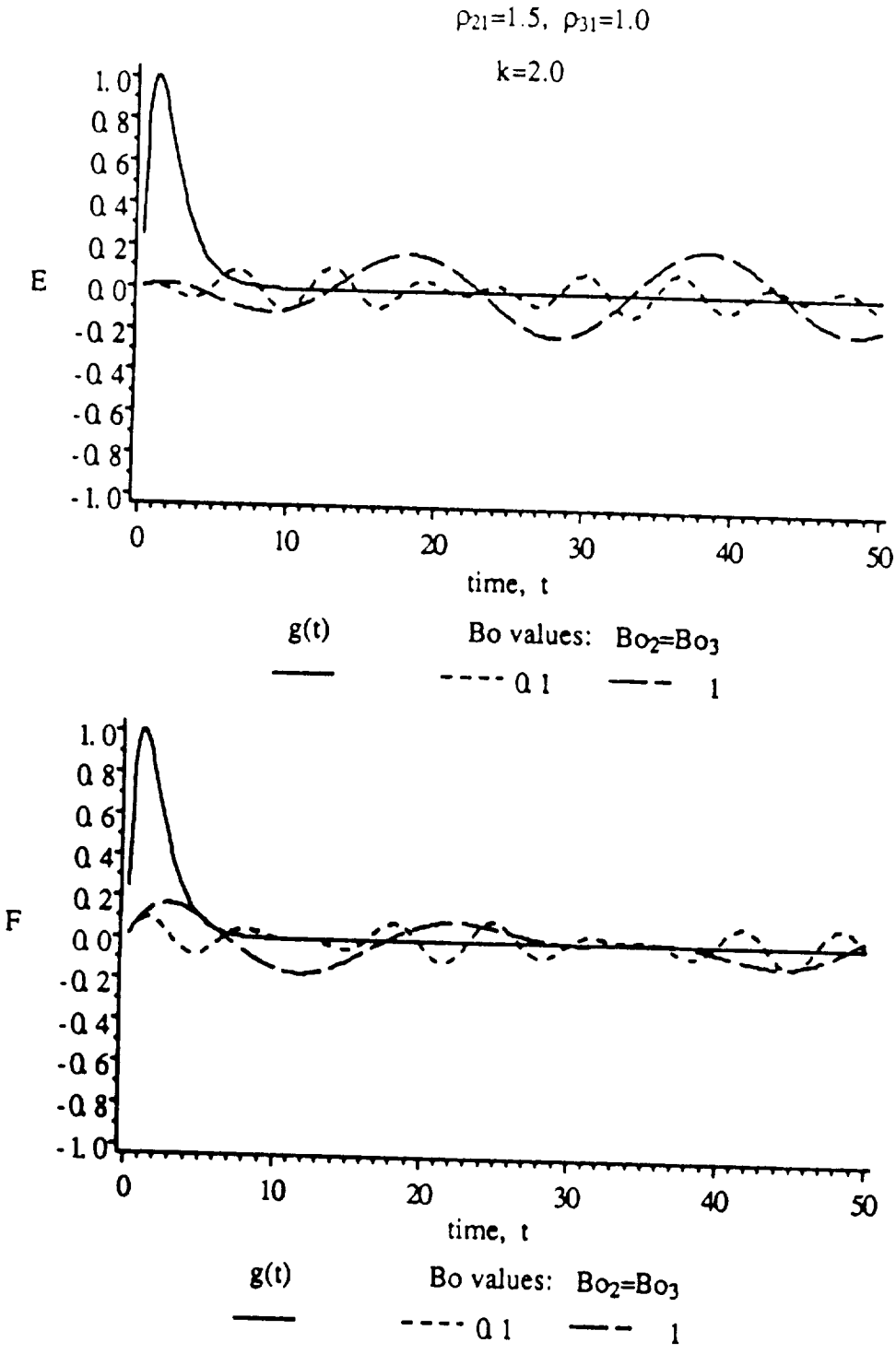
Time Response of the Interfaces
ρ21=1.5, ρ31=1.0
k=2.0
E
1.0
0.8
0.6
0.4
0.2
0.0
-0.2
-0.4
-0.6
-0.8
-1.0
0
10
20
30
40
50
time, t
g(t)
Bo values: Bo2=Bo3
0.1
1
F
1.0
0.8
0.6
0.4
0.2
0.0
-0.2
-0.4
-0.6
-0.8
-1.0
0
10
20
30
40
50
time, t
g(t)
Bo values: Bo2=Bo3
0.1
1

Figure 4.16

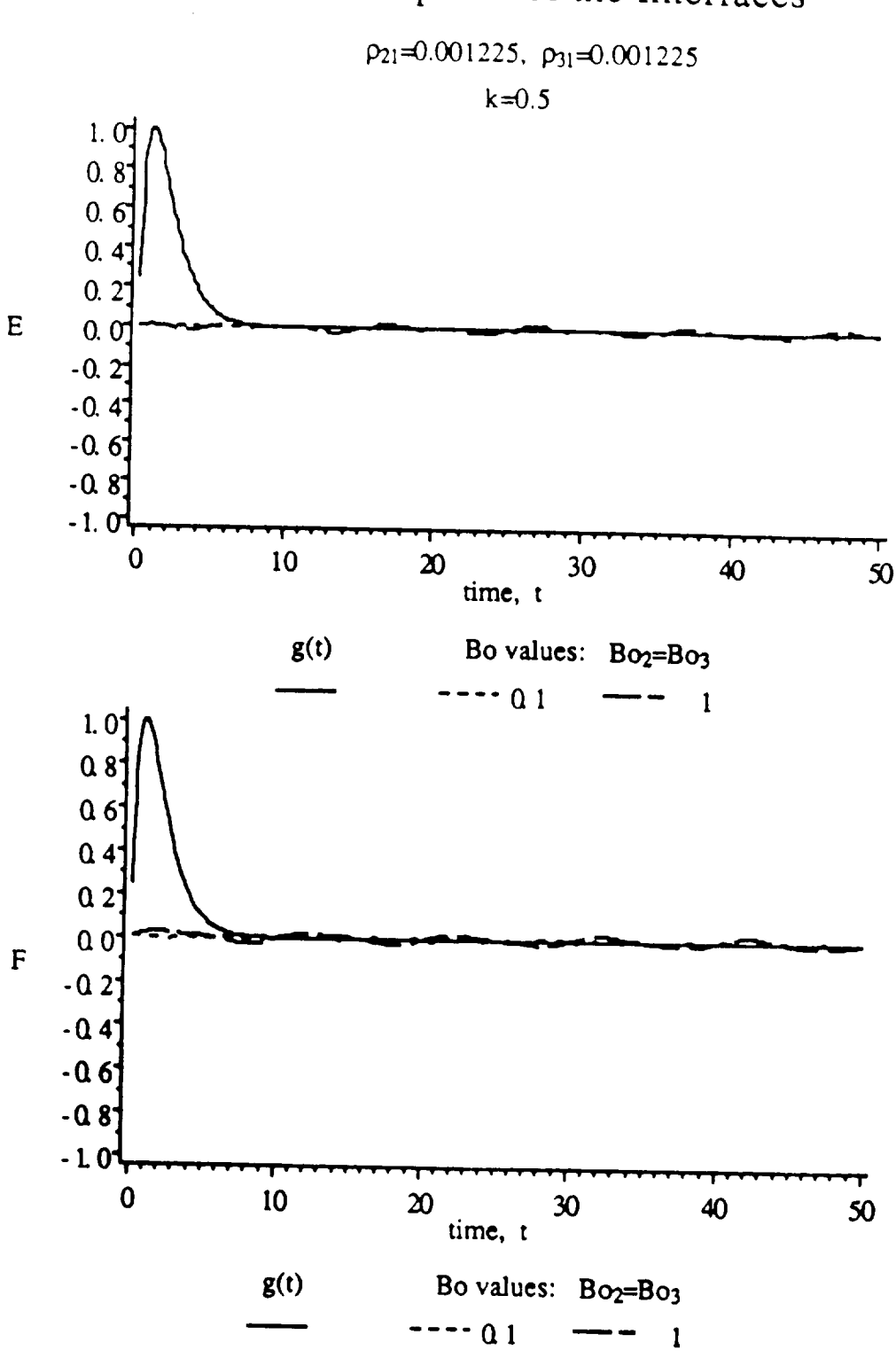
Time Response of the Interfaces
ρ21=0.001225, ρ31=0.001225
k=0.5
E
1.0
0.8
0.6
0.4
0.2
0.0
-0.2
-0.4
-0.6
-0.8
-1.0
0
10
20
30
40
50
time, t
g(t)
Bo values: Bo2=Bo3
0.1
1
F
1.0
0.8
0.6
0.4
0.2
0.0
-0.2
-0.4
-0.6
-0.8
-1.0
0
10
20
30
40
50
time, t
g(t)
Bo values: Bo2=Bo3
0.1
1

Figure 4.17

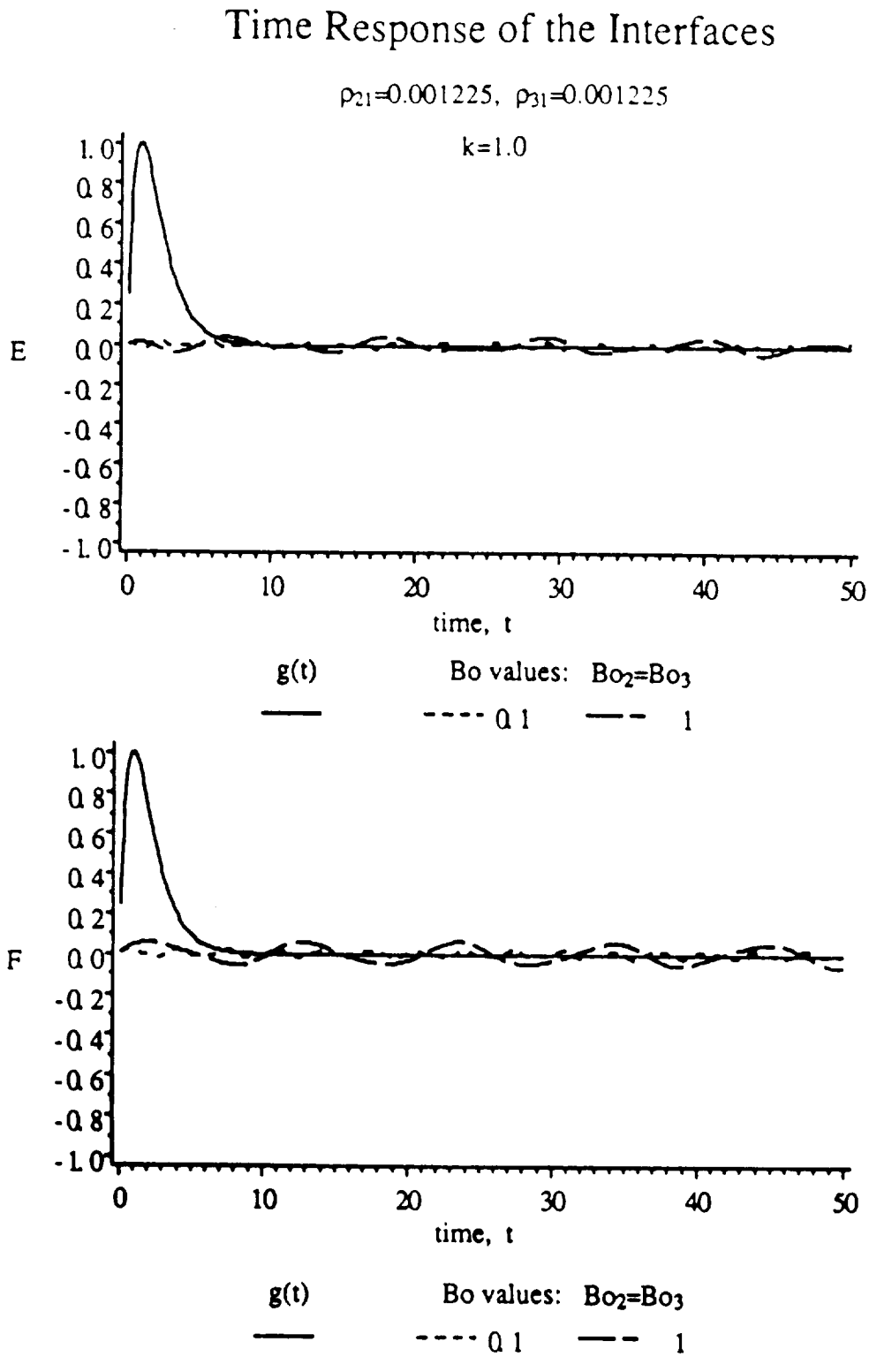
Time Response of the Interfaces
ρ21=0.001225, ρ31=0.001225
k=1.0
E
F
1.0
0.8
0.6
0.4
0.2
0.0
-0.2
-0.4
-0.6
-0.8
-1.0
0
10
20
30
40
50
time, t
g(t)
Bo values: Bo2=Bo3
0.1
1

Figure 4.18

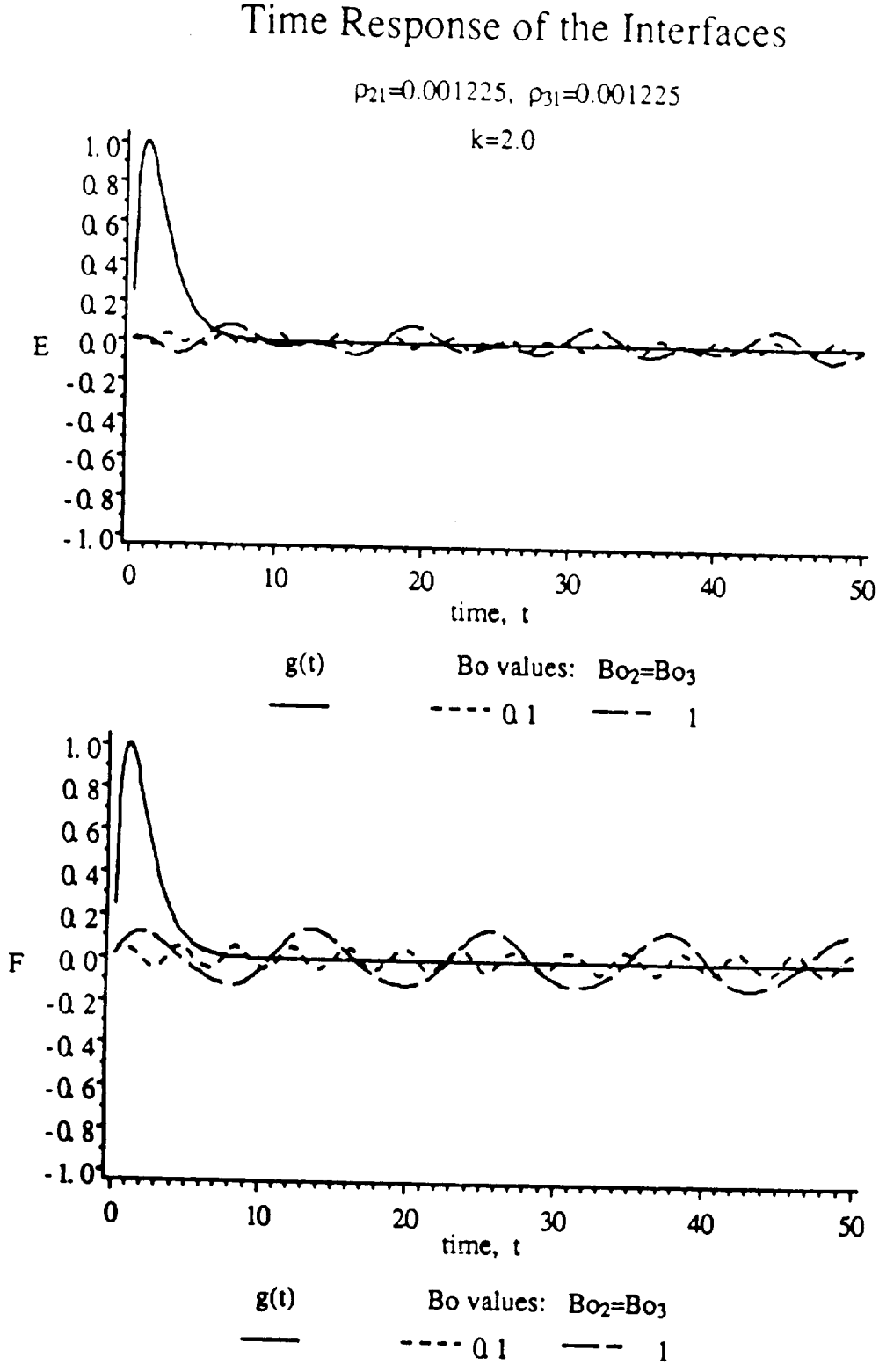
Time Response of the Interfaces
ρ21=0.001225, ρ31=0.001225
k=2.0
E
F
time, t
g(t)
Bo values: Bo2=Bo3
0.1
1

Figure 4.19

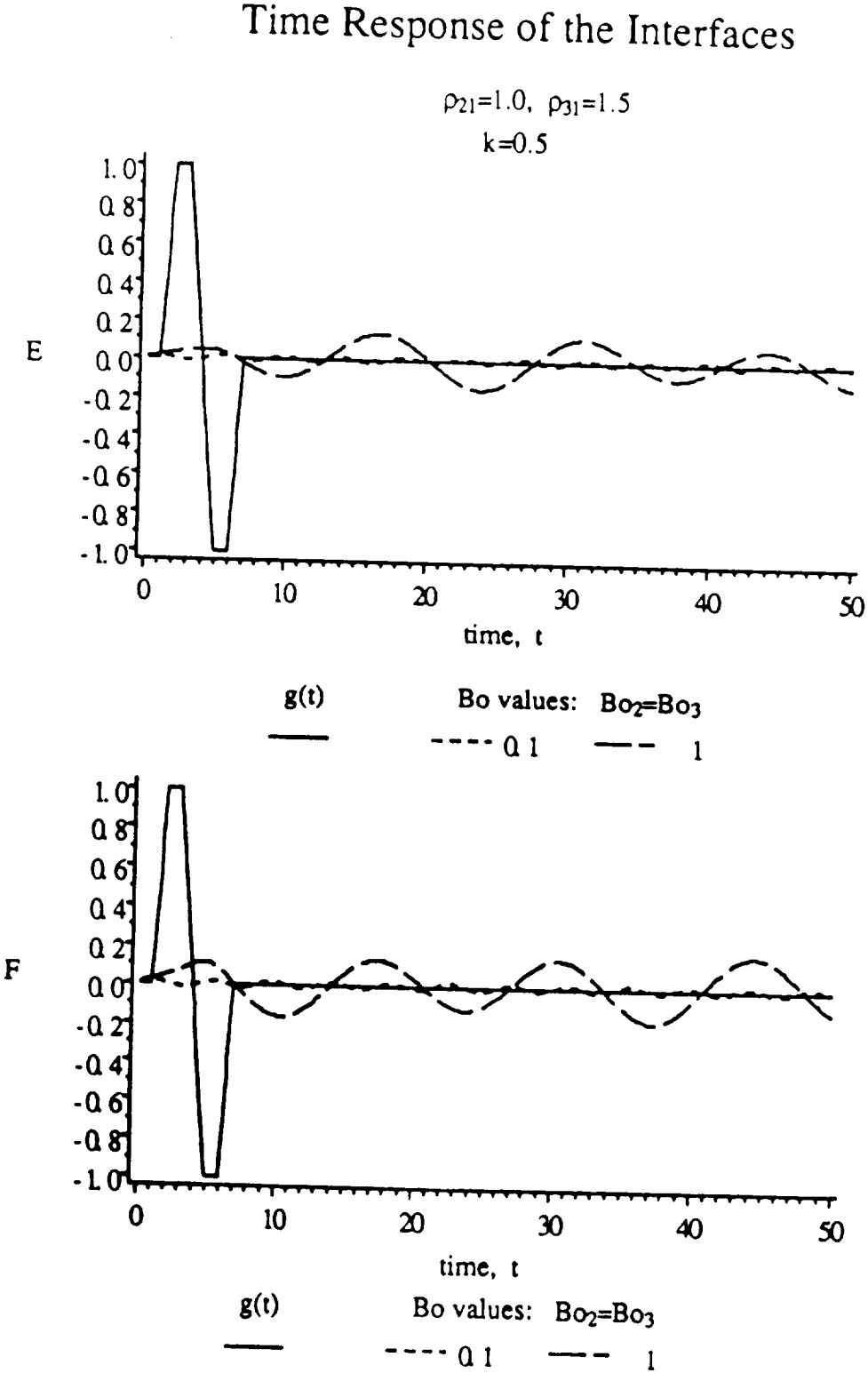
Time Response of the Interfaces
ρ_{21}=1.0, ρ_{31}=1.5
k=0.5
E
1.0
0.8
0.6
0.4
0.2
0.0
-0.2
-0.4
-0.6
-0.8
-1.0
0
10
20
30
40
50
time, t
g(t)
Bo values: Bo_2=Bo_3
0.1
1
F
time, t
g(t)
Bo values: Bo_2=Bo_3
0.1
1

Figure 4.20

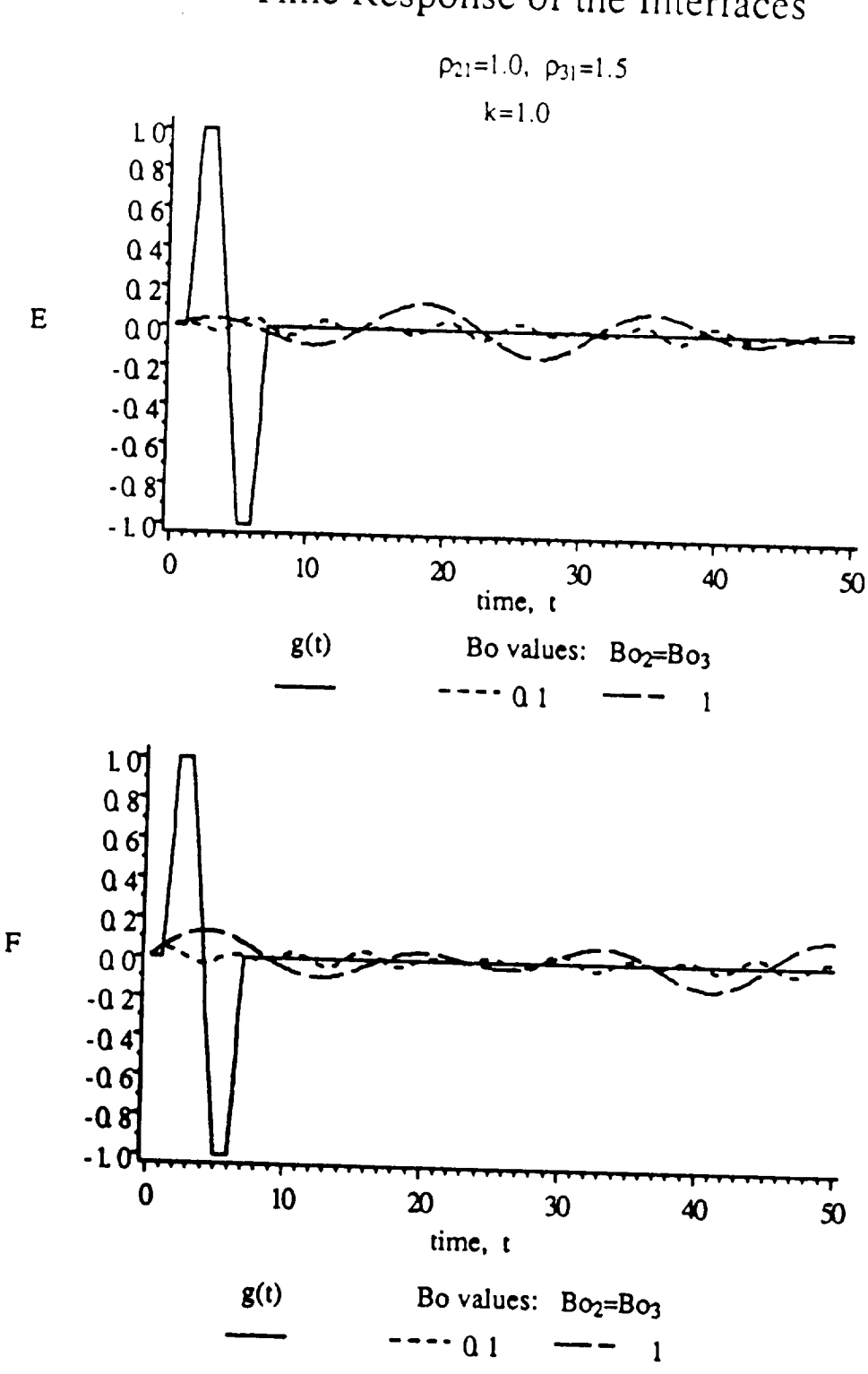
Time Response of the Interfaces
ρ21=1.0, ρ31=1.5
k=1.0
E
1.0
0.8
0.6
0.4
0.2
0.0
-0.2
-0.4
-0.6
-0.8
-1.0
0
10
20
30
40
50
time, t
g(t)
Bo values: Bo2=Bo3
0.1
1
F
1.0
0.8
0.6
0.4
0.2
0.0
-0.2
-0.4
-0.6
-0.8
-1.0
0
10
20
30
40
50
time, t
g(t)
Bo values: Bo2=Bo3
0.1
1

Figure 4.21

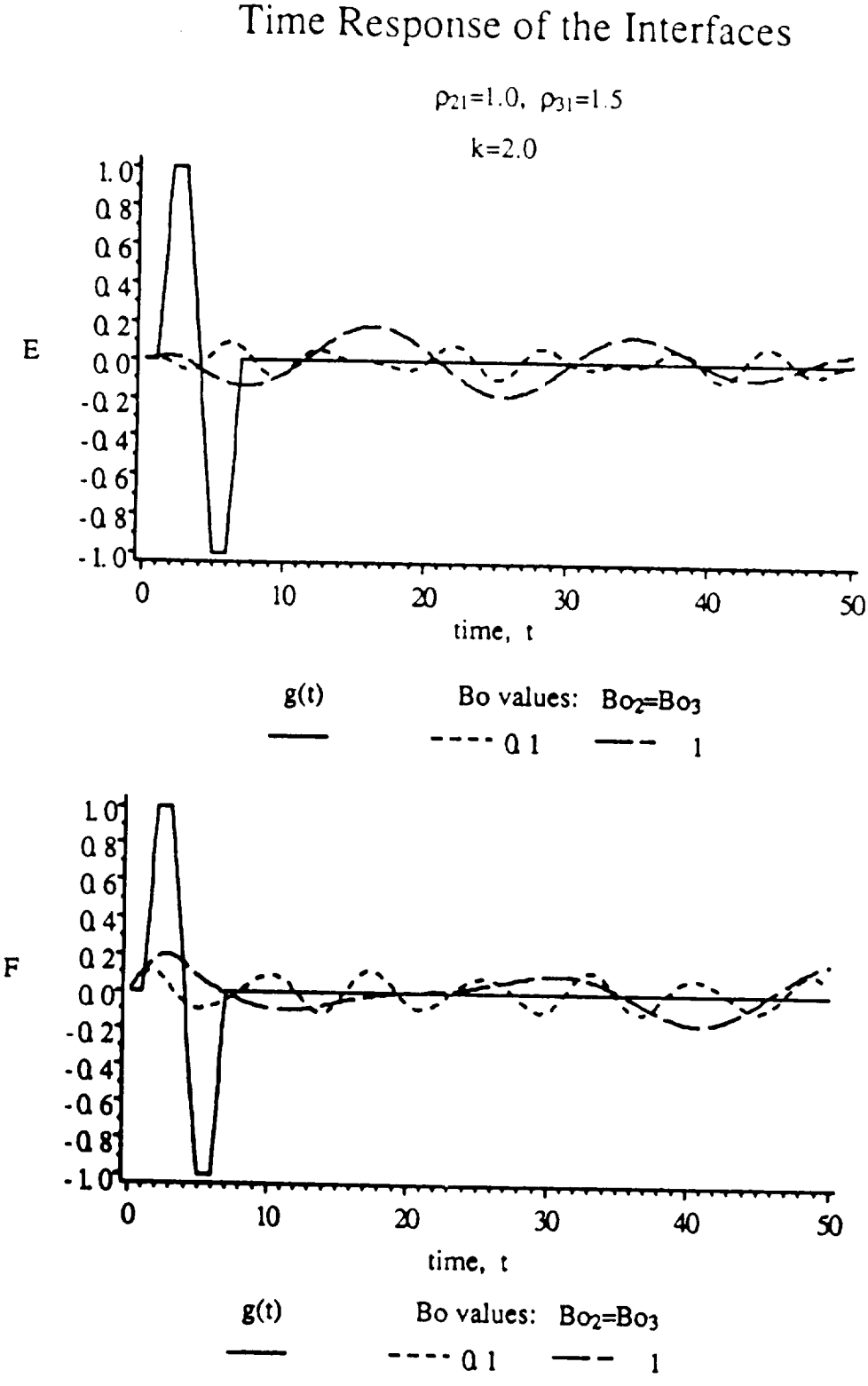
Time Response of the Interfaces
ρ21=1.0, ρ31=1.5
k=2.0
E
1.0
0.8
0.6
0.4
0.2
0.0
-0.2
-0.4
-0.6
-0.8
-1.0
0
10
20
30
40
50
time, t
g(t)
Bo values: Bo2=Bo3
0.1
1
F
1.0
0.8
0.6
0.4
0.2
0.0
-0.2
-0.4
-0.6
-0.8
-1.0
0
10
20
30
40
50
time, t
g(t)
Bo values: Bo2=Bo3
0.1
1

Figure 4.22

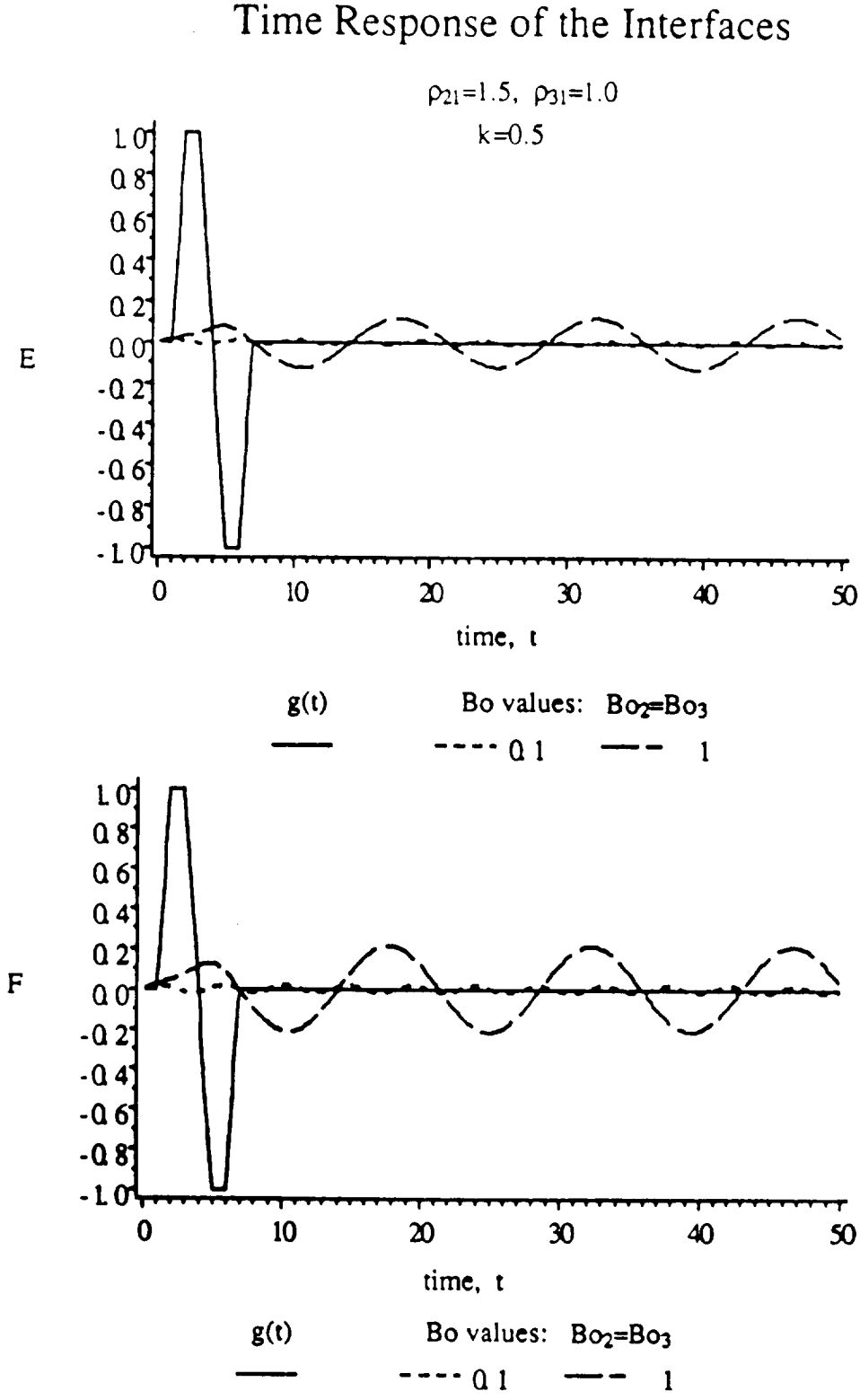
Time Response of the Interfaces
ρ21=1.5, ρ31=1.0
k=0.5
E
1.0
0.8
0.6
0.4
0.2
0.0
-0.2
-0.4
-0.6
-0.8
-1.0
0
10
20
30
40
50
time, t
g(t)
Bo values: Bo2=Bo3
0.1
1
F
1.0
0.8
0.6
0.4
0.2
0.0
-0.2
-0.4
-0.6
-0.8
-1.0
0
10
20
30
40
50
time, t
g(t)
Bo values: Bo2=Bo3
0.1
1

Figure 4.23

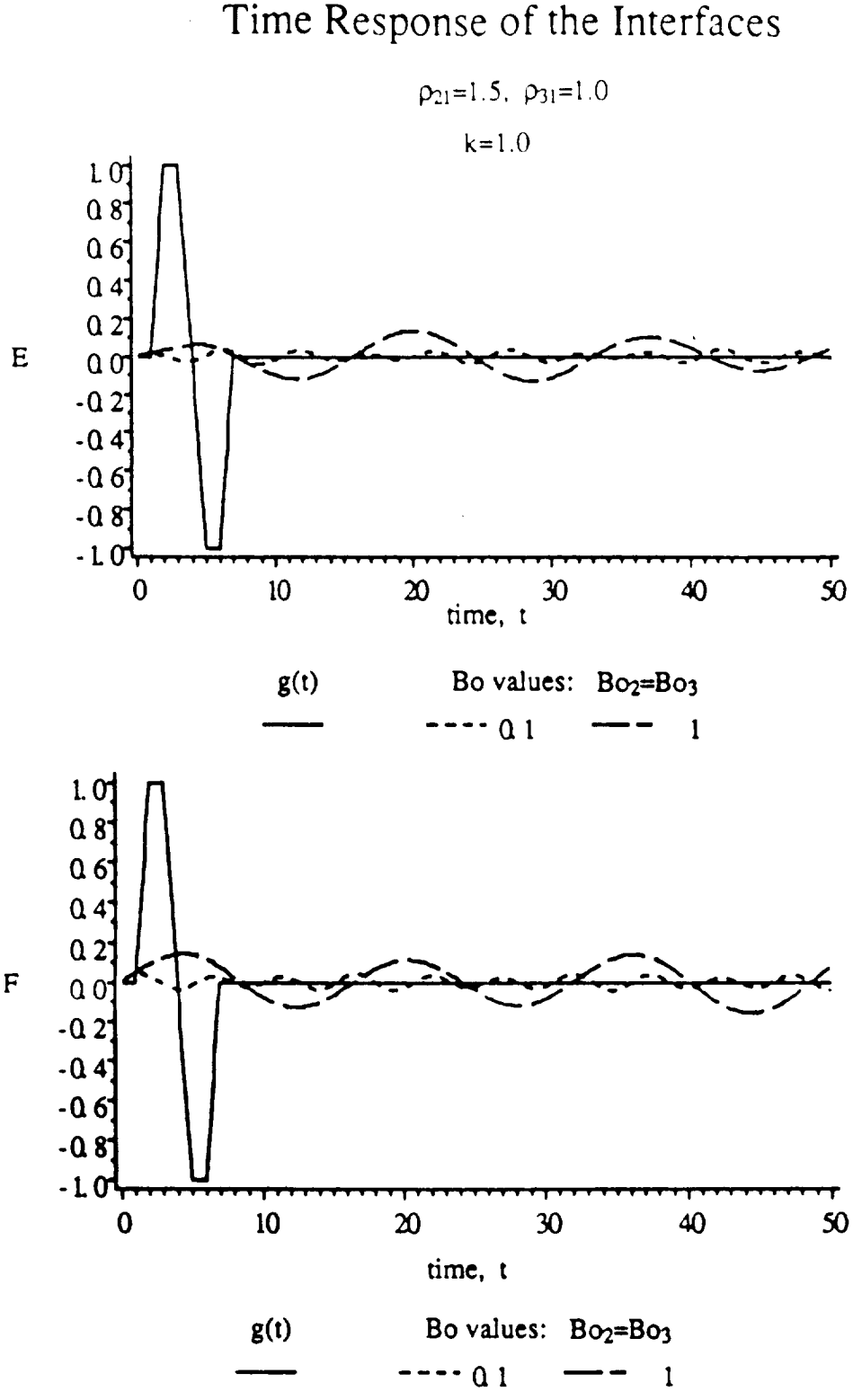
Time Response of the Interfaces
ρ21=1.5, ρ31=1.0
k=1.0
E
1.0
0.8
0.6
0.4
0.2
0.0
-0.2
-0.4
-0.6
-0.8
-1.0
0
10
20
30
40
50
time, t
g(t)
Bo values: Bo2=Bo3
0.1
1
F
1.0
0.8
0.6
0.4
0.2
0.0
-0.2
-0.4
-0.6
-0.8
-1.0
0
10
20
30
40
50
time, t
g(t)
Bo values: Bo2=Bo3
0.1
1

Figure 4.24

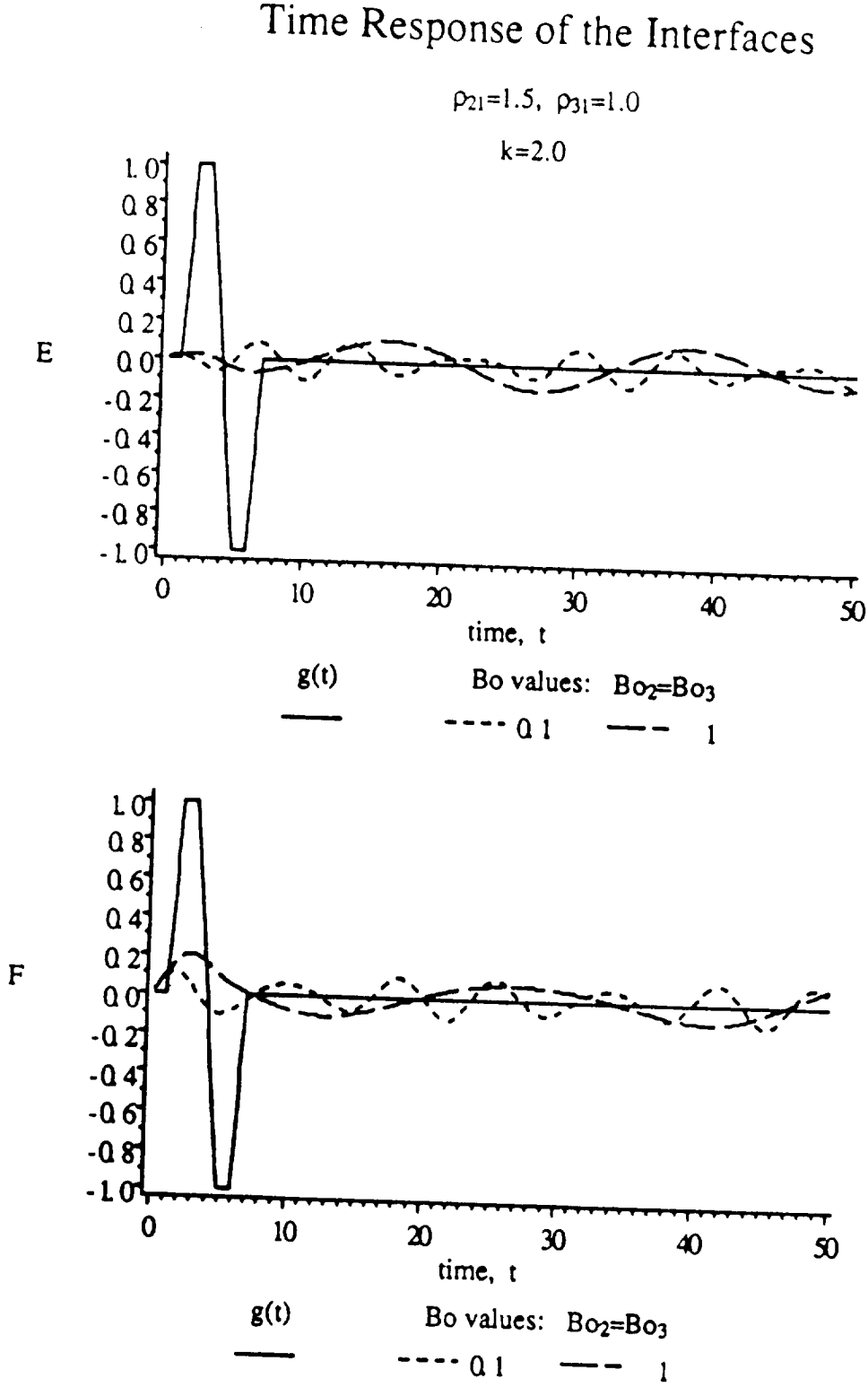
Time Response of the Interfaces
ρ21=1.5, ρ31=1.0
k=2.0
E
1.0
0.8
0.6
0.4
0.2
0.0
-0.2
-0.4
-0.6
-0.8
-1.0
0
10
20
30
40
50
time, t
g(t)
Bo values: Bo2=Bo3
0.1
1
F
1.0
0.8
0.6
0.4
0.2
0.0
-0.2
-0.4
-0.6
-0.8
-1.0
0
10
20
30
40
50
time, t
g(t)
Bo values: Bo2=Bo3
0.1
1

Figure 4.25

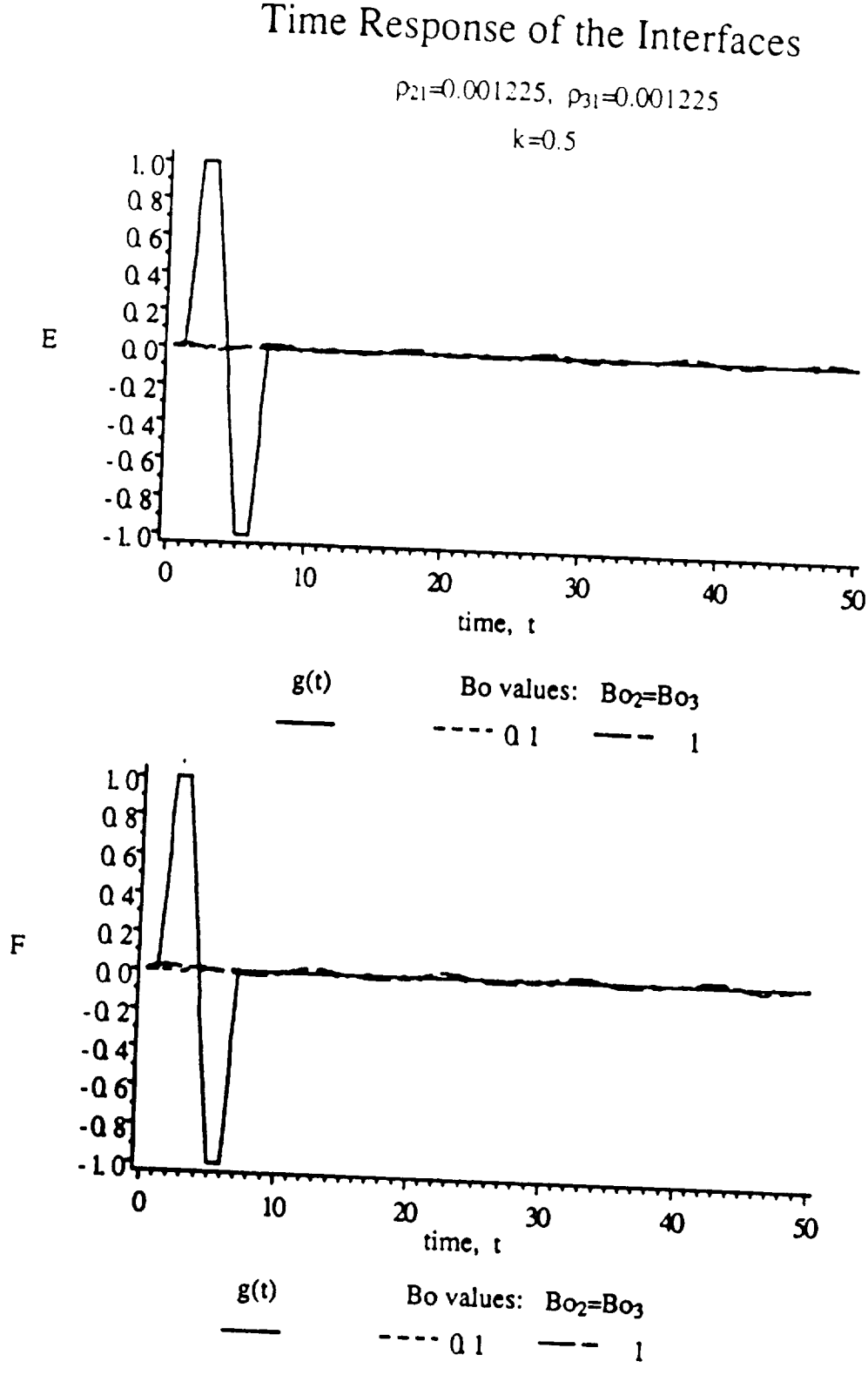
Time Response of the Interfaces
ρ21=0.001225, ρ31=0.001225
k=0.5
E
1.0
0.8
0.6
0.4
0.2
0.0
-0.2
-0.4
-0.6
-0.8
-1.0
0
10
20
30
40
50
time, t
g(t)
Bo values: Bo2=Bo3
0.1
1
F
1.0
0.8
0.6
0.4
0.2
0.0
-0.2
-0.4
-0.6
-0.8
-1.0
0
10
20
30
40
50
time, t
g(t)
Bo values: Bo2=Bo3
0.1
1

Figure 4.26

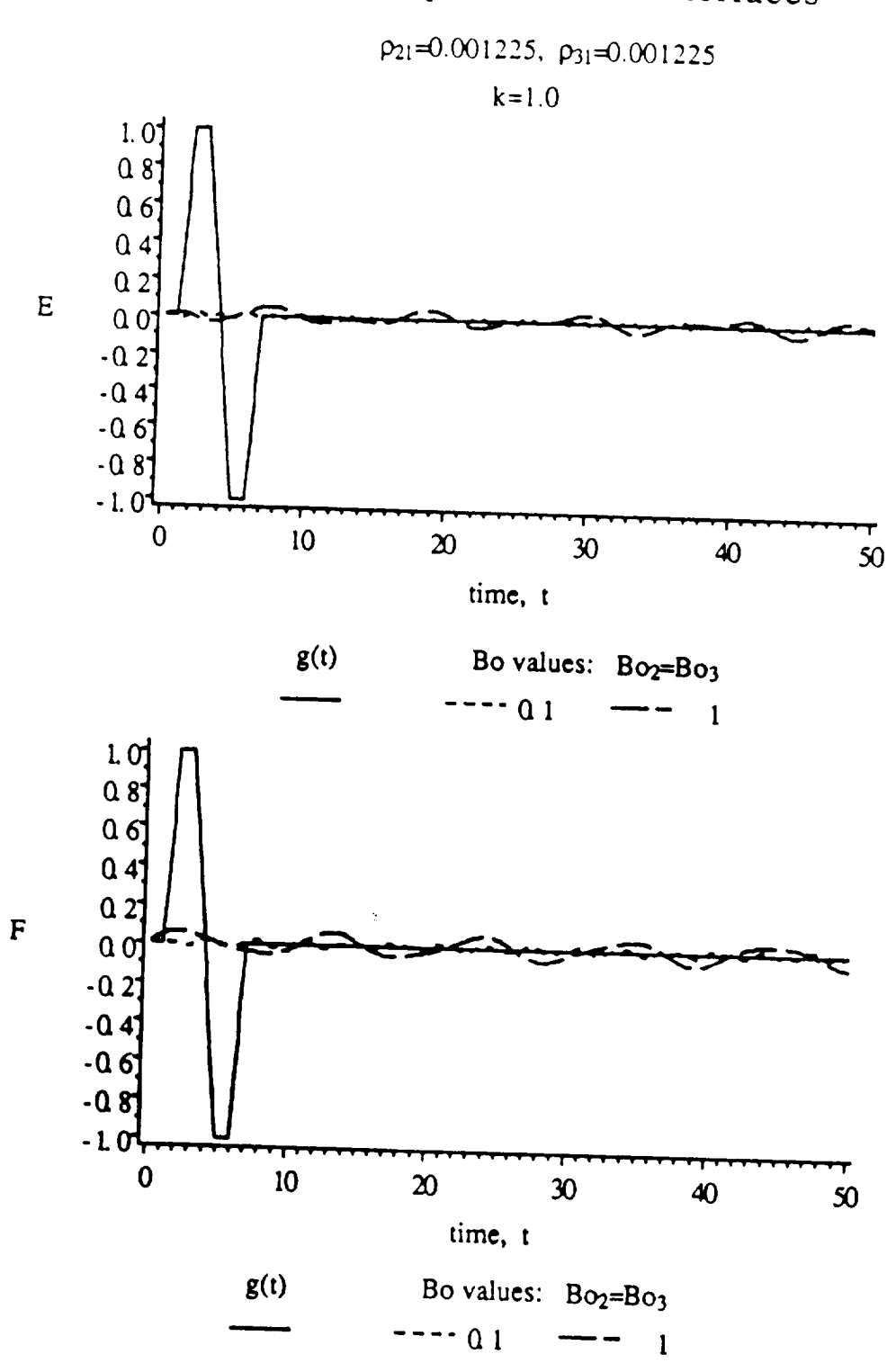
Time Response of the Interfaces
ρ21=0.001225, ρ31=0.001225
k=1.0
E
1.0
0.8
0.6
0.4
0.2
0.0
-0.2
-0.4
-0.6
-0.8
-1.0
0
10
20
30
40
50
time, t
g(t)
Bo values: Bo2=Bo3
0.1
1
F
time, t
g(t)
Bo values: Bo2=Bo3
0.1
1

Figure 4.27

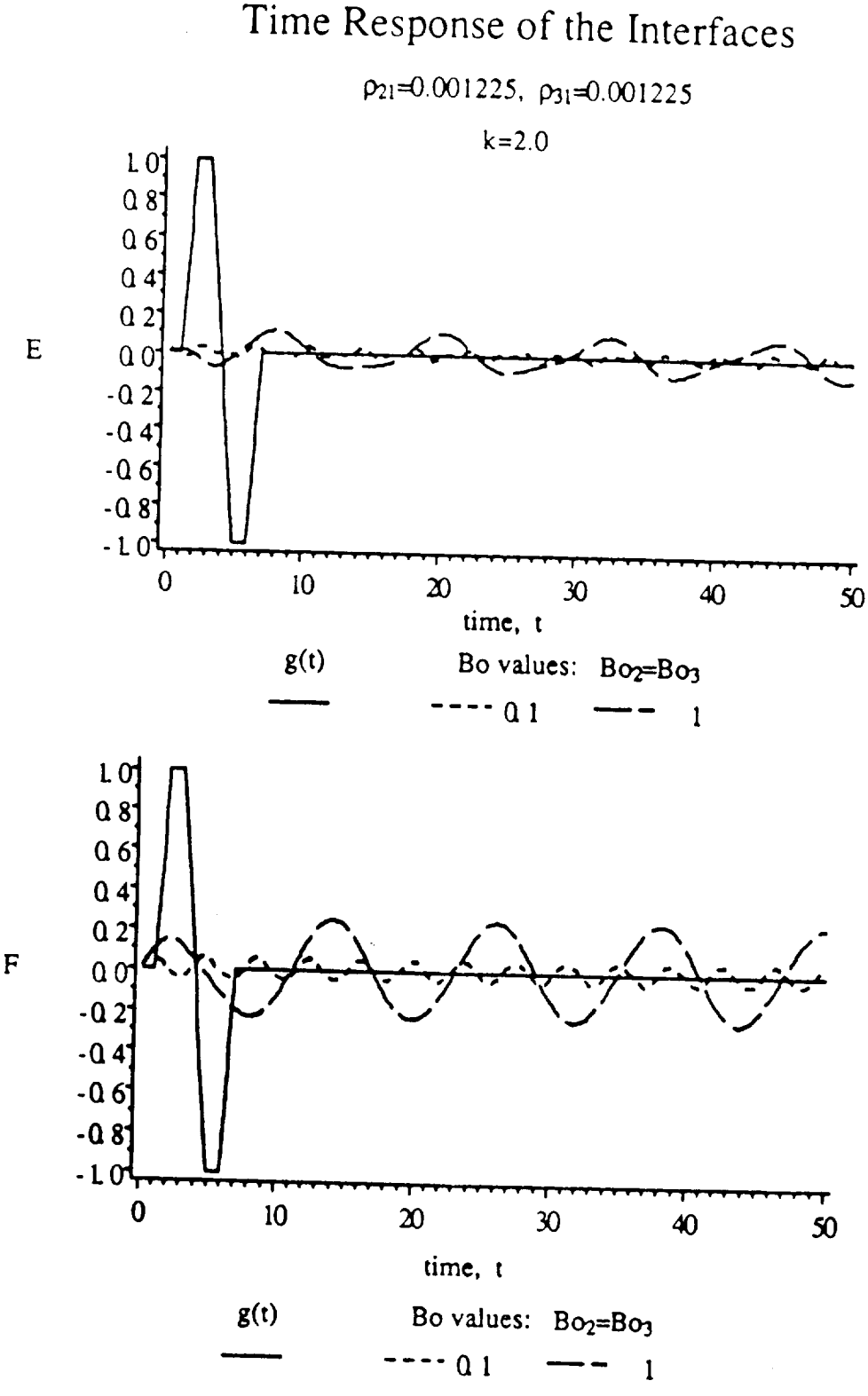
Time Response of the Interfaces
ρ21=0.001225, ρ31=0.001225
k=2.0
E
1.0
0.8
0.6
0.4
0.2
0.0
-0.2
-0.4
-0.6
-0.8
-1.0
0
10
20
30
40
50
time, t
g(t)
Bo values: Bo2=Bo3
0.1
1
F
1.0
0.8
0.6
0.4
0.2
0.0
-0.2
-0.4
-0.6
-0.8
-1.0
0
10
20
30
40
50
time, t
g(t)
Bo values: Bo2=Bo3
0.1
1

Figure 4.28

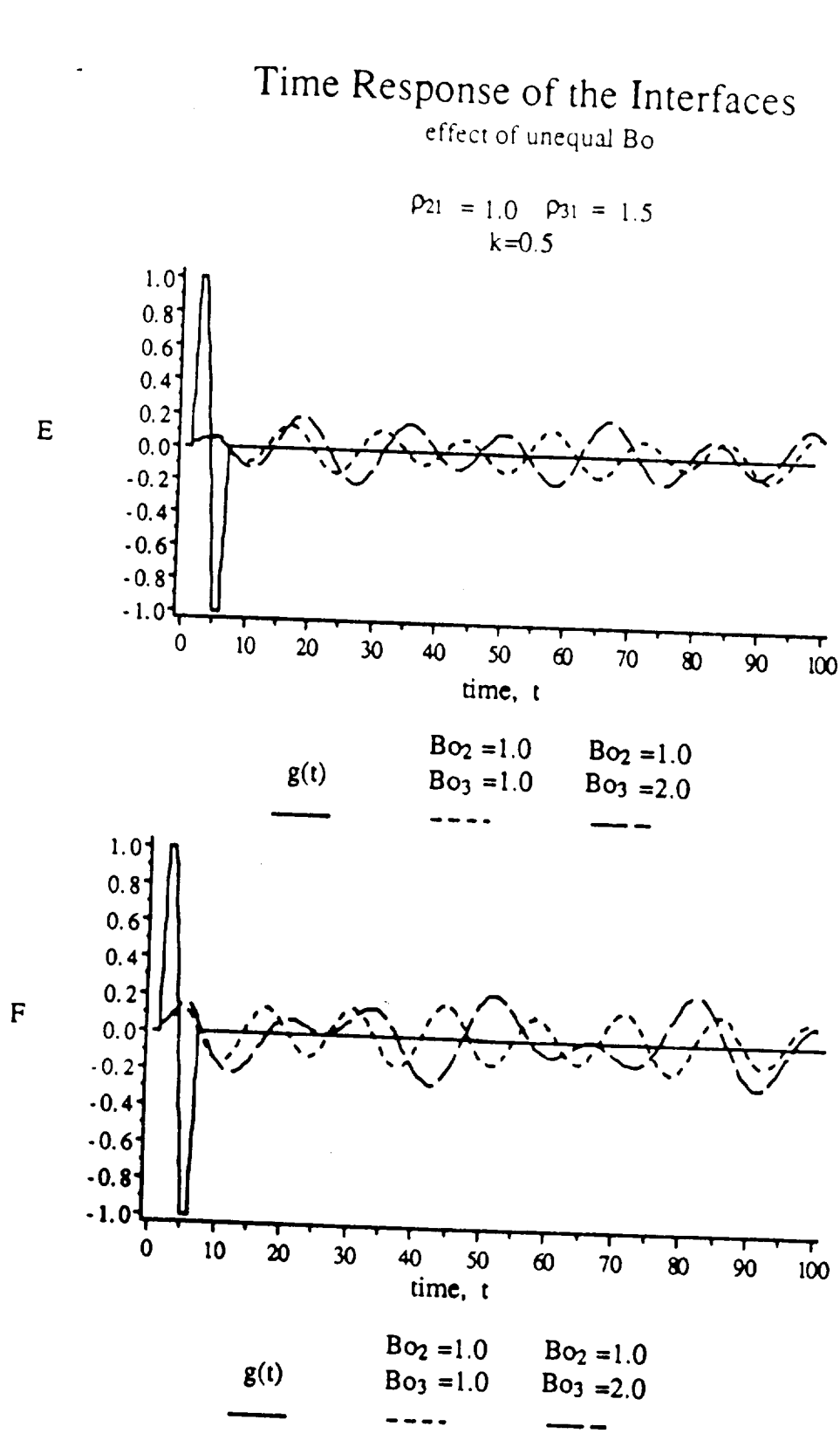
Time Response of the Interfaces
effect of unequal Bo
ρ21 = 1.0 ρ31 = 1.5
k=0.5
E
1.0
0.8
0.6
0.4
0.2
0.0
-0.2
-0.4
-0.6
-0.8
-1.0
0 10 20 30 40 50 60 70 80 90 100
time, t
g(t)
Bo2 =1.0
Bo3 =1.0
Bo2 =1.0
Bo3 =2.0
F
1.0
0.8
0.6
0.4
0.2
0.0
-0.2
-0.4
-0.6
-0.8
-1.0
0 10 20 30 40 50 60 70 80 90 100
time, t
g(t)
Bo2 =1.0
Bo3 =1.0
Bo2 =1.0
Bo3 =2.0

Figure 4.29

Time Response of the Interfaces

effect of unequal Bo

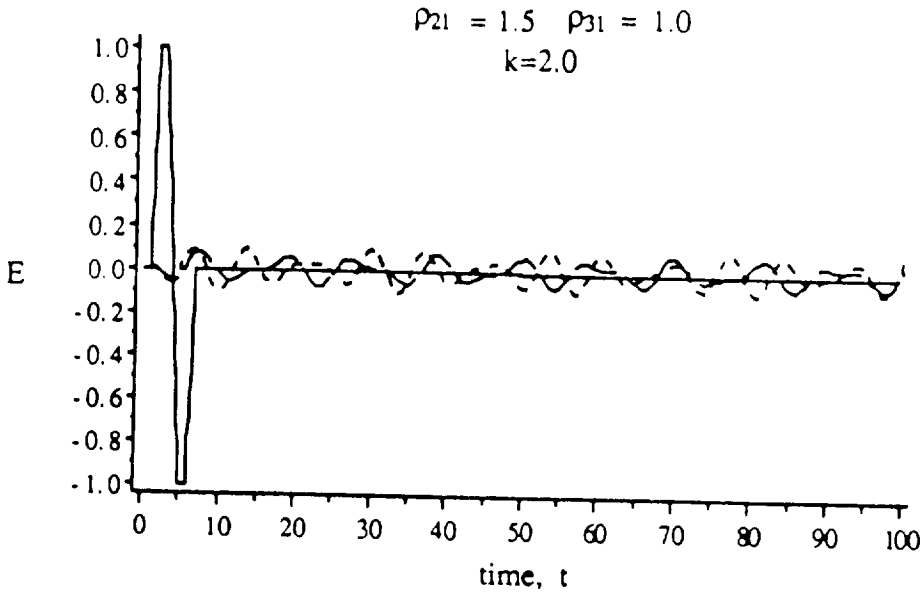

g(t) Bo_2 =0.1 Bo_3 =0.1 ——— Bo_2 =0.1 Bo_3 =0.2 - - - -

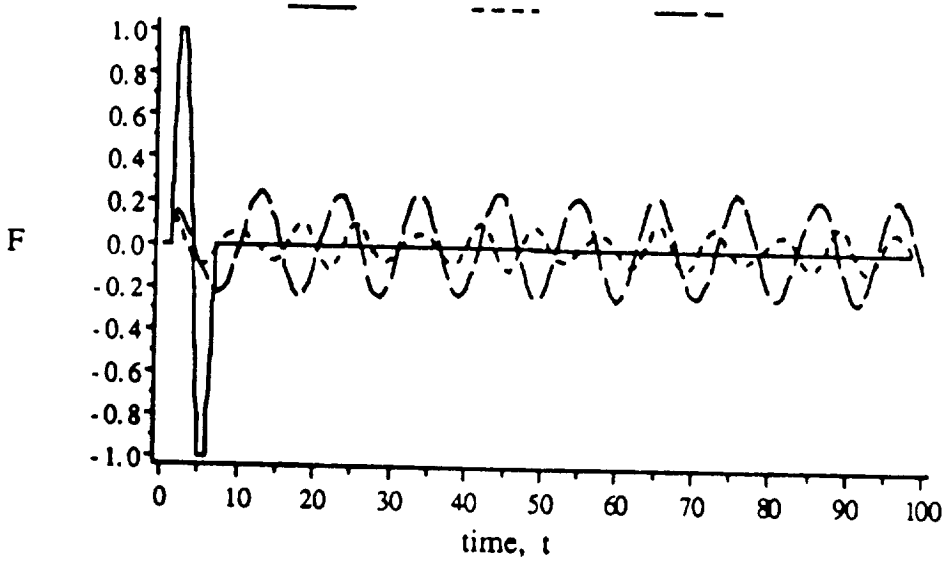

g(t) Bo_2 =0.1 Bo_3 =0.1 ——— Bo_2 =0.1 Bo_3 =0.2 - - - -

Figure 4.30

Time Response of the Interfaces

effect of unequal Bo

$\rho_{21} = \rho_{31} = 0.001225$

k=2.0

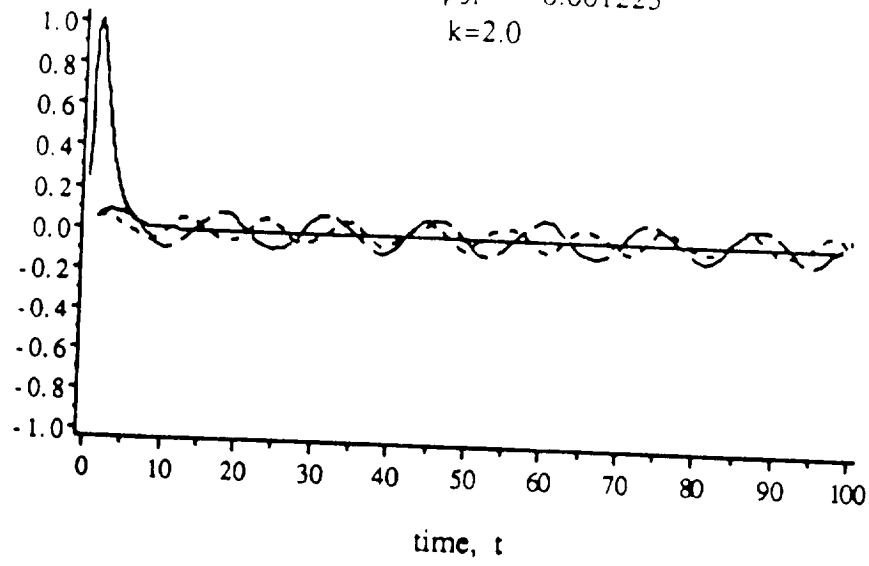

g(t) — $Bo_2 = 1.0$, $Bo_3 = 1.0$ ---- $Bo_2 = 1.0$, $Bo_3 = 2.0$ — —

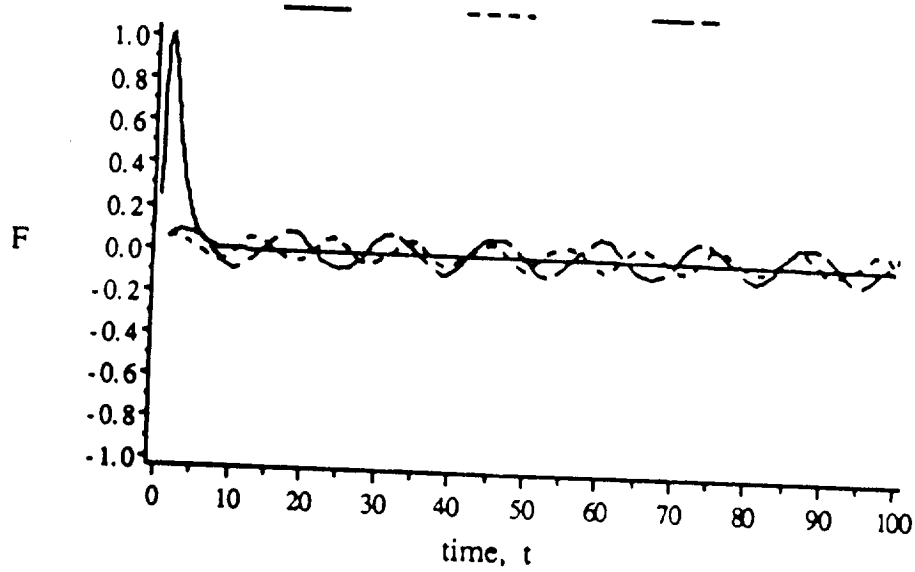

g(t) — $Bo_2 = 1.0$, $Bo_3 = 1.0$ ---- $Bo_2 = 1.0$, $Bo_3 = 2.0$ — —

Figure 4.31

Long Duration Response: Comparison of Zero Forcing with Impulse Forcing

$\rho_{21}=1.5,\ \rho_{31}=1.0,\ Bo_2=Bo_3=1.0,\ k=0.5$

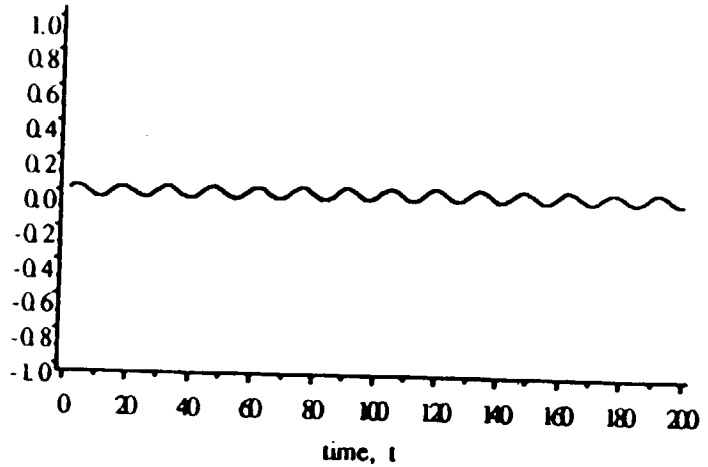

g=0 E ——

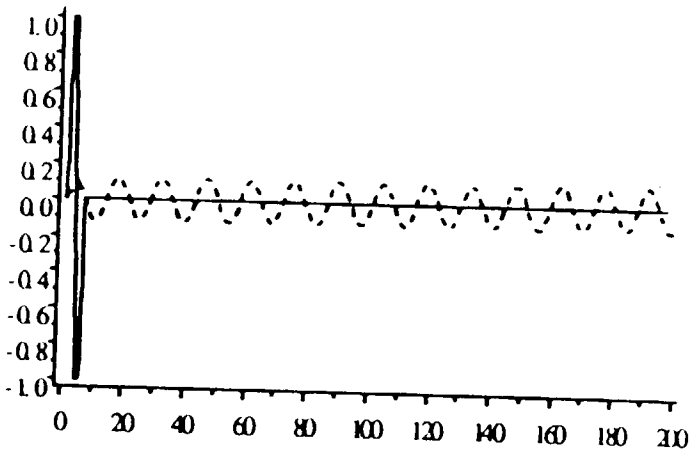

g(t) —— E----

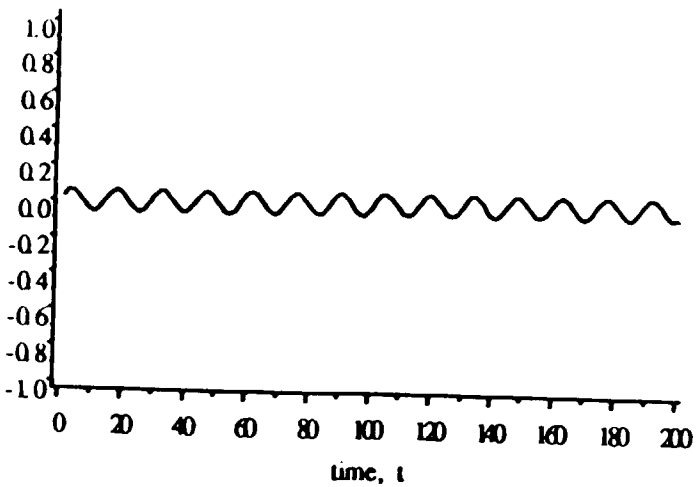

g=0 F ——

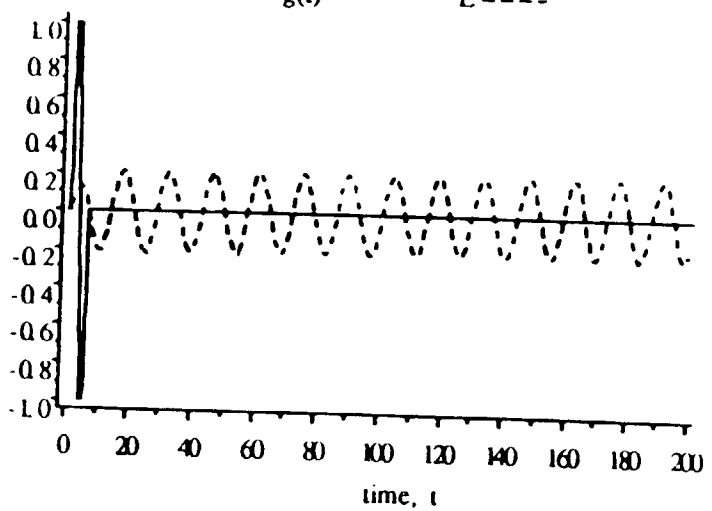

g(t) —— F----

Figure 4.32

Long Duration Response: Comparison of Zero Forcing with Impulse Forcing

$\rho_{21} = 1.0,\ \rho_{31} = 1.5\ ,\ Bo_2=Bo_3=1.0,\ k=0.5$

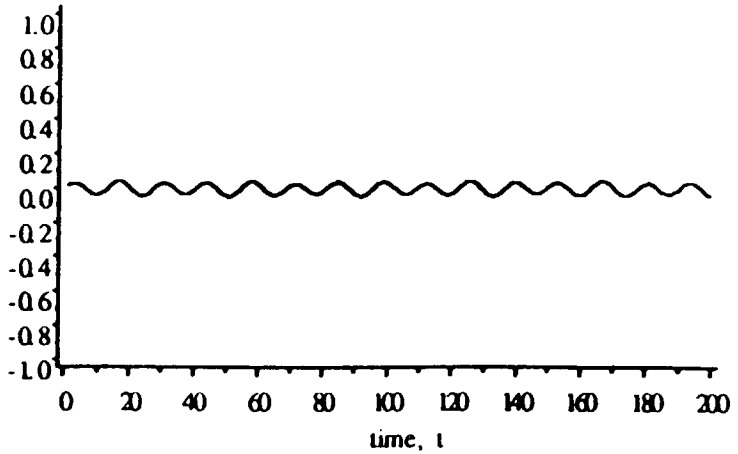

g=0 E ——

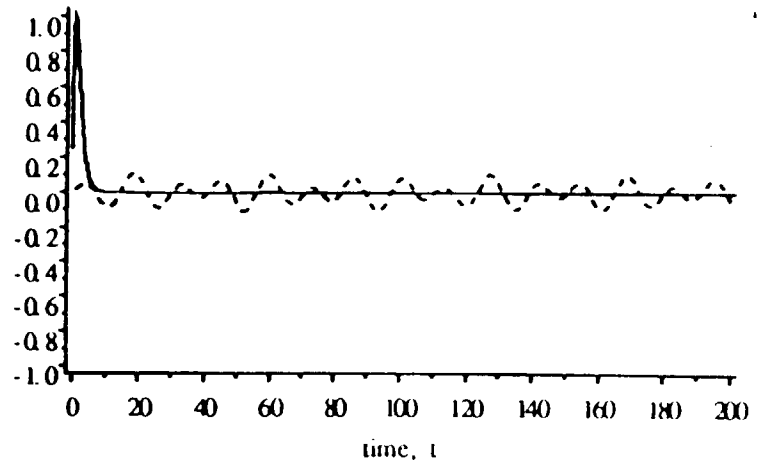

g(t) —— E - - - -

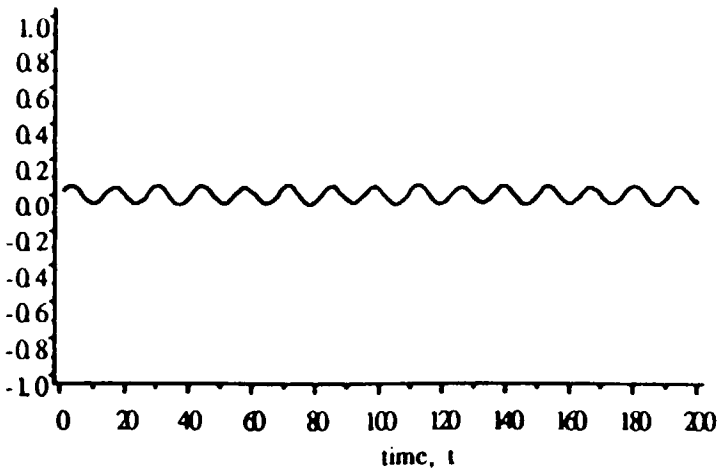

g=0 F ——

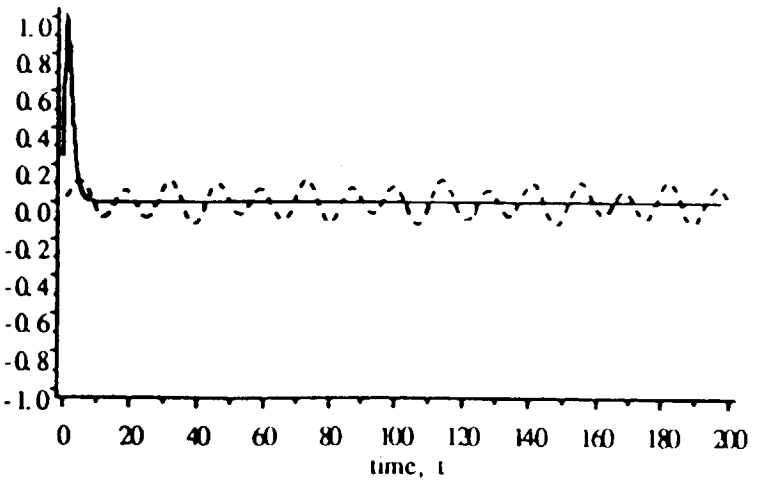

g(t) —— F - - - -

Figure 4.33

Long Duration Response: Comparison of Zero Forcing with Impulse Forcing

$\rho_{21}=\rho_{31}=0.001225$, $Bo_2=Bo_3=1.0$, $k=2.0$

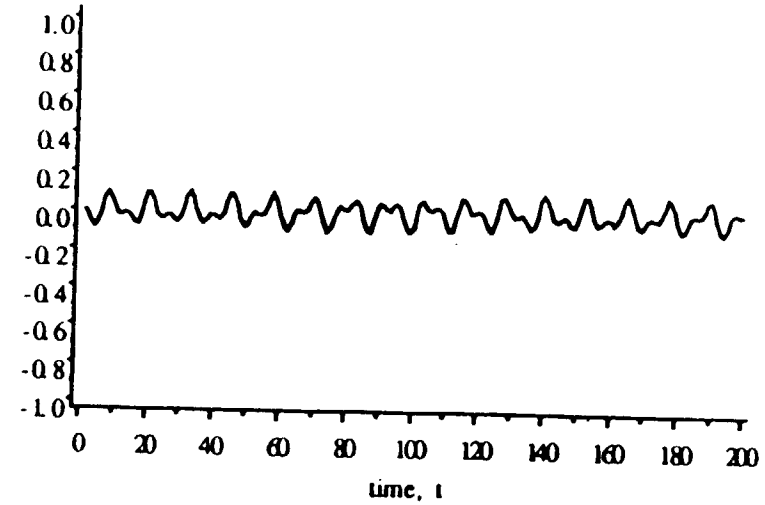

g=0 E ——

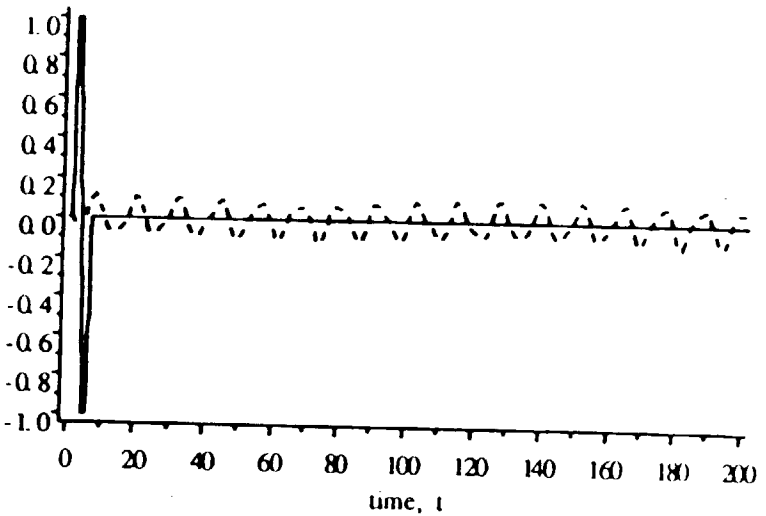

g(t) —— E ----

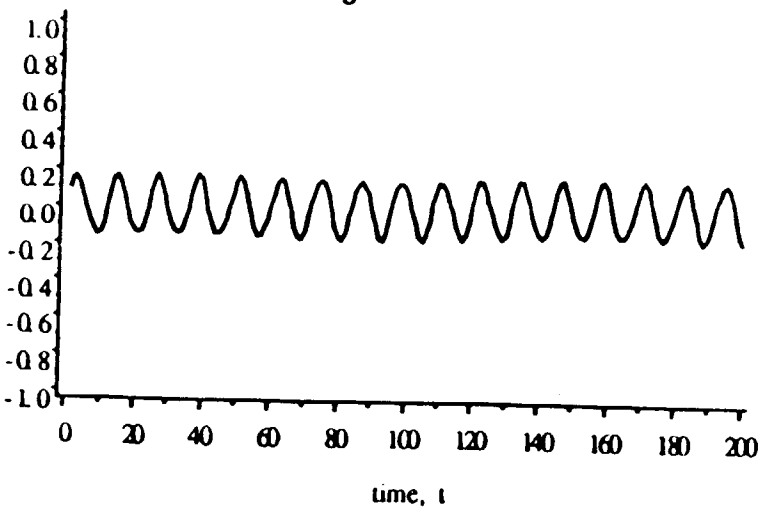

g=0 F ——

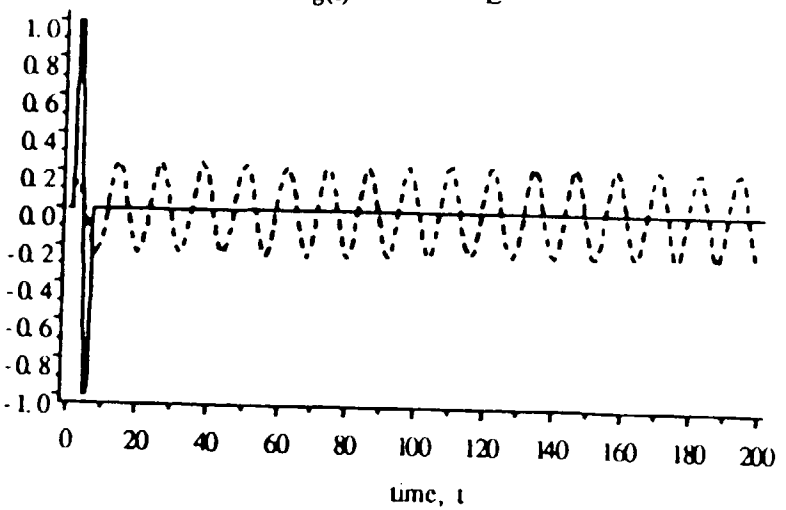

g(t) —— F ----

Figure 4.34

CHAPTER 5

CONCLUSIONS

The effect of microgravity environment accelerations on the behavior of a multi-layered idealized fluid configuration has been investigated. The analysis was linear, and each fluid region was considered inviscid, incompressible, irrotational, and immiscible. A normal mode approach was taken with regard to the spatial variables.

As a preliminary study, the stability of the configuration was investigated in the presence of constant acceleration fields. Dimensional equation development resulted in a dispersion relation. The nature of the roots of the dispersion relation determined the stability of the configuration.

Three parameters were studied, including the wave number of the perturbation, height of the middle layer, and the value of the constant forcing. The stability regimes of these parameters were investigated for various configurations involving air, water, and silicone oil.

The results show that the configuration is most stable to larger values of the wave number. This implies that the fluid system is susceptible to long wavelength perturbations. The change in height of the middle layer has a negligible effect if the quantity h/λ is greater or on the order of one. For values of $h/\lambda < O(1)$, faster growing instabilities are associated with smaller values of h/λ.

Results indicate that as the constant forcing value is decreased, the configuration becomes more stable. The limit case of zero forcing was investigated and found to be stable for all parameter values. The zero mean gravity state served as the basis for the ensuing time-dependent cases.

For the periodic case, the equations were non-dimensionalized. Floquet theory was applied to the system of equations (3.29-3.32) resulting in an infinite set of algebraic equations. A truncation was made, and the problem was posed as a generalized eigenvalue problem. Solutions to the eigensystem determined the stability of the configuration.

Six non-dimensional parameters were investigated: the Bond type number at each interface (Bo_2,Bo_3), the density ratios of the outer to middle layer (ρ_{21},ρ_{31}), the Froude type number (Fr), and the wave number (k). Ranges of values studied are pertinent to a microgravity environment and satisfy conditions of linearity. Results indicate several trends involving these parameters.

As Bo values are increased, the configuration becomes more unstable. That is, the unstable range encompasses a wider range of wave numbers. This trend can be interpreted as resulting from a decrease in the surface tension (inversely proportional to Bo) at the interfaces which expectedly would be more unstable. For unequal Bo values (Bo_3= 2*Bo_2), the range of unstable wave numbers is even greater.

A density difference parameter (ρ_{D1}) is expressed in

terms of ρ_{21} and ρ_{31}. Essentially it equals the average of the density differences across each interface. In general, as ρ_{D1} increases, the configuration becomes more unstable. This trend corresponds within certain "families" of configurations (for example, gas/liquid/liquid or liquid/liquid/liquid, etc.)

An decrease in the Froude type parameter (inversely proportional to the square of the forcing frequency) corresponds to larger bands of unstable wave numbers. Hence, the configuration is more unstable to high frequency forcing.

The multi-layered fluid system was found to be "more unstable" than the one interface configuration. That is, the range of unstable wave numbers is smaller in the one interface case. In particular, one area of contrast was in the very low k region where regions of stability were present for the one interface case.

For the non-periodic forcing case, the non-dimensionalized equations resulted in four ordinary differential equations in time. The system was integrated numerically, and the time responses of the interfaces were obtained.

Two short-duration impulse type functions were imposed on the system. Asymptotic stability of the fluid system in the presence of short-duration accelerations was ascertained via mathematical analysis, and the numerical results were consistent. The interfaces respond in a wavelike fashion, but do not grow exponentially in time, providing that certain conditions on the forcing function are satisfied.

In general, the presence of an impulse causes enhancement of interface perturbation amplitudes (for long wavelength perturbations) as compared to the zero forcing case. For higher wave numbers, different impulse accelerations can affect a given configuration quite differently. If the oscillation of the perturbation has "phase correspondence" with the period of the forcing, a reduction in interface amplitude may occur. Perturbation enhancement is generally greater in the presence of the bi-directional step forcing as compared to the one-directional ramp forcing. While the wave is not growing exponentially in time, enhancement could cause undesired consequences for an experiment. For example, a solidification experiment could be adversely affected by the presence of impulse forcing.

The results of the idealized fluid system are qualitatively relevant to specific configuration geometries. For example, it was determined that the multi-layered case is generally unstable for low wave numbers (long wavelengths). Certain float zone processing techniques involve a fluid column which is multi-layered. Such a configuration would need to avoid long wavelength perturbations. In general, it was found that the multi-layered configuration has a wider band of unstable wavelengths than the single interface fluid system. Hence, any space-processing geometry involving multiple layers of fluids would be more susceptible to instabilities than a one interface configuration.

Additionally, the subharmonic case is relevant to space-processing applications. It was discovered that the fluid system is most unstable at low values of Fr (inversely proportional to the forcing frequency). The investigation into the subharmonic case showed that at low Fr values, the subharmonic (λ=1/2) occurs at higher wave numbers.

This study involves values of non-dimensional parameters which are relevant to a microgravity environment. Configurations involving fluids of specific interest may be investigated. For example, a typical configuration may have the following dimensional parameters: ρ_D= 0.8 g/cm^3, γ_{II}= γ_{III}= 25 dynes/cm, G_o= 10^{-3}* g_{earth}, ω_f= 0.5 s^{-1}, and H= 4.0 cm. These values, according to the definition of the non-dimensional parameters, correspond to values of Fr=1.54 and $Bo_2(Bo_3)$=0.03. The configuration parameters are typical of what may be expected in microgravity processing applications. Fluid systems of specific interest may be investigated in such a manner.

The multi-layer configuration utilized in this study was idealized. In an actual space-processing application, the fluid system would be bounded in space; the boundary conditions pertinent to the container would need to be considered. A suggested area of future investigation is to consider finite configurations.

BIBLIOGRAPHY

1) Avduyevsky,V.S. (ed.) Scientific Foundations of Space Manufacturing, MIR Publishers, Moscow, 1984.

2) Bauer,H.F., "Natural Damped Frequencies of an Infinitely Long Column of Immiscible Viscous Liquids", Z. Angew. Math. u. Mech., 64, 475, 1984.

3) Benjamin,T.B. and Ursell,F., "The Stability of the Plane Free Surface of a Liquid in Vertical Periodic Motion", Proc. Roy. Soc. Lond., A225, 505, 1954.

4) Byrne,G.D. and Hindmarsh,A.C., "Stiff ODE Solvers: A Review of Current and Coming Attractions", J. of Computational Physics, 70, 1, 1987.

5) Drazin,P.G. and Reid,W.H., Hydrodynamic Stability, Cambridge University Press, Cambridge,1981.

6) Gu,X.M., "Nonlinear Surface Waves of a Fluid in Rectangular Containers Subjected to Vertical Periodic Excitations", Ph.D. Dissertation, U. of Minnesota., 1986.

7) Gu,X.M., Sethna,P.M., and Narain,N., "On Three-Dimensional Non-linear Subharmonic Resonant Surface Waves in a Fluid: Part 1-Theory", J. Appl. Mech.,55, 213, 1988.

8) Hasewaga, E., "Waves on the Interface of Two Liquid Layers in Vertical Periodic Motion",JSME Bull.,26, 51, 1983.

9) Hung,R., Lee,C., and Wu,J., "Gravity-Jitters and Excitation of Slosh Waves", AIAA Paper 90-0655, 1990.

10) IMSL User's Manual, Version 2.0, IMSL,Inc., Houston, 1987.

11) Jacqmin,D., "Stability of an Oscillated Fluid with a Uniform Density Gradient", J. Fluid Mech., 219, 449, 1990.

12) Jacqmin,D. and Duval,W.M., "Instabilities Caused by Oscillating Accelerations Normal to a Viscous Fluid-Fluid Interface", J. Fluid Mech.,196, 495, 1988.

13) Jenkins,M.A., and Traub,J.F., "A Three-Stage Algorithm For Real Polynomials Using Quadratic Iteration, SIAM J.on Num. Anal., 7, 545, 1970.

14) Kaufman,L.C., "The LZ Algorithm to Solve the Generalized Eigenvalue Problem", SIAM J. on Num. Anal., 11, 997, 1974.

15) Kaufman,L.C., "The LZ Algorithm to Solve the Generalized Eigenvalue Problem for Complex Matrices", ACM Transactions on Mathematical Software, 1, 271, 1975.

16) Lyell,M.J. and Roh,M. "Instability of Multi-Layer Configurations in the Presence of Time-Dependent Accelerations in a Microgravity Environment", AIAA Paper 91-0109, 1991.

17) Malacinski,G.M. "Developmental Biology in Outerspace", Bioscience, 39, 314, 1989.

18) Martinez,J., "Stability of Liquid Bridges: Results of SL-D1 Experiment", Acta Astronautica, 15, 449, 1987.

19) Moler,C. and Stewart,G.W., "An Algorithm for Generalized Matrix Eigenvalue Problems", SIAM J. on Num. Anal., 10, 241, 1973.

20) NASA. (n.d.) Science in Orbit- The Shuttle and Spacelab Experience: 1981-1986, U.S. Government Printing Office, Washington D.C., 1988.

21) Pool,R. "Zero Gravity Produces Weighty Improvements", Science, 246, 580, 1989.

22) Ramachandran,N. and Winter,C.M., "The Effects of G-Jitter and Surface Tension Induced Convection on Float Zones", AIAA Paper 90-0654, 1990.

23) Sanchez,D., Ordinary Differential Equations and Stability Theory: An Introduction, W.H. Freeman, San Francisco, 1968.

24) Smith,B.T. et al., Matrix Eigensystem Routines-EISPACK Guide, Springer-Verlag, New York, 1976.

25) Stoker,J.J., Nonlinear Vibrations, Interscience Publishers, New York, 1950.

26) Tyc,G., Cleghorn,W.L., and Rimrott,F.P.J., "Infinite Eigenvalue Method for Stability Analyses of Canonical Linear Systems with Periodic Coefficients", AIAA Journal, 28, 869, 1990.

27) Walter,H. (Ed.), Fluid Sciences and Materials Sciences in Space: A European Perspective, Springer-Verlag, New York, 1987.

28) Wang,T.G., Thrinh,E.H, Croonquist,A.P., and Elleman,D.D., "Shapes of Rotating Free Drops: Spacelab Experimental Results", Phys.Rev. Letter,56, 452, 1986.

APPENDIX 1

Utilization of WVNET Resources

The numerical solution and graphical representation of the present analytical problem requires a well-integrated host of computer resources. The CMS system was accessed via WVNET on a VT320 terminal. A remote site at the Engineering Sciences building was used.

A1.1 Numerical Results

The numerical results for Chapters 2,3,and 4 were obtained by accessing several routines from the IMSL library[10]. Programs which were utilized are found in Appendices 4-9. One solution, in the case of periodic forcing, involved the eigenvalues of a very large complex matrix system. An enormous amount of storage space was required for computation. Upon request, WVNET increased the storage capacity from 4M to 12M. This was sufficient to run the programs. Alternatively, temporary disks could be accessed to provide the necessary space. The following steps were taken to declare the temporary disk space:

```
TDSK 192 DISK B CYL 15
FORMAT 192 B
RELEASE A
RELEASE B
ACCESS 192 A
ACCESS 191 B
```

These steps free 15 spare cylinders of disk space. The computer now interprets this disk as the A disk and the original disk as the B disk. Hence, to bring files over to the temporary diskspace, the following command must be used:

COPY filename FORTRAN B filename FORTRAN A

Once a data file is created, the file can be transferred back to the permanent storage using the following command:

COPY filename filetype A filename filetype B

This file is now saved in the permanent directory. After logging off, the temporary disk memory will be destroyed. This method was solely used prior to the increase of storage space.

A typical session using the expanded memory is as follows: (After logging on to CMS via WVNET.)

```
DEF STOR 12M
IPL CMS
GETDISK IMSL
FORTVS2 filename
GLOBAL TXTLIB VSF2FORT CMSLIB IMSL1 IMSL2
GLOBAL LOADLIB VSF2LOAD
LOAD filename
START
```

Execution will create the desired datafile.

A1.2 Graphical Results

Two options were explored for graphing the results. Initially the data was downloaded to a diskette via Kermit, which in turn was plotted using Lotus/123 graphics package on a Zenith DS computer. While the output was satisfactory, it was inconvenient and time-consuming to change terminal sites.

The second, and preferred, option was to access CMS directly through a WVNET line connected to a MacIntosh II PC. This was accomplished via VersaTerm and VersaTerm Pro communications. The program calling IMSL routines was run in the same manner as with a VT320. The data was then transferred to a SAS/Graph routine emulating TEK4014 device, which presented the results graphically. A typical graphing session is as follows:

```
COPY datafilename filetype A FOR017 LISTING A
SAS filename of sas program
TEK4014
```

A typical SAS/Graph program is as follows:

```
CMS FILEDEF FOR017 DISK FOR017 LISTING;
DATA;
INFILE FOR017;
```

```
INPUT X Y BO;
PROC GPLOT;
PLOT X*Y=BO;
SYMBOL1 I=SPLINE L=1;
SYMBOL2 I=SPLINE L=21;
SYMBOL3 I=SPLINE L=20;
SYMBOL4 I=SPLINE L=22;
```

This routine will take three columns of data as input and graphically sort according to equal values of Bo.

The plots are converted to MacDraw files from which hardcopies were obtained from MacDraw I and II graphic packages. The advantages to this option are the one-terminal site capabilities as well as good resolution.

Utilization of WVNET Resources:

Method 1:

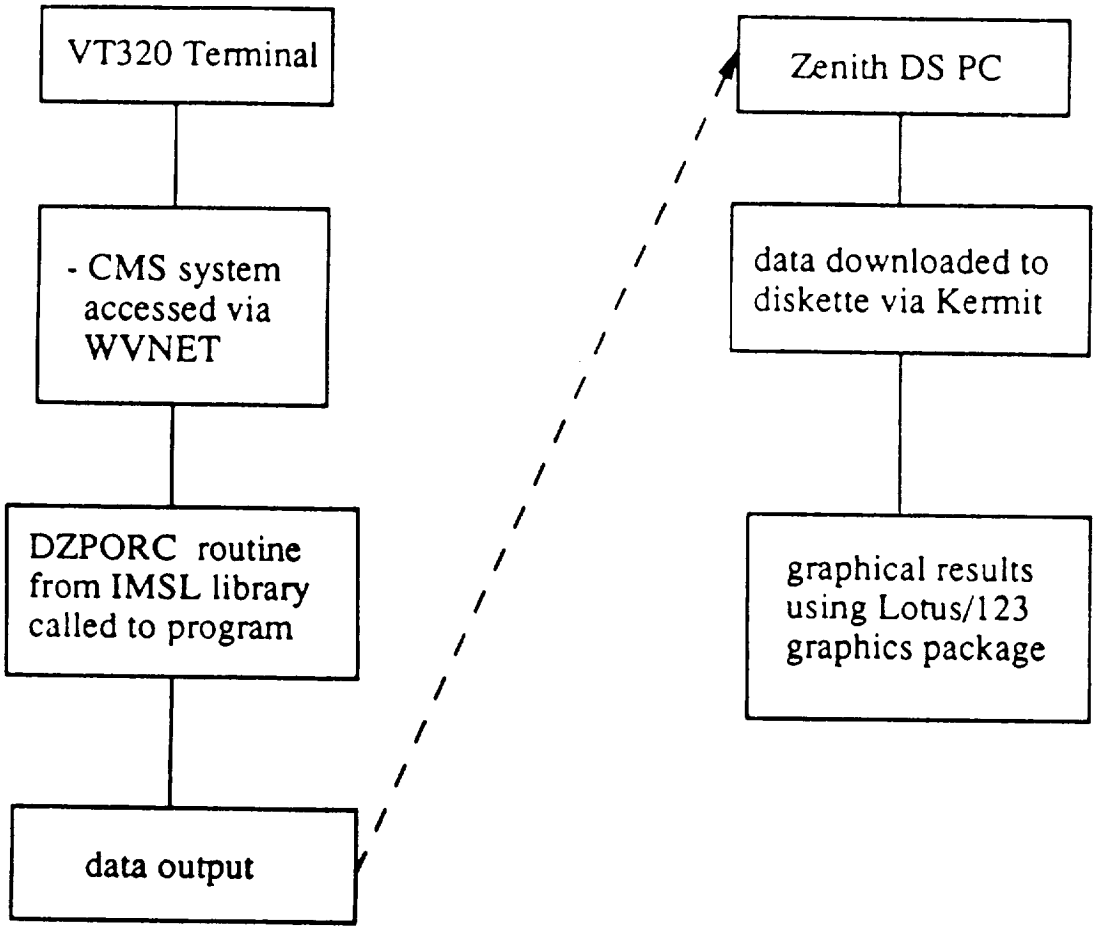

- satisfactory output
- inconvenient and time-consuming to change sites

method 2:

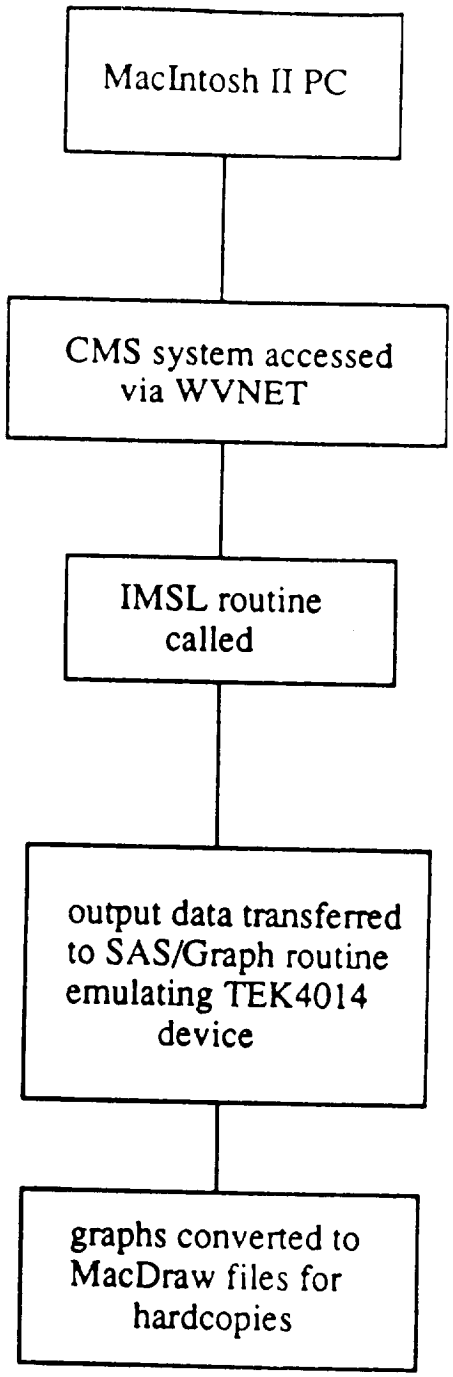

- option of choice
- one-terminal site capabilities

APPENDIX 2

One Interface System of Equations

The fluid system and analysis is the same as for the multi-layer configuration except that there is only one interface. The upper region is subscripted by a 2 and the lower region is subscripted by a 1.

The same governing equations are utilized with the following non-dimensionalization:

$$\underline{u} = (G_o/\omega_f)\ \tilde{\underline{u}} \tag{A2.1}$$

$$x = (G_o/\omega_f^2)\ \tilde{x} \tag{A2.2}$$

$$t = (1/\omega_f)\ \tilde{t} \tag{A2.3}$$

$$p = \rho_D(G_o/\omega_f)^2\ \tilde{p} \tag{A2.4}$$

The interface is given by:

$$Fe = z - 0 - \varepsilon C(t)e^{i(lx+my)} \tag{A2.5}$$

The velocity potentials in each region are described by:

$$\phi_1 = [A(t)e^{kz}\ ]\ e^{i(lx+my)} \tag{A2.6}$$

$$\phi_2 = [B(t)e^{-kz}\ ]\ e^{i(lx+my)} \tag{A2.7}$$

(Note that tildes have been dropped. All quantities are non-dimensional.)

Application of boundary conditions is similar to that of the multi-layer configuration. This system reduces to two linear differential equations which are solved using Floquet analysis. The one interface system is as follows:

$$(\lambda+in)C_n - kA_n = 0 \tag{A2.8}$$

$$(\lambda+in)A_n - \frac{(1-\rho_{21})}{2(1+\rho_{21})}(C_{n-1} + C_{n+1}) + \frac{k^2\rho_{D1}}{Q(1+\rho_{21})}C_n = 0 \tag{A2.9}$$

where $$\rho_{D1} = \frac{(1-\rho_{21})}{2}$$

$$Q = \frac{\rho_{D1} G_o^{\,3}}{\gamma \omega_f^{\,4}} = Bo\left[\frac{G_o}{H\omega_f^{\,2}}\right]^2 \qquad \text{(A2.10)}$$

but there is no H, thus the lengthscale $(G_o/\omega_f^{\,2})$ is used.

$$\therefore \quad Q = Bo(1.0)^2 \qquad \text{(A2.11)}$$

The problem can now be posed as an eigensystem which is truncated and solved numerically.

APPENDIX 3

Stability of Characteristic Equation

According to condition (1) of Sanchez[23] (Section 4.3), the characteristic polynomial of $\underset{\sim}{R}$ must be stable (ie. the four roots of the polynomial must have non-positive real components). The polynomial is of the form

$$\Lambda^4 + a\Lambda^2 + b = 0 \quad \text{or} \quad s^2 + as + b = 0 \qquad (s=\Lambda^2) \qquad \text{(A3.1)}$$

$$s = \frac{-a \pm \sqrt{a^2 - 4b}}{2} \qquad \text{(A3.2)}$$

For guaranteed non-positive real components:

i) $a \geq 0$

ii) $b > 0$

iii) $a^2 > 4b$

Conditions i) and ii) are satisfied simply by the signs of their components. Condition iii) requires that the following inequality must hold true

$$\tau_1(\tau_2+\tau_3)^2 > \tau_4\tau_5\tau_5 \qquad \text{(A3.3)}$$

where

$$\tau_1 = \frac{-k^3\ \rho_{D1}}{-(1+\rho_{21})(1+\rho_{31})e^{k} + (\rho_{21}-1)(1-\rho_{31})e^{-k}}$$

$$\tau_2 = \frac{-(1-\rho_{31})e^{-k} + (1+\rho_{31})e^{k}}{Bo_2\ \rho_{D1}}$$

$$\tau_3 = \frac{(1-\rho_{21})e^{-k} + (1+\rho_{21})e^{k}}{Bo_3\ \rho_{D1}}$$

$$\tau_4 = \frac{4\ \rho_{D1}^{\ 2}}{-(1+\rho_{21})(1+\rho_{31})e^{k} + (\rho_{21}-1)(1-\rho_{31})e^{-k}}$$

$$\tau_5 = (-e^{k} + e^{-k}) \qquad \tau_6 = \frac{k^6}{Bo_2\ Bo_3}$$

As an analytical check, condition iii) was investigated for $\rho = \rho_{21} = \rho_{31}$, $Bo_2 = Bo_3$. The following requirement of stability was obtained:

$$0 > -4\rho - (1-\rho)^2 e^{-2k} \qquad \text{(A3.4)}$$

This is true for all values of ρ.

Using a root finder, the roots of the characteristic polynomial were determined for the other parameter cases, and all roots had non-positive real components. Hence, condition (1) of Sanchez is satisified.

APPENDIX 4

Dispersion Solution - Chap 2

This program solves the dispersion relation which was derived in Chapter 2 of the thesis (equation (2.19)). The dispersion relation is a fourth order polynomial, the roots of which are the propagation speeds of the disturbance.

An IMSL routine, 'DZPORC', is called. This routine is a complex root finder. Solutions are obtained for the various configurations of interest.

```
C THIS IS IN FILE: 'LAYERS FORTRAN'
C
C THIS ROUTINE SOLVES THE DISPERSION RELATION FOR THE CASE OF
C CONSTANT GRAVITATIONAL FIELD.
C THE DISPERSION RELATION IS A FOURTH ORDER POLYNOMIAL.  THE
C FOUR ROOTS ARE COMPLEX AND ARE SOLVED BY CALLING A ROOT
C FINDER ROUTINE, 'DZPORC', FROM THE IMSL LIBRARY.
C
C SOLUTIONS ARE OBTAINED FOR THE FOUR CONFIGURATION CASES ACROSS
C THE PARAMETER SPACE OF INTEREST.
C
C
C
      IMPLICIT REAL*8 (A-H,O-Z)
      DIMENSION DEN(3),GAM(3)
      REAL*8 COEFF(5),ACFS(5)
      COMPLEX*16 ROOT(4)
C
C
C
      COMMON/DAT/R1,R2,R3,AH,AG2,AG3,AGRAV,AWN
      NDEG=4
      G0=980.0D0
C
C
      OPEN(UNIT=14,STATUS='NEW',FILE='FOR014')
C
C
C
C  DENSITIES OF FLUIDS
      DEN(1)=1.0D0
      DEN(2)=0.96D0
      DEN(3)=0.001225D0
C
C  SURFACE TENSIONS
      GAM(1)=72.0D0
      GAM(2)=40.0D0
      GAM(3)=25.0D0
C
C
C
C
C  DO CASES
C
C CASE 1: AIR/SILICON OIL/WATER
      R2=DEN(3)
      R1=DEN(2)
```

```
            R3=DEN(1)
            AG2=GAM(3)
            AG3=GAM(2)
C
            WRITE(14,*)'AIR OVER SILICON OIL OVER WATER'
            WRITE(14,*)'DEN2=',R2
            WRITE(14,*)'DEN1=',R1
            WRITE(14,*)'DEN3=',R3
            WRITE(14,*)'SUR TEN2=',AG2,'SUR TEN3=',AG3
C
            DO 100 I3=1,5
            DO 90 I2=1,6
            DO 80 I1=1,7
C
            AH=0.5D0+(I3-1)*0.25D0
            AGRAV=G0*(1.0D0-(I2-1)*0.2D0)
            AWN=0.25D0+(I1-1)*0.5D0
C
            WRITE(14,*)'H=',AH,'GRAV=',AGRAV
            CALL DISP(ACFS)
            DO 40 I=1,5
            COEFF(I)=ACFS(I)
 40         CONTINUE
C
            CALL DZPORC(NDEG,COEFF,ROOT)
C
            WRITE(14,*)'RT1=',ROOT(1)
            WRITE(14,*)'RT2=',ROOT(2)
            WRITE(14,*)'RT3=',ROOT(3)
            WRITE(14,*)'RT4=',ROOT(4)
 80         CONTINUE
 90         CONTINUE
 100        CONTINUE
C
C
C CASE 2: AIR/WATER/AIR
            R2=DEN(3)
            R1=DEN(1)
            R3=DEN(3)
            AG2=GAM(1)
            AG3=GAM(1)
C
            WRITE(14,*)' '
            WRITE(14,*)' '
            WRITE(14,*)'AIR OVER WATER OVER AIR'
            WRITE(14,*)'DEN2=',R2
            WRITE(14,*)'DEN1=',R1
```

```
      WRITE(14,*)'DEN3=',R3
      WRITE(14,*)'SUR TEN2=',AG2,'SUR TEN3=',AG3
C
      DO 200 J3=1,5
      DO 190 J2=1,6
      DO 180 J1=1,7
      AH=0.5D0+(J3-1)*0.25D0
      AGRAV=G0*(1.0D0-(J2-1)*0.2D0)
      AWN=0.25D0+(J1-1)*0.5D0
C
      WRITE(14,*)'H=',AH,'GRAV=',AGRAV
      WRITE(14,*)'WAVE NUMBER=',AWN
      CALL DISP(ACFS)
      DO 50 J=1,5
      COEFF(J)=ACFS(J)
 50   CONTINUE
C
      CALL DZPORC(NDEG,COEFF,ROOT)
C
      WRITE(14,*)'RT1=',ROOT(1)
      WRITE(14,*)'RT2=',ROOT(2)
      WRITE(14,*)'RT3=',ROOT(3)
      WRITE(14,*)'RT4=',ROOT(4)
180   CONTINUE
190   CONTINUE
200   CONTINUE
C
C
C CASE 3: AIR/SILICON OIL/AIR
      R2=DEN(3)
      R1=DEN(2)
      R3=DEN(3)
      AG2=GAM(3)
C
      WRITE(14,*)' '
      WRITE(14,*)' '
      WRITE(14,*)'AIR OVER SILICON OIL OVER AIR'
      WRITE(14,*)'DEN2=',R2
      WRITE(14,*)'DEN1=',R1
      WRITE(14,*)'DEN3=',R3
      WRITE(14,*)'SUR TEN2=',AG2,'SUR TEN3=',AG3
C
      DO 300 K3=1,5
      DO 290 K2=1,6
      DO 280 K1=1,7
      AH=0.5D0+(K3-1)*0.25D0
      AGRAV=G0*(1.0D0-(K2-1)*0.2D0)
```

```
            AWN=0.25D0+(K1-1)*0.5D0
C
            WRITE(14,*)'H=',AH,'GRAV=',AGRAV
            WRITE(14,*)'WAVE NUMBER=',AWN
            CALL DISP(ACFS)
            DO 60 K=1,5
 60         CONTINUE
C
            CALL DZPORC(NDEG,COEFF,ROOT)
C
            WRITE(14,*)'RT1=',ROOT(1)
            WRITE(14,*)'RT2=',ROOT(2)
            WRITE(14,*)'RT3=',ROOT(3)
            WRITE(14,*)'RT4=',ROOT(4)
 280        CONTINUE
 290        CONTINUE
 300        CONTINUE
C
C
C CASE 4: WATER/SILICON OIL/WATER
            R2=DEN(1)
            R1=DEN(2)
            R3=DEN(1)
            AG2=GAM(2)
            AG3=GAM(2)
C
            WRITE(14,*)' '
            WRITE(14,*)' '
            WRITE(14,*)'WATER OVER SILICON OIL OVER WATER'
            WRITE(14,*)'DEN2=',R2
            WRITE(14,*)'DEN1=',R1
            WRITE(14,*)'DEN3=',R3
C
            DO 400 L3=1,5
            DO 390 L2=1,6
            DO 380 L1=1,7
            AH=0.5D0+(L3-1)*0.25D0
            AGRAV=G0*(1.0D0-(L2-1)*0.2D0)
            AWN=0.25D0+(L1-1)*0.5D0
C
            WRITE(14,*)'H=',AH,'GRAV=',AGRAV
            WRITE(14,*)'WAVE NUMBER=',AWN
            CALL DISP(ACFS)
            DO 70 L=1,5
            COEFF(L)=ACFS(L)
 70         CONTINUE
C
```

```
            CALL DZPORC(NDEG,COEFF,ROOT)
C
            WRITE(14,*)'RT1=',ROOT(1)
            WRITE(14,*)'RT2=',ROOT(2)
            WRITE(14,*)'RT3=',ROOT(3)
            WRITE(14,*)'RT4=',ROOT(4)
 380        CONTINUE
 390        CONTINUE
 400        CONTINUE
C
C
            CLOSE(14)
            STOP
            END
C
C
C
            SUBROUTINE DISP(ACFS)
            IMPLICIT REAL*8 (A-H,O-Z)
            DIMENSION ACFS(5)
            COMMON/DAT/R1,R2,R3,AH,AG2,AG3,AGRAV,AWN
C
C
C COEFFICIENTS
            A=R1+R3
            B=((AGRAV/AWN)*(R1-R3))-(AG3*AWN)
            C=R1+R2
            D=((AGRAV/AWN)*(R2-R1))-(AG2*AWN)
            W=R2-R1
            X=((AGRAV/AWN)*(R2-R1))-(AG2*AWN)
            Y=R1-R3
            Z=((AGRAV/AWN)*(R3-R1))+(AG3*AWN)
C
            ACFS(1)=(X+Z)+(B*D*EXP(2.0D0*AWN*AH))
            ACFS(2)=0.0D0
            ACFS(3)=(W*Z)+(X*Y)+((A*D+B*C)*EXP(2.0D0*AWN*AH))
            ACFS(4)=0.0D0
            ACFS(5)=(W*Y)+(A*C*EXP(2.0D0*AWN*AH))
C
            RETURN
            END
```

APPENDIX 5

Generalized Eigenvalue Solution - Chap 3

This program solves the large, sparse, generalized eigenvalue problem which is represented by equation (3.41) of Chapter 3 (periodic forcing case). Truncation was made at N=|25| giving rise to an eigensystem of 204 equations.

The complex eigenvalues are determined using 'DGVLCG' of the IMSL library. The eigenvalues are the Floquet exponents of equations (3.35-3.38). Following computation of the eigenvalues, only the largest real component will be extracted for the data set. This represents the fastest growing Floquet exponent.

```
C   PROGRAM: NEWPER FORTRAN
C
C
C   3/21/90
C
C   RE: PERIODIC MULTI-SLAB ANALYSIS
C
C
C   THIS PROGRAM IS STRUCTURED TO SOLVE A LARGE, SPARSE GENERALIZED
C   EIGEN VALUE MATRIX, RESULTING FROM AN ANALYSIS OF MULTI-LAYERED
C   SLABS OF LIQUID UNDER A NORMAL PERIODIC FORCING FUNCTION IN A
C   MICROGRAVITY ENVIRONMENT.
C

C   FLOQUET THEORY WAS APPLIED, GENERATING A SYSTEM OF AN INFINITE
C   NUMBER OF LINEAR EQUATIONS.  THIS SYSTEM WAS TRUNCATED AT 25
C   WHICH RESULTS IN 204 EQUATIONS.
C
C   SINCE THE PROBLEM IS ESSENTIALLY A GENERALIZED COMPLEX
C   EIGENSYSTEM OF THE FORM, A*Z=W*B*Z, THE ROUTINE 'DGVLCG' OF THE
C   IMSL LIBRARY WILL BE CALLED TO SOLVE FOR THE EIGENVALUES.
C   THE EIGENVALUES(W) ARE THE FLOQUET EXPONENTS OF THE SYSTEM.
C
C   FOLLOWING COMPUTATION OF THE EIGENVALUES, THE LARGEST POSITIVE
C   COMPONENT IS EXTRACTED FROM EACH ITERATION OF VARIOUS PARAMETERS.
C   THIS COMPONENT WILL DETERMINE THE STABILITY OF THE CONFIGURATION.
C
C
C
      PARAMETER (N=204, NG=51)
      IMPLICIT REAL*8(A-H,O-Z)
      COMPLEX*16 A(N,N),BLK(4,4),B(N,N)
      COMPLEX*16 ALPHA(N),BETA(N), EVAL(N)
      COMPLEX*16 Y11,Y12,Y13,Y14,Y21,Y22,Y23,Y24,Y31,Y32,Y33,Y34
      COMPLEX*16 Y41,Y42,Y43,Y44,Y1,Y2,YB,YT,YDIA
      REAL RECO(4),Q(4)
      REAL AK
      EXTERNAL DGVLCG
      COMMON /WORKSP/ RWKSP
      REAL RWKSP(332948)
      CALL IWKIN(332948)
C
      LDA=N
      LDB=N
C
      OPEN(UNIT=16,STATUS='NEW',FILE='FOR016')
C
C   FILLING THE A AND B MATRICES WITH ZEROES PRIOR TO LOADING
```

```
C  THE NON-ZERO TERMS
C
      DO 5 II=1,N
      DO 4 JJ=1,N
      A(II,JJ)=(0.0D0,0.0D0)
      B(II,JJ)=(0.0D0,0.0D0)
   4  CONTINUE
   5  CONTINUE
C
C
C
C
C  THIS IS THE PARAMETER BLOCK.  LOOPS ARE PERFORMED ON THE BOND
C  NUMBERS (BO2,BO3), THE FROUDE NUMBER (FR), AND THE WAVE NUMBER
C  (K).VALUES OF THE DENSITY RATIOS (RH21,RH31) ARE SPECIFIED.
C
      RH21=10.0D0
      RH31=0.001225D0
      RHD1=(DABS(RH21-1.0D0)+DABS(RH31-1.0D0))/2.0D0
C
      DO 500 NJ=0,0
      DO 400 NT=0,0
      DO 300 IY=1,1
         WN=0.0D0
      DO 200 IX=1,50
         WN=WN+0.1D0
C
C
C
      FR=0.01D0
C
      DO 160 NP=0,3
      NPP=NP+1
      BO2=10.0D0**(-NP)
      BO3=BO2
C
C  CALCULATING NON-ZERO ELEMENTS THAT WILL BE INSERTED INTO
C  MATRICES A AND B.
C
      DO 20 M=1,NG
      SUB=((NG*1.0D0)+1.0D0)/2.0D0
C
      CF=(M*1.0D0)-SUB
      X13=-1.0D0*WN*DEXP(WN)
      X14=1.0D0*WN*DEXP(-1.0D0*WN)
      X23=-1.0D0*WN
```

```
      X24=1.0D0*WN
      X31N=FR*WN*WN*DEXP(-1.0D0*WN)*(RHD1)
      X31D=BO2*(RH21+1.0D0)
      X31=X31N/X31D
      X34=((1.0D0-RH21)*DEXP(-2.0D0*WN))/(1.0D0+RH21)
      X42=(-FR*WN*WN*(RHD1))/(BO3*(1.0D0+RH31))
      X43=(1.0D0-RH31)/(1.0D0+RH31)
      XB=-1.0D0*(1.0D0-RH31)/(1.0D0+RH31)
      XT=(DEXP(-2.0D0*WN)*(RH21-1.0D0))/(RH21+1.0D0)
      X1=(FR*(1.0D0-RH21))/((1.0D0+RH21)*2.0D0*DEXP(WN))
      X2=FR*(1.0D0-RH31)/(2.0D0*(1.0D0+RH31))
      X34M=X34*CF
      X43M=X43*CF
C
C ELEMENTS OF 4X4 SUBMATRIX FOR A GIVEN NG.
C
          XZER=0.0D0
          Y11=DCMPLX(XZER,CF)
      BLK(1,1)=Y11
          Y12=DCMPLX(XZER,XZER)
      BLK(1,2)=Y12
          Y13=DCMPLX(X13,XZER)
      BLK(1,3)=Y13
          Y14=DCMPLX(X14,XZER)
      BLK(1,4)=Y14
          Y21=DCMPLX(XZER,XZER)
      BLK(2,1)=Y21
          Y22=DCMPLX(XZER,CF)
      BLK(2,2)=Y22
          Y23=DCMPLX(X23,XZER)
      BLK(2,3)=Y23
          Y24=DCMPLX(X24,XZER)
      BLK(2,4)=Y24
          Y31=DCMPLX(X31,XZER)
      BLK(3,1)=Y31
          Y32=DCMPLX(XZER,XZER)
      BLK(3,2)=Y32
          Y33=DCMPLX(XZER,CF)
      BLK(3,3)=Y33
          Y34=DCMPLX(XZER,X34)
      BLK(3,4)=Y34
          Y41=DCMPLX(XZER,XZER)
      BLK(4,1)=Y41
          Y42=DCMPLX(X42,XZER)
      BLK(4,2)=Y42
          Y43=DCMPLX(XZER,X43)
      BLK(4,3)=Y43
          Y44=DCMPLX(XZER,CF)
```

```
      BLK(4,4)=Y44
C
C  LOADING NON-ZERO TERMS IN MATRIX A
C
         Y1=DCMPLX(X1,XZER)
         Y2=DCMPLX(X2,XZER)
      NL=(4*M)-3
      NU=(4*M)
      K1=0
      DO 15 I=NL,NU
      K2=0
      K1=K1+1
      DO 10 J=NL,NU
      K2=K2+1
      A(I,J)=BLK(K1,K2)
      IF(M.EQ.1.OR.M.EQ.NG) GO TO 8
      IF(K1.EQ.3)THEN
          JB=I-6
          JF=I+2
          IP1=I+1
          JFP=JF+1
          JBP=JB+1
          A(I,JF)=Y1
          A(I,JB)=Y1
          A(IP1,JFP)=Y2
          A(IP1,JBP)=Y2
        ELSE
      END IF
      GO TO 10
 8    IF(M.EQ.1.AND.K1.EQ.3)THEN
          JF=I+2
          IP1=I+1
          JFP=JF+1
          A(I,JF)=Y1
          A(IP1,JFP)=Y2
        ELSE
      END IF
      IF(M.EQ.NG.AND.K1.EQ.3)THEN
          JB=I-6
          IP1=I+1
          JBP=JB+1
          A(I,JB)=Y1
          A(IP1,JBP)=Y2
        ELSE
        END IF
 10   CONTINUE
 15   CONTINUE
 20   CONTINUE
```

```
C
C
C  LOADING NON-ZERO TERMS OF MATRIX B
C
          YB=DCMPLX(XB,XZER)
          YT=DCMPLX(XT,XZER)
          XN1=-1.0D0
          YDIA=DCMPLX(XN1,XZER)
        NCT=0
        DO 30 L=1,NG
        DO 25 MOP=1,4
        NCT=NCT+1
        B(NCT,NCT)=YDIA
        IF(MOP.EQ.4)THEN
           NM1=NCT-1
           B(NCT,NM1)=YB
           B(NM1,NCT)=YT
         ELSE
         END IF
   25   CONTINUE
   30   CONTINUE
C
C
        CALL DGVLCG (N, A, LDA, B, LDB, ALPHA, BETA)
C
C  PROGRAM DGVLCG CALCULATES THE EIGENVALUES OF A GENERALIZED
C  COMPLEX EIGENSYSTEM.
C  THE EIGENVALUE (EVAL(N)) IS COMPUTED BY DIVIDING COMPLEX
C  VECTORS ALPHA(N) BY BETA(N).
C
C  THE EIGENVALUES ARE SWEPT OUT IN ORDER OF INCREASING SIZE OF
C  THE REAL COMPONENT.  THUS TO EXTRACT THAT VALUE, ONE NEEDS
C  ONLY THE N-TH REAL VALUE OF EVAL.
C  THIS LARGEST REAL COMPONENT (RECO), IS THEN SENT TO A DATA
C  FILE FOR VARIOUS PARAMETER VARIATIONS.
C
        DO 50 IM=1,N
          EVAL(IM)=ALPHA(IM)/BETA(IM)
  50    CONTINUE
        RECO(NPP)=EVAL(N)
C
C
C
        WRITE(16,2)WN,RECO(NPP),BO2
   2    FORMAT(1X,F5.2,E10.3,F6.3)
 160    CONTINUE
 200    CONTINUE
 300    CONTINUE
```

```
 400    CONTINUE
 500    CONTINUE
C
C
        CLOSE(16)
        STOP
        END
```

APPENDIX 6

Standard Eigenvalue Problem - Chap 3

This program converts the generalized eigenvalue problem (of form $\underset{\sim}{A}\ \underline{X} = \lambda\ \underset{\sim}{B}\ \underline{X}$) to the standard form of $\underset{\sim}{C}\ \underline{X} = \lambda\ \underline{X}$. This requires premultiplication of both sides by B^{-1} using IMSL routine 'DLINGC'.

The eigenvalues are calculated using routine 'DEVLCG' which utilizes a different algorithm than the generalized eigenvalue problem. The Floquet exponents as determined by both methods will be compared to check accuracy.

```
C PROGRAM 'LONG'
C
C  THIS PROGRAM IS STRUCTURED TO SOLVE A LARGE, SPARSE GENERALIZED
C  EIGEN VALUE MATRIX, RESULTING FROM AN ANALYSIS OF MULTI-LAYERED
C  SLABS OF LIQUID UNDER A NORMAL PERIODIC FORCING FUNCTION IN A
C  MICROGRAVITY ENVIRONMENT.
C
C  THE PROBLEM CAN BE CONVERTED FROM A GENERALIZED TO A REGULAR
C  EIGENVALUE PROBLEM BY PREMULTIPLYING BOTH SIDES BY BINV. THIS
C  CAN BE CARRIED OUT BY IMPLEMENTING IMSL ROUTINES 'DLINCG',
C  'DMCRCR', AND FINALLY THE EIGENVALUES CAN BE DETERMINED BY
C  USING ROUTINE 'DEVLCG'.
C
C
C
C
      PARAMETER (N=204, NG=51)
      IMPLICIT REAL*8(A-H,O-Z)
      COMPLEX*16 A(N,N),BLK(4,4),B(N,N)
      COMPLEX*16 ALPHA(N),BETA(N), EVAL(N)
      COMPLEX*16 Y11,Y12,Y13,Y14,Y21,Y22,Y23,Y24,Y31,Y32,Y33,Y34
      COMPLEX*16 Y41,Y42,Y43,Y44,Y1,Y2,YB,YT,YDIA
      COMPLEX*16 BINV(N,N),C(N,N)
      EXTERNAL DGVLCG, DLINCG, DMCRCR, DEVLCG
      COMMON /WORKSP/ RWKSP
      REAL RWKSP(332948)
      CALL IWKIN(332948)
C
      LDA=N
      LDB=N
      LDBINV=N
      NR=N
      LDC=N
C
      OPEN(UNIT=16,STATUS='NEW',FILE='FOR016')
C
C  FILLING THE MATRICES WITH ZEROES
C
      DO 5 II=1,N
      DO 4 JJ=1,N
      A(II,JJ)=(0.0D0,0.0D0)
      B(II,JJ)=(0.0D0,0.0D0)
    4 CONTINUE
    5 CONTINUE
C
C
C
```

```
C
C  PARAMETER BLOCK
C
      BET=0.01D0
      WN=1.0D0
      DO 300 IY=1,1
      WN=WN+0.5D0
      DO 200 IX=1,1
      BET=BET*(5.0D0*IX)
      T2=0.001D0
      T3=0.001D0
      RH21=0.001225D0
      RH31=0.001225D0
      RHD1=(DABS(RH21-1.0D0)+DABS(RH31-1.0D0))/2.0D0
C
C
C CALCULATING NON-ZERO ELEMENTS
C
      DO 20 M=1,NG
      SUB=((NG*1.0D0)+1.0D0)/2.0D0
C
      CF=(M*1.0D0)-SUB
      X13=-1.0D0*WN*BET*DEXP(WN)
      X14=1.0D0*WN*BET*DEXP(-1.0D0*WN)
      X23=-1.0D0*WN*BET
      X24=1.0D0*WN*BET
      X31N=WN*WN*DEXP(-1.0D0*WN)*(RHD1)
      X31D=T2*(RH21+1.0D0)
      X31=X31N/X31D
      X34=(-1.0D0*DEXP(-1.0D0*WN)*(RH21-1.0D0)*CF)/(RH21+1.0D0)
      X42=(-1.0D0*WN*WN*(RHD1))/(T3*(1.0D0+RH31))
      X43=((1.0D0-RH31)*CF)/(1.0D0+RH31)
      XB=-1.0D0*(1.0D0-RH31)/(1.0D0+RH31)
      XT=(DEXP(-1.0D0*WN)*(RH21-1.0D0))/(RH21+1.0D0)
      X1=-1.0D0*(RH21-1.0D0)/(2.0D0*(RH21+1.0D0)*DEXP(WN))
      X2=(1.0D0-RH31)/(2.0D0*(1.0D0+RH31))
      X34M=X34*CF
      X43M=X43*CF
C
C ELEMENTS OF 4X4 SUBMATRIX
C
          XZER=0.0D0
          Y11=DCMPLX(XZER,CF)
      BLK(1,1)=Y11
          Y12=DCMPLX(XZER,XZER)
      BLK(1,2)=Y12
          Y13=DCMPLX(X13,XZER)
      BLK(1,3)=Y13
          Y14=DCMPLX(X14,XZER)
```

```
      BLK(1,4)=Y14
           Y21=DCMPLX(XZER,XZER)
      BLK(2,1)=Y21
           Y22=DCMPLX(XZER,CF)
      BLK(2,2)=Y22
           Y23=DCMPLX(X23,XZER)
      BLK(2,3)=Y23
           Y24=DCMPLX(X24,XZER)
      BLK(2,4)=Y24
           Y31=DCMPLX(X31,XZER)
      BLK(3,1)=Y31
           Y32=DCMPLX(XZER,XZER)
      BLK(3,2)=Y32
           Y33=DCMPLX(XZER,CF)
      BLK(3,3)=Y33
           Y34=DCMPLX(XZER,X34)
      BLK(3,4)=Y34
           Y41=DCMPLX(XZER,XZER)
      BLK(4,1)=Y41
           Y42=DCMPLX(X42,XZER)
      BLK(4,2)=Y42
           Y43=DCMPLX(XZER,X43)
      BLK(4,3)=Y43
           Y44=DCMPLX(XZER,CF)
      BLK(4,4)=Y44
C
C  LOADING NON-ZERO TERMS IN MATRIX A
C
          Y1=DCMPLX(X1,XZER)
          Y2=DCMPLX(X2,XZER)
      NL=(4*M)-3
      NU=(4*M)
      K1=0
      DO 15 I=NL,NU
      K2=0
      K1=K1+1
      DO 10 J=NL,NU
      K2=K2+1
      A(I,J)=BLK(K1,K2)
      IF(M.EQ.1.OR.M.EQ.NG) GO TO 8
      IF(K1.EQ.3)THEN
           JB=I-6
           JF=I+2
           IP1=I+1
           JFP=JF+1
           JBP=JB+1
           A(I,JF)=Y1
           A(I,JB)=Y1
```

```
            A(IP1,JFP)=Y2
            A(IP1,JBP)=Y2
          ELSE
        END IF
        GO TO 10
    8   IF(M.EQ.1.AND.K1.EQ.3)THEN
            JF=I+2
            IP1=I+1
            JFP=JF+1
            A(I,JF)=Y1
            A(IP1,JFP)=Y2
          ELSE
        END IF
        IF(M.EQ.NG.AND.K1.EQ.3)THEN
            JB=I-6
            IP1=I+1
            JBP=JB+1
            A(I,JB)=Y1
            A(IP1,JBP)=Y2
          ELSE
          END IF
   10   CONTINUE
   15   CONTINUE
   20   CONTINUE
C
C
C  LOADING NON-ZERO TERMS OF MATRIX B
C
          YB=DCMPLX(XB,XZER)
          YT=DCMPLX(XT,XZER)
          XN1=-1.0D0
          YDIA=DCMPLX(XN1,XZER)
        NCT=0
        DO 30 L=1,NG
        DO 25 MOP=1,4
        NCT=NCT+1
        B(NCT,NCT)=YDIA
        IF(MOP.EQ.4)THEN
           NM1=NCT-1
           B(NCT,NM1)=YB
           B(NM1,NCT)=YT
         ELSE
         END IF
   25   CONTINUE
   30   CONTINUE
C
C COMPUTING THE INVERSE OF B
```

```
C
      CALL DLINCG (N, B, LDB, BINV, LDBINV)
C
C
C MULTIPLYING BINV AND A
C
      CALL DMCRCR (NR,NR,BINV,LDA,NR,NR,A,LDB,NR,NR,C,LDC)
C
C
C SOLVING FOR THE EIGENVALUES
C
      CALL DEVLCG (N, C, LDC, EVAL)
C
C
      DO 50 IM=1,N
      WRITE(16,*)'EVAL=',EVAL(IM)
  50  CONTINUE
C
 200  CONTINUE
 300  CONTINUE
C
C
      CLOSE(16)
      STOP
      END
```

APPENDIX 7

Determinant Calculation

This program takes the eigenvalues which were determined by Appendix 5 and substitutes them into equation (3.39). The determinant of the resulting matrix is calculated to check for accuracy of the eigenvalues. The determinant should equal zero if the eigenvalues are accurate.

Routine 'DLFTCG' is utilized for LU factorization of the matrix and computation of the determinant.

```
C  THIS PROGRAM 'DET FORTRAN' WILL CALCULATE THE DETERMINANT OF
C  THE SPARSE MATRIX TO DETERMINE THE ACCURACY OF THE SOLUTION.
C  THE ROUTINE 'DLFDCG' OF THE IMSL PACKAGE WILL BE UTILIZED.  THE
C  LU FACTORIZATION WILL BE NEEDED AND WILL PROVIDED BY CALLING THE
C  'DLFTCG' ROUTINE.
C
C
C  THIS PROGRAM IS STRUCTURED TO SOLVE A LARGE, SPARSE GENERALIZED
C  EIGEN VALUE MATRIX, RESULTING FROM AN ANALYSIS OF MULTI-LAYERED
C  SLABS OF LIQUID UNDER A NORMAL PERIODIC FORCING FUNCTION IN A
C  MICROGRAVITY ENVIRONMENT.
C
C  SINCE THE PROBLEM IS ESSENTIALLY A GENERALIZED COMPLEX
C  EIGENSYSTEM OF THE FORM, A*Z=W*B*Z, THE ROUTINE 'DGVLCG' OF THE
C  IMSL LIBRARY WILL BE CALLED TO SOLVE FOR THE EIGENVALUES.
C
C
C
C
      PARAMETER (N=204, NG=51)
      IMPLICIT REAL*8(A-H,O-Z)
      COMPLEX*16 A(N,N),BLK(4,4),B(N,N)
      COMPLEX*16 ALPHA(N),BETA(N), EVAL(N)
      COMPLEX*16 FAC(N,N),DET1,AMAT(N,N)
      COMPLEX*16 Y11,Y12,Y13,Y14,Y21,Y22,Y23,Y24,Y31,Y32,Y33,Y34
      COMPLEX*16 Y41,Y42,Y43,Y44,Y1,Y2,YB,YT,YDIA
      REAL*8 DET2
      INTEGER IPVT(N)
      EXTERNAL DGVLCG, DLFDCG, DLFTCG
      COMMON /WORKSP/ RWKSP
      REAL RWKSP(332948)
      CALL IWKIN(332948)
C
      LDA=N
      LDB=N
      LDFAC=N
C
      OPEN(UNIT=19,STATUS='NEW',FILE='FOR019')
C
C  FILLING THE MATRICES WITH ZEROES
C
      DO 5 II=1,N
      DO 4 JJ=1,N
      A(II,JJ)=(0.0D0,0.0D0)
      B(II,JJ)=(0.0D0,0.0D0)
4     CONTINUE
5     CONTINUE
```

```
C
C
C
C
C  PARAMETER BLOCK
C
      BET=0.01D0
      WN=1.0D0
      DO 300 IY=1,1
      WN=WN+0.5D0
      DO 200 IX=1,1
      BET=BET*(5.0D0*IX)
      T2=0.001D0
      T3=0.001D0
      RH21=0.001225D0
      RH31=0.001225D0
      RHD1=(DABS(RH21-1.0D0)+DABS(RH31-1.0D0))/2.0D0
C
C
C CALCULATING NON-ZERO ELEMENTS
C
      DO 20 M=1,NG
      SUB=((NG*1.0D0)+1.0D0)/2.0D0
C
      CF=(M*1.0D0)-SUB
      X13=-1.0D0*WN*BET*DEXP(WN)
      X14=1.0D0*WN*BET*DEXP(-1.0D0*WN)
      X23=-1.0D0*WN*BET
      X24=1.0D0*WN*BET
      X31N=WN*WN*DEXP(-1.0D0*WN)*(RHD1)
      X31D=T2*(RH21+1.0D0)
      X31=X31N/X31D
      X34=(-1.0D0*DEXP(-1.0D0*WN)*(RH21-1.0D0)*CF)/(RH21+1.0D0)
      X42=(-1.0D0*WN*WN*(RHD1))/(T3*(1.0D0+RH31))
      X43=((1.0D0-RH31)*CF)/(1.0D0+RH31)
      XB=-1.0D0*(1.0D0-RH31)/(1.0D0+RH31)
      XT=(DEXP(-1.0D0*WN)*(RH21-1.0D0))/(RH21+1.0D0)
      X1=-1.0D0*(RH21-1.0D0)/(2.0D0*(RH21+1.0D0)*DEXP(WN))
      X2=(1.0D0-RH31)/(2.0D0*(1.0D0+RH31))
      X34M=X34*CF
      X43M=X43*CF
C
C ELEMENTS OF 4X4 SUBMATRIX
C
          XZER=0.0D0
          Y11=DCMPLX(XZER,CF)
      BLK(1,1)=Y11
          Y12=DCMPLX(XZER,XZER)
      BLK(1,2)=Y12
```

```
          Y13=DCMPLX(X13,XZER)
        BLK(1,3)=Y13
          Y14=DCMPLX(X14,XZER)
        BLK(1,4)=Y14
          Y21=DCMPLX(XZER,XZER)
        BLK(2,1)=Y21
          Y22=DCMPLX(XZER,CF)
        BLK(2,2)=Y22
          Y23=DCMPLX(X23,XZER)
        BLK(2,3)=Y23
          Y24=DCMPLX(X24,XZER)
        BLK(2,4)=Y24
          Y31=DCMPLX(X31,XZER)
        BLK(3,1)=Y31
          Y32=DCMPLX(XZER,XZER)
        BLK(3,2)=Y32
          Y33=DCMPLX(XZER,CF)
        BLK(3,3)=Y33
          Y34=DCMPLX(XZER,X34)
        BLK(3,4)=Y34
          Y41=DCMPLX(XZER,XZER)
        BLK(4,1)=Y41
          Y42=DCMPLX(X42,XZER)
        BLK(4,2)=Y42
          Y43=DCMPLX(XZER,X43)
        BLK(4,3)=Y43
          Y44=DCMPLX(XZER,CF)
        BLK(4,4)=Y44
C
C  LOADING NON-ZERO TERMS IN MATRIX A
C
          Y1=DCMPLX(X1,XZER)
          Y2=DCMPLX(X2,XZER)
        NL=(4*M)-3
        NU=(4*M)
        K1=0
        DO 15 I=NL,NU
        K2=0
        K1=K1+1
        DO 10 J=NL,NU
        K2=K2+1
        A(I,J)=BLK(K1,K2)
        IF(M.EQ.1.OR.M.EQ.NG) GO TO 8
        IF(K1.EQ.3)THEN
          JB=I-6
          JF=I+2
          IP1=I+1
          JFP=JF+1
```

```
            JBP=JB+1
            A(I,JF)=Y1
            A(I,JB)=Y1
            A(IP1,JFP)=Y2
            A(IP1,JBP)=Y2
          ELSE
        END IF
        GO TO 10
    8   IF(M.EQ.1.AND.K1.EQ.3)THEN
            JF=I+2
            IP1=I+1
            JFP=JF+1
            A(I,JF)=Y1
            A(IP1,JFP)=Y2
          ELSE
        END IF
        IF(M.EQ.NG.AND.K1.EQ.3)THEN
            JB=I-6
            IP1=I+1
            JBP=JB+1
            A(I,JB)=Y1
            A(IP1,JBP)=Y2
          ELSE
          END IF
   10   CONTINUE
   15   CONTINUE
   20   CONTINUE
C
C
C  LOADING NON-ZERO TERMS OF MATRIX B
C
          YB=DCMPLX(XB,XZER)
          YT=DCMPLX(XT,XZER)
          XN1=-1.0D0
          YDIA=DCMPLX(XN1,XZER)
        NCT=0
        DO 30 L=1,NG
        DO 25 MOP=1,4
        NCT=NCT+1
        B(NCT,NCT)=YDIA
        IF(MOP.EQ.4)THEN
           NM1=NCT-1
           B(NCT,NM1)=YB
           B(NM1,NCT)=YT
         ELSE
         END IF
   25   CONTINUE
   30   CONTINUE
```

```
C
C
      CALL DGVLCG (N, A, LDA, B, LDB, ALPHA, BETA)
C
      DO 50 IM=1,N
        EVAL(IM)=ALPHA(IM)/BETA(IM)
 50   CONTINUE
C
C
200   CONTINUE
300   CONTINUE
C
C
C
C  COMPUTE NEW MATRIX A=A-W*B
C
      DO 500 MM=1,N
      DO 400 IL=1,N
      DO 350 JL=1,N
      AMAT(IL,JL)=A(IL,JL)
      A(IL,JL)=AMAT(IL,JL)-(EVAL(MM)*B(IL,JL))
350   CONTINUE
400   CONTINUE
C
C  FACTORING MATRIX A
C
      CALL DLFTCG (N, A, LDA, FAC, LDFAC, IPVT)
C
C
C  COMPUTE THE DETERMINANT OF THE FACTORED MATRIX
C
      CALL DLFDCG (N, FAC, LDFAC, IPVT, DET1, DET2)
C
C
      WRITE(19,*)DET1,DET2
C
      DO 460 IR=1,N
      DO 450 JR=1,N
      A(IR,JR)=AMAT(IR,JR)
450   CONTINUE
460   CONTINUE
500   CONTINUE
      CLOSE(19)
      STOP
      END
```

APPENDIX 8

One Interface Solution -Chap 3

As discussed in section 3.4a, a limit approximation is compared to the 1 interface system of equations (see Appendix 2). The two linear equations (A2.8,A2.9) are solved using Floquet analysis resulting in a standard eigensystem.

Routine 'DEVLCG' is used to determine the eigenvalues of the 1 interface configuration. The results are used to compare the limit approximation for the 2 interface system.

```
C THIS IS A CHECK FOR ONE INTERFACE
C
C THIS PROGRAM SOLVES THE EIGENSYSTEM RESULTING FROM A ONE
C INTERFACE CONFIGURATION.
C
C THE SYSTEM REDUCES TO TWO LINEAR DIFFERENTIAL EQUATIONS WHICH
C ARE SOLVED VIA FLOQUET ANALYSIS IN THE SAME MANNER AS THE
C TWO INTERFACE SYSTEM.
C A STANDARD EIGENVALUE PROBLEM IS OBTAINED AND IS SOLVED USING
C 'DEVLCG' FROM THE IMSL LIBRARY.
C
C
      PARAMETER (N=102,NG=51)
      IMPLICIT REAL*8 (A-H,O-Z)
      COMPLEX*16 A(N,N), BLK(2,2)
      COMPLEX*16 EVAL(N)
      COMPLEX*16 Y11, Y12, Y21, Y22, YOUT
      EXTERNAL DEVLCG
      COMMON /WORKSP/ RWKSP
      REAL RWKSP(332948)
      CALL IWKIN(332948)
C
C
      LDA=N
C
      OPEN(UNIT=16,STATUS='NEW',FILE='FOR016')
C
C FILLING THE A MATRIX WITH ZEROES
      DO 5 I=1,N
      DO 4 J=1,N
      A(I,J)=(0.0D0,0.0D0)
   4  CONTINUE
   5  CONTINUE
C
C
C PARAMETER BLOCK
      RH21=0.001225D0
      DO 500 NJ=0,0
      Q=1.0D0*10.0D0**NJ
      WN=0.0D0
      DO 400 NT=1,50
      WN=WN+0.05D0
C
C CALCULATING NON-ZERO TERMS OF A
      DO 100 M=1,NG
      SUB=((NG*1.0D0)+1.0D0)/2.0D0
```

```
C
      CF=(M*1.0D0)-SUB
      X21=-Q*WN*WN
      X12=WN
      XOUT=(1.0D0-RH21)/(2.0D0*(1.0D0+RH21))
      FC=-CF
C
C ELEMENTS OF 2X2 BLOCK
      XZER=0.0D0
      Y11=DCMPLX(XZER,FC)
        BLK(1,1)=Y11
      Y12=DCMPLX(X12,XZER)
        BLK(1,2)=Y12
      Y21=DCMPLX(X21,XZER)
        BLK(2,1)=Y21
      Y22=DCMPLX(XZER,FC)
        BLK(2,2)=Y22
      YOUT=DCMPLX(XOUT,XZER)
C
C LOADING TERMS OF A
      MP=(2*M)-1
      MP1=MP+1
      MPM=MP1-3
      MPP=MP1+1
      A(MP,MP)=BLK(1,1)
      A(MP,MP1)=BLK(1,2)
      A(MP1,MP)=BLK(2,1)
      A(MP1,MP1)=BLK(2,2)
      IF(M.NE.1)THEN
        A(MP1,MPM)=YOUT
        ELSE
        END IF
      IF(M.NE.NG)THEN
        A(MP1,MPP)=YOUT
        ELSE
        END IF
C
  100 CONTINUE
C
C
      CALL DEVLCG (N, A, LDA, EVAL)
C
C
      RECO=EVAL(N)
C
      UNUM=1.0
C
      WN=WN+0.05D0
```

```
      WRITE(16,28)WN,UNUM,RECO
 28   FORMAT(1X,F5.2,F6.3,E10.3)
C
      WN=WN-0.05D0
C
  400 CONTINUE
  500 CONTINUE
C
      CLOSE(16)
      STOP
      END
```

APPENDIX 9

Time Response of Interfaces - Chap 4

For the non-periodic forcing case, a system of linear differential equations in terms of $(E,F,\dot{E},\dot{F})$ is obtained (equations (4.22,4.23)). E and F are the displacements of the upper and lower interfaces, respectively.

The system of equations is integrated numerically using 'DIVPAG' of the IMSL library. This routine utilizes Gear's to solve for the time-dependent coefficients.

```
C     THIS FILE IS CSLAB   FORTRAN
C     THIS PROGRAM INTEGRATES THE FOURTH ORDER MULTI-SLAB
C     FORCED LINEAR SYSTEM, CONSISTING OF E(T),F,DE/DT,DF/DT
C         ( ALL FCNS. OF T)
C     THE FORCING IS **NOT*** PERIODIC
C       GEAR'S METHOD IS USED--PROB MAY BE STIFF.
C                    IMSL LIBRARIES ARE USED.
C     PARAMETER VALUES ARE CHOSEN.
C
C
        INTEGER NEQ,NPARAM
        PARAMETER (NPARAM=50,NEQ=4)
C
        INTEGER IDO,IEND,IMETH,INORM,NOUT
        REAL*8 A(1,1),FCN,FCNJ,HINIT,PARAM(NPARAM),TOL,T,TEND,Y(NEQ)
        REAL*8 AK,B2,B3,R21,R31,RHD1
        REAL*8 EE(3),FF(3)
        EXTERNAL FCN,DIVPAG,SSET,UMACH
C
        COMMON/DAT/AK,B2,B3,R21,R31,RHD1
C
C
        OPEN(UNIT=24,STATUS='NEW',FILE='FOR024')
C
C  COUNTER
         KK=0
        JEDE=0
C  PARAMETER VALUES
        AK=1.0D0
        B2=1.0D0
        B3=1.0D0
        R21=0.001225D0
        R31=0.001225D0
        RHD1=(DABS(R21-1.0D0)+DABS(R31-1.0D0))/2.0D0
C
C
        DO 200 ID=0,1
C
        B2=10.0D0**(-ID)
        B3=B2
C
        PP=ID+1
C
C
C SET INITIAL CONDITIONS
        T=0.00D0
C
```

```
C    E=Y1, DE/DT=Y2, F=Y3, DF/DT=Y4
C
        CC=-0.05D0
        DD=0.05D0
C
        Y(1)=0.00D0
        Y(2)=-AK*CC*DEXP(-AK)
        Y(3)=0.00D0
        Y(4)=AK*DD
C
C   SET PROGRAM SWITCHES/VALUES
        HINIT=0.0001D0
        INORM=1
        IMETH=2
        CALL SSET(NPARAM,0.0,PARAM,1)
        PARAM(1)=HINIT
        PARAM(10)=INORM
        PARAM(12)=IMETH
C   SET ERROR TOLERANCE
        TOL=1.0D-5
C
C
C
C
        WN=AK
        BO2=B2
        BO3=B3
C
        IDO=1
        DO 100 II=1,5000
C
        TEND=0.01D0*II
        CALL DIVPAG(IDO,NEQ,FCN,FCNJ,A,T,TEND,TOL,PARAM,Y)
        KK=KK+1
        IF (KK.EQ.10) GO TO 50
        GO TO 60
 50     CONTINUE
C
C
        JEDE=JEDE+1
        TT=T
        GRAV=G(T)
        IF(JEDE.GE.150)GRAV=0.0D0
        WRITE(24,28)T,Y(1),Y(3),BO2
 28     FORMAT(1X,4F9.4)
C
        KK=0
 60     CONTINUE
```

```
 100   CONTINUE
C
C     RELEASE WORKSPACE
         IDO=3
         CALL DIVPAG(IDO,NEQ,FCN,FCNJ,A,T,TEND,TOL,PARAM,Y)
C
 200   CONTINUE
C
         CLOSE(24)
         END
C
         SUBROUTINE FCN(NEQ,T,Y,YP)
         INTEGER NEQ
         REAL*8 T,Y(NEQ),YP(NEQ)
         REAL*8 CF1N,CF1D,CF1,CF2N,CF2D,CF2,CBLK2,CBLK3,CFA,CFB
         REAL*8 AK,R2,R3,RHD1,B2,B3
         COMMON/DAT/AK,B2,B3,R2,R3,RHD1
C
         CF1N=-2.0D0*AK*DEXP(-AK)
         CF1D=(1.0D0+R3)*(1.0D0+R2)+(1.0D0-R3)*(R2-1.0D0)
     & *DEXP(-2.0D0*AK)
         CF1=CF1N/CF1D
         CF2N=AK*((R2-1.0D0)*DEXP(-2.0D0*AK)-(R2+1.0D0))
         CF2D=CF1D
         CF2=CF2N/CF2D
         CBLK2=(AK*AK/B2)*(RHD1)-(R2-1.0D0)*G(T)
         CBLK3=(AK*AK/B3)*(RHD1)-(1.0D0-R3)*G(T)
         CFA=(1.0D0-R3)/(1.0D0+R2)
         CFB=AK/(1.0D0+R2)
C
C
         YP(1)=Y(2)
         YP(2)=(CF1*CFA*DEXP(-AK)-CFB)*CBLK2*Y(1)
     & +CF1*CBLK3*Y(3)
         YP(3)=Y(4)
         YP(4)=(DEXP(-AK)*(CF2*CFA-CFB)*CBLK2)*Y(1)+CF2*CBLK3*Y(3)
         RETURN
         END
C
C
         FUNCTION G(T)
         REAL*8 G,T
         IF(T.LT.1.0) G=0.0D0
         IF(T.GE.1.0.AND.T.LT.2.0)G=T-1.0D0
         IF(T.GE.2.0.AND.T.LT.3.0)G=1.0D0
         IF(T.GE.3.0.AND.T.LT.5.0)G=-T+4.0D0
         IF(T.GE.5.0.AND.T.LT.6.0)G=-1.0D0
```

```
      IF(T.GE.6.0.AND.T.LT.7.0)G=T-7.0D0
      IF(T.GE.7.0D0)G=0.0D0
      RETURN
      END
C
      SUBROUTINE FCNJ(NEQ,T,Y,YP)
C     DUMMY
      RETURN
      END
```

APPROVAL OF EXAMINING COMMITTEE

John Kuhlman, Ph.D.

Gary Morris, Ph.D.

7 March 1991
Date

Margaret J. Lyell, Ph.D., Chair